Aleksander Nawrat
Zygmunt Kuś (Eds.)

Vision Based Systems for UAV Applications

Springer

Studies in Computational Intelligence

Volume 481

Series Editor

J. Kacprzyk, Warsaw, Poland

Aleksander Nawrat · Zygmunt Kuś
Editors

Vision Based Systems for UAV Applications

Springer

Editors
Prof. Aleksander Nawrat
Silesian University of Technology
Gliwice
Poland

Dr. Zygmunt Kuś
Silesian University of Technology
Gliwice
Poland

Printed on acid-free paper

*"In God We Trust, All others we observe
and keep very close..."*
                              To our friends

Preface

The book was motivated by a significant number of vision based algorithms for Unmanned Aerial Vehicles (UAV) that are developed during research and development projects. Nowadays, it can be observed a significant increase in a number of UAV applications. One of the main factors in the development of UAV is rapid progress of development of advanced sensory and considerable increase of computing power. Aerial observation is currently used for both military and civilian purposes. The variety of drones and their parameters gives almost unlimited possibilities in areas like vision surveillance, cartography, geodesy, cinematography or meteorology. Most if not all of these applications utilize some kind of vision based sensor like video camera, thermal imaging camera or laser range finders. Therefore it is essential to improve the existing general video acquisition devices and design and construct innovative dedicated for special purposes cameras. The amount of high and low frequencies disruptions is significantly greater than for traditional handheld cameras. It is a matter of high importance to design devices to reduce the impact in order to deliver proper video stream stabilization. Additionally bearing capacity of quick response class UAV is highly limited. Therefore video acquisition devices are required to be as light as possible but at the same time rugged and reliable. However, there is also a considerable group of vision based control algorithms that are used e.g. for target detection or collision-free navigation. It is worth mentioning about the task of controlling a group of mobile robots within line of sight. There is also an active field of classification of actions and patterns based on information often fused from multiple video stream sources. Finally the video stream has to be compressed and transmitted wirelessly from UAV to ground station over heterogeneous networks with different dynamically changing topologies.

Main idea of visual surveillance is to detect any specified targets or abnormal situations in the line of sight. Targets can be detected due to their characteristic features e.g. face, character of movement, size, color or shape. Those features are detected, tracked and recognized by a dedicated set of algorithms processing images acquired from live video stream. Detection and recognition are usually a time consuming thus there is object tracking phase in the middle. The main challenge of such algorithms is to reconcile the tracking quality with simplicity required for real time processing. Regardless the application object recognition is an essential task for complex systems where a certain amount of system autonomy is required. The book contains

valuable information in the field of detection, tracking and recognition of objects. Presented challenges and solutions are the results of research conducted by the team.

Nowadays, image acquisition devices are mainly used by human operators or large tactical or strategic class UAVs. Therefore there is a need for innovative video sources that are characterized by small weight, low energy consumption and at the same time high resistance to vibrations, shock and temperature. Traditionally used visible light cameras cover only a small part of the magnetic spectrum and are easily covered by dust, smoke, fog, etc. In order to continue aerial observation thermal imaging and omnidirectional cameras have to be used.

It is commonly accepted that over 80% of all perceptual information being received by human brain is perceived through eyes. It is natural for control algorithms developers to try to utilize the information as it is done by both human and animal brains. Vision information can be utilized not only for control a single device but also for controlling a group of e.g. mobile robots. An alternative approach is to use aerial vision information for controlling detected and recognized objects on the ground.

Main aim of design and construction of UAVs is their practical application. However, their design is a lengthy process and requires intensive evaluation using both simulation and experimental data. Even then, it is often necessary to apply amendments based on the actual real life experience of the application. Misrecognition can sometimes lead to irreversible consequences therefore in order to improve the quality of recognition frequently fusion of data from multiple sources of information is used. However it is worth mentioning that before the video stream from a camera mounted on an UAV it is necessary to wirelessly transmit to human operator using ground base station. In addition, video data transmission requires a significant network bandwidth. Communication over long distances is charged a considerable limitation in this regard. Therefore it is necessary to use a dedicated image and sound compression algorithms.

The topics covered in this book also includes practical applications of classification algorithms used in video streams for UAV. This book is not only intended for researchers involved in image processing field. Aim of the book was to create a valuable source of information for researchers and constructors of solutions utilizing vision from UAV. Scientists and researchers involved in computer vision, image processing, data fusion, control algorithms, mechanics, data mining, navigation and IC can find many valuable, useful and practical suggestions and solutions. The latest challenges for vision based systems are also presented. Furthermore the information included in the book can benefit greatly students of higher years of study in the fields of computer science, automation, robotics, mechanical engineering or data mining. The author strongly encourage all readers to explore the following chapters of the book and invite to open and honest discussion of any questions or concerns encountered during the lecture.

Gliwice   Aleksander Nawrat
February 2012   Zygmunt Kuś

Acknowledgments

Contents

Part III: Design of Vision Based Control Algorithms

Part IV: Practical Applications of Classification Algorithms Used in Video Streams for UAV

List of Contributors

Artur Babiarz
Silesian University of Technology, Institute of Automatic Control, Akademicka 16,
44-101 Gliwice, Poland
e-mail: `artur.babiarz@polsl.pl`

Damian Bereska
Silesian University of Technology, Institute of Automatic Control, Akademicka 16,
44-101 Gliwice, Poland
e-mail: `damian.bereska@polsl.pl`

Robert Bieda
Silesian University of Technology, Institute of Automatic Control, Akademicka 16,
44-101 Gliwice, Poland
e-mail: `robert.bieda@polsl.pl`

Grzegorz Bieszczad
Military University of Technology, Institute of Optoelectronics, Warsaw, Poland
e-mail: `gbieszczad@wat.edu.pl`

Dawid Cedrych
Silesian University of Technology, Institute of Automatic Control, Akademicka 16,
44-101 Gliwice, Poland
e-mail: `dawid.cedrych@polsl.pl`

Tomasz Czapla
Silesian University of Technology, Faculty of Mechanical Engineering, Division of
Theoretical and Applied Mechanics, ul. Konarskiego 18A, 44-101 Gliwice, Poland
e-mail: `tomasz.czapla@polsl.pl`

Adam Czornik
Silesian University of Technology, Institute of Automatic Control, Akademicka 16,
44-101 Gliwice, Poland
e-mail: `adam.czornik@polsl.pl`

Krzysztof Daniec
Silesian University of Technology, Institute of Automatic Control, Akademicka 16,
44-101 Gliwice, Poland
e-mail: `krzysztof.daniec@polsl.pl`

Piotr Demski
Silesian University of Technology, Institute of Automatic Control, Akademicka 16,
44-101 Gliwice, Poland
e-mail: `piotr.demski@polsl.pl`

Sławomir Fraś
Silesian University of Technology, Institute of Automatic Control, Akademicka 16,
44-101 Gliwice, Poland
e-mail: `slawomir.fras@polsl.pl`

Adam Gałuszka
Silesian University of Technology, Institute of Automatic Control, Akademicka 16,
44-101 Gliwice, Poland
e-mail: `adam.galuszka@polsl.pl`

Tomasz Grzejszczak
Silesian University of Technology, Institute of Automatic Control, Akademicka 16,
44-101 Gliwice, Poland
e-mail: `tomasz.grzejszczak@polsl.pl`

Paweł Iwaneczko
Silesian University of Technology, Institute of Automatic Control, Akademicka 16,
44-101 Gliwice, Poland
e-mail: `pawel.iwaneczko@polsl.pl`

Krzysztof Jaskot
Silesian University of Technology, Institute of Automatic Control, Akademicka 16,
44-101 Gliwice, Poland
e-mail: `krzysztof.jaskot@polsl.pl`

Karol Jędrasiak
Silesian University of Technology, Institute of Automatic Control, Akademicka 16,
44-101 Gliwice, Poland
e-mail: `karol.jedrasiak@polsl.pl`

Henryk Josiński
Silesian University of Technology, Institute of Computer Science, Akademicka 16,
44-101 Gliwice, Poland
e-mail: henryk.josinski@polsl.pl

Daniel Kostrzewa
Silesian University of Technology, Institute of Computer Science, Akademicka 16,
44-101 Gliwice, Poland
e-mail: Daniel.kostrzewa@polsl.pl

Roman Koteras
Silesian University of Technology, Institute of Automatic Control, Akademicka 16,
44-101 Gliwice, Poland
e-mail: roman.koteras@polsl.pl

Marek Koźlak
Ośrodek Badawczo-Rozwojowy Urządzeń Mechanicznych "OBRUM" sp. z o.o. ul.
Toszecka 102, 44-117 Gliwice, Poland
email: mkozlak@obrum.gliwice.pl
Silesian University of Technology, Technopark, ul. Konarskiego 18C, 44-100 Gli-
wice, Poland
email: marek.kozlak@polsl.pl

Michał Krupiński
Military University of Technology, Institute of Optoelectronics, Warsaw, Poland
e-mail: mkrupinski@wat.edu.pl

Antoni Kurzeja
Ośrodek Badawczo-Rozwojowy Urządzeń Mechanicznych "OBRUM" sp. z o.o. ul.
Toszecka 102, 44-117 Gliwice, Poland
email: akurzeja@obrum.gliwice.pl

Zygmunt Kuś
Silesian University of Technology, Institute of Automatic Control, Akademicka 16,
44-101 Gliwice, Poland
e-mail: zygmunt.kus@polsl.pl

Jan Kwiatkowski
Silesian University of Technology, Institute of Automatic Control, Akademicka 16,
44-101 Gliwice, Poland
e-mail: jan.kwiatkowski@polsl.pl

Henryk Madura
Military University of Technology, Institute of Optoelectronics, Warsaw, Poland
e-mail: hmadura@wat.edu.pl

Mateusz Malinowski
Silesian University of Technology, Institute of Automatic Control, Akademicka 16,
44-101 Gliwice, Poland
e-mail: mateusz.malinowski@polsl.pl

Martin Mellado
Instituto de Automatica e Informatica Industrial, Universidad Plitecnica de Valencia
e-mail: marin@ai2.upv.es

Agnieszka Michalczuk
Silesian University of Technology, Institute of Computer Science, Akademicka 16,
44-101 Gliwice, Poland
e-mail: agnieszka.michalczuk@polsl.pl

Michał Mikulski
Silesian University of Technology, Institute of Automatic Control, Akademicka 16,
44-101 Gliwice, Poland
e-mail: michal.mikulski@polsl.pl

Aleksander Nawrat
Silesian University of Technology, Institute of Automatic Control, Akademicka 16,
44-101 Gliwice, Poland
e-mail: aleksander.nawrat@polsl.pl
Ośrodek Badawczo-Rozwojowy Urządzeń Mechanicznych "OBRUM" sp. z o.o. ul.
Toszecka 102, 44-117 Gliwice, Poland
email: anawrat@obrum.gliwice.pl

Michał Niezabitowski
Silesian University of Technology, Institute of Automatic Control, Akademicka 16,
44-101 Gliwice, Poland
e-mail: michal.niezabitowski@polsl.pl

Marcin Pacholczyk
Silesian University of Technology, Institute of Automatic Control, Akademicka 16,
44-101 Gliwice, Poland
e-mail: marcin.pacholczyk@polsl.pl

Anna Piaskowy
Silesian University of Technology,
44-101 Gliwice, Poland
e-mail: anna.piaskowy@polsl.pl

Andrzej Polański
Silesian University of Technology, Institute of Computer Science, Akademicka 16,
44-101 Gliwice, Poland
e-mail: andrzej.polanski@polsl.pl

Artur Skórkowski
Silesian University of Technology,
44-101 Gliwice, Poland
e-mail: artur.skorkowski@polsl.pl

Krzysztof Skrzypczyk
Silesian University of Technology, Institute of Automatic Control, Akademicka 16,
44-101 Gliwice, Poland
e-mail: Krzysztof.skrzypczyk@polsl.pl

Dawid Sobel
Silesian University of Technology, Institute of Automatic Control, Akademicka 16,
44-101 Gliwice, Poland
e-mail: dawid.sobel@polsl.pl

Tomasz Sosnowski
Military University of Technology, Institute of Optoelectronics, Warsaw, Poland
e-mail: tsosnowski@wat.edu.pl

Adam Świtoński
Silesian University of Technology, Institute of Computer Science, Akademicka 16,
44-101 Gliwice, Poland
e-mail: adam.switonski@polsl.pl

Tadeusz Topór-Kamiński
Silesian University of Technology, Institute of Automatic Control, Akademicka 16,
44-101 Gliwice, Poland
e-mail: tadeusz.kaminski@polsl.pl

Konrad Wojciechowski
Silesian University of Technology, Institute of Computer Science, Akademicka 16,
44-101 Gliwice, Poland
e-mail: konrad.wojciechowski@polsl.pl

Józef Wrona
Military University of Technology, ul. gen. Sylwestra Kaliskiego 2, Warsaw, Poland,
Industrial Research Institute of Automation and Measurements, Aleje Jerozolimskie
2022, 02-486 Warsaw, Poland
e-mail: jwrona@wat.edu.pl

Part I
Design of Object Detection, Recognition and Tracking Algorithms

Visual surveillance is one of the most active fields of research. Its main idea is to detect any specified targets or abnormal situations in the line of sight. Targets can be detected due to their characteristic features e.g. face, character of movement, size, color or shape. Those features are detected by a dedicated set of algorithms processing images acquired from live video stream. Traditionally detection is performed within 2D images acquired from the video stream. Recently also depth images from various structural light or lidar systems are taken into account. Real time processing is essential for accurate system or human observer reaction therefore the time of computation is an important limitation that has to be coped with. There are multiple abnormal situations that might be detected. A typical example is detection of abandoned objects like suitcases or small size packages that might contain highly energetic materials. Another example is road surveillance where incidents breaking the traffic law are aim of the detection process. Similar approach is utilized by city surveillance systems where average people trajectories are computed and any unusual activities are detected and reported to the human staff.

Detection is usually a time consuming process thus it is followed by less time consuming object tracking phase. During tracking previously detected characteristic object features are tracked from frame to frame usually only in a specified local surroundings. Forasmuch as tracked object may change its perceived appearance during tracking it is frequently assumed that the model update is necessary for maintaining satisfactory quality of the tracking process. Real time object tracking is often used for surveillance purposes. However it can also be used for instance for creation of automatic target sentry turrets or as a base information for control algorithm of camera gimbal mounted to the UAV. Such applications could be applied in a variety of environments like critical infrastructure protection or for national border security.

Information acquired by tracking the detected objects can be also used for higher level algorithms like object and activity recognition. There is a variety of object recognition applications e.g. car owner recognition based on car plates, person recognition based on facial features, etc. Regardless the application object recognition is an essential task for complex systems where a certain amount of system autonomy is required. However classification large number of features is time consuming. In order to reduce the number of features often data dimensionality reduction algorithms like FLD or PCA are used.

Computer vision system combining detection, tracking and recognition mounted in gimbal under UAV can be successfully applied to various important tasks like monitoring watercourses or critical infrastructure like pumping gas stations or high-voltage lines.

Another important challenge is how to track objects in rapid disturbance conditions. For instance the changes a helicopter position and orientation during the time of disturbance result in losing tracked object from the field of view. Due to this fact the helicopter control system uses not only the visual information. The essence of the potential solution is to compute the object position only in such time intervals when the object is in the center of the image. It allows the camera head regulators to compensate change of the camera position and set the camera towards the object. The solution could comprise of turning the camera head towards the trucked object in horizontal and vertical planes.

Machine Vision in Autonomous Systems of Detection and Location of Objects in Digital Images

Artur Babiarz, Robert Bieda, Karol Jędrasiak, and Aleksander Nawrat

Abstract. In the article a group of vi libraries ("virtual instrument") of the simulation – programming LabVIEW environment, enabling the construction of a program that would be the basics of the image programming and analysis system, are presented. Presented libraries are dedicated for the Vivotek, supporting the SDK module ("VitaminCtrl"). They provide the ability to connect the camera that works on the Internet, configuration of the transmission protocol, acquisition parameters and audio and video streaming. In addition, while operating the PTZ ("pan-tilt-zoom") cameras, suggested module allow to control the camera motion from the client application level which was created in the National Instruments' firm environment. With the use of the designed libraries, the LabVIEW environments and PTZ cameras of Vivotek a post was made to make algorithm and synthesis of the processing algorithms and for the analysis of digital images. At the stage of the development of the functional modules, a consistent idea of input and output signals definition was also developed. The created modules rely on both the commands of the controlling module SDK and syntax URL format commands. What is more, designed modules enable capturing the video signal frames and their conversation to a LabVIEW variable environment of Image type ("IMAQ Image.ctl"). With the achieved functionality a simple construction of an application for the synthesis and analysis of algorithms for image processing and for the analysis of images acquired in the real time, directly from the camera, is possible.

Artur Babiarz · Robert Bieda · Karol Jędrasiak · Aleksander Nawrat
Silesian University of Technology, Institute of Automatic Control,
Akademicka 16, 44-101 Gliwice, Poland
e-mail: {robert.bieda,karol.jedrasiak,
       artur.babiarz,anawrat}@polsl.pl

1   Introduction

A group of functional module of LabVIEW environment, enabling configuration and control of a PTZ ("pan-tilt-zoom") camera, that is used autonomous [7] platforms of different types (flying [9], ridding) was designed and implemented in the presented article. The following are examples of exemplary camera models of type PTZ of 7000 series, that presented modules cooperate with.

Fig. 1. An example cameras

The idea of designed module is based on using the SDK ("VitaminCtrl") libraries, that are supporting the cooperation with the VIVOEK camera in the simulation- programming environment of LabVIEW. With the development of functional modules, allowing for the configuration and control of the camera and the acquisition of images, it is possible to test processing algorithms and the analysis of images on sequences obtained at the time of the algorithms being tested. The convention of proposed arrangement of the input and output signals of particular module is presented in fig.2.

Optional In/Out

input. no. 1	op. no. 1	op. no. 2	output. no. 1
input. no. 2			output. no. 2
input. no. 3	op. no. 3	op. no. 4	output. no. 3
input. no. 4			output. no. 4

Input   Output

Optional input/output.
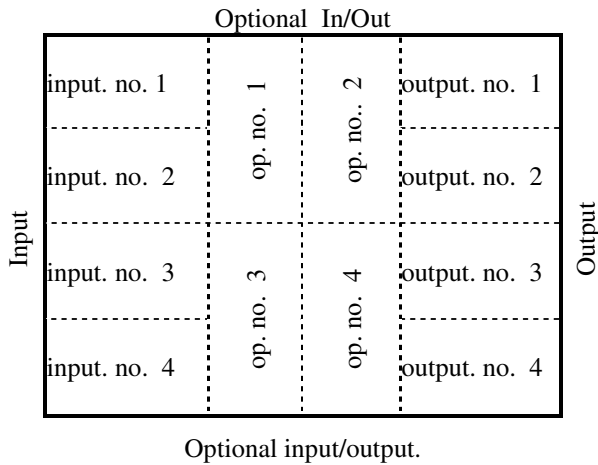
Fig. 2. The ideological arrangement of input and output controls in the vi modules

The left side (according to the convention of the "information flow direction") provides the controls of input signals. The controls placed in the upper or lover part allow for optional configuration of our module's work. A permanent and necessary element of the operation is the "VitaminCrtl" libraries reference control - in this convention it is input no.1. Accordingly transferred references to another module is input no.1 The input/output controls no.4 are responsible for the control of possible mistakes of the realization of particular modules. Inputs no.2 and no.3 and no.1 to no.4 optional controls are the input parameters essential to realization of a task defined with the module functionality. Outputs no.2 and no.4 and no.1 to no.4 optional controls consist information connected with the realization of the task defined with the module functionality. The video camera could be used for telemetry of UAVs [5] in order to support collision-free path planning [6] or for target detection and tracking [10].

A description of the developed modules and their functions and input/output parameters is given below.

2 Description of Completed Communication Modules and Camera Control

2.1 The Module Connected with Camera

The main requirement for usage of the PTZ camera in the image analysis system is connecting with the device of image acquisition. Camera is equipped with a server available via Internet or localhost. The process of connecting with the camera is also a process of login in through the Internet. The operation of connecting and disconnecting the client's application with the sever/camera is made by the VVT_STARTSTOP.vi module. The pattern of controls outputs of the connection module is presented by the Fig. 3a.
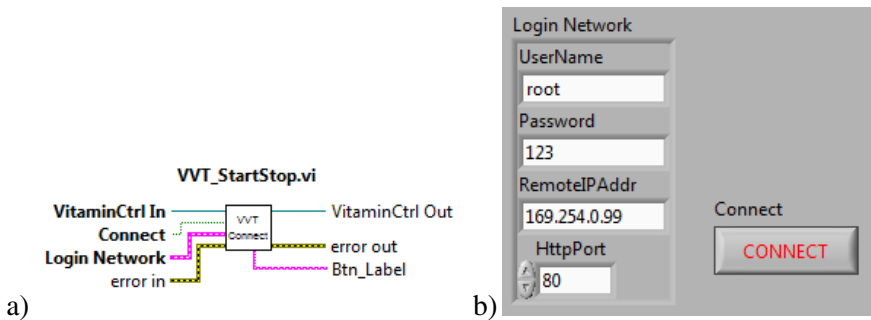
Fig. 3. The view of the module control connected to the camera and its input/output parameters

The description of the input/output signals:

The module connecting with the camera requires two input parameters (fig. 3b):

- "connect" controls of binary variable describe the type of the conducted task – "true" – connection, "false"- disconnection;
- "login network" controls consist the information set of connecting parameters :
    - o "username" – the name of the user;
    - o "password" – the password of access for a particular user;
    - o "remoteipaddr" –IP address of the server (camera);
    - o "httpport" – the address of port on which the communications with the camera takes place (default no. 80).

2.2   The Module Connected with Camera

The PTZ camera used in the research enables communication basing on one of few of the standard protocols. A configuration of parameters responsible for the control of the connection "stability" of the client's application with the server/camera is also possible. control In the basic version such functionality is enabled by : VVT_PROTOCOL_GET_SET.vi module presented on Fig. 4a. Module this, enables also to acquire above information about the actual condition of the parameters of the communication protocol.
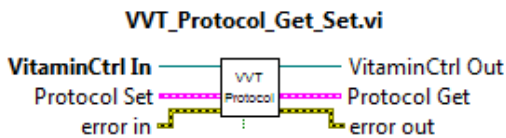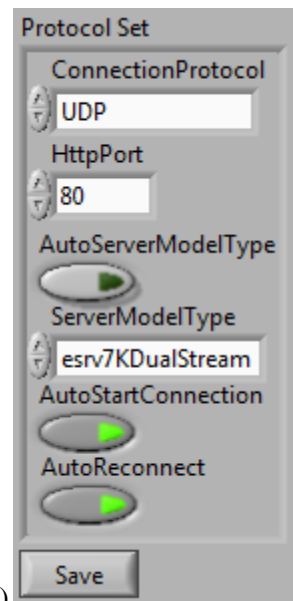
a)   b)

Fig. 4. The configuration module control view of the connecting protocol and its inputs/outputs parameters

The description of the input/output signals:

The configuration module of the protocol can work in a desired parameter setting mode ("set") or until the acquisition of information about their actual condition ("get"). The change in functionality is realized by the optional control no.3 defined as binary value - "true" where arrangement of parameters ("set") is consistent with "protocol set" and "false" controls of the actual parameter reading state ("get") returned in "protocol get" control. The content of the "protocol set/get"control is described on Fig. 4b:

- "protocol set/get" controls consist of the following information set:
  - "connectionprotocol" – Communications protocol type [None, HTTP, UDP, TCP] – a change in the protocol type forces a new connection with the camera;
  - "httpport" –the address of port on which the communications with the camera takes place (default no. 80);
  - "autoservermodeltype" – defines if the type of the camera (Server) should be defined automatically or manually (the type of the server corresponds to the camera type of Vivotex – the tested model was of 70000 series);
  - "servermodeltype" – enables the choice of the server/camera type in case of a defining a server manually ("autoservermodeltype "control);
  - "autostartconnection" – defines whether the camera should connect automatically after being connected to the Internet Network and also the change of the transmission protocol.

2.3 User Interface Configuration Module

SDK "VitaminCtrl" module allows for a preview of the image registered by the camera with its configuration of its appearance and functionality provided by the application of the Vivotek camera's Server. The possibility of configuration is realized by the VVT_USERINTERFACE_GET_SET.vi module. The designed module enables both the change in individual parameters of "ui set" and reading of the actual values of those "ui get" parameters (Fig. 5a).

The description of the input/output signals:

The configuration interface module of the user can work in desired parameter setting mode ("set") or until the acquisition of information about their actual condition ("get"). The change in functionality is realized by the optional control no.3 defined as binary value - "true" where arrangement of parameters ("set") is consistent with "ui get" and "false" controls of the actual parameter reading state ("get") returned in "ui get" control. The content of the ""ui set/get""control is described on Fig. 5b:
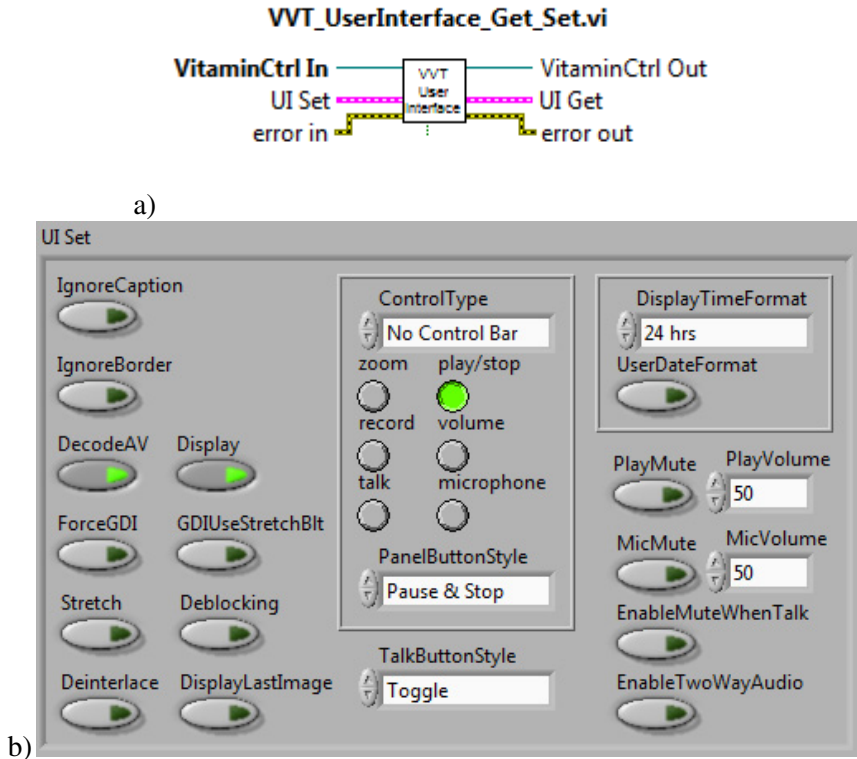
Fig. 5. The view on the user's interface control module and its input/output parameters

- "ui set/get" controls of appearance and improving the quality of the projected image:
  - "ignorecaption" – switches on/off the information bar in the Upper part of the image from the camera containing information about the type of the streaking audio-video transmission and about the actual date and camera work;
  - "ignoreborder" – switches on/off the "frame" around the projected from the camera;
  - "decodeav" – switches on/off decoding of the transmitted audio-video stream (with MPEG4video transmission);
  - "display" – switches on/off projection options of the video stream transmitted from the camera;
  - "forcegdi" – switches on/off the back-up for older graphic cards improving the projected image quality;
  - "gdiusestrechblt" – switches on/off (only with activated "forcegdi" control) the option fitting the levels of color intensity in the projected image (useful when using an older graphic card)

- o "stretch" – switches on/off the option of adjusting the projected image to the size of the active control of client's panel regardless of resolution of the registered image;
  - o "deblocking" – switches on/off the options minimizing the effect of blocks that are created Turing the compressiom process of the developer image in the MJPEG stream form;
  - o "interlace" – switches on/off the decoding of streaming video;
  - o "displaylastimage" – switches on/off the ability to put the last registered video frame into the image frame, in case where the connection is lost or the client's application is disconnected from the sever/camera;
- The controls connected with the configuration of the preview window toolbar of the recorded image and sound:
  - o "controltype" – enables the choice of the image window toolbar [No control bar, Normal control, Morion control, Mask Edit];
  - o "zoom" – switches on/off the magnifying of an image fragment control (in "Normal control" mode);
  - o "play/stop" – switches on/off streaming video preview controls (in "Normal control" mode);
  - o "record" – switches on/off streaming video saving controls (only in "Normal control" mode);
  - o "volume" – switches on/off the streaming audio signal controls (in "Normal control" mode of MPEG4 stream);
  - o "talk" – switches on/off biodirectional audio stream communication controls (in "Normal control" mode of MPEG4 stream);
  - o "microphone" – switches on/off controls associated with the audio signalc sent from the client application to the camera (in "Normal control"mode of MPEG4 stream);
  - o "panelbuttonstyle" – allows the selection of style/pe of display controls tolbar (in "Normal control" mode);
- The controls defining the format of the information display made at defined time (the upper image window control bar from the client application camera):
  - o "displaytimeformat" – pozwala wybrać rodzaj reprezentacji czasu pracy kamery [24 hrs, 12 hrs, userdefine];
  - o "userdateformat" – switches on/off the way of displaying the date;
- The controls responsible for the configuration of the audio stream in both monitored listening mode from the internal/external microphone of the camera and in the transmitting from the client application to the camera mode :
  - o "playmute" – switches on/off the audio-listening of the stream from the camera's microphone ;
  - o "playvolume" – determines the intensity of the audio-listening [0,1,…,100];
  - o "micmute" – switches on/off transmitting the audio stream to the camera;

- o "micvolume" –determines the intensity of the outgoing audio signal to the camera [0,1,…,100];
- o "enablemutewhentalk" – switches on/off silence mode of the audio-listening at the time of transmitting the audio signal to the camera;
- o "enabletwowayaudio" – switches on/off the two-way mode of the audio transmission (for the cameras operating the two-way audio transmission).

2.4   The Module of the CC Matrix Parameters

The flexibility of the tested camera allows the configuration the parameters of the sourced image. Those parameters are strictly connected with the hardware configuration of the acquisition module and are not dependable from the type of the transmitted video signal. The control and parameter settings of the camera matrix are made by the **VVT_IMAGECONTROL_GET_SET.vi** module (Fig. 6a.) Due to the use of the URL commands in the module it is required to determine the IP of the camera server and it is recommended to elicit a module in command of another 'internal' event (for e.g. record/reading parameter controls). This recommendation is related with the "long" time of the ULR command realization by the camera server.
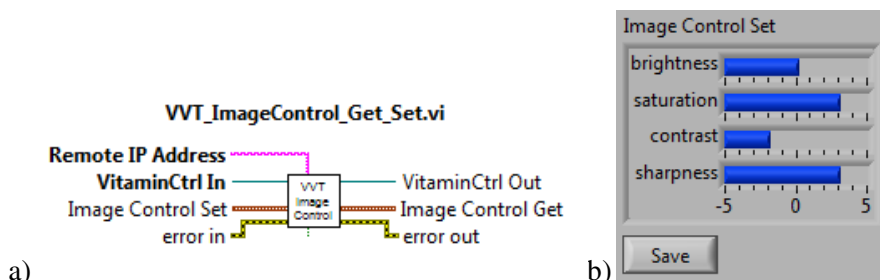
Fig. 6. The view on the CCmatrix parameters module control and its input/output parameters

The description of the input/output signals:

The configuration of the camera matrix can work in desired parameter setting mode ("set") or until the acquisition of information about their actual condition ("get"). The change in functionality is realized by the optional control no.3 defined as binary value - "true" where arrangement of parameters ("set") is consistent with " image control set" and "false" controls of the actual parameter reading state ("get") returned in "image control set control. The content of the "image control set/get"control is described on Fig. 6b:

- The camera IP address control ("remote ip address") in optional input no.1 is a required parameter for realization of the task connected with the rekord/Reading pof image acquisition parameters; this value is defined as a

chain of signs (text) of a structure commonly used in IP address definition: [A.B.C.D – where A, B, C parameters and D are the values of the 0 – 255 set, for e.g. 168.254.0.99]

- "image control set/get" controls of the image acquisition parameters:
  - o "brightness" – defines the value of the image brightness ratio [-5,-4,…,+5];
  - o "saturation" – defines the value of the image color saturation ratio [-5, -4,…,+5];
  - o "contrast" – defines the value of the registered image contrast ratio [-5,-4,…,+5];
  - o "sharpness" – defines the value of the image "sharpness" ratio (strengthening the sharpness of the content details) [-5,-4,…,+5].

2.5   The Module of the PTZ Camera Velocity

In case of the PTZ cameras a vertical axis rotation ("pan"),horizontal axis ("tilt") and "move" along the optical axis ("zoom") of the camera is possible. It is also possible to determine the camera speed movement (the change of the scale ratio in case of the optical axis) and speed movement in "auto pan" or "patrol" traffic mode. In case, where the camera is equipped the automatic/manual module of focus ("focus") it is possible also to define the "speed" of changes that are being made. The control of the "speed" parameters of the camera movement is realized in the **VVT_PTZSPEED.vi** module in Fig. 7a. Due to the use of the URL commands in the module it is required(in the process of the parameters read-out) to determine the IP of the camera server. Moreover, in the speed setting mode an information about the speed in time " before the made change" to minimize the number of commands needed for determination of only "new/changed' individual speed values, is needed.

Such recommendation are connected with the "long" time of the URL command realization by the camera sever and to elicit of multiple commands which could put the speed values in case where it does not undergoes a change.

The description of the input/output signals:

The configuration of the camera speed movement can work in desired parameter setting mode ("set") or in the acquisition of information about their actual condition ("get" – and IP address of the camera is required). The change in functionality is realized by the optional control no.3 defined as binary value - "true" where arrangement of parameters ("set") is consistent with " ptz control speed set" and "false" controls of the actual parameter reading state ("get") returned in "ptz control speed get" control. The content of the "ptz control speed set/get "control is described on Fig. 7b:
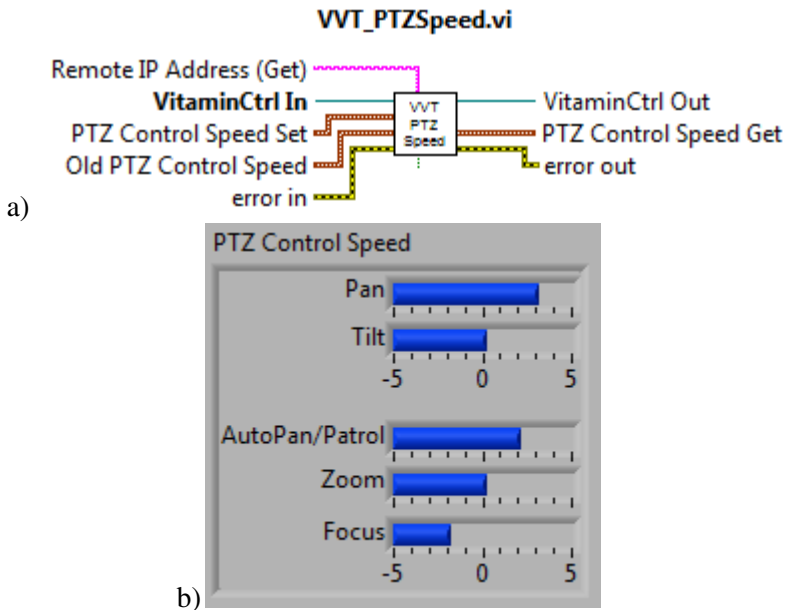
Fig. 7. The view on the speed control module and its input /output parameters

- The camera IP address control ("remote ip address") in optional input no.1 is a required parameter for realization of the task connected with the camera speed movement parameters; this value is defined as a chain of signs (text) of a structure commonly used in IP address definition: [A.B.C.D – where A, B, C parameters and D are the values of the 0 – 255 set, for e.g. 168.254.0.99]
- The "ptz control speed set/get" controls of the camera movement parameters:
  - o "pan" – defines the rotation speed value(the rotation increment size) horizontally [-5,-4,…,+5];
  - o "tilt" – defines the rotation speed value (the rotation increment size) vertically[-5,-4,…,+5];
  - o "autopan/patrol" – defines the rotation speed value (the rotation increment size) horizontally ("auto pan") or between the base points in "patrol" mode [-5,-4,…,+5];
  - o "zoom" – defines the "speed" value of the zooming in the image (the zooming in increment size) in the optical axis of the camera[-5,-4,…,+5];
  - o "focus" – defines the speed of image focus change (in manual mode) [-5,-4,…,+5].

2.6 *The Configuration of the Streaming Video Mode*

Most of the Vivotek cameras transmit a video signal streaming mode form, which is often used for transmitting film sequences player online on numerous websites

and applications such as QuickTime or RealPlayer. The camera under tests offered a support for streaming transmission in two formats: MPEG4 and MJPEG. A configuration of the above streaming formats is also possible. The functionality was realized in **VVT_VIDEOCONTROL_SET_GET.vi** module (Fig.8a). Due to the use of the URL commands in the module it is required to determine the IP address of the camera server and it is recommended to elicit a module in command of another 'internal" event (for e.g. record/reading parameter controls). This recommendation is related with the "long" time of the ULR command realization by the camera server.

a)   b)
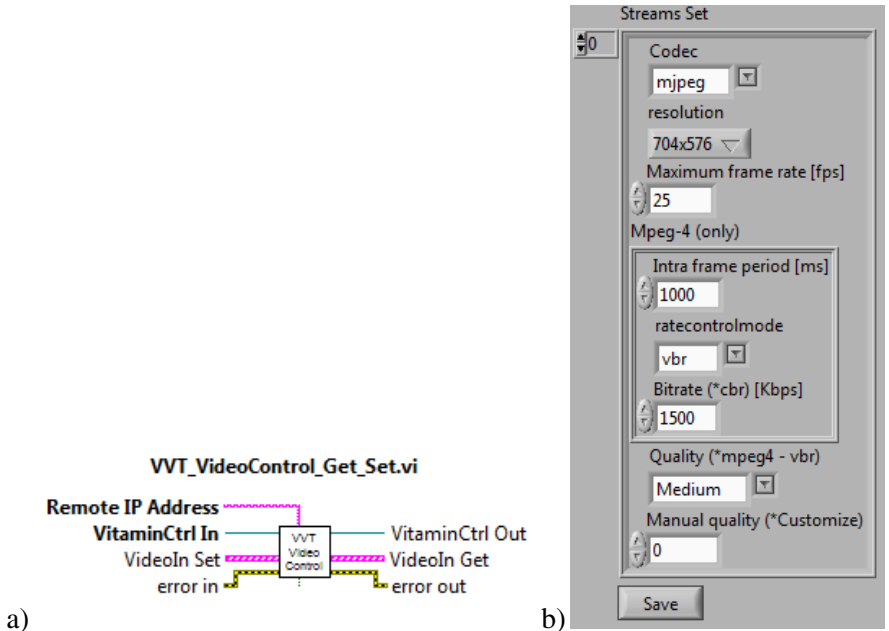
Fig. 8. The view on the video streaming configuration module and its input/output parameters

The description of the input/output signals:

The configuration of the video streaming transmission parameters can work in desired parameter setting mode ("set") or in the acquisition of information about their actual condition ("get"). The change in functionality is realized by the optional control no.3 defined as binary value - "true" where arrangement of parameters ("set") is consistent with " videoin set" and "false" controls of the actual parameter reading state ("get") returned in "videoin get" control. The content of the "videoin set/get" control is described on Fig. 8b:

- The camera IP address control ("remote ip address") in optional input no.1 is a required parameter for realization of the task connected with the camera speed movement parameters; this value is defined as a chain of signs (text) of a structure commonly used in IP address definition : [A.B.C.D – where A, B, C parameters and D are the values of the 0 – 255 set, for e.g. 168.254.0.99]
- The "videoin set/get" of streaming video transmission controls:
  - o "codec" –a type of streaming image transmission [mpeg4, mjpeg];
  - o "resolution" – the resolution of the registered image [704x576, 352x288, 176x144];
  - o "maximum frame rate" – a number of video frames sent by second(fps) [1,…,25];
  - o "intra frame period" – defines the time of "refreshing" individual video frames in milliseconds (only in the MPEG4 transmission type);
  - o "ratecontrolmode" – defines the type of the video stream flow [fixed value "cbr" or variable value "vbr"] (only in the MPEG4 transmission type);
  - o "bitrate" – th value of the intensity of the video stream in "cbr" module in kilobytes per second (only in the MPEG4 transmission type);
  - o "quality" – defines in "descriptive" way the average intensity rate of the video stream (the quality of the image) MJPEG and MPEG4 format of "vbr" type [Customize, Medium, Standard, Good, Detailed, Excellent];
  - o "manual quality" – defines the intensity of the stream (the quality of the image) in "quality" = "customize" mode [1,…,31].

2.7   The Audio-Stream Configuration Module

The camera under tests offers a support for two-way audio-stream transmission in two formats: AAC4 and GSM-AMR. There is also a possibility of configuration of the above streaming formats. The functionality was realized in module **VVT_AUDIOCONTROL_SET_GET.vi** (Fig.8a). Due to the use of the URL commands in the module it is required to determine the IP address of the camera server and it is recommended to elicit a module in command of another 'internal' event (for e.g. record/reading parameter controls). This recommendation is related with the "long" time of the ULR command realization by the camera server.

The description of the input/output signals:

The configuration of the audio transmission module parameters can work in desired parameter setting mode ("set") or in the acquisition of information about their actual condition ("get"). The change in functionality is realized by the

optional control no.3 defined as binary value - "true" where arrangement of parameters ("set") is consistent with " audioin set" and "false" controls of the actual parameter reading state ("get") returned in "audioin get" control. The content of the "audioin set/get " control is described on Fig. 9b:
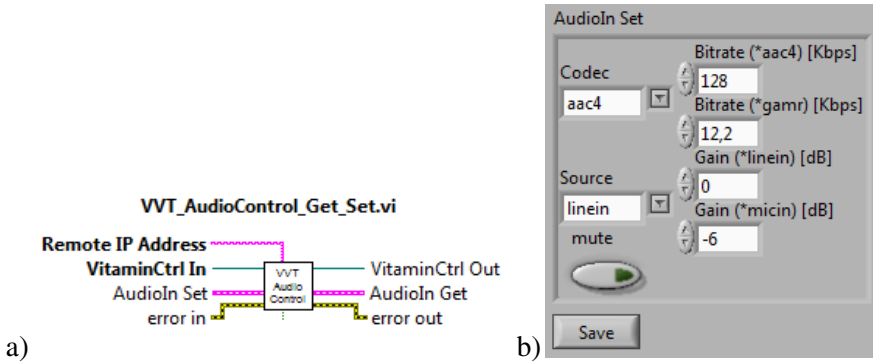
Fig. 9. The view on the audio-stream configuration control and its input/output parameters

- The camera IP address control ("remote ip address") in optional input no.1 is a required parameter for realization of the task connected with the camera speed movement parameters; this value is defined as a chain of signs (text) of a structure commonly used in IP address definition : [A.B.C.D – where A, B, C parameters and D are the values of the 0 – 255 set, for e.g. 168.254.0.99]
- The "audioin set/get" controls of audio transmission:
  - o "codec" –a kind of an audio-stream transmission [aac4, gsm-amr];
  - o "bitrate (aac4/gamr)" – The intensity of audio-stream in kilobytes per second respectively for audio formats   AACE/GSM-AMR [1,…,128/12,2];
  - o "source" – defines the source of the audio-stream (internal "linein" microphone, external microphone "micin");
  - o "gain (linein/micin)" – the value of sensitivity of the internal/external microphone defined in decibels [-33,…,+21];
  - o "mute" – switches on/off the audio-stream transmission.

2.8   *The Configuration of the Camera Functioning Module*

The camera under tests was an observation camera often used for objects or room monitoring. As a result, the manufacturers enable us to tailor the camera to different working conditions, in which the image acquisition takes place. The configurative abilities of the camera functioning functions was gathered in **VVT_CAMERACONTROL_GET_SET.vi** module (Fig. 10a). Due to the use of the URL commands in the module it is required to determine the IP address of

the camera server and it is recommended to elicit a module in command of another 'internal" event (for e.g. record/reading parameter controls). This recommendation is related with the "long" time of the ULR command realization by the camera server.
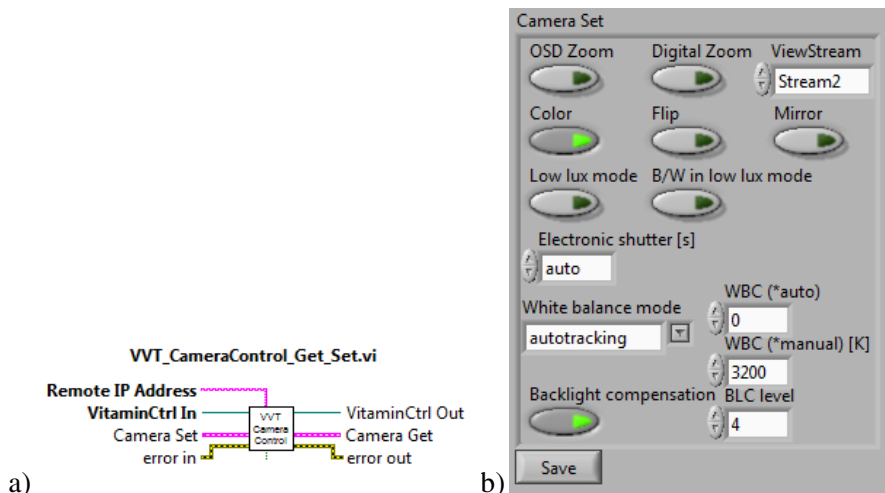
Fig. 10. The view on the configuration of camera functioning functions controls and its input/output parameters

The description of the input/output signals:

The configuration of the audio transmission module parameters can work in desired parameter setting mode ("set") or in the acquisition of information about their actual condition ("get"). The change in functionality is realized by the optional control no.3 defined as binary value - "true" where arrangement of parameters ("set") is consistent with " camera set" and "false" controls of the actual parameter reading state ("get") returned in "camera get" control. The content of the "camera set/get " control is described on Fig. 11b:

- The camera IP address control ("remote ip address") in optional input no.1 is a required parameter for realization of the task connected with the record/reading of the image stream transmission parameters; this value is defined as a chain of signs (text) of a structure commonly used in IP address definition : [A.B.C.D – where A, B, C parameters and D are the values of the 0 – 255 set, for e.g. 168.254.0.99]
- The "camera set/get" of audio transmission controls:
  - o "osd zoom" – switches on/off the OSD of actual image magnifying value (of both the optical and digital image);
  - o "digital zoom" – switches on/off the digital magnification

o "viewstream" – defines the video stream number passed from the camera to the client application image control (for cameras operating on few video streams at one time);

o "color" – switches on/off the option from colorful image to monochrome (when the "b/w ni low lux mode" is inactive);

o "flip" – switches on/off the option of reflexion of an image on its horizontal axis;

o "mirror" – switches on/off the option of reflexion of an image on its vertical axis;

o "low lux mode" – switches on/off the CCD matrix functioning in difficult lighting conditions (increases the sensor sensitiveness);

o "b/w in low lux mode" – switches on/off the automatic switch to monochrome function type of the image when the camera works in difficult lighting conditions. ("low lux mode");

o "electronic shutter" – defines the time(by seconds) of activation of one frame in the video sequence (the time of opening the aperture) [auto, 1/50, 1/100, 1/250, 1/500, 1/1000, 1/2000, 1/4000];

o "white balance mode" – defines the whiteness correlation balance of the acquired image [autotracking, manualcontrol];

o "wbc (auto/manual)" – defines, respectively, the whiteness balance in the automatic mode [0,…,8] and the light source temperature defined in Kelvins. [3200, 4000, 4800, 5600, 6400, 7200, 8000, 8800, 9600];

o "backlight compensation" – switches on/off the compensation options of bright light sources in the view field of the camera;

o "blc level" – defines the compensation level of the light sources in the view field of the camera [0,…,7].

2.9   The Movement Control Module of PTC Camera

The tested camera enables the rotation of the matrix CCD head around both axis and its "dislocation" in the optical axis of the image (magnification of the image). Moreover, as a camera designer for monitoring, it allowed functioning in "auto pan" mode (automatic scanning of the environment in the horizontal of the camera's rotation movement) and in the "patrol" mode (scanning the environment including the defined control points). Additionally it also enables the control over the zooming (magnification) degree, the image sharpness and aperture opening size. The functionality of the camera enabling the control of the "movement" of its individual element was included in VVT_PTZCONTROL.vi module, Fig. 10a.

   The description of the input/output signals:

   The module of controlling the camera movement works primarily in the input parameter definition module (commanding succeeding movement orders). The content of the "ptz camera control" is presented on fig. 11b:

VVT_PTZControl.vi

VitaminCtrl In ————————— VitaminCtrl Out
PTZ Camera Control ⊣
                          error out
error in

a)   b)
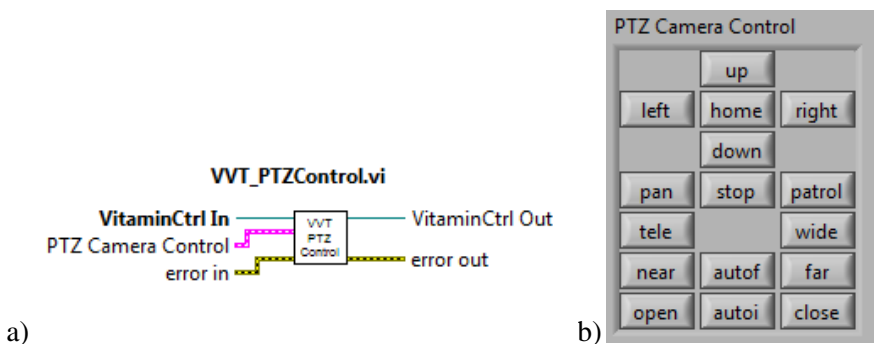
Fig. 11. The view on the control of the camera movement controls and its input/output parameters

- "ptz camera control" controls defining the possible for realization modes of automatic/manual movement:
  - "up, down, left, right" – movement orders (rotations) for the camera respectively up and down ("tilt") and right and left ("pan");
  - "home" – an order of return to basic position ("pan=0", "tilt=0", "zoom=1"),it is a position in which the camera is places itself after being plugged to power;
  - "pan, stop" – respectively starts or finishes the automatic Canning in the movement/rotation plane of the camera;
  - "patrol" – automatically starts the space scanning with the compliance of the defined characteristic points in the observed area;
  - "tele, wide" – respectively a zoom in and zoom out option ("zoom") of the analyzed image area;
  - "near, far" – commands responsible for a manual setup of the focus of registered image;
  - "autof" – switching off the automatic image sharpness adjustment ("auto focus");
  - "open, close" – commands responsible for manual opening/closure of the shutter;
  - "autoi" – switching off the automatic adjustment of the shutter opening ("auto iris").

2.10 The Module of the Digital Image Acquisition from the Video Stream

During the experiments on the modules enabling communication and configuration of the camera was created a module, which is necessary for the realization of the objective task which was made for those researches. It concerns the possibility of using the obtained video images for the synthesis and analysis of the processing and

recognition system of the digital images. The desired functionality of obtained library provides the **VVT_GETFRAME.vi** module (fig. 12). It allows, as a result of calls to the client's application, to obtain an image represented by the variable of Image type("IMAQ Image.ctl"). Such representation allows for a simple use of obtained image as a input parameter of processing methods and analysis of images available in the LabVIEW environment. Moreover, it enables a conversion for array representation (2-D array type) of the obtained digital image. Such representation enables the construction of own processing algorithms and analysis of objects being the research goal of constructed mechanic vision system.

VVT_GetFrame.vi

VitaminCtrl In —————— VVT Get Frame —————— VitaminCtrl Out
                                              Image Out
error in   error out
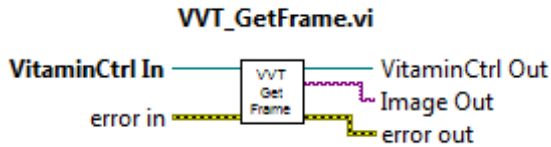
Fig. 12. The view on the registration and conversion of digital image module

The description of input/output signals:
The module of digital image frame acquisition from the video-stream practically works only in the module of the input parameter definition (a variable turning of Image type).

2.11 The Module of Obtaining the Information in the Patrol Point

Cameras equipped with a structure of moving PTZ head usually enable to identify the characteristic points defining the route of scanning the patrolled area, in the authentic work mode. For the purpose of defining the patrol points in the camera system, coordinates allowing, in synonymous way, reproduction of the patrol route, are recorded. The camera analysis, for which the presented module were constructed, has shown that among those information, data about the value of the increments of individual control devices that are responsible for reaching a require position, are contained. This approach was used for the construction of VVT_GETPOSITION.vi module (fig. 13). It allows the creation realization of

VVT_GetPosition.vi

Remote IP Address
VitaminCtrl In —————— VVT PTZ position —————— VitaminCtrl Out
bstrPosition   PTZ_poz [pan,tilt,zoom] #[3x1]
error in   String
                                            error out
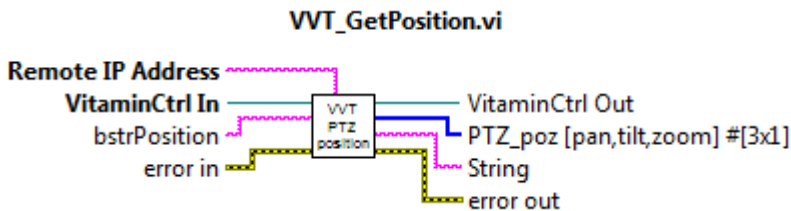
Fig. 13. The view of module control of obtaining information about the patrol point

patrol point in the actual camera position and then reading the information of the elements values responsible for the camera position. Information this is returned in two ways: in text form and in the vector form of the figure values. Alternatively an inertial measurement unit could be used [4].

The description of input/output signals:

The module of obtaining information about the patrol point of the camera works only in the module of reading/obtaining information about the increment for individual position of the PTZ head:

- The camera IP address control ("remote ip address") in optional input no.1 is a required parameter for realization of the task connected with the record/reading of the image stream transmission parameters; this value is defined as a chain of signs (text) of a structure commonly used in IP address definition : [A.B.C.D – where A, B, C parameters and D are the values of the 0 – 255 set, for e.g. 168.254.0.99]
- A control of the name of the patrol point ("bstrPosition") describes the label which the patrol point is going to be written under: the value of this control is defined as a chain of signs (text)unique in relation to other patrol points defined in the camera as the patrol rout out automatic work mode;
- The array/vector control ("ptz_poz") is a vector of Tyree numbers defining Reading of the increment values for given configuration of the variable Pan, Tilt and Zoom positions;
- Testing control ("string") contains information about the increments value returned in "ptz_poz" vector in text format (chain of signs);

3   Examples of Use of Control Modules

3.1   *Reconstruction of the Feedback Information on the Position of the Camera*

One of the most import ant information that are required in the process of control realization, especially camera control, is the knowledge about the current state (e.g. the position)of the controlled object. In case of presented modules and their use for controlling PTZ cameras, this information can be understood as value vector (signals) defining the camera head position in relation to its base. Presented on fig.1 sample cameras are the finished solutions, in which the information about the actual position of the camera' s head was not revealed. Those cameras, from the point of their usage in monitoring, so to say, work on open-track control. In reality, the control configurations which are the construction of those camera and which complete the controlling of the camera's movement, use the information about the actual location of particular rotation units (in case of a rotation around the Pan and Tilt axes) and the virtual image unit of the relocation of the realized by the optical change in the image zoom (zoom). Below, a an exemplary realization of a task of feedback information acquisition, this mean the rotate

angle Pan and Tilt values and the magnification factor Zoom, for the purpose of controlling the camera from the level of LabView application environment is presented.

The analysis of the given measures defining the position of the camera dependence was carried out on the Vivotek model of PT72x2 series. The measurement of dependences of the increments values of the characteristic points and the field of variability of Pan, Tilt and Zoom values was carried out. The range of the two first values responsible for the rotation of particular axis, is presented on fig.14.
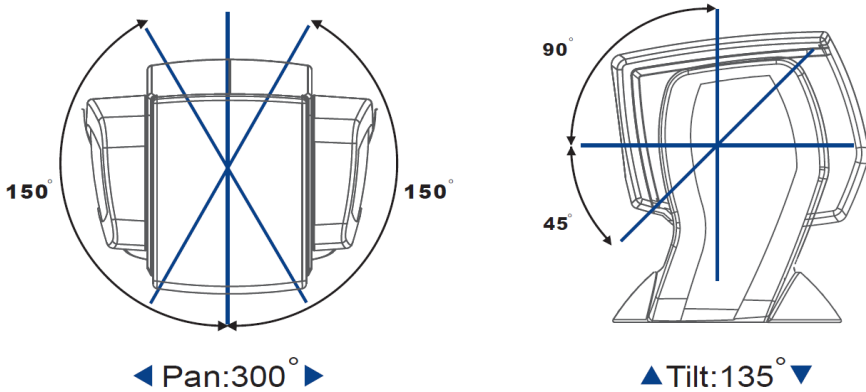
Fig. 14. The illustration of the range of the variability of the rotation angle for particular axes on the PZ72x2 camera model

The values of increments for the positions characteristic for particular variables defining the position/configuration of the camera are presented in the table 1.

Table 1. The range of the variability of the camera position configuration parameters and increment values corresponding with them

Parameter	Range of variability of parameters			Rage of variability of increments		
	min	ini	max	min	ini	Max
Pan	-150	0	150	-6790	0	6790
Tilt	-45	0	90	-786	0	1572
Zoom	1x	-	10x	4096	-	5211

The experimental analysis of repetition of achieving a given position in case of Pan and Tilt values has shown that it is consistent, repeatable and independent of the direction in which the change of a particular angle rotation value was made. At the same time, it appeared that the values responsible for the rotation speed defined by the use of the speed control mode of the **PTZ VVT_PTZSPEED.vi** camera, point 2.5, in reality defines the size of the growth in the value of the

particular angle changes. Moreover, particular "speed" values from the [-5, -4, …
,+5] range are the total multiplicity of the smallest "speed". This analysis allowed
to define the dependence between the increment value defining the rotation of a
given axis and the value of the particular angle expressed in degrees. Respectively,
in the analyzed camera model, for the Pan and Tilt parameters, the dependencies
are described with the formulas:

$$Pan = \frac{15}{679}x \tag{1}$$

$$Tile = \frac{15}{262}y \tag{2}$$

where x, y are respectively the increment values in the configuration connected
with the rotation of the camera head around the axes to Pan and Tilt.

In the case of the third parameter (Zoom) defining such a simple model was not
possible. During the analyzed experiments, the changes dependence of the optical
object magnification in the function of values of corresponding increments proved to
be ambiguous, dependent on the direction (the growth or reduction of the
magnification value factor) to which the Zoom parameter value was being changed.
The route of the characteristic determined by the Reading of the increment values
and the OSD module displaying the image about the magnification of the image
from the camera was show on a logarithmic scale on fig.15.
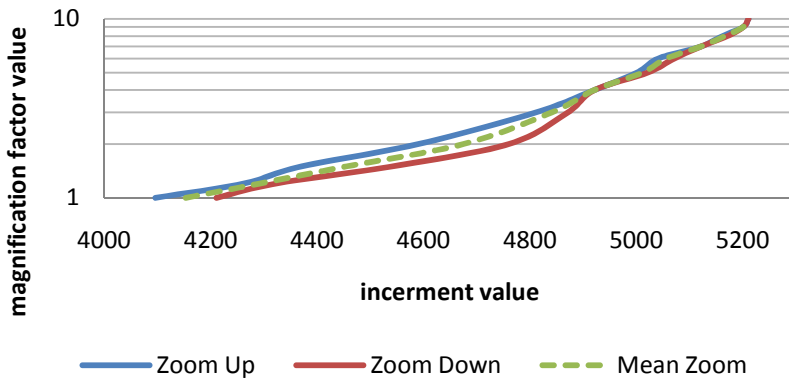
Fig. 15. The characteristic of the change dependencies of the magnification factor
depending on the increment values

The characteristic shown onfig.15 was defined on the semi-logarithmic plane.
For such representation, the averaged dependency (Mean Zoom) appears to be
approximately linear. This suggests a model class, among which one should
search for analytic dependencies defining the relationship between the Zoom value
and increment value. The first, tested class are the exponential form models:

$$zoom_{(a,b,c)} = a\,z^b + c \tag{3}$$

The second class, are the polynomial n models:

$$zoom_{(n)} = \sum_{i=0}^{n} a_i z^i = a_n z^n + a_{n-1}z^{n-1} + \cdots + a_1 z + a_0 \tag{4}$$

where z is the increment value in configuration of the camera connected with magnification of the image.

In the process of model parameter identification it was assumed :
- in the case of the first model the following range of acceptable variability of the parameters: $a, b, c \in [0,100]$;
- in case of the polynomial models only the functions of the row $n \in \{1,2,3,\dots,5\}$ were tested.

As the best (optimum) choice of individual model parameters were chosen those, which minimized the mean absolute error (MAE). Respectively, as a result of conducted identifications, the structure of the optimal model
- in the class of exponential models is described with the dependency:

$$zoom_{(a,b,c)} = 1.29281 \cdot 10^{-63} \cdot z^{17.1711} + 0.665295 \tag{5}$$

For the smallest value in this class MAE = 0.165195;
- in the class of exponential models for a polynomial degree $n = 3$:

$$zoom_{(n)} = 1.31792 \cdot 10^{-8} \cdot z^3 - 1.74023 \cdot 10^{-4} \cdot z^2 + 0.76697 \cdot z \\ - 1126.84 \tag{6}$$

For the smallest value in this class MAE = 0.126602.

The route of the dependencies of the Zoom values in the increment value function for particular models is presented on fig.16.
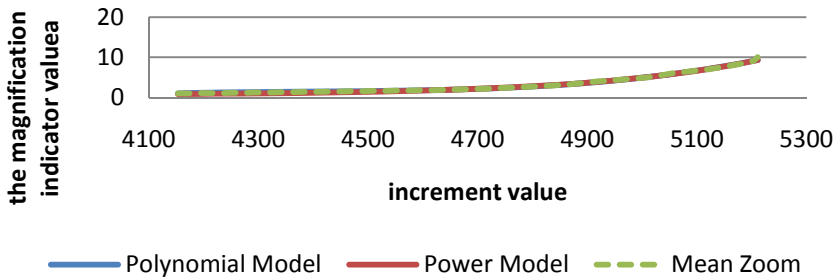
Fig. 16. The route of the Zoom dependencies from the increment value for particular linear models

The sample code realizing the reconstruction of the return signal on the camera's position, with the use of constructed module in G language of the LabView environment, was described on fig.17. The magnification value, returned by the camera system was shown on the fig.18a using, at the same time, the VVT_PTZSPEED.vi module together with the reconstruction parameters models of Pan, Tilt and Zoom location, obtained information about those values was shown on fig.18b.

The experience acquired during tests and experiments might be useful for improving the quality of operation and stabilization of opto-electronic gimbals for UAVs[8].
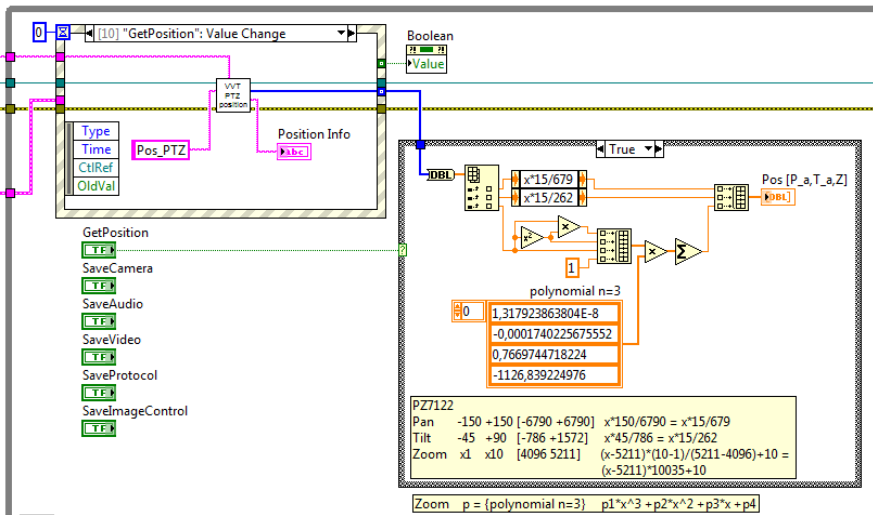
Fig. 17. A part of a program in G language realizing the obtaining information about the position of the PTZ camera head
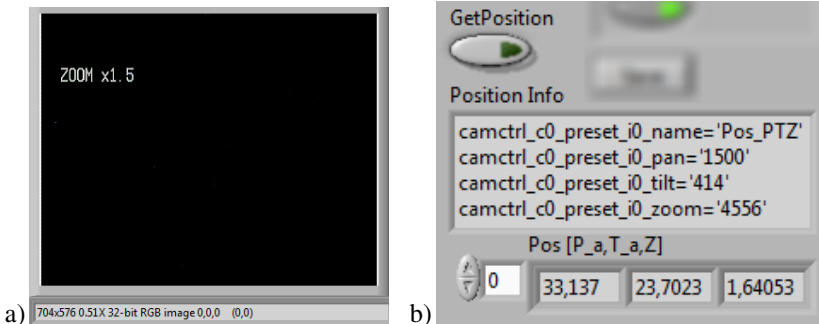
Fig. 18. The outcome of the reconstruction activity of the Pan, Tilt and Zoom algorithms; The outcome of the reconstruction algorithm. Information on the camera image a) information returned by the program b) computed.

References

[1]   Vivotek activex SDK VitaminControl v.4.0.0.3 (July 13, 2011),
      `http://www.vivotek.com`

[2]   Network Camera User's Manual PZ7111/PZ7112/PZ7121/PZ7122 (July 07, 2010),
      `http://www.vivotek.com`

[3]   Vivotek URL commands for 7000 series V2 v.1.1 (June 06, 2009),
       `http://www.vivotek.com`

[4]   Jaskot, K., Babiarz, A.: The inertial measurement unit for detection of position.
      Przegląd Elektrotechniczny 86, 323–333 (2010)

[5]   Babiarz, A., Jaskot, K., Koralewicz, P.: The control system for autonomous mobile
      platform. In: Nawrat, A., Simek, K., Świerniak, A. (eds.) Advanced Technologies
      for Intelligent Systems. SCI, vol. 440, pp. 15–28. Springer, Heidelberg (2013)

[6]   Babiarz, A., Jaskot, K.: The concept of collision-free path planning of UAV objects.
      In: Nawrat, A., Simek, K., Świerniak, A. (eds.) Advanced Technologies for
      Intelligent Systems. SCI, vol. 440, pp. 81–94. Springer, Heidelberg (2013)

[7]   Daniec, K., Jedrasiak, K., Koteras, R., Nawrat, A.: Embedded micro inertial
      navigation system. Applied Mechanics and Materials 249-250, 1234–1246 (2013)

[8]   Jędrasiak, K., Bereska, D., Nawrat, A.: The prototype of gyro-stabilized UAV
      gimbal for day-night surveillance. In: Nawrat, A., Simek, K., Świerniak, A. (eds.)
      Advanced Technologies for Intelligent Systems. SCI, vol. 440, pp. 107–115.
      Springer, Heidelberg (2013)

[9]   Iwaneczko, P., Jędrasiak, K., Daniec, K., Nawrat, A.: A prototype of unmanned
      aerial vehicle for image acquisition. In: Bolc, L., Tadeusiewicz, R., Chmielewski,
      L.J., Wojciechowski, K. (eds.) ICCVG 2012. LNCS, vol. 7594, pp. 87–94. Springer,
      Heidelberg (2012)

[10] Jędrasiak, K., Nawrat, A.: Image recognition technique for unmanned aerial
      vehicles. In: Bolc, L., Kulikowski, J.L., Wojciechowski, K. (eds.) ICCVG 2008.
      LNCS, vol. 5337, pp. 391–399. Springer, Heidelberg (2009)

Recognition and Location of Objects in the Visual Field of a UAV Vision System

Robert Bieda, Krzysztof Jaskot, Karol Jędrasiak, and Aleksander Nawrat

Abstract. The aim of this methodology is a creation of a tool which would be able to construct a system for obtaining information about objects in the environment of the vision system. This task is often defined as a sub-task in the primary problem of the automatic task completion by the independent UAV unit using visual information. These researches concerned the construction of the algorithm that would allow the location of objects in the image, identification of these objects by classifying them into appropriate (previously declared) class, and then sending information about the sought-after object / objects to the actuator control module.

1   Detection of Objects in the Image

The first step aimed at detecting the object(s) in the surrounding field of the camera view is carrying out the image segmentation. The video camera could be mounted under an UAV [12] and controlled by micro navigation system [10] via communication system with multiple mobile vehicles [11]. Operator using the UAV in order to acquire aerial images requires real time image processing. Therefore the main requirement for practical image processing algorithms is the time of execution [13]. Image segmentation allow to distinct the areas representing different elements of the analyzed scene. To achieve this purpose, there was used a simple operation involving the segmentation of individual pixels assigned to one of two predefined classes: the background or the object. The process of classification of individual points is made based on the brightness level of the individual points. The value of the brightness of a point is compared with the value of the

Robert Bieda · Krzysztof Jaskot · Karol Jędrasiak · Aleksander Nawrat
Silesian University of Technology, Institute of Automatic Control,
Akademicka 16, 44-101 Gliwice, Poland
e-mail: `{robert.bieda,karol.jedrasiak,krzysztof.jaskot,`
`anawrat}@polsl.pl`

cut-off. The value of the brightness of a measured point is compared with the value of the T cut-off.

All points with the level of brightness of less than the threshold value will be assigned to the class object {1} and all pixels with values greater than the cut-off shall be considered as the background in the picture {0}.

The classification is therefore reduced to a simple segmentation operation with a single cut-off threshold:

$$B(x,y) = \begin{cases} 1 \ for \ I(x,t) < T, \\ 0 \ for \ I(x,y) \geq T, \end{cases} \tag{1}$$

where: B – binary image after segmentation, I – input image undergoing segmentation.

The problem that had to be solved at this point was to propose a method of automatic selection of the threshold value segmentation. In the experiments several known techniques for automatic threshold selection, based on the analysis of the image's histogram undergoing segmentation, were analyzed.

The analysis included techniques based on clustering, the size of the entropy in the image, using moments and techniques based on the principle of maximizing the variance between classes. Among the tested techniques, in terms of derived image segmentation workspace, the technique applied by Otsu was proposed as the best.

This technique allows, in general, an assignation of numerous threshold cut-offs. The choice of these thresholds at the same time ensures the greatest possible "separation" in the set histogram image classes. This method is based on the analysis of the factor is interpreted as the between-class variance. In the described problem, two classes are defined, which leads the problem of assignation of thresholds separating classes that would lead to defining the worth of a single T threshold:

$$\sigma_B^2(T) = \frac{[\mu\omega(T) - \mu(T)]^2}{\omega(T)[1 - \omega(T)]}, \tag{2}$$

where:

$$\mu(T) = \sum_{i=0}^{T} ip(i), \quad \mu = \sum_{i=0}^{255} ip(i), \quad \omega(T) = \sum_{i=0}^{T} p(i). \tag{3}$$

Values such as $p(i), \mu, \mu(T), \omega(T)$, are respectively: the likelihood of existence of the same level-brightness image (normalized histogram value), average value of image brightness (average histogram value),the average T- value of first performances in the image brightness and the value of the normalized cumulative histogram of the image for the T level brightness.

Picture 1 shows an exemplary result of using operations of the analyzed image segmentation.
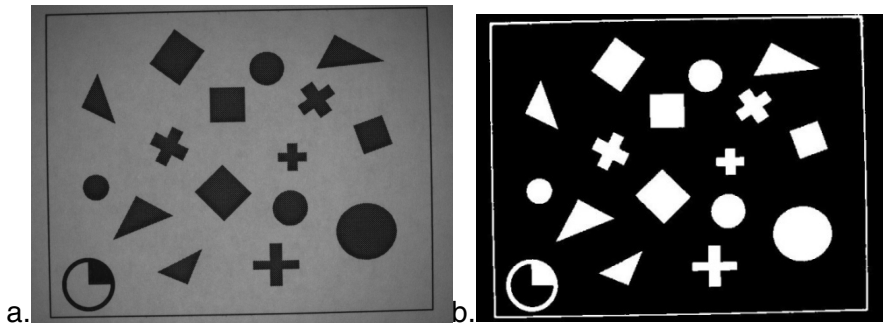
Fig. 1 The example segmentation: a. the image of the working scene of a manipulator, b. binary image

Such binary image is then subjected to a labeling process. This process allows to clearly define the belonging of individual points in the image to the appropriate areas, designated in the process of segmentation. A similar process could be applied to detection of objects in IR cameras [9].

2   Extraction of the Objects' Characteristics

You In order to clearly describe the designated areas-objects in the image the use of different techniques is applied to determine the characteristics of clearly describing the properties of objects. In the described solution the image undergoing the analyzis was binarized. Binary areas are often described using the so-called shape factors or description with the use of geometric moments.

Set of features describing objects in an image is often called a vector x of those features. In the analyzed case, for description of the separated areas-objects in the image, a 24-elements vector used. The basis of the features' vector construction was the analysis of the areas-objects binary with the usage of geometric moments.

Moment of geometric order/row $(p + q)$ of picture B is defined as follows:

$$m_{pq} = \int_{-\infty}^{\infty} \int_{-\infty}^{\infty} x^p y^q B(x,y) dx dy, \quad p,q = 0,1,2,\dots \tag{4}$$

The independence of the area- object characteristics   from translation (displacement In the picture) is defined by the definition of the central moments of geometric order $(p + q)$:

$$\mu_{pq} = \int_{-\infty}^{\infty} \int_{-\infty}^{\infty} (x - x_0)^p (y - y_0)^q B(x,y) dx dy, \quad p,q = 0,1,2,... \tag{5}$$

where, $x = \frac{m_{10}}{m_{00}}, y_0 = m_{01}/m_{00}$, are the coordinates of the geometric center of the analyzed area.

In addition, the invariance of the characteristics of the scale changes, have been implemented using standard geometric moments:

$$\eta_{pq} = \frac{\mu_{pq}}{\mu_{00}^{(p+q+2)/2}} \tag{6}$$

The complete independence of the position, scale and rotation is achieved by the use of for description the characteristics of geometric invariant Hu moments objects features:

$$h_1 = \eta_{20} + \eta_{02}; \tag{7.a}$$

$$h_2 = (\eta_{20} - \eta_{02})^2 + 4\eta_{11}^2; \tag{7.b}$$

$$h_3 = (\eta_{30} - 3\eta_{12})^2 + (3\eta_{21} - \eta_{03})^2; \tag{7.c}$$

$$h_4 = (\eta_{30} - \eta_{12})^2 + (\eta_{21} + \eta_{03})^2; \tag{7.d}$$

$$h_5 = (\eta_{30} - 3\eta_{12})(\eta_{30} + \eta_{12})[(\eta_{30} + \eta_{12})^2 - (\eta_{21} + \eta_{03})^2] + 3(\eta_{21} - \eta_{03})(\eta_{21} + \eta_{03})[3(\eta_{30} + \eta_{12})^2 - (\eta_{21} + \eta_{03})^2]; \tag{7.e}$$

$$h_6 = (\eta_{20} - \eta_{02})[(\eta_{30} + \eta_{12})^2 - (\eta_{21} + \eta_{03})^2] + 4\eta_{11}(\eta_{30} + \eta_{12})(\eta_{21} + \eta_{03}); \tag{7.f}$$

$$h_7 = (3\eta_{21} - \eta_{03})(\eta_{30} + \eta_{12})[(\eta_{30} + \eta_{12})^2 - 3(\eta_{21} + \eta_{03})^2] + (3\eta_{12} - \eta_{30})(\eta_{21} + \eta_{03})[3(\eta_{30} + \eta_{12})^2 - (\eta_{21} + \eta_{03})^2]; \tag{7.g}$$

Additional information which was helpful in the design of the vector characteristics was obtained using classical indicators describing the geometric relationships of the analyzed objects. Among the many existing indicators following shape aspect ratios were selected:

- hydraulic radius:

$$R_h = \frac{A}{P} \tag{8}$$

- the diameter of a circle with an area equivalent to the area under test:

$$D_A = 2\sqrt{\frac{A}{\pi}} \qquad (9)$$

- compactness factor:

$$Compactness = \frac{4\pi A}{P^2} \qquad (10)$$

where A, P respectively the surface area and the length of the circuit of the analyzed object;

- The ratio of the sides of the rectangle described on the object :

$$AspectRatio_{rectangle} = \frac{W_{MER}}{L_{MER}} \qquad (11)$$

where, $L_{MER} = \max_\alpha\{D(\alpha)\} = D$; $W_{MER} = D(\alpha_{max} \pm 90°)$ are respectively the length and width of the Minimum Enclosing Rectangle, and where $D(\alpha)$ is the projection of the analyzed object into the direction of α;

- circularity ratio:

$$Roundness = \frac{4A}{\pi D^2} \qquad (12)$$

where $D = \max\left\{\sqrt{(x_i - x_j)^2 + (y_i - y_j)^2}\right\}$ is the maximum length of the line

(the diameter of the circle described in the analyzed object);

- elongation factor:

$$Elongation = \frac{F}{W} \qquad (13)$$

where, $F = \frac{P - \sqrt{P^2 - 16\cdot A}}{4}$; $W = \frac{A}{F}$ are respectively the length and the width of the rectangle's surface and circumference equal to the surface and circumference of the object;

- ratio of the axis of the ellipse described on the object:

$$AspectRatio_{elipse} = \frac{\lambda_{min}}{\lambda_{max}} \qquad (14)$$

where, $\lambda_k = \frac{\mu_{20} + \mu_{02} \pm \sqrt{(\mu_{20} - \mu_{02})^2 + 4\mu_{11}^2}}{2}$ are the eigenvalue of the so-called geometric moments of inertia matrix;

- elongation „surface-moment" factor:

$$eccentricity = \frac{(\mu_{20} - \mu_{02})^2 + 4\mu_{11}^2}{(\mu_{20} + \mu_{02})^2} \tag{15}$$

Vector design features describing the objects is shown in the table 1.

Table 1. The vector design features

L.P.	The name of the feature	No.
1	The X coordinate of the geometric center of the area - x_0	-
2	The Y coordinate of the geometric center of the area - y_0	-
3	Hydraulic radius (ratio of surface area to the circuit area)	(8)
4	The diameter of the circle with an surface equivalent to the area	(9)
5	Axis of the ellipse corresponding to the ratio of the area	(14)
6	The ratio of the dimensions of the rectangle corresponding to the area	(11)
7	Elongation factor	(13)
8	The compactness factor	(10)
9	Roundness factor	(12)
10	„Surface-moment" factor	(15)
11	Normalized moment of geometric order $2 \cdot XX \cdot \eta_{20}$	(6)
12	Normalized moment of geometric order $2 \cdot XY \cdot \eta_{11}$	(6)
13	Normalized moment of geometric order $2 \cdot YY \cdot \eta_{02}$	(6)
14	Normalized moment of geometric order $3 \cdot XXX \cdot \eta_{30}$	(6)
15	Normalized moment of geometric order $3 \cdot XXY \cdot \eta_{21}$	(6)
16	Normalized moment of geometric order $3 \cdot XYY \cdot \eta_{12}$	(6)
17	Normalized moment of geometric order $3 \cdot YYY \cdot \eta_{03}$	(6)
18	Torque invariant Hu 1	(7.a)
19	Torque invariant Hu 2	(7.b)
20	Torque invariant Hu 3	(7.c)
21	Torque invariant Hu 4	(7.d)
22	Torque invariant Hu 5	(7.e)
23	Torque invariant Hu 6	(7.f)
24	Torque invariant Hu 7	(7.g)

The first two features of the x vector do not carry a strict information about the properties of the object, but only information about the location of the object in the image. These figures were, however, included in the feature vector due to the overriding task that they have been confronted with the vision system, a task associated with the detection of the object and its location in the surroundings of the UAV unit.

In the process of describing and object recognition using feature X vector only 22 elements were actually used.

3   The Algorithm of the Objects Classification

For the purpose of the realization of the recognition of the objects, a perceptron algorithm, a simple algorithm of a linear classifier was used. This method allows for the solution of the hyperplane designation problem that exists in the l – dimensional features' space of the objects dividing the given space into two dimensions. The determined hyperplane, at the same time, divides features vectors belonging to two different objects classes. In the perceptron algorithm it is assumed that two classes ω_1 and ω_2 linearly separated exist. Therefore it is possible to determine such a hyperplane $w^T x = 0$ where:

$$\mathbf{w}^{*T}\mathbf{x} > 0 \quad \forall \mathbf{x} \in \omega_1 \tag{16.1}$$

$$\mathbf{w}^{*T}\mathbf{x} < 0 \quad \forall \mathbf{x} \in \omega_2 \tag{16.2}$$

The case described by the definition is the one where the hyperplane passes by the beginning of the coordinates system connected with the space features. In more general case the hyperplane equation is $w^{*T}x + w_0^* = 0$. Taking into account how to write the equation for the definition (16) the features space should be extended with an extra dimension. As a result, in $(l + 1)$ - of the dimensional space the features vector is defined as follows: $x' \equiv [x^T, 1]^T$, where the vector of the hyperplane coefficients: $w' \equiv [w^T, w_0]^T$. Then $w^T x + w_0 = w'^T x'$. The problem of discovering the coefficients vector w described in the hyperplane is brought down to the classical optimization problem. In the perceptrone algorithm a following cost function is minimized:

$$J(w) = \sum_{x \in Y} (\delta_x w^T x), \tag{17}$$

where Y is a subset of the training feature vectors of the two classes ω_i, that were incorrectly classified by the weight vector w. Parameter δ_x takes the value -1if $x \in \omega_1$ and $\delta_x = 1$ where $x \in \omega_2$. With the above assumptions and definitions it can be easily shown that the rate of (17) shall always take the positive or zero values when the set Y is empty (all training vectors are correctly classified).

   It can be shown that this optimization problem is resolvable using the following iterative rule:

$$w(t + 1) = w(t) - \rho_t \sum_{x \in Y} \delta_x x \tag{18}$$

with a proper selection of the parameter values ρ_t the training algorithm (18) converges the minimizing quality index solution (17).

The classifier based on the perceptron algorithm is often described as a simple neural network consisting of a single neuron of l-inputs and one output. The perceptron model was shown on the picture no. 2
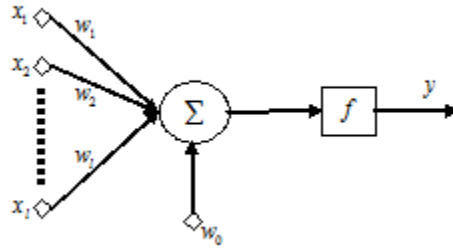
Fig. 2 The perceptron model as a linear classifier

The f function, which is usually called the activating function, can take on many form. The easiest and the most common form of the activating function is signum function:

$$f(z) = sign(z) = \begin{cases} +1 \; when \; z > 0 \\ 0 \; when \; z = 0 \; , \\ -1 \; when \; z < 0. \end{cases} \qquad (19)$$

In the literature devoted to classifiers it is possible to run cross different algorithms which enable to learn the w weight values which describe the hiperplane separated into two classes of objects in the features vectors dimension.

3.1 Rosenblatt Algorithm

The most famous algorithm is the one suggested by the inventor of the perceptron conception at the end of the 50s of the past century. This algorithm is iterative and it allows to find a solution of the indicator minimization problem (17), assuming the linear separability of the classes ω_1 and ω_2. The idea of this algorithm can be represented in the form of the following dependence:

$$w(t + 1) = w(t) + \rho x_{(t)} \; when \; x_{(t)} \in \omega_1 \; and \; w^T(t)x_{(t)} \leq 0 \qquad (20.1)$$

$$w(t + 1) = w(t) - \rho x_{(t)} \; when \; x_{(t)} \in \omega_2 \; and \; w^T(t)x_{(t)} \geq 0 \qquad (20.2)$$

$$w(t + 1) = w(t) \; otherwise \qquad (20.3)$$

Features $x_{(t)}$ vector is a vector which , in the iteration t constantly belongs to the learning set Y. The calculations are terminated when a subset of the learning feature vector is empty, which is equivalent to the classification of all learning vectors to the correct class which they belong to.

3.2   The MSE Algorithm

The idea, that is used in this algorithm, relies on estimating the parameters of the w weight vector, which could minimize the mean square error, MSE between the known perceptron output value, for the training set Y, and the value obtained from the hyperplane described in weight W vector equation. Therefore, this problem can be written as follows:

$$\hat{w} = \min_{w} J^*(w) \qquad (21)$$

For the following quality indicator:

$$J^*(w) = E[|y - w^T x|^2] \qquad (22)$$

It can be also show that, the following weight vector is the solution of the above problem:

$$\hat{w} = R_x^{-1} Y_x \qquad (23)$$

where the matrix:

$$\mathbf{R_x} = E\left[\mathbf{xx}^T \right] = \begin{bmatrix} E[x_1 x_1] & \cdots & E[x_1 x_l] \\ E[x_2 x_1] & \cdots & E[x_2 x_l] \\ \vdots & \vdots & \vdots \\ E[x_l x_1] & \cdots & E[x_l x_l] \end{bmatrix} \qquad (24)$$

Is also called a correlation matrix and in many cases it is also equal to the covariance matrix. The vector

$$\mathbf{Y_x} = E[\mathbf{xy}] = \begin{bmatrix} E[x_1 y] \\ E[x_2 y] \\ \vdots \\ E[x_l y] \end{bmatrix} \qquad (25)$$

Is a cross-correlation vector between the expected output and the ((entrance)of the learning feature vectors.

4   Classification of Objects in the Multiclass Case

The above methods describe the case of appointing the hyperplane in the problem of the dimension separation of features of two class objects. In the described approach, the number of objects in the works pace May, in general, be greater. This raises the question how to take advantage of those algorithms in the multiclass

case, where it is possible to distinguish M- different objects classes. The easiest solution is the M- hyperplane construction in the values dimension, where each of them separates one $(M - 1)$ class from the others. The multiclass problem is actually the problem of resolving the one dimensional problems of M. In that case the weight w_i vector for $i = 1 ..., M$ allows to determine the attachment of the value vector to the class ω_i. The classification problem of the M- class process can be defined as follows:

$$w_i^T x > 0 \; and \; w_j^T x < 0, \qquad \forall x \in \omega_i, \; \forall i \neq j \; (i, j = 1, ..., M) \qquad (26)$$

The idea of the construction of such a M -class perceptron is shown on the picture 3.
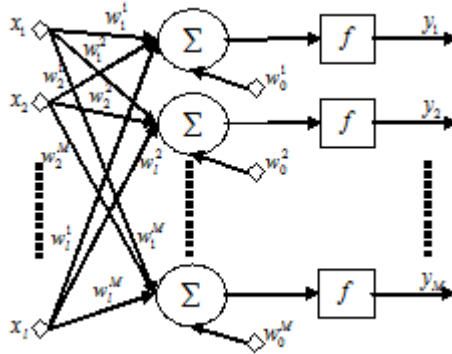
Fig. 3. Perceptron construction for a multiclass problem

4.1   The Kesler Algorithm

In this algorithm, a methodology that is used is the developed idea of the perceptron as a linear classifier from the dual-class to multiclass problem. As before, the linear discrimination function with ω_i weights, $i = 1, ..., M$ is defined for every class of the ω_i objects. The vector of x features described in the object is being assigned to the class ω_i if:

$$w_i^T x > w_j^T x, \forall j \neq i \qquad (27)$$

For all the training vectors of all ω_i classes, $i = 1, ..., M$ are constructed $(M - 1)$ vectors $x_{ij} = [0^T, 0^T, ..., x^T, ..., -x^T, ..., 0^T]^T$ of a dimension $(l + 1)M \times 1$. This gives us a vector block with zero everywhere except for positions i and j in the block, for which we have, respectively, x vector and $-x$ (for $j \neq i$). There is also constructed a block weight vector $w = [w_1^T, ..., w_M^T]^T$. If $x \in \omega_i$ then a natural consequence is that $w^T x_{ij} > 0, \forall j = 1, ..., M \; and \; j \neq i$. This is how the linear

classifier in the extended $(l+1)M$-dimensional features space is constructed, where for each of $(M-1)N$ of training vectors is placed on the "positive" side of the hyperplane. This is the algorithm that is named the Kesler construction.

5   Experimental Researches

In the tests related to the classification that were carried out, four groups of objects forming for classes consisting of $n_i = 15, i = 1, \ldots 4$ training vectors in each of ω_i class. Picture 4 shows the analyzed pictorial scenes containing objects, , on the basis of which a training set Y of $N = 60$ abundance was created.
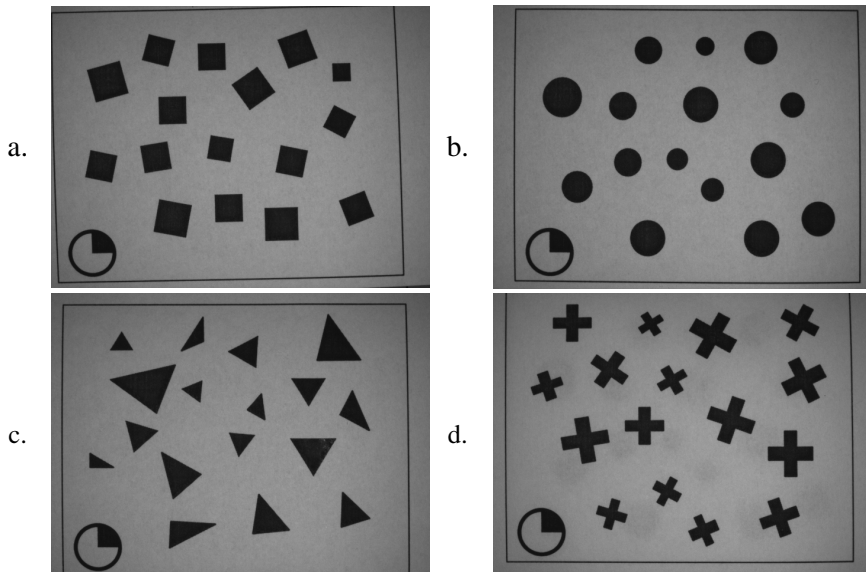
Fig. 4. Pictures containing the objects creating the training set of the classified: a. class ω_1-squares, b. class ω_2-circles, c. class ω_3 triangles, d. ω_4-crosses

   Multiple tests carried out on the training set constructed in such a way, did not resulted in a fully satisfactory outcome. In the iterative Rosenblatt algorithms for the problem of the $M = 4$ independent perceptrons and for the Kesler construction a correct solution was not obtained. Regardless of the choice of the starting point $(w(0))$ and the value of the training factor $,\rho$ the algorithms did not find the hyperplane (-y), for which all of the training actors of the Y set were correctly classified. This problem is probably the outcome of the assumptions failure, which were required in the construction of the perceptron, and which relate to the linear separation of the classes in the features dimension. Further investigation into the authenticity of such an assumption is pretty difficult due to the large dimension of the features' space (l = 22).

In the case of the MSE algorithm, the solution to the problem of finding then M vectors od the weight vectors described in M perceptrons is always possible if only the correlation matrix R_x is reversible. In the case of the MSE algorithm, the linear separation assumption is not essentials in individual classes $\omega_i, i = 1, ... M$ the features' dimension. However, if the given assumption is not fulfilled there is no guarantee that the obtained $\hat{w}$ vector will make it possible to correctly classify all the training vectors. What follows is that the value of the vector (4) will always be more than zero. Sample results of the classification of the objects based on the multiclass perceptron are shown on picture 5.

(ω_1 -red, ω_2 -green, ω_3 -blue, ω_4 -baby blue)
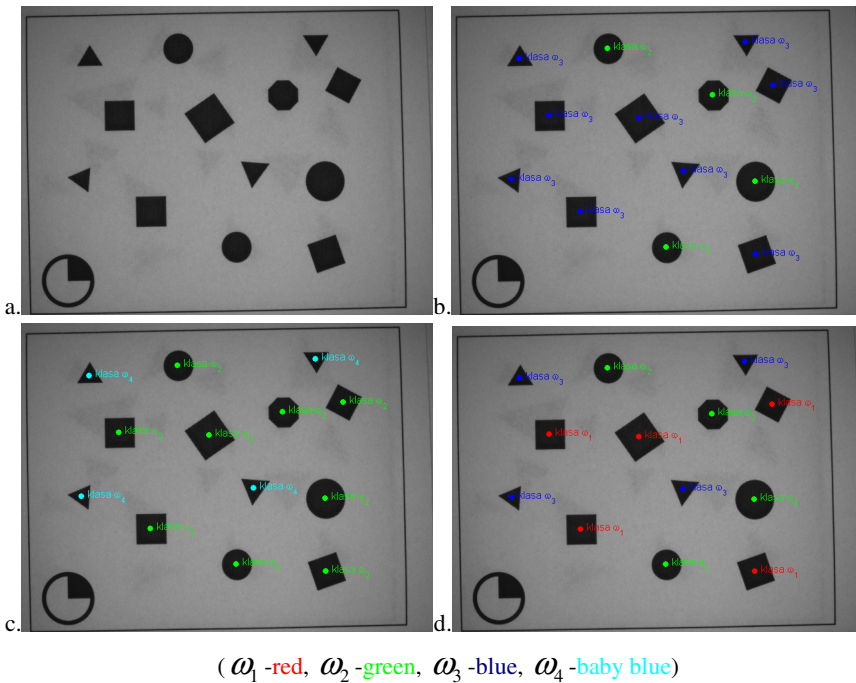
Fig. 5. The result of the object classification with the usage of the perceptron : a. analyzed picture, b. the result for the perceptron trained on the Rosenblatt algorithm, c. the result for the perceptron trained on the Kesler algorithm, d. the result for the perceptron trained on the MSE algorithm.

6   Reduction of the Features Dimension

One of the stages of designing a classifier is often the extraction or feature selection. This process is designed to minimize the number of features in the vector that is described in the object. Very often, the information contained in the selected l is in excess, and the values ,that describe different object values, are strongly

correlated. In consequence, the description is redundant, and repeatedly the large dimension of features makes the analysis more difficult. One of the stages of designing the classified is the extraction stage or features selection. This process is used to minimize the number of features in the vector that is described in the given object. Many times the information contained in the selected l is in excess, and the values describing different objects are greatly corralled with each other. In consequence, the description is redundant and a big features' dimension makes the analysis more difficult.

In the experiment that was carried out, some algorithms enabling to determine the transition to the other m-dimensional space were analyzed, in the space, which features describing will not be redundant and at the same time, where there space of this ($m \leq l$) dimension can be reduced.

In general, the transformation of the state vector x from the space l-dimensional to space m-dimensional can be described as

$$y = A^T x, \tag{28}$$

where A is the matrix of a $l \times m$ dimension.

6.1 The FLD Algorithm

One of the methods allowing to distinguish the matrix of A^T transformation is the method that is based on the analysis of so-called scatter matrices. The genesis of this method taken from the description of the construction of the Fisher's linear discriminant also known as the FLD. The size of the constructed index of discrimination enables to describe both the degree of the separation of given ω_i classes and the degree of scattering vectors from each class.

In order to determine the transformation matrix it is necessary to define and determine the few values describing the classes in our features' dimension.

The scattering matrix of the intra-class

$$S_{w = \sum_{i=1}^{M} P_i S_i}, \tag{29}$$

where S_i is the covariance matrix of class ω_i elements:

$$S_i = E[(x - \mu_i)(x - \mu_i)^T] \tag{30}$$

P_i is the given a'priori probability of the appearance of the i-th class. Such greatness is of the appointed as a ratio of the abundance of the i-th class to the abundance of all the elements in M analyzed classes

$$P_i = \frac{n_i}{N} \tag{31}$$

Vector μ_i is the mean vector of the elements composing a given ω_i class. The $trac\{S_w\}$ value is the average to all classes of features variation.

The scattering matrix of inter-class

$$S_b = \sum_{i=1}^{M} P_i(\mu_i - \mu_0)(\mu_i - \mu_0)^T, \tag{32}$$

where μ_0 is the global mean vector

$$\mu_0 = \sum_{i=1}^{M} P_i \mu_i \tag{33}$$

The greatness of $trace\{S_b\}$ defines the average distance between given mean vectors of given ω_i classes.

This is the form of the mixture of the matrix dispersal/scattered matrix:

$$S_m = E[(x - \mu_0)(x - \mu_0)^T] \tag{34}$$

Such matrix is known as the covariance matrix of the feature vectors in relation to the global mean vector of all the analyzed classes. It can be easily shown that this matrix can be determined using the (29) and (32) values in their form:

$$S_m = S_w + S_b \tag{35}$$

The Fisher ratio describing the separation degree of the classes In the feature dimension is often defined in the following way:

$$J_F = trace\{S_w^{-1} S_m\} \tag{36}$$

The construction of the transformation matrix is based on the problem of maximizing the ratio (36). The problem of maximizing J_F is a classical problem of appointing the individual value and the value of individual $S_w^{-1} S_m$ matrices corresponding with them

$$(S_w^{-1} S_m)V = VD \tag{37}$$

where matrix D is a diagonal matrix of which the elements on the diagonal are the individual values of $S_w^{-1} S_m$ matrix:

$$\mathbf{D} = \begin{bmatrix} \lambda_1 & 0 & \cdots & 0 \\ 0 & \lambda_2 & \cdots & 0 \\ \vdots & \vdots & \vdots & \vdots \\ 0 & 0 & \cdots & \lambda_q \end{bmatrix} \tag{38}$$

Whereas the V matrix is the column matrix with the $l \times l$ dimension, that is corresponding to its individual λ_i values of specific vectors v_i, $V = [v_1 \quad v_2 \quad \dots \quad v_l]$.

6.2   The PCA Algorithm

The second, frequently used technique of determining the reducing redundancy transformation and „increasing" separability between the classes is the principal component analysis PCA. This technique is also often named a KL (Karhunen-Loève) transformation The task of appointing the transformation matrix A^T (28), as before, is All about determining the eigenvalues of the matrix D (38) and its corresponding column matrix V (39) of individual vectors. The analysis is made on the basis of the covariance matrix R_x (24) (or S_m (34) and (35)):

$$R_x V = S_m V = VD \tag{39}$$

The individual values λ_i are often interpreter as cumulative energy content, thanks to which we can determine the amount of information carried by the individual components of the feature vectors after the transformation with the usage of the matrix V^T. The percentage amount of the carried information can be determined using he following formula:

$$E_v = \frac{\sum_{i=1}^{m} \lambda_{(i)}}{\sum_{j=1}^{l} \lambda_{(j)}} 100\% \tag{40}$$

where $\lambda_{(i)}$ is i-th quantity of the individual value.

The amount of the information In the feature vector after transformation with the usage of matrix V^T is the same as the amount of information in the given vector before its transformation. However, while determining the transformation matrix A^T based on the matrix of the individual vectors V only m-vectors, to which the m-biggest eigenvalues correspond to, are taken into the account. Assuming the accuracy of the mapping information E_v, carried with the feature vector of the transformation matrix A^T can be constructed using the m-first individual vectors grouped according to the corresponding individual values $\lambda_{(i)}$, $\lambda_{(1)} \geq \lambda_{(2)} \geq \dots \geq \lambda_{(m)}$, $for\ m \leq l$,

$$A^T = V_m^T = \begin{bmatrix} V_{(1)} & V_{(2)} & \dots & V_{(m)} \end{bmatrix}^T \tag{41}$$

In the described experiment the previously presented methods of the transformation matrix construction were analyzed with the aim of construction the object classifier defined In four classes. The accuracy of mapping the information E_v by the feature vectors y obtained after the transformation of the primary vectors x, is
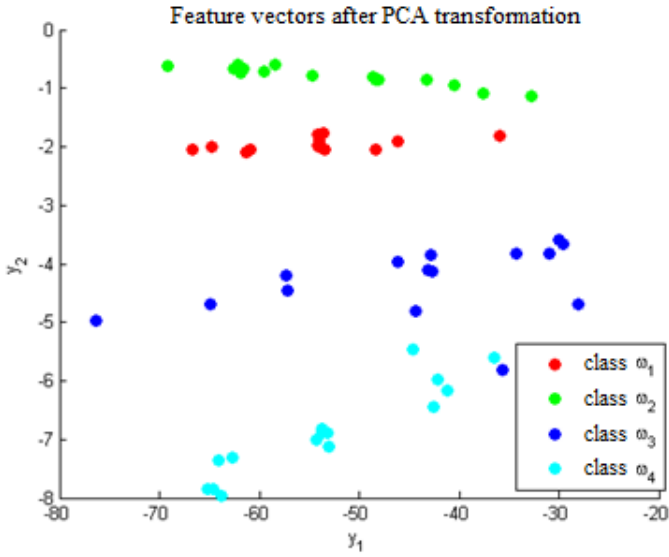
a.
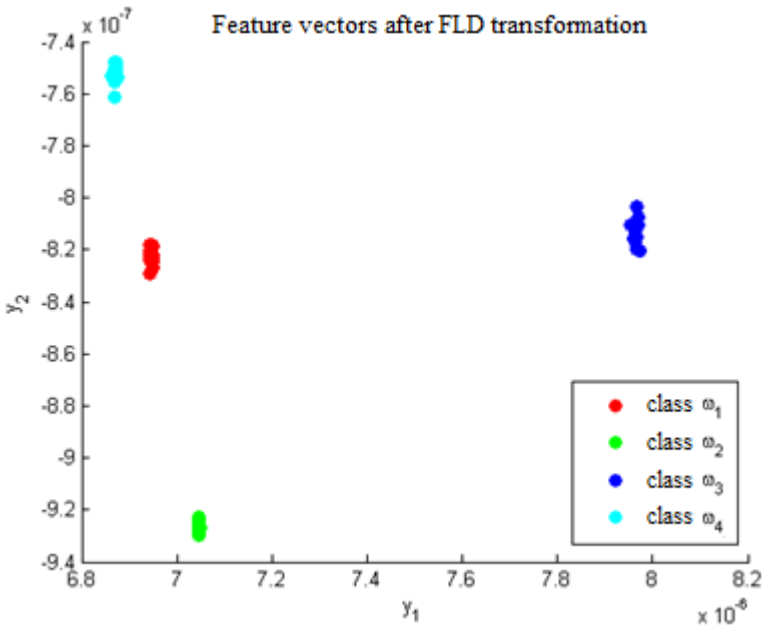
b.

Fig. 6. The visualization of the training set after the transformation: a. PCA b. FDL with the 98% mapping information

set to 98%. As a result, the analysis using the algorithms FLD and PCA the feature dimension space is reduced from $l = 22$ to $m = 2$. This suggests, that the values (features forming the feature vector x) describing objects in particular classes ω_i were strongly correlated. As a result, the representation of classes ω_i using the feature vector $y = [y_1\ y_2]^T$ was shown graphically on picture 6. The dimension of the vectors representing, in the transformation (7), where the transformation matrix A^T is described by the following relation (42) (for $m = 2$).

From the picture 6 analysis it is visible that a better representation, In terms of classifier construction, can be achieved by using the FLD algorithm. The classes of the training set objects are more concentrated around the average values than it is in the case of the PCA algorithm. This is also confirmed by the numerical analysis of the result of the transformation. To estimate this, both the degree of separation (the distance between the mean vectors) of classes ω_i and the degree of aggregation of individual vectors in the given object classes were used.

The value of the J_{F2} indicator is the greater when the concentration of individual vectors around the middle class ω_i vector is greater (small value of $trace\{S_w\}$), and the greater is the distance between the middle vectors of particular object classes (great value of $trace\{S_b\}$). In the analyzed case the indicator J_{F2} value confirms the observations from the analysis of the Fig 6. The value of the class indicator after the PCA transformation equals to $J_{F2}^{PCA} = 25.7$, whereas to each class of a training set after the transformation with FLD equals to $J_{F2}^{FLD} = 20260$. However, despite such impressive outcome it is easily noticeable (pic.6b) that in the dimension of the feature vector y it is not possible to mark the hyperplane (for $m = 2$ straight line), which would clearly divide the class ω_i from other classes. Therefore, the Assumption that the feature vectors x describing the four object classes in the space $l = 22$-dimensional are linearly inseparable. This fact   explains the impossibility of Winding the hypeplane using the described perceptron algorithm as a linear classifier.

7   The Minimum-Distance Classifier

As a result, to every class of the training set after the transformation with the FDL algorithm, a Simple minimum-distance classifier can be used. In this study the classification process is all about the finding the class ω_i, to which a given vector of y feature (according to the similarity function $g(y)$) is the most similar. The g function, describing the 'similarity' of the feature vector to one class, for each separate class, was defined as follows:

$$g_i(y) = \exp\left(-\frac{1}{2}(y - \mu_i)S_i^{-1}(y - \mu_i)^T\right) \tag{42}$$

where S_i and μ_i are respectively the covariance matrix and the mean class vector ω_i, $i = 1, ..., M = 4$, designated for vectors forming a class after the FLD transformation. The process of the classification with the use of function (44) processes as follows : Feature vector y belongs to class ω_i when:

$$g_i(y) = \max\{g_1(y), g_2(y), ..., g_M(y)\}, when \; y \in \omega_i \tag{43}$$

In case, where the zoom ratio E_v will be set on a bit lover level (for e.g. 96%) then the dimension of feature vectors x after FLD transformation will reduce itself to the one-dimension space ($m = 1$). The arrangement of the classes can be described as an outcome of projection of the $y_1 y_2$ plane on picture 6b on y_1 axis. In this case, the classification process can be carried out on the basis of the minimizing the differences between the feature y_1 and the mean value of this feature for the particular $\omega_i$classes:

$$j = \min_{i=1,..M} \{|y_1 - \mu_1|\} \; when \; y_1 \in \omega_j \tag{44}$$

The outcome of the activity of the classifier which bases on the above example is show on Fig 7.
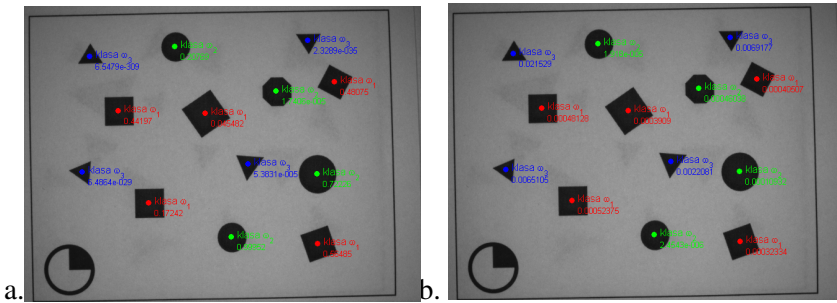
Fig. 7. The outcome of the classification in the dimension of the features after the FLD transformation : a. case 2D b. case 1D

   As it can be noticed in Fig 7 in both cases the outcome of the classification is correct. This gives hope for the construction of a autonomic visual system. Such system, 'pre-learned" is able to independently analyze the image of the surroundings of the manipulator and send him the data needed to completion of the overriding task.

8   Summary

The results obtained show that the construction of the co-operating classifier and the visual system is possible. The obtained results are promising and appear to

augur well for the further work on this issue. Additionally, in the above, shortened description of the issue, it was shown which problems must be solved to construct such a classifier.

References

[1] Obinata, G., Dutta, A.: Vision-Systems Segmentation and Pattern Recognition. I_Tech Education and Publishing (2007)

[2] Russ, J.C.: The Image Processing Handbook, 5th edn. CRC Pressm, Taylor and Francis Group (2007)

[3] Webb, A.R.: Statistical Pattern Recognition, 2nd edn. Wiley (2002)

[4] Theodoridis, S., Koutroumbas, K.: Pattern Recognition, 4th edn. Academic Press (2009)

[5] Gonzalez, R.C., Wood, R.E.: Digital Image Processing, 3rd edn. Prentice Hall (2008)

[6] Tadeusiewicz, R., Korohoda, P.: Komputerowa analiza i przetwarzanie obrazów. Fundacja Postępu Telekomunikacji (1997)

[7] Nixon, M.S., Aguado, A.S.: Feature Extraction & Image Processing, 2nd edn. Academic Press (2008)

[8] Bishop, C.M.: Pattern Recognition and Machine Learning. Springer (2006)

[9] Nawrat, A., Daniec, K., Warmuz, T.: Object detection using IR camera. In: Nawrat, A., Simek, K., Świerniak, A. (eds.) Advanced Technologies for Intelligent Systems. SCI, vol. 440, pp. 129–142. Springer, Heidelberg (2013)

[10] Daniec, K., Jedrasiak, K., Koteras, R., Nawrat, A.: Embedded micro inertial navigation system. Applied Mechanics and Materials 249-250, 1234–1246 (2013)

[11] Jędrasiak, K., Nawrat, A., Wydmańska, K.: SETh-link the distributed management system for unmanned mobile vehicles. In: Nawrat, A., Simek, K., Świerniak, A. (eds.) Advanced Technologies for Intelligent Systems. SCI, vol. 440, pp. 247–256. Springer, Heidelberg (2013)

[12] Iwaneczko, P., Jędrasiak, K., Daniec, K., Nawrat, A.: A prototype of unmanned aerial vehicle for image acquisition. In: Bolc, L., Tadeusiewicz, R., Chmielewski, L.J., Wojciechowski, K. (eds.) ICCVG 2012. LNCS, vol. 7594, pp. 87–94. Springer, Heidelberg (2012)

[13] Jędrasiak, K., Nawrat, A.: Image recognition technique for unmanned aerial vehicles. In: Bolc, L., Kulikowski, J.L., Wojciechowski, K. (eds.) ICCVG 2008. LNCS, vol. 5337, pp. 391–399. Springer, Heidelberg (2009)

Automatic Targeting Sentry Turret
for Distributed Systems

Piotr Demski, Tomasz Grzejszczak, Karol Jędrasiak, and Michał Mikulski

Abstract. Today most popular systems are constructed with the idea of collaboration. In software we can see a drastic increase of cloud-oriented applications, in electronics more devices are designed with CAN and Ethernet communications, and in robotics and defense whole systems are linked as unmanned sensor and agent networks. This paper describes the fundamental design principles of an automatic sentry turret in a distributed multi-agent system. The work is focused on the design of the turret system itself and the system architecture for distributed robotic applications. The papers is divided into the following sections: introduction, turret construction, system architecture, automatic target detection and aiming, and summary. Module.

1   Introduction

Increased collaboration in applications, communications, electronics extends rapidly to the field of robotics. Multi-agent networks can be used for sharing vital information, either for control purposes or intelligence. This approach to the development of specialized robots is essential if a more complex system can be achieved. This article presents the construction, system architecture, and aiming algorithms of a specialized robotic platform: a sentry turret, as a part of a bigger and more complex robotics system that is being deployed at the Silesian University of Technology. This article presents a thought process behind specialized units as seen from an agent-network, but the principles presented here can be applied, but not limited to: exoskeletons, UAVs [11],[9],[14] and mobile robots [3][1].

Piotr Demski · Tomasz Grzejszczak · Karol Jędrasiak · Michał Mikulski
Silesian University of Technology, Institute of Automatic Control,
Akademicka 16, 44-101 Gliwice, Poland
e-mail: {michal.mikulski,tomasz.grzejszczak,piotr.demski,
    karol.jedrasiak}@polsl.pl
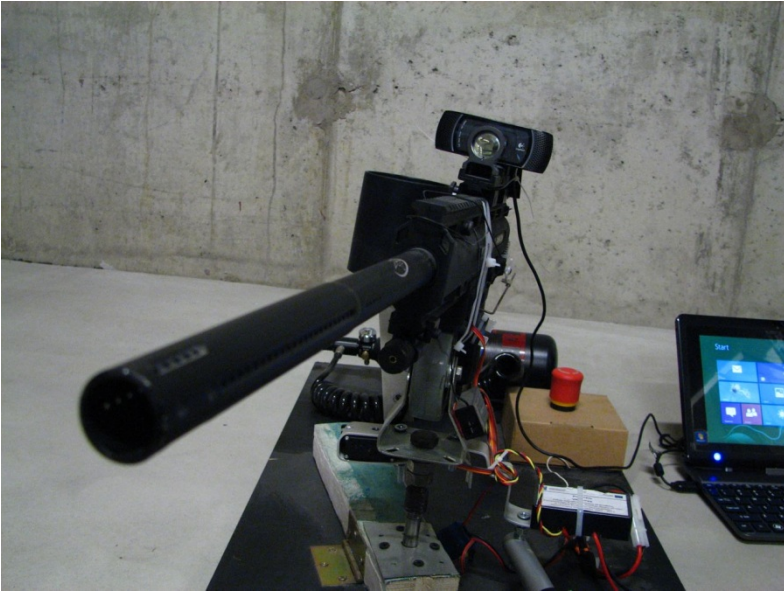
Fig. 1. Automatic sentry turret

Sentry turrets that can be attached to distributed systems can be used for more complex systems, such as multi-target attack, or cooperative decision-making as seen in [7]. They can be either stand-alone [6], deployable, or mounted on tactical vehicles, guard posts, or wearable robots such as exoskeletons, or "mech" like machines like KURATAS [4] .

2   Turret Construction

The project's goals was to construct an automatic targeting system, that would consist of two rotary joints, allowing the gun to aim freely at stationary and moving targets. Because the main focus of this article was on the control systems: both visual and distributed, a paintball marker was used instead of a live-ammo firearm.

Automatic turret elements (spotted in Fig.2):

- Tippmann X7 Phenom paintball marker, (a)
- Tippmann E-Grip - electronic powered automatic trigger system, (integrated with a)
- Tippmann X7 Phenom Cyclone Feed System, (b)
- Tiberius Arms Dual Illumination Open Dot Sight (swappable with Tiberius Arms 4x32 or 1x30 Dot Scope), (c)
- Tiberius Arms Tactical Laser, (d)
- 48cl 3000 psi HPA Tank, (e)

- Coiled Remote HPA Line, (f)
- 45MHz wireless receiver, (g)
- Linear electric actuator responsible for horizontal turret rotation, (h)
- Pitch servomechanism (TowerPro MG-995), (not seen on image)
- Trigger servomechanism (TowerPro MG-995), (i)
- H-Bridge integrated speed controller, (j)
- Emergency Stop button, (k)
- Li-Pol battery pack, (inside k)
- Logitech C910 HD Webcam, (l)
- Windows 8 tablet PC.(m)
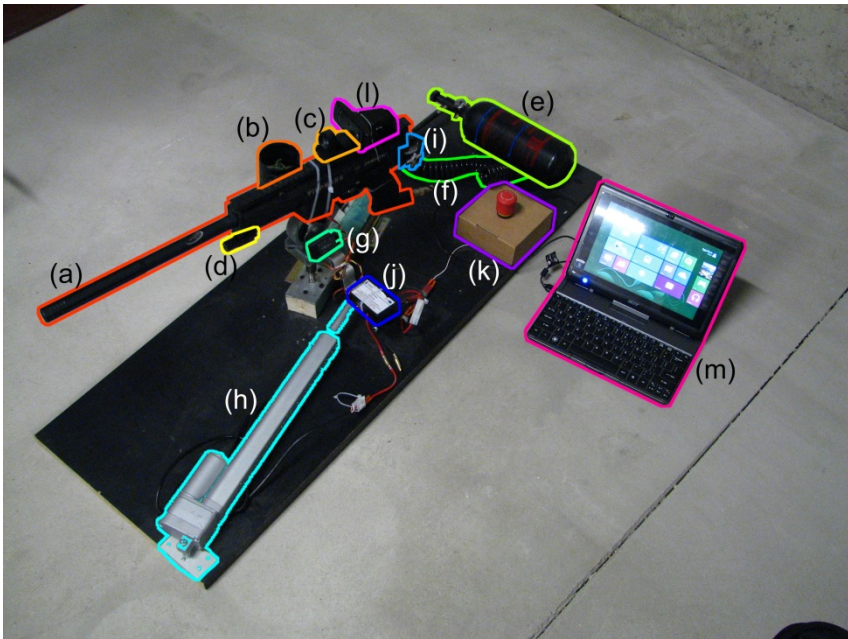
Fig. 2. Solution elements

The trigger in the presented system is based on a TowerPro MG-995 servomechanism, that presses and releases the Tippmann E-Grip automatic trigger. This is the easiest solution, that doesn't require any modification of the Tippmann's electronic components.

Because the automatic turret presented in this paper was created to be a universal construction - compatible with any mechanical trigger firearm, only the automatic firing was done using the E-Grip electronic control board, that was powered by it's own 9 Volt Battery hidden inside the grip.

E-Grip firing modes according to Tippmann:

- Semi-Auto: Fires 1 Shot for each trigger pull.
- Auto-Response: Fires 1 Shot for each trigger pull or release.
- Full Auto: Fires Repeatedly as long as the trigger is held.
- 3 Shot Burst: Fires 3 Shots for each trigger pull.
- Turbo: Fires 1 shot for every trigger pull, fires 1 shot for every trigger pull or release if the time between trigger pulls is less than .25 seconds.

3 System Architecture

The system network architecture is organized so it allows remote connection, monitoring and control of multiple devices and platforms. There was a need to choose architecture which can incorporate communication methods with varying devices, such as UAVs, exoskeletons and sentry turrets. Each of those have different functionality, which must be clearly defined so the remote (Internet) user can quickly and easily connect to them. System should also be expandable in a way which allows the addition of other devices without need to recreate whole system, or even breaking the connection with existing devices.

The answer for all those needs was the Windows Communication Foundation (WCF) API. Its object-oriented architecture gives the desired flexibility to the system. WCF was already tested and has proven its value in previous Authors works, such as [5].
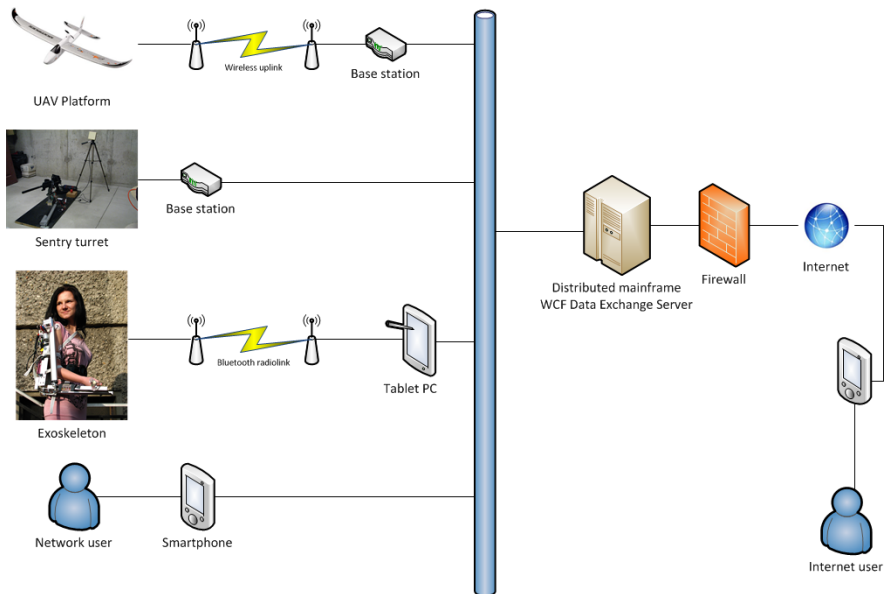
Fig. 3. An overview schema of the system

The WCF Data Exchange Server is a central communication point between re-mote users and devices, as shown in Fig.3. Each device is connected to system via base station, which can be dedicated - as in sentry turret application, or some other general-purpose device adapted to the application (such as PC tablet or smart-phone).

The sentry turret can be operated in two modes. In first mode, the turret is con-trolled manually (Fig.4). The position of the turret is set using Graupner RC equipment. The camera image is transmitted to video goggles, so the operator can see which way he is pointing the turret.
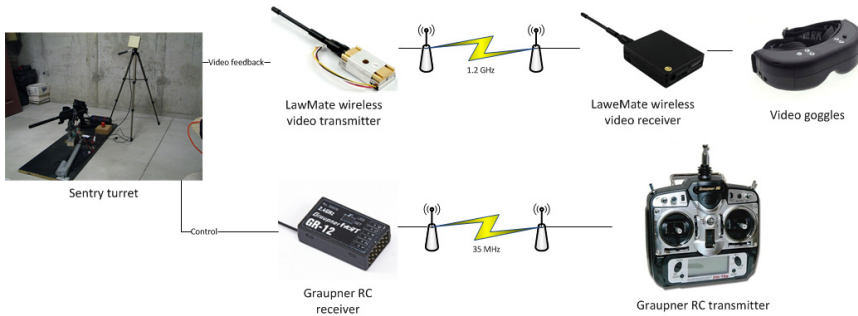
Fig. 4. An overview of the manual operation schema

The second operating mode is automatic (Fig. 5). In this mode, images from the camera is send to base station. Their image processing and other algorithms de-termine the position of the tracked object. The detection and aiming of the turret will be described later. After processing the image data, the desired turret position is sent to turret motors using xBee wireless network [2]. It is notable that all the communication with the turret itself is wireless, so the operator or the base station can be placed safely away from the turret.

The base station also implements the client functionality of WCF, using the software written in C\#. Base station is connected to WCF server, so the remote user can monitor the work of the turret.
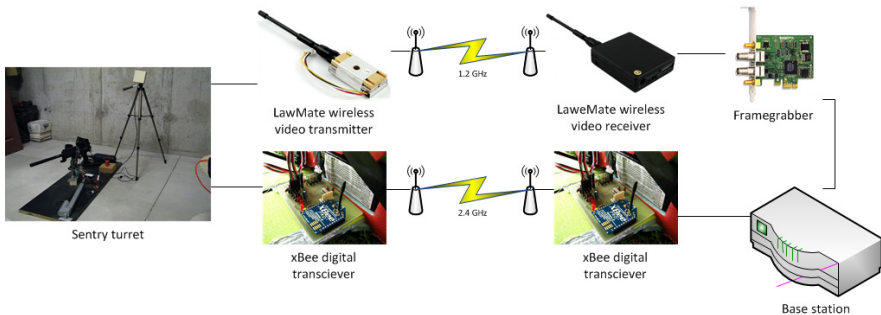
Fig. 5. An overview of base station control schema

4   Automatic Target Detection and Aiming

The turret aiming motors are capable of moving the gun and its sight vertically and horizontally. Depending on the accuracy of mechanisms, it is possible to create a coordinate system, where x and y axes corresponds to motors adjustments or indirectly to angles of barrel deflection or sight position.

The field of all possible sight positions is similar to image from mounted or stationary camera. After proper system calibration it is possible to get the adjustment of motors from the wanted sight position, which corresponds to position of object on image. By the assumption of mounting camera directly on barrel or mounting stationary camera with the same field of view and orientation as gun it is possible to easily correlate the image coordinates with simple construction of two motors working horizontally and vertically in two dimensions.

As it was mentioned previously, it is possible to handle two approaches. The camera can be mounted on gun or it can be set stationary with the same field of view. In case of stationary camera, the calibration process begins with gun aiming at certain points and user indicating those points on camera field of view. Then by means of linear interpolation the correlation between motors adjustment and detected object position on image is set.

In case of camera mounted on gun, there no need of software calibration. There is only a need to properly mount the camera, so the gun is aiming directly to the center of image. In this case, the position of detected objects and their displacement from center of image would be treated as correction to motors position. If the object is detected to the right of image center, there is an order send to move gun to the right. The algorithm previously was prototyped in simulation environment [8] and implemented in opto-electronic gimbal [10]. Depending on how far the object is from the center of image, the correction presets are chosen with use of fuzzy logic. Example of camera mounted on gun is presented in Fig. 6.

Fig. 6. Camera mounted on the gun

The most important information from vision system is the position of object and real time processing [12]. Objects are tracked with use of history of motion and optical flow algorithm. It is assumed that the scene is static, and the camera is not moving. If a new moving object appears it is separated from the background and its center of mass is calculated. As long as an object is moving its position is tracked and its coordinates are sent as control of gun positioning variables.

Each turret is mounted in one place and as a process of setting up the equipment it is possible to provide the GPS coordinates so the turret can work in slave mode. In this case turret is receiving orders about objects and targets position that are detected from other systems. Aiming targets is done by calculating the position of object due to turret position and setting the proper orientation.

It is also possible that the user is manually operating the gun. It can work with two ways. In fully manual mode user is controlling the gun actuators. In semi-automatic mode user is working with vision system and can point objects on camera output frames in order to move the gun to that position or to track objects.

The presented solution was made with use of easy methods and its purpose was to point out all disadvantages that should be handled. The parameters that should be considered are: wind speed, bullet speed while shooting moving targets, distance from object that indicates bullet descending due to gravity. Each of those variables cause the inaccuracy of the gun. For example it is possible that if the object is moving fast, the gun would not shoot the object, but the place where the object was small amount of time ago.

5   Future Work

The proposed architecture of distributed system for monitoring and control of robotic application has proven its usefulness in sentry turret application. It is possible to use such architecture for other devices, such as exoskeletons. It is important to be able to remotely monitor the health of the exoskeleton application elements, such as batteries, actuators and controllers, to ensure safety of the user. The experience from sentry turret application showed that this is possible and doesn't even need dedicated architecture written from the very bottom, but the usage of existing, universal architectures is possible. Current work will be focused on the usage of different devices, such as tablets or smartphones, to allow interconnection between robotic applications and remote users.

6   Summary

Targeting system requires extensive testing, as far as dispersion, recoil and different ranges are concerned. One of the biggest issues are shooting the moving targets, because in this case a lot of arguments should be taken into account, some of them are difficult to measure, some demand high measurement accuracy. However it was shown and proven that the system can work with multi agent approach and

implementing such system is an effective way of terrain control. It is practical implementation of the idea presented in [13] and [15].

References

[1] Demski, P., Mikulski, M., Koteras, R.: Characterization of hokuyo UTM-30LX laser range finder for an autonomous mobile robot. In: Nawrat, A., Simek, K., Świerniak, A. (eds.) Advanced Technologies for Intelligent Systems. SCI, vol. 440, pp. 143–154. Springer, Heidelberg (2013)

[2] Digi International Inc.: XBee/XBee-PRO ZB RF Modules Manual (2009)

[3] Ho-Chung, C., Ta-Ming, S.: Visual servo control of a three degree of freedom robotic arm system. In: IEEE International Conference on Advanced Robotics and its Social Impacts. IEEE, Taipei (2008)

[4] Suidobashi Heavy Industry: Kuratas (2012), `http://suidobashijuko.jp/`

[5] Mikulski, M.A., Szkodny, T.: Remote control and monitoring of ax-12 robotic arm based on windows communication foundation. In: Czachórski, T., Kozielski, S., Stańczyk, U. (eds.) Man-Machine Interactions 2. AISC, vol. 103, pp. 77–83. Springer, Heidelberg (2011)

[6] Moore, S.: A robotic sentry for korea's demilitarized zone. In: IEEE Spectrum (2007)

[7] Wolcott, R., Bishop, B.: Cooperative decision-making and multi-target attack using multiple sentry guns. In: 41st Southeastern Symposium on System Theory. IEEE, Tullahoma (2009)

[8] Grygiel, R., Pacholczyk, M.: Prototyping of control algorithms in matlab/Simulink. In: 14th World Multi-Conference on Systemics, Cybernetics and Informatis, WMSCI 2010, vol. 2, pp. 141–145 (2010)

[9] Daniec, K., Jedrasiak, K., Koteras, R., Nawrat, A.: Embedded micro inertial navigation system. Applied Mechanics and Materials 249-250, 1234–1246 (2013)

[10] Jędrasiak, K., Bereska, D., Nawrat, A.: The Prototype of Gyro-Stabilized UAV Gimbal for Day-Night Surveillance. In: Nawrat, A., Simek, K., Świerniak, A. (eds.) Advanced Technologies for Intelligent Systems. SCI, vol. 440, pp. 107–115. Springer, Heidelberg (2013)

[11] Iwaneczko, P., Jędrasiak, K., Daniec, K., Nawrat, A.: A prototype of unmanned aerial vehicle for image acquisition. In: Bolc, L., Tadeusiewicz, R., Chmielewski, L.J., Wojciechowski, K. (eds.) ICCVG 2012. LNCS, vol. 7594, pp. 87–94. Springer, Heidelberg (2012)

[12] Jędrasiak, K., Nawrat, A.: Image recognition technique for unmanned aerial vehicles. In: Bolc, L., Kulikowski, J.L., Wojciechowski, K. (eds.) ICCVG 2008. LNCS, vol. 5337, pp. 391–399. Springer, Heidelberg (2009)

[13] Jędrasiak, K., Nawrat, A., Wydmańska, K.: SETh-link the distributed management system for unmanned mobile vehicles. In: Nawrat, A., Simek, K., Świerniak, A. (eds.) Advanced Technologies for Intelligent Systems. SCI, vol. 440, pp. 247–256. Springer, Heidelberg (2013)

[14] Nawrat, N., Kozak, K., Daniec, K., Koteras, R.: Differential navigation for UAV platforms with mobile reference station. In: Proceedings of the International Conference on Applied Computer Science, pp. 465–471 (2010)

[15] Kozak, K., Koteras, R., Daniec, K., Nawrat, A.: qB-Distributed real time control system in UAV design. In: Proceedings of the 13th WSEAS International Conference on Systems, pp. 185–189 (2009)

Object Tracking for Rapid Camera Movements in 3D Space

Zygmunt Kuś and Aleksander Nawrat

Abstract. The solution of the camera head control problem was presented in the paper. The main goal of developed control algorithm is the object tracking in rapid disturbance conditions. The changes of the helicopter position and orientation during the time of disturbance result in losing tracked object from the field of view. Due to this fact the helicopter control system uses not only the visual information. The essence of the proposed solution is to compute the object position only in such time intervals when the object is in the center of the image. It allows the camera head regulators to compensate change of the camera position and set the camera towards the object. The proposed solution comprises of turning the camera head towards the trucked object in horizontal and vertical planes. The appropriate angles were computed on the basis of rangefinder data (distance between the camera and the object) and GPS and IMU data (the camera position and orientation). Furthermore, examples of the situation when the distortion changes the helicopter position in horizontal and vertical plane were presented in the paper.

1 Introduction

UAVs which are used to track terrestial objects have a wide range of use. Tracking of such objects results in problems with recognition and following the object by the UAV [32]. One of the possible solutions of the latter is the use of the

Zygmunt Kuś · Aleksander Nawrat
Silesian University of Technology, Institute of Automatic Control,
Akademicka 16, 44-101 Gliwice, Poland
e-mail: {zygmunt.kus,aleksander.nawrat}@polsl.pl

Aleksander Nawrat
Ośrodek Badawczo-Rozwojowy Urządzeń Mechanicznych "OBRUM" sp. z o.o., ul. Toszecka 102, 44-117 Gliwice, Poland
e-mail: anawrat@obrum.gliwice.pl

camera operator. Utilizing such an approach requires the operator to observe camera image on the screen which is located on the ground. The video is streamed via a communication system like [33] or [35].

However, this approach is considerably limited by the manual skills of the operator. This limitation is crucial in case of the occurrence of flight trajectory disturbances. An example of such a disturbance is strong gust of wind. It results in the object loss from the operator's screen and the operator cannot track the object any longer. Moreover, the same problem occurs when we use methods based on the image processing. These methods [1, 2, 3, 4, 5, 6, 7] are very effective when the tracked object occurs in the camera field of view. Rapid disturbances can make that the tracked object is out of the picture. When the tracked object movements are not the reason that we can not see the object then the image processing methods [14] – [23] do not give us any valuable information. The aforementioned situation is examined in the following paper. Hence the automatic object tracking method for rapid camera movements will be proposed herein.

2   Camera Movements Correction in 3D Space

The following section will focus on the basic elements of the solution of the problem presented in the introduction. The 3D modeling of a helicopter equipped with the camera is far more complex; however, it considerably increases the possibilities of camera control.

Below there are presented basic assumptions concerning geometrical relations for the examined problem:

a) the helicopter position equals camera position (displacement of the optical center of the camera lens in relation to the center of mass of the helicopter is minor and easy to take into account);

b) the camera orientation is a sum of helicopter orientation and camera head rotation (we do not model helicopter behavior, but we utilize a dynamic model of the impact of helicopter rotations on a camera - taking into consideration that the helicopter has its own flight trajectory control system e.g [26], [27]);

c) the tracked object moves on a flat ground $z_0 = 0$;

d) prior to commencing automatic object tracking the helicopter is manually directed at the area where the tracked object is situated. Next, the camera working in manual mode is directed at the object tracked by the operator. Then the operator marks the object on a screen or the object is located by image processing algorithms;

e) automatic object tracking is commenced when the object is in the center of the camera field of view;

f) the camera head may rotate within the range of 360 degrees in horizontal plane - parallel to the bottom of helicopter.

g) the camera is always above the object;

h) the helicopter with the camera mounted at the bottom of a helicopter body flies in a position approximate to horizontal;

It is assumed that connection between the helicopter and camera is rigid therefore there are not any dynamic relationships between the location and orientation of the camera and the location and orientation of the helicopter. As a consequence, the camera head control algorithm is based on fundamental geometrical relationships between camera and tracked object locations. Similarly, as it was presented in [25] the current object position is calculated only in the moment when pattern recognition algorithms give information that the object is in the picture. It allows to direct the camera to the tracked object immediately after distortion occurrence which turns the camera in an incorrect direction (orientation measured by IMU [28]).

Fig.1 presents the examined 3D scene.
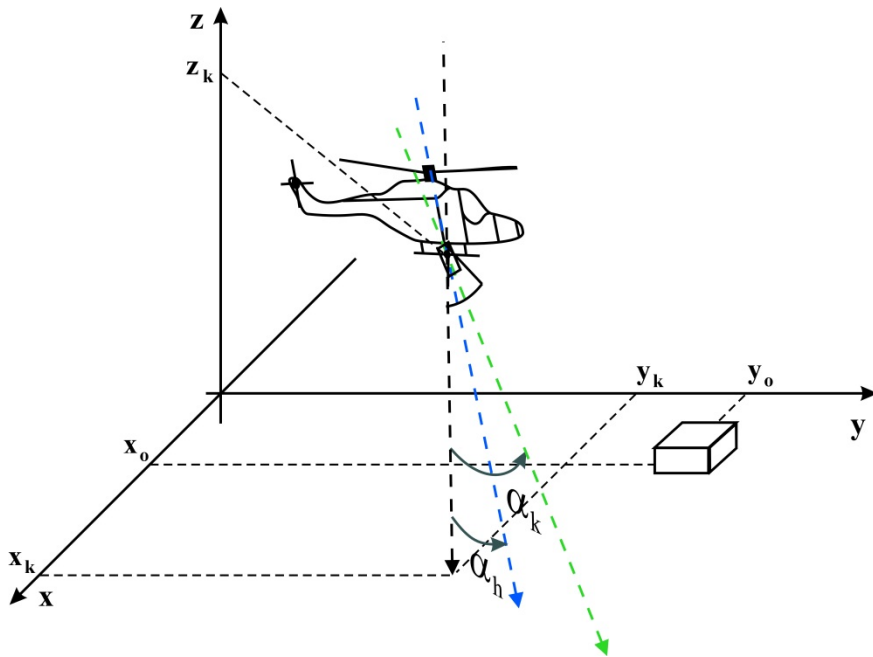
Fig. 1. The scheme of a camera and helicopter in 3D space

Fig.2 presents notations and the range of camera rotation angles in an (x, y) plane view.

As it is shown in figure 2 it is assumed that an x axis direction is a reference direction for determining the camera rotation angle in an (x, y) plane.

For the clockwise rotation direction we assume that $\beta < 0$ within the range 0 to -180 degrees. For the counter-clockwise rotation direction we assume that $\beta > 0$ within the range 0 to 180 degrees. Conclusively, the aforementioned description of a camera rotation angle defines the camera rotation in a horizontal plane around the circle for the complete range of the camera rotation. Figure 3 presents notations and the range of camera rotation angles α on a projection on a vertical plane S.
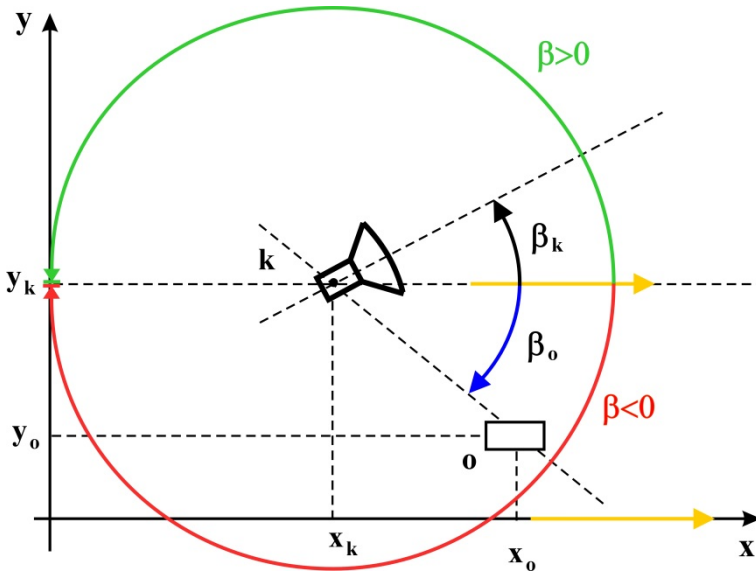
Fig. 2. Camera rotation angles as projection on a (x,y) plane
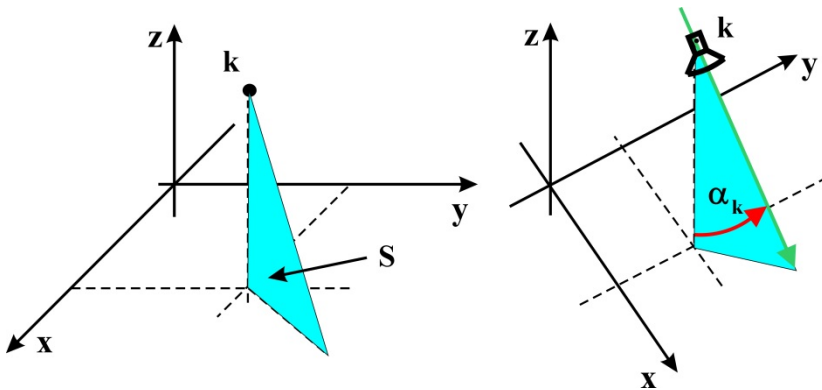
Fig. 3. Camera rotation angles α on a projection vertical plane S

The direction of an axis z is a reference direction for defining the camera rotation angle in a vertical plane (cf. fig. 3). It is assumed that the camera may rotate within the range of 0 to 90 degrees. It denotes that $\alpha \in (0°, 90°)$.

The range of the camera rotation in vertical plane, as shown in figure 3, is sufficient regarding the following assumption: the first step comprises of setting the camera in an (x, y) plane towards an object which guarantees that $\beta_k = \beta_{kset}$ in the second step the camera is being set in a vertical plane towards the object. Figure 4 presents spatial distribution of the camera and object before and after distortion.
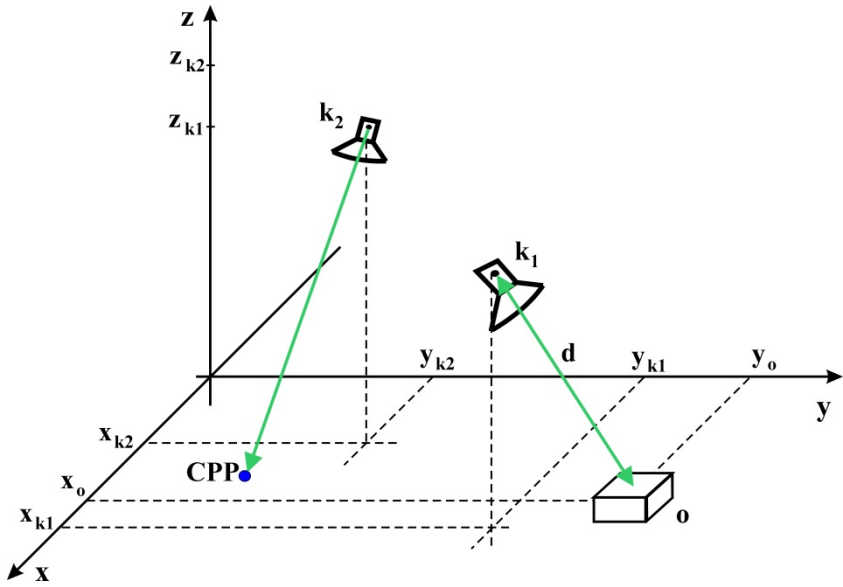
Fig. 4. Spatial distribution of the camera and object before and after distortion
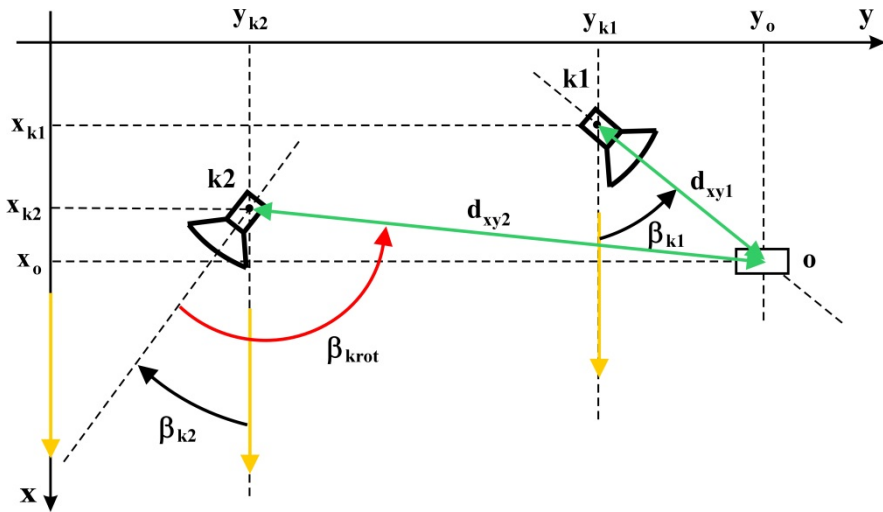
Fig. 5. Camera rotation angles and locations in a projection on an (x,y) plane before and after distortion

According to figure 4 we assume the following terms:

(x_{k1}, y_{k1}, z_{k1})- the camera coordinates before distortion;
(x_{k2}, y_{k2}, z_{k2}) - the camera coordinates after distortion;
d- the distance between the object and the camera measured before distortion;

(x_0, y_0, z_0) - the tracked object coordinates, assuming $z_0 = 0$;
CPP- point on the (x, y) plane visible in the center of the camera picture after distortion.

Furthermore, figure 4 indicates on the fact that distortion moved the camera towards the center of the coordinates system $(x_{k2} < x_{k1}, y_{k2} < y_{k1})$ and it additionally increased the camera level above the ground $(z_{k2} > z_{k1})$ The camera rotation angles in planes (x, y) and S were changed as well. Figure 5 represents the changes of angles in a greater detail.

Figure 5 depicts notations for camera locations and rotations in relation to the object. It is a projection on an (x, y) plane before and after distortion.

According to figure 5 we assume the following terms:

βk_1- the angle of a camera deviation in a projection on an (x, y) plane when the camera is directed towards the object (before distortion);

βk_2- the angle of a camera deviation in a projection on an (x, y) plane when the camera is not directed towards the object (after distortion);

βk_{krot}- the angle of a camera rotation in a projection on an (x, y) plane which compensates distortion (the camera is directed towards the object);

βk_{kset} - the angle in a projection on an (x, y) plane which defines direction towards the object;

d_{xy1} - the distance between the object and the camera in a projection on an (x, y) plane measured before distortion;

d_{xy2} - the distance between the object and the camera in a projection on an (x, y) plane measured after distortion;

Figure 6 depicts notations for camera locations and rotations in relation to the object. It is a projection on an S plane before and after distortion.
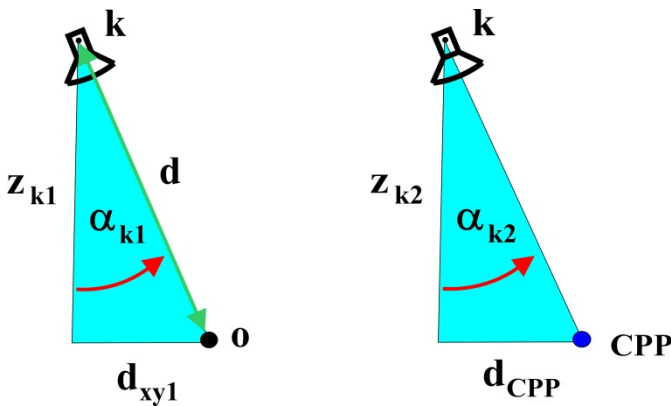
Fig. 6. Camera rotation angles and locations in a projection on a plane S before and after distortion

According to figure 6 we assume the following terms:

α_{k1}- the angle of a camera deviation from the vertical direction when the camera is directed towards the object (before distortion) ;

α_{k2}- the angle of a camera deviation from the vertical direction when the camera is not directed towards the object (after distortion);

When the first step of control algorithm is performed and the camera is set in an (x, y) plane towards an object ($\beta_k = \beta_{kset}$) then it is possible to calculate a correction angle α_{krot} in an S plane. The location of the camera and the object on an S plane after the correction on an (x, y) plane is presented in figure 7.

According to figure 7 we assume the following terms:

α_{kset}- the angle in a projection on the S plane which defines direction towards the object;

a_{krot}- the angle of a camera rotation in a projection on the S plane which compensates distortion.

The camera settings changes, which will occur after distortion, aim at turning the camera head in such a way which allows the object to appear in the camera field of view. Similarly, as it was presented in [25], we assume that when the object is in the center of the field of view then $OFVD = 0$ otherwise $OFVD > 0$. $OFVD$ is a signal produced by the image processing system. Hence we assume that in the moment of object position computing ($OFVD = 0$) the object is directly in the axis of the camera. The first step of control algorithm comprises of computing of the object location before distortion. The position of the object (x_0, y_0, z_0) is calculated on the basis of rangefinder data (distance d), GPS[30] and IMU ($x_{k1}, y_{k1}, z_{k1}, \alpha_{k1}, \beta_{k1}$):

$$\left.\begin{cases} x_0 = x_{k1} + d_{xy1} \cdot \sin (90° - \beta_{k1}) \\ y_0 = y_{k1} + d_{xy1} \cdot \cos (90° - \beta_{k1}) \end{cases}\right\} for\ \beta_{k1} \in \langle 0°, 180°\rangle \qquad (1.1)$$

$$\left.\begin{cases} x_0 = x_{k1} + d_{xy1} \cdot \sin (90° + \beta_{k1}) \\ y_0 = y_{k1} - d_{xy1} \cdot \cos (90° - \beta_{k1}) \end{cases}\right\} for\ \beta_{k1} \in (0°, 180°) \qquad (1.2)$$

As was it mentioned above, it is assumed that during object position calculation the object is in the center of the field of view. The aforementioned calculations are processed during the helicopter flight when $OFVD = 0$. The manifestation of distortion is the loss of the object in the picture and considerable changes of the object position or orientation. Then the helicopter control system turns the helicopter to a nearly horizontal position. Afterwards $x_{k2}, y_{k2}, z_{k2}, \alpha_{k2}, \beta_{k2}$ are measured. The goal of the control algorithm is to turn the camera towards the object. Required values of camera tilt angles α_{kset} and β_{kset} are calculated on the basis of the object and camera positions. These angles are calculated by the equations stated below:

$$\beta_{kset} = -90° - \arctan\left(\frac{x_{k2} - x_0}{y_{k2} - y_0}\right) \ for \ y_{k2} \geq y_0 \qquad (2.1)$$

$$\beta_{kset} = 90° - \arctan\left(\frac{x_{k2} - x_0}{y_{k2} - y_0}\right) \ for \ y_{k2} < y_0 \qquad (2.2)$$
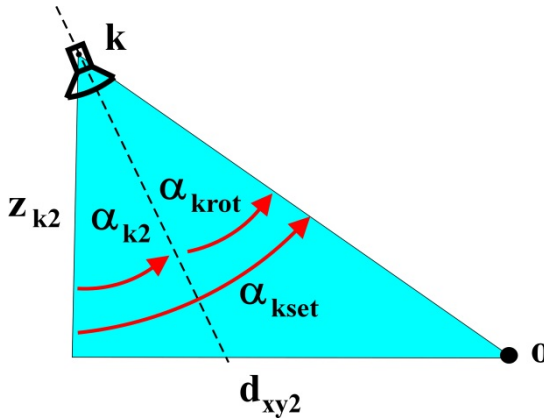
Fig. 7. Camera rotation angles and location in a projection on the S plane after the correction on the (x,y) plane

In the next step the correction angles α_{krot} and β_{krot} are computed. The camera must be turned at these angles. These angles are calculated as shown in the equation (3).

$$\alpha_{rot} = \alpha_{kset} - \alpha_{k2} \qquad (3)$$

3   Helicopter Dynamics Modeling in 3D Space

In order to check the correctness of the developed algorithm the simplified dynamic helicopter model is used. It indicates how distortion affects the helicopter position and orientation in 3D space. Hence the first order lag element represents the aforementioned properties. It is possible when the results shown in [8,9,10,11,12,13] and flight controllers are taken into account. Moreover, the camera heads dynamics was defined by the first order lag for both directions of rotation. It must be assumed that the camera movements are faster than the helicopter reactions on the control signal. It must be assumed that the helicopter movements are faster than tracked object movements.

Figure 8 represents the model of helicopter dynamics for 3D space. It must be assumed that the trajectory control system ensures flight along a set trajectory.

Therefore the following transfer functions denoting helicopter behavior are proposed:

$$K_{xh}(s) = \frac{k_{xh}}{(1+sT_{xh})}$$ - transfer function for distortion in axis x

$$K_{yh}(s) = \frac{k_{yh}}{(1+sT_{yh})}$$ - transfer function for distortion in axis y

$$K_{zh}(s) = \frac{k_{zh}}{(1+sT_{zh})}$$ - transfer function for distortion in axis z

$$K_{\alpha h}(s) = \frac{k_{\alpha h}}{(1+sT_{\alpha h})}$$ - transfer function for distortion which results in helicopter rotation in a vertical plane.

$$K_{\beta h}(s) = \frac{k_{\beta h}}{(1+sT_{\beta h})}$$ - transfer function for distortion which results in helicopter rotation in the horizontal plane.

Fig. 8. The helicopter dynamic model for particular control loops in 3D space

Figure 9 shows the camera head control system. The goal of this control system is to compute the required set values for α_k and β_k variables. This signal allows to set camera direction to the object regardless of the helicopter position. The first block computes the position of the object (x_0, y_0) on the basis of the distance d and the camera position. The influence of the helicopter rotations on the (x, y) plane and on an S plane on the camera is defined as an adder. The

position of the object is calculated from (1). The next block is Key1 closed for $OFVD = 0$ which means that the object is in the center of the camera picture. Block Mem remembers the current value of computed x_0. The required set camera angle is calculated on the basis of the camera and object positions. It allows to set camera direction towards the object. Firstly, we calculate the angle of the set α_k β_k values. The block after the adder is the Key2 block which is closed for $OFVD \neq 0$. It means the object is out of the center of the picture. Transfer function $K_{Gk}(s)$ denotes the dynamics of the camera head and it is equal (4) for the rotation in the (x, y) plane and 3 for the rotation in the S plane.

$$K_{Gk\alpha}(s) = \frac{k_{\alpha k}}{s \cdot (1 + sT\alpha k)} \tag{4}$$

$$K_{Gk\beta}(s) = \frac{k_{\beta k}}{s \cdot (1 + sT\beta k)} \tag{5}$$

The first order lag denotes inert properties while the integral denotes the motor.
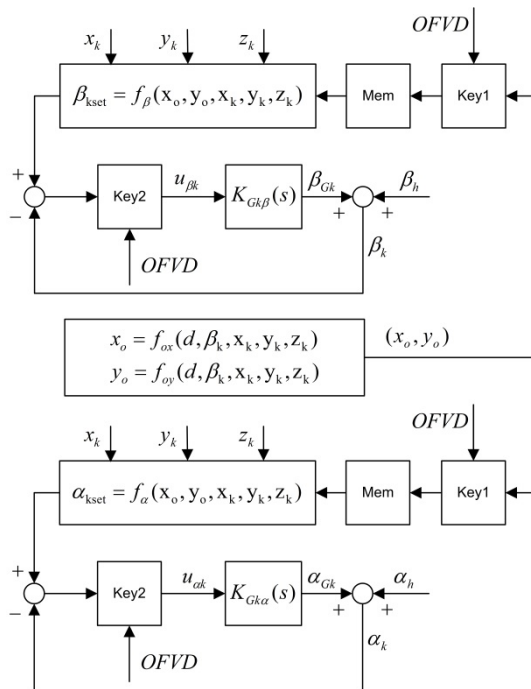
Fig. 9. The camera head control system

This way we obtain correct measurement of the object position. We measure it only if the object is in the center of the picture. However, the control signal changes the camera position only if the object is out of the center of the picture.

4   Examples of Tracking Algorithms Operation in the Presence of Disturbances

In 3D space the possibilities of various disturbances occurrence are significantly increased. These changes of helicopter position in the horizontal and vertical plane impact on the camera position. What is more, distortion in the form of the helicopter rotation has an impact on the camera rotation in two rotation axes ((x, y) and S planes).

Figure 10 represents the situation after distortion when the helicopter changes its position only in the (x, y) plane where $z_k = const$. The helicopter with the camera moves between the points, in projection on the (x. y) plane, and at the same time it goes around the object.

Fig. 10. The camera position during disturbance in the form of the helicopter position changes in the (x,y) plane

Fig. 11. Transients α_k and β_k defining the object tracking in the response to the disturbance which impact the helicopter only in the horizontal plane

Transients $\alpha_{kset}, \alpha_k, \beta_{kset}$ and β_k in the response to the camera position changes in the (x, y) plane, which were presented in figure 10, are presented in figure 11.

The change of the camera position is equal to the change of the helicopter position which is the result of wind blowing in a horizontal plane. As figure 11 presents the change of the (x_k, y_k) position caused the change of the required angles $\alpha_{kset}, \beta_{kset}$ of the camera rotation towards the tracked object. The camera head turns in order to set the camera rotation angles to set values ($\alpha_k = \alpha_{kset}$ and $\beta_k = \beta_{kset}$). Transients α_k and β_k have some minor overshoots, however, steady state error approaches zero.

We can improve the control quality by means of adding lead compensator PD in close loop in the position where the signals $U_{\alpha k}$ and $U_{\beta k}$ can be found (cf. fig. 9).

The transfer functions of these lead compensators PD, which will also be used in the following examples, are as presented below:

$$K_c(s) = \frac{10 \cdot (s+1)}{(1 + s \cdot 0.01)} \tag{6}$$

The compensator was tuned in such way that it is reducing dominant time constant [24].

The transients $\alpha_{kset}, \alpha_k, \beta_{kset}$ and β_k for the disturbance which was defined in figure 10 for the system with the lead compensator PD are presented in figure 12.
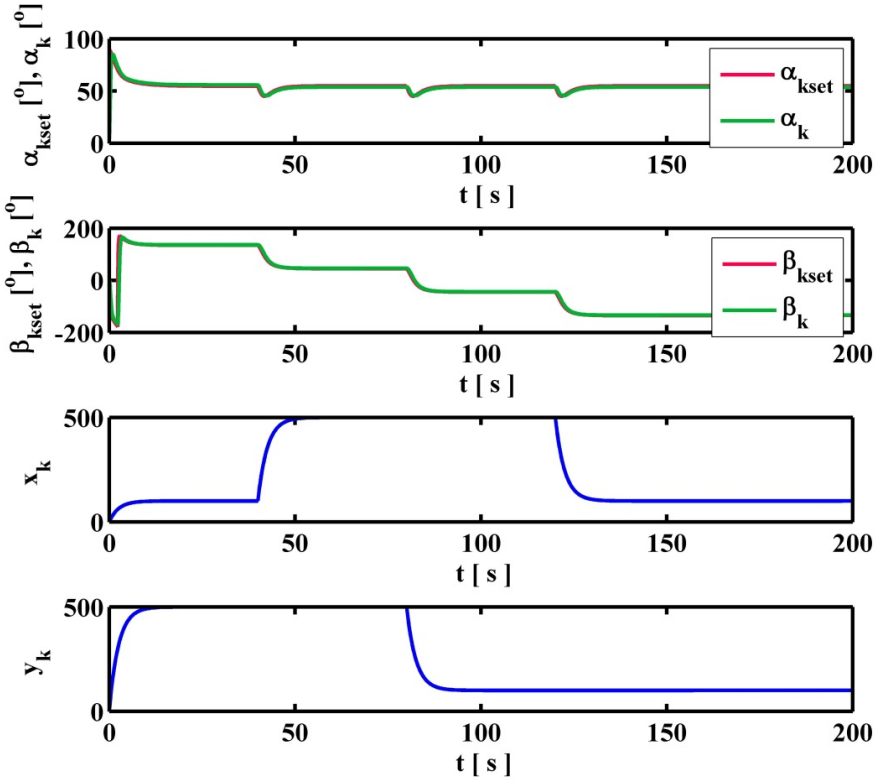
Fig. 12. The responses of the system in case of excitation defined in figure 10 for the system with the lead compensator PD

As figure 12 presents there is a considerable enhancement of the transients quality and the steady state error remains equal zero. Figure 13 represents the situation after distortion when the camera changes its position only in the (y, z) plane where $x_k = x_0 = const$ .In this case the camera sequentially moves upwards, above the object, downwards and finally back to the starting position.
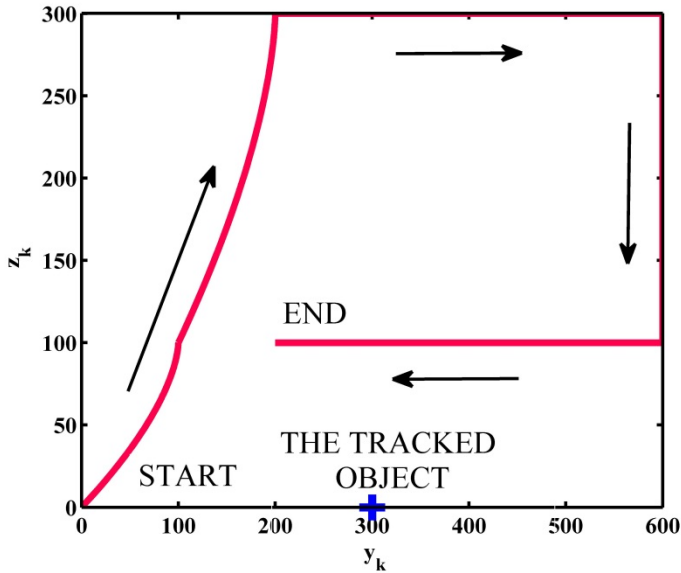
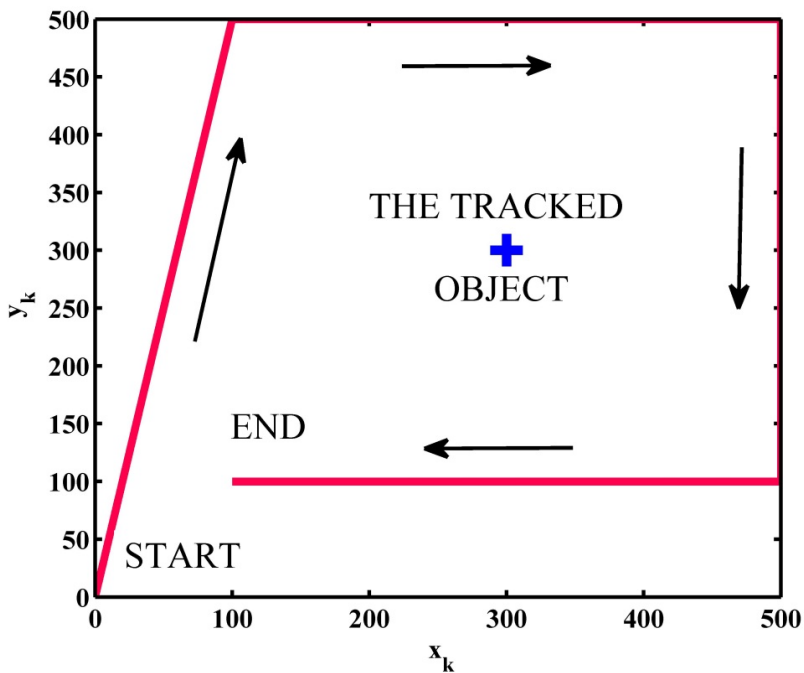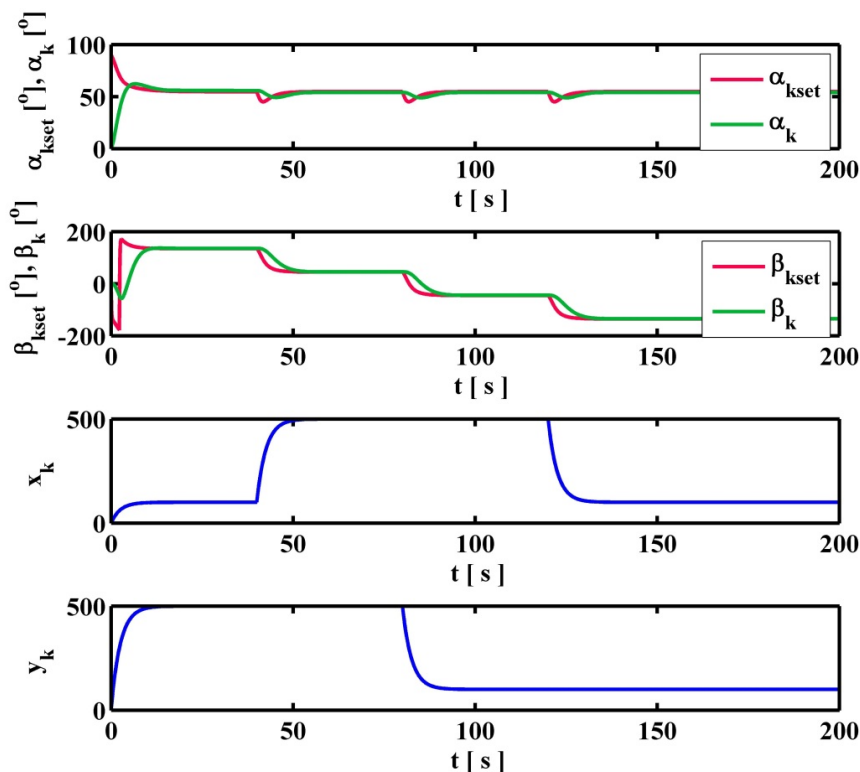**Fig. 13.** The camera position during disturbance in the form of the helicopter changes in the (y,z) plane
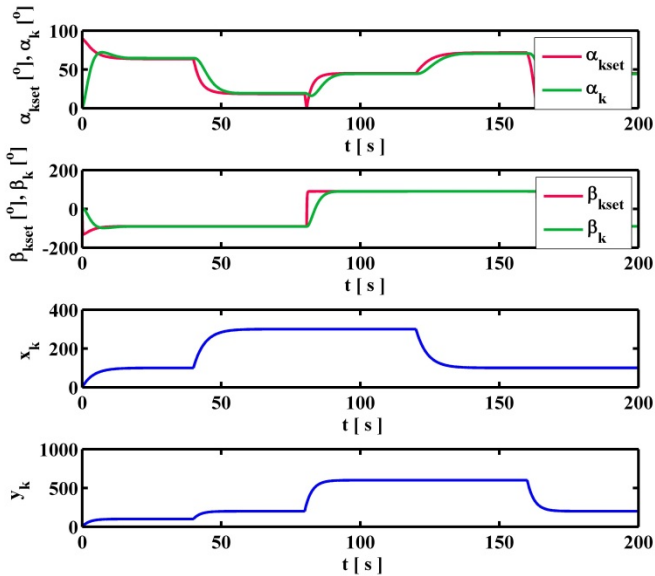
Fig. 14. Transients α_k and β_k defining the object tracking in the response to the disturbance which impacts the helicopter only in the vertical plane

Transients $\alpha_{kset}, \alpha_k, \beta_{kset}$ and β_k in the response to the camera position changes in the (y, z) plane, which were presented in figure 13, are presented in figure 14.

The change of the camera position is equal to the change of the helicopter position which is the result of wind blowing in a vertical plane. As figure 11 presents the change of the (x_k, y_k) position caused the change of the required angles α_{kset} and β_{kset} of the camera rotation towards the tracked object. The camera head turns in order to set the camera rotation angles to set values ($\alpha_k = \alpha_{kset}$ and $\beta_k = \beta_{kset}$). Transients α_k and β_k have some transient error, however, steady state error approaches zero. In this very example we can achieve the improvement of control quality likewise by means of lead compensator PD in close loop in the position where the signals $I_{\alpha k}$ and $U_{\beta k}$ can be found (cf. fig 9). The same lead compensators PD which were used previously were used herein. The transients $\alpha_{kset}, \alpha_k, \beta_{kset}$ and β_k for the disturbance which was defined in figure 13 for the system with the lead compensator PD are presented in figure 15.
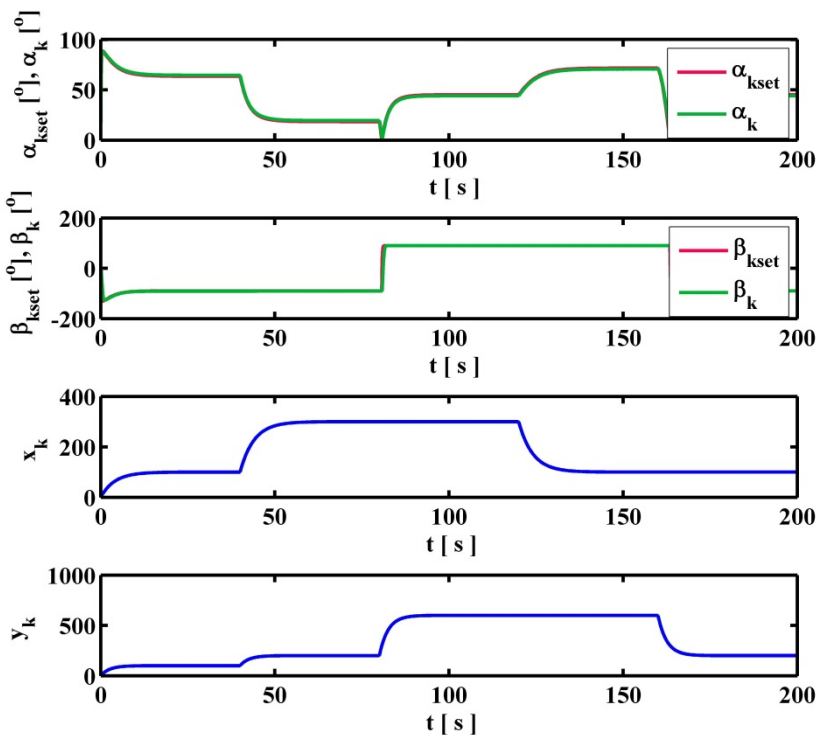
Fig. 15. The responses of the system in case of excitation defined in figure 13 for the system with the lead compensator PD

As figure 15 presents there is a considerable enhancement of the transients quality and the steady state error remains equal zero. Figure 16 represents the situation after distortion when the helicopter changes its position both in the

vertical and horizontal planes. The helicopter moves between the points which are located on different altitudes and situated on different sides in relation to the very object.
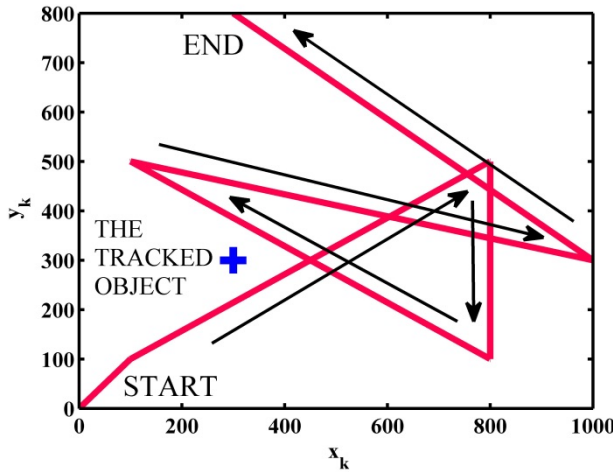
Fig. 16. The camera position in the projection on the (x,y) plane during disturbance which influences the helicopter both in horizontal and vertical planes
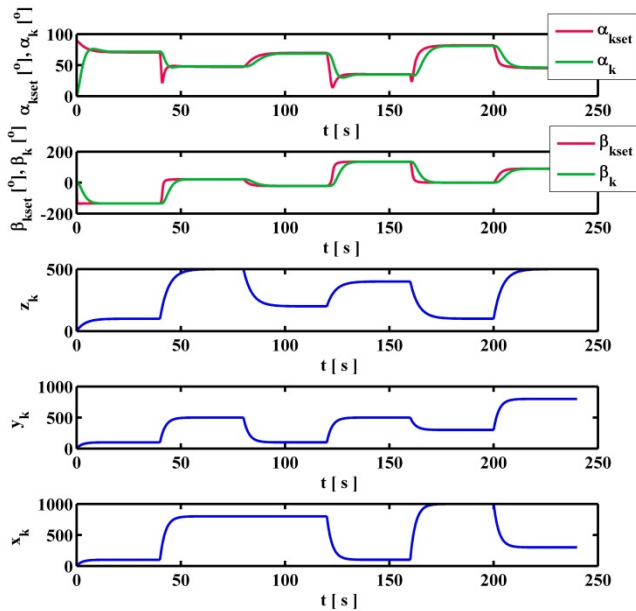
Fig. 17. Transients α_k and β_k defining the object tracking in the response to the disturbance which impacts the helicopter both in horizontal and vertical planes

Transients $\alpha_{kset}, \alpha_k, \beta_{kset}$ and β_k in the response to the camera position changes in the (y, z) plane, which were presented in figure 16, are presented in figure 17.

Transients α_k, β_k have some transient error, however, steady state error approaches zero. In this very example we can achieve the improvement of control quality likewise by means of lead compensator PD in close loop in the position where the signals $U_{\alpha k}$ and $U_{\beta k}$ can be found (cf. fig. 9). The same lead compensators PD which were used previously were used herein.

The transients $\alpha_{kset}, \alpha_k, \beta_{kset}$ and β_k for the disturbance which was defined in figure 15 for the system with the lead compensator PD are presented in figure 18.
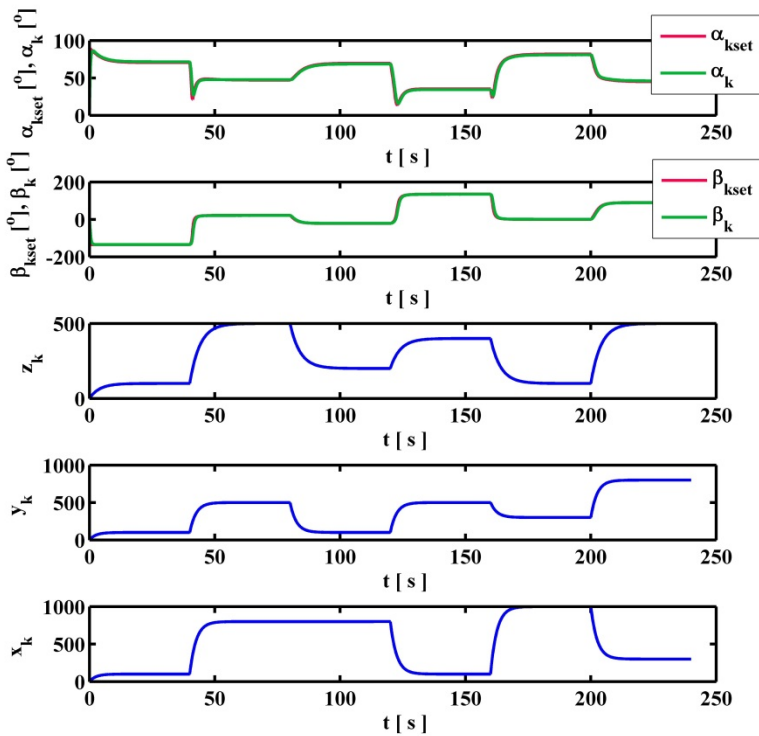

Fig. 18. The responses of the system in case of excitation defined in figure 16 for the system with the lead compensator PD

As figure 18 presents there is a considerable enhancement of the transients quality and the steady state error remains equal zero. As the presented examples indicate, the developed control system provides the correct object tracking during disturbances which occur in various directions in 3D.

5   Summary

This chapter has presented a solution of the camera head control problem. It allows to track objects in rapid disturbance conditions. The paper assumes that the object moves considerably slower than UAV during autonomous navigation [34]. Such an approach provides that the tracked object will not move too far during the time of disturbance. Due to this fact the helicopter control system [31] will manage to return to the basic helicopter orientation which is taken up during a regular flight. It allows the camera head regulators to compensate change of the camera position and set the camera towards the object. In case of fast-moving objects it is indispensable to use information obtained from the image processing system. This image processing system informs us about the moving object direction.

Conclusively, the essence of the proposed solution is to compute the object position only in such time intervals when the object is in the center of the image.

Lead compensators PD used in close loops allow to considerably enhance the control quality for the assumed camera head model. For the specific camera head type it is necessary to find the mathematical model appropriate for this very type of the camera head. In this case the choice of the regulator depends on the previously obtained camera head mathematical model. All aforementioned examples illustrate that the developed solution operates correctly

References

[1]   Davies, D., Palmer, P.L., Mirmehdi, M.: Detection and tracking of very small low contrast objects. In: Proceedings of the 9th British Machine Vision Conference (September 1998)

[2]   Zhang, S., Karim, M.A.: Automatic target tracking for video annotation. Op. Eng. 43, 1867–1873 (2004)

[3]   Irani, M., Peleg, S.: Improving resolution by image registration. CVGIP: Graph. Models and Image Process. 53, 231–239 (1991)

[4]   Chesnaud, C., Refegier, P., Boulet, V.: Statistical region snake-based segmentation adapted to different physical noise models. IEEE Trans. Patt. Anal. Mach. Intell. 21, 1145–1157 (1999)

[5]   Gordon, N., Ristic, B., Arulampalam, S.: Beyond the Kalman Filter: Particle Filters for Tracking Applications. Artech House, Boston (2004)

[6]   Sharp, C., Shakernia, O., Sastry, S.: A Vision System for Landing an Unmanned Aerial Vehicle. In: Proceedings of the 2001 IEEE International Conference on Robotics and Automation, vol. 2, pp. 1720–1727. IEEE, Los Alamitos (2001)

[7]   Casbeer, D., Li, S., Beard, R., Mehra, R., McLain, T.: Forest Fire Monitoring With Multiple Small UAVs, Porland, OR (April 2005)

[8]   Kuś, Z., Fraś, S.: Helicopter control algorithms from the set orientation to the set geographical Location. In: Nawrat, A., Simek, K., Świerniak, A. (eds.) Advanced Technologies for Intelligent Systems. SCI, vol. 440, pp. 3–14. Springer, Heidelberg (2013)

[9]   Nawrat, A.: Modelowanie i sterowanie bezzałogowych obiektów latających. Wydawnictwo Politechniki Śląskiej, Gliwice (2009)

[10]   Valavanis, K.P. (ed.): Advances In Unmanned Aerial Vehicles. Springer (2007)

[11] Castillo, P., Lozano, R., Dzul, A.E.: Modelling and Control of Mini-Flying Machines. Springer (2005)
[12] Padfield, G.D.: Helicopter Flight Dynamics. Backwell Science Ltd. (1996)
[13] Manerowski, J.: Identyfikacja modeli dynamiki ruchu sterowanych obiektów latających, WN ASKON, Warszawa (1999)
[14] Kearney, J.K., Thompson, W.B.: Optical flow estimation: An error analysis of gradient-based methods with local optimization. IEEE Transactions on Pattern Analysis and Machine Intelligence 9, 229–243 (1987)
[15] Anandan, P.: A computational framework and an algorithm for the measurement of visual motion. International Journal of Computer Vision 2, 283–310 (1989)
[16] Barman, H., Haglund, L., Knutsson, H., Granlund, G.: Estimation of velocity, acceleration, and disparity in time sequences. In: Proc. IEEE Workshop on Visual Motion, Princeton, NJ, pp. 44–51 (1991)
[17] Bascle, B., Bouthemy, E., Deriche, N., Meyer, E.: Tracking complex primitives in an image sequence. In: Proc. 12th International Conference on Pattern Recognition, Jerusalem, pp. 426–431 (1994)
[18] Butt, E.J., Yen, C., Xu, X.: Local correlation measures for motion analysis: A comparative study. In: Pattern Recognition and Image Processing Conference, Las Vegas, pp. 269–274 (1982)
[19] Butt, E.J., Bergen, J.R., Hingorani, R., Kolczynski, R., Lee, W.A., Leung, A., Lubin, J., Shvayster, H.: Object tracking with a moving camera. In: Proc. IEEE Workshop on Visual Motion, Irving, pp. 2–12 (1989)
[20] Buxton, B.E., Buxton, H.: Computation of optical flow from the motion of edges features in image sequences. Image and Vision Computing 2(2), 59–75 (1984)
[21] Campani, M., Verri, A.: Computing optical flow from an overconstrained system of linear algebraic equations. In: Proc. 3rd International Conference on Computer Vision, Osaka, pp. 22–26 (1990)
[22] Campani, M., Verri, A.: Motion analysis from firstorder properties of optical flow. CVGIP: Image Understanding 56(1), 90–107 (1992)
[23] Carlsson, S.: Information in the geometric structure of retinal flow field. In: Proc. 2nd International Conference on Computer Vision, pp. 629–633 (1988)
[24] Gessing, R.: Control Fundamentals. Silesian University of Technology, Gliwice (2004)
[25] Kuś, Z.: Object tracking in a picture during rapid camera movements
[26] Babiarz, A., Jaskot, K., Koralewicz, P.: The control system for autonomous mobile platform. In: Nawrat, A., Simek, K., Świerniak, A. (eds.) Advanced Technologies for Intelligent Systems. SCI, vol. 440, pp. 15–28. Springer, Heidelberg (2013)
[27] Babiarz, A., Jaskot, K.: The concept of collision-free path planning of UAV objects. In: Nawrat, A., Simek, K., Świerniak, A. (eds.) Advanced Technologies for Intelligent Systems. SCI, vol. 440, pp. 81–94. Springer, Heidelberg (2013)
[28] Jaskot, K., Babiarz, A.: The inertial measurement unit for detection of position. Przegląd Elektrotechniczny 86, 323–333 (2010)
[29] Grygiel, R., Pacholczyk, M.: Prototyping of control algorithms in matlab/Simulink. In: 14th World Multi-Conference on Systemics, Cybernetics and Informatis, WMSCI 2010, vol. 2, pp. 141–145 (2010)
[30] Skorkowski, A., Topor-Kaminski, T.: Analysis of EGNOS-augmented receiver positioning accuracy. Acta Physica Polonica A 122(5), 821–824 (2012)
[31] Daniec, K., Jedrasiak, K., Koteras, R., Nawrat, A.: Embedded micro inertial navigation system. Applied Mechanics and Materials 249-250, 1234–1246 (2013)

[32] Iwaneczko, P., Jędrasiak, K., Daniec, K., Nawrat, A.: A prototype of unmanned aerial vehicle for image acquisition. In: Bolc, L., Tadeusiewicz, R., Chmielewski, L.J., Wojciechowski, K. (eds.) ICCVG 2012. LNCS, vol. 7594, pp. 87–94. Springer, Heidelberg (2012)

[33] Jędrasiak, K., Nawrat, A., Wydmańska, K.: SETh-link the distributed management system for unmanned mobile vehicles. In: Nawrat, A., Simek, K., Świerniak, A. (eds.) Advanced Technologies for Intelligent Systems. SCI, vol. 440, pp. 247–256. Springer, Heidelberg (2013)

[34] Nawrat, N., Kozak, K., Daniec, K., Koteras, R.: Differential navigation for UAV platforms with mobile reference station. In: Proceedings of the International Conference on Applied Computer Science, pp. 465–471 (2010)

[35] Kozak, K., Koteras, R., Daniec, K., Nawrat, A.: qB-Distributed real time control system in UAV design. In: Proceedings of the 13th WSEAS International Conference on Systems, pp. 185–189 (2009)

Object Tracking in a Picture during Rapid Camera Movements

Zygmunt Kuś and Aleksander Nawrat

Abstract. Unmanned aerial vehicles (UAV) are very useful platforms for detecting and tracking objects which are located on the ground. The crux of the considered problem is the tracked object which disappears from a field of view. The above mentioned may be caused by rapid camera movements. One of the examples of such a situation is the camera being attached to helicopter. In case of sudden gust of wind a helicopter trajectory can be considerably and rapidly changed. This results in losing tracked object from the picture we get from the camera. The fundamental idea of the solution, which was presented here in, was based on additional data concerning camera orientation and location. Moreover the distance of a tracked object from the camera is also utilized to correct camera movements.

1 Introduction

Unmanned aerial vehicles (UAV) are very useful platforms for detecting and tracking objects which are located on the ground. There are many solutions of an object tracking problem which are based on image processing methods [1,2,3,4,5,6,7]. UAV behavior depends on the weather and type [32]. One of the problems may be rapid changes of wind and gusts. The following paper describes the problem of a tracked object which disappears from a field of view. There are three reasons which may cause this problem. Firstly, the object moves faster than the tracking camera head. Secondly, a pattern recognition algorithm has a fault and as a result it does not recognize the object. Finally, external distortion changes the position of the camera in the way that the object is out of the range of the field

Zygmunt Kuś · Aleksander Nawrat
Silesian University of Technology, Institute of Automatic Control,
Akademicka 16, 44-101 Gliwice, Poland
e-mail: {zygmunt.kus,aleksander.nawrat}@polsl.pl

Aleksander Nawrat
Ośrodek Badawczo-Rozwojowy Urządzeń Mechanicznych "OBRUM" sp. z o.o.,
ul. Toszecka 102, 44-117 Gliwice, Poland
e-mail: anawrat@obrum.gliwice.pl

of view. This paper examines the third case exclusively. In this case it is not poss-
ible to use image processing methods [14] – [23] because of disappearing object
from the picture.

It is assumed that the camera is mounted under a helicopter whereas the tracked
object moves on the ground. It must be also assumed that the object moves on the
flat surface. In the abovementioned case a rapid gust of wind may result in losing
the object from the picture streamed via communication system [33]. The helicop-
ter position determines which part of ground is being observed. Thus the first
stage of control algorithm is the return of the helicopter to the horizontal position.
Next, the camera is set by the developed control algorithm to the direction defined
by the last object position. For the lucidity of the work the author concentrates
only on 2D space.

2   Camera Movements Correction

Main elements of the algorithm are based on the basic geometrical relationships
between the helicopter, camera and tracked object positions. The current object
position is calculated only in the moment when pattern recognition algorithms
give information that object is in the picture. This current object position is uti-
lized when the distortion causes camera turn in a completely different direction.
Figure 1 presents the assumed 2D scene.

The tracked object is on a flat surface and the camera is above it. It is assumed
that the helicopter flies in a position approximate to horizontal. The camera is
mounted at the bottom.
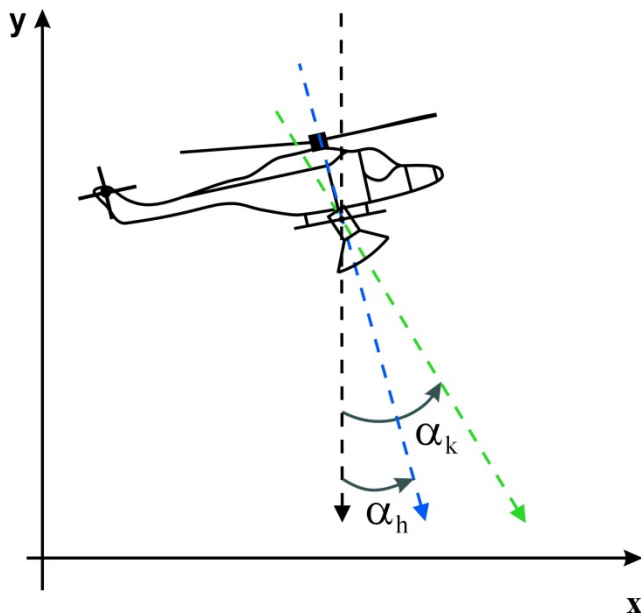
Fig. 1. The scheme of mounting a camera in a helicopter

There are assumed the following terms:

α_h - the angle of deviation of a helicopter from the vertical position,

α_k - the angle of deviation of a camera from the vertical position (it is equal 0 when the camera is directed to the ground,

$\alpha_k > 0$ - for clockwise angles, $\alpha_k < 0$ for counter-clockwise angles, maximum of α_k is 90°),

x - an axis representing the helicopter and the object position connected with the ground in horizontal direction,

y - an axis representing the helicopter and the object position connected with the ground in vertical direction.

For the object we assume that $y_0 = 0$ which means the object is always on the ground.
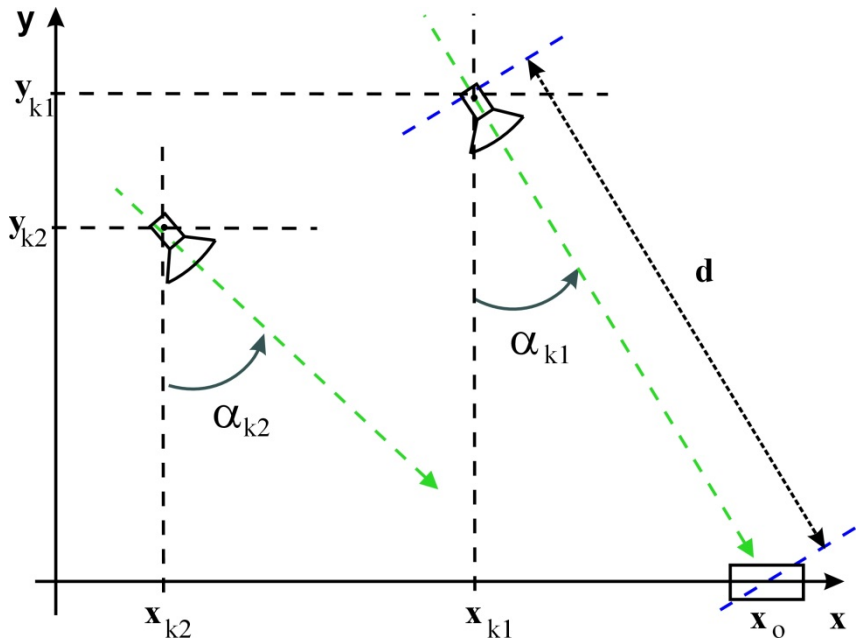
Fig. 2. The position of the tracked object in relation of the camera

The figure 2 represents the way of determining the object position in relation to the camera and its corresponding angles. Index 1 denotes the position before distortion whereas index 2 denotes the position after distortion. As we can see in the picture distortion caused the change of position and orientation. The object position was marked herein as well. We assume that the object is on the level $y = 0$.

According to figure 2 we assume the following terms:

(x_{k1}, y_{k1}) - the camera coordinates before distortion,
(x_{k2}, y_{k2}) - the camera coordinates after distortion,
d - the distance between the object and the camera measured before distortion,
(x_0, y_0) - the tracked object coordinates, assuming $y\_o=0$,

α_{k1} - the angle of deviation of a camera from the vertical position when the camera is directed to the object (before distortion) ,

α_{k2} - the angle of deviation of a camera from the vertical position when the camera is not directed to the object (after distortion).

The aim of the camera settings correction is to turn the head of the camera in a manner which allows the object to appear in the camera field of view. The figure 3 represents the object position in relation to the camera field of view. Furthermore, we assume that when the object is in the center of the field of view then $OFVD = 0$. $OFVD$ is a signal produced by the image processing system otherwise $OFVD > 0$. Hence we assume that in the moment of object position computing ($OFVD = 0$) the object is directly in the axis of the camera.
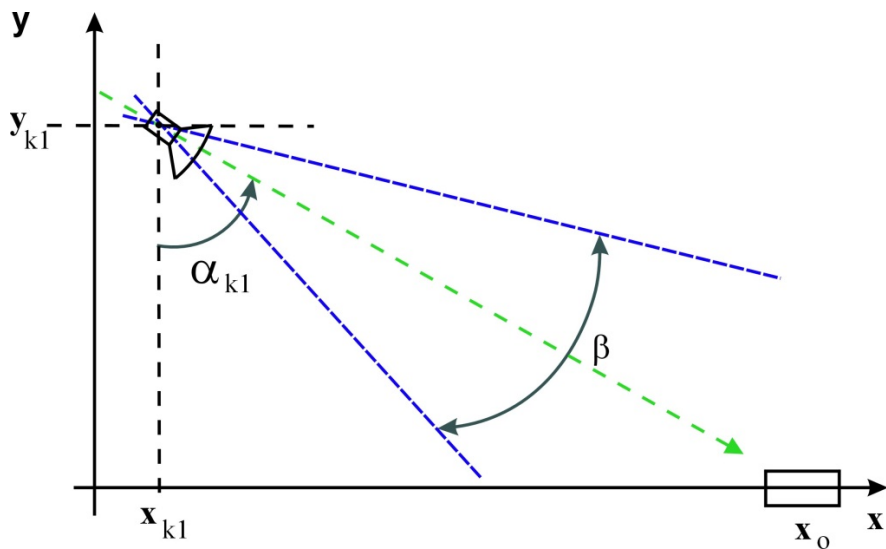
Fig. 3. The object position in the field of view of the camera

The position of the object is calculated on the basis of rangefinder data (distance d), GPS [30] and IMU data $(x_{k1}, y_{k1}, \alpha_{k1})$:

$$x_0 = d \cdot \sin(\alpha_{k1}) + x_{k1} \ or \ x_0 = (d^2 - y_{k1}^2)^{0.5} + x_{k1} \tag{1}$$

As was it mentioned above, it is assumed that the object is in the center of the field of view. The aforementioned calculations are processed during the helicopter

flight. When there is distortion the object ceases to be visible in the picture. In the case of distortion it may be stated that there is no object in the picture and considerable changes of the object position or orientation appear. Then the helicopter control system turns the helicopter to a nearly horizontal position. Afterwards $x_{k2}, y_{k2}, \alpha_{k2}$ are measured. In the next step the correction angle is computed. The helicopter must be turned at this angle. As figure 4 presents the position and orientation of the camera are known. The position of the tracked object is known too. This position was calculated before distortion. The angle α_{rot} is calculated on the basis of camera and object positions. The angle α_{rot} is the angle of rotation which compensates distortion.
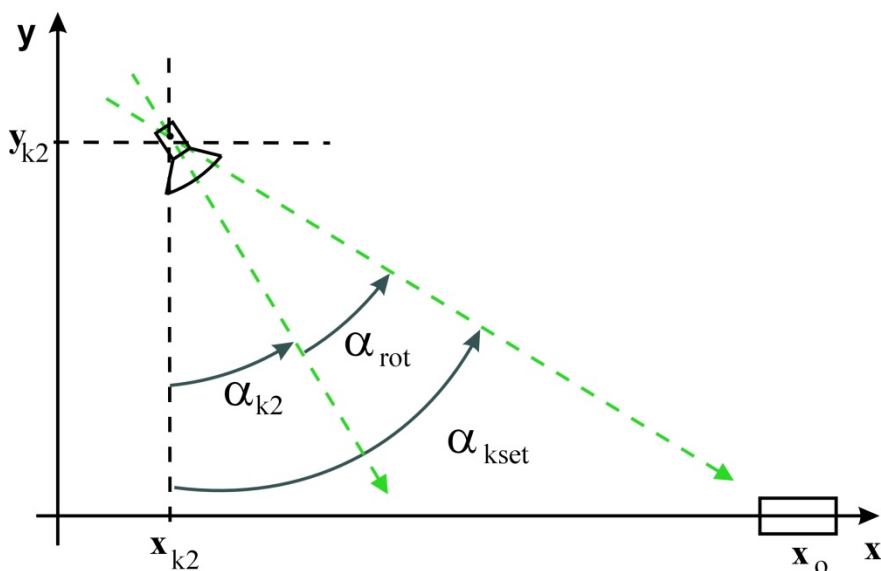
Fig. 4. Terms of camera angles in relation to the tracked object

Required value of camera tilt angle α_{kset} is calculated on the basis of the object and camera positions:

$$\alpha_{kset} = arctan\left(\frac{x_0 - x_{k2}}{y_{k2}}\right) \tag{2}$$

According to the terms in figure 4 it is obtained

$$\alpha_{rot} = \alpha_{kset} - \alpha_{k2} \tag{3}$$

It is necessary to account a sign of the angles. It depends on the object position in relation to the camera position.

3   The Modeling of the System for Tracking Algorithms Testing for a Dynamic Helicopter Model

In order to check the correctness of the developed algorithm the dynamic helicopter model is used. It is not a complete helicopter model. It shows how distortion affects the helicopter position and orientation. First order lag element represents this properties. It is possible when the results shown in [8,9,10,11,12,13] and flight controllers are taken into account. Moreover, the camera head dynamics was defined by first order lag. It must be assumed that the camera movements are faster than the reactions of helicopter on control signal. It must be assumed that the helicopter movements are faster than tracked object movements. Figure 5 represents the model of helicopter dynamics. It is assumed that the trajectory control system ensures flight along set trajectory [25, 26].
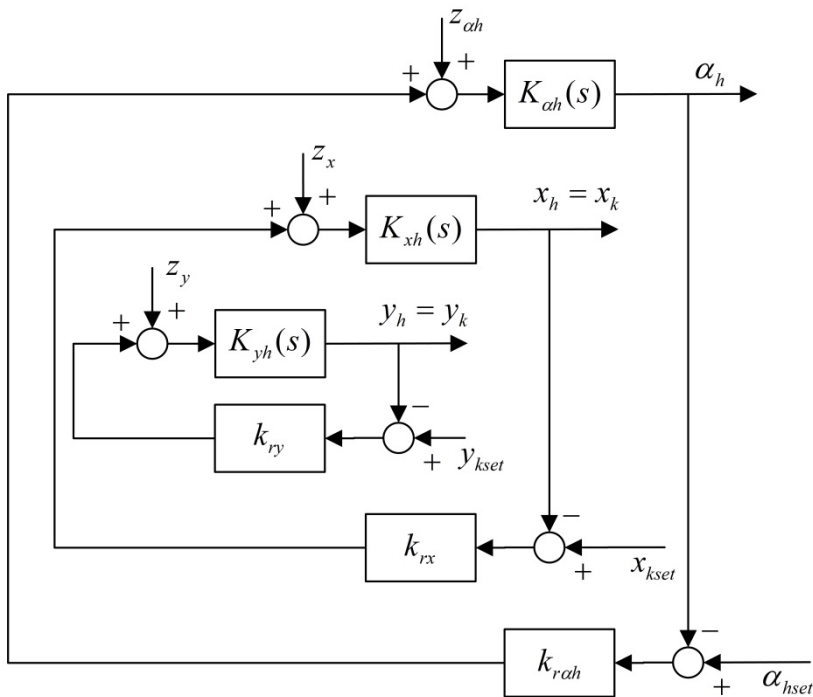
Fig. 5. The helicopter dynamic model for particular control loops

Therefore the following transfer functions denoting helicopter behavior are proposed:

$$K_{xh}(s) = \frac{k_{xh}}{(1+sT_{xh})} \text{ - transfer function for distortion in axis } x \qquad (4)$$

$$K_{yh}(s) = \frac{k_{yh}}{(1+sT_{yh})} \text{ - transfer function for distortion in axis } y \qquad (5)$$

$$K_{\alpha h}(s) = \frac{k_{\alpha h}}{(1+sT_{\alpha h})} \text{ - transfer function for distortion which results} \qquad (6)$$
$$\text{in helicopter rotation.}$$

Figure 6 shows   camera head control system. The aim of this control system is to compute required set value for α_k variable. This signal allows to set camera direction to the object regardless of the helicopter position. The first block computes the position of the object on the basis of the distance d and camera position. The next block is Key1 closed for $OFVD = 0$ which means the object is in the center of the camera picture.

Mem block remember current value of computed x_0. Required set camera angle is calculated on the basis of the camera and object positions. It allows to set camera direction to the object. The block after the adder is block Key2 which is closed for $OFVD \neq 0$ which means the object is out of the center of the picture. Transfer function $K_{Gk}(s)$ denotes the dynamics of camera head. It is as follows:

$$K_{Gk}(s) = \frac{k_{\alpha k}}{s \cdot (1 + sT_{\alpha k})} \qquad (7)$$

The first order lag denotes inert properties and integrator denotes the motor.
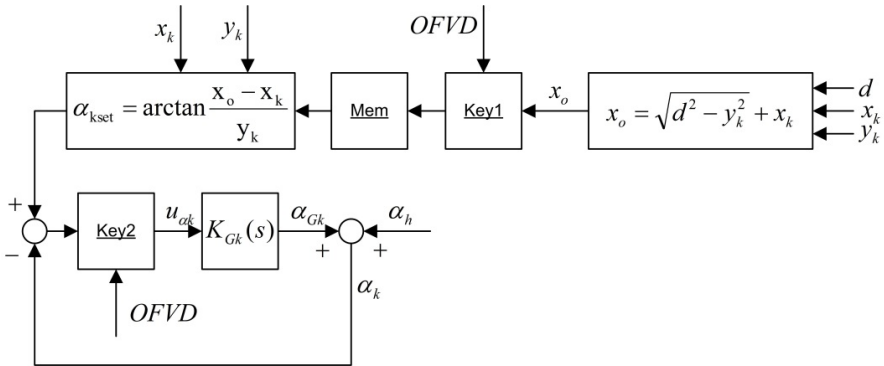
Fig. 6. Camera head control system

This way we obtain correct measurement of the object position. We measure it only if the object is in the center of the picture. However, the control signal changes the camera position only the object is out of the center of the picture.

4   Examples of Control System Operation in the Presence of Disturbances

Distortion in the form of the helicopter position change in horizontal and vertical axes is transmitted to the camera position. Distortion in the form of the helicopter rotation has impact on the camera rotation. The rotation of the head of the camera corrects the camera position which was disturbed before. Because of small size of the helicopter and camera it is assumed that the camera position is equal to the helicopter position. The helicopter rotation is added to the camera rotation.

Figure 7 represents the situation when the helicopter changes its position only in the axis x after distortion occurs.
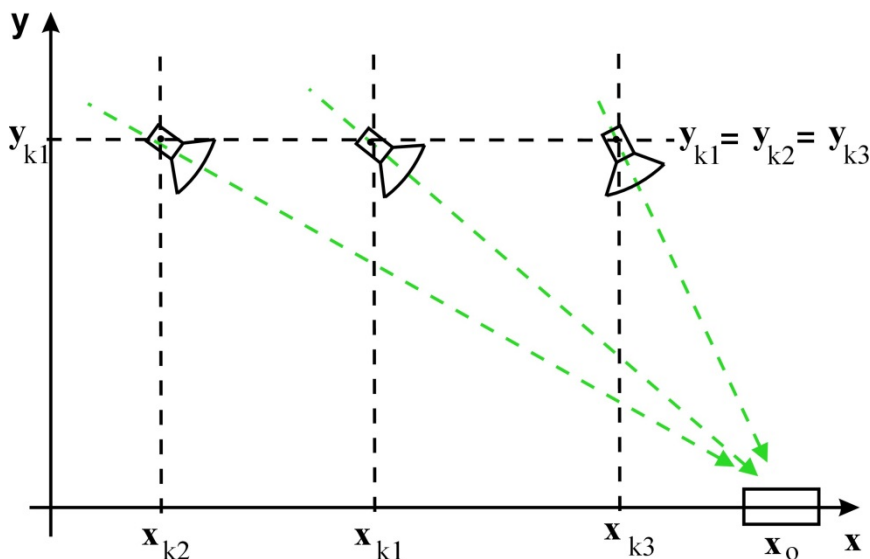
Fig. 7. Disturbance in the form of the helicopter position changes in the horizontal axis

Transients α_{kset} and α_k in the response to the camera position changes in axis x are presented in figure 8. The change of the camera position is equal to the change of the helicopter position which is the result of wind blowing in a horizontal surface. As figure 8 presents the change of the position caused the change of the required angle of camera rotation in direction of the tracked object. The camera head turns in order to set the camera rotation angle to set value α_{kset}. Transient α_k has some minor overshoots. We can improve the control quality by means of adding lead compensator PD in close loop with signal α_k.

Fig. 8. Transients α_{kset} and α_k in the response to the camera position changes in axis x

Figure 9 represents the situation when the helicopter changes its position only in the axis y after distortion occurs.

Fig. 9. Transients α_{kset} and α_k in the response to the camera position changes in axis x

Transients α_{kset} and $\boldsymbol{\alpha_k}$ in the response to the camera position changes in axis y are presented in figure 10. The change of the camera position is equal to the change of the helicopter position which is the result of wind blowing in a vertical surface. As figure 10 presents the change of the position y_k caused the change of the required angle of camera rotation in direction of the tracked object α_{kset}. The camera head turns in order to set the camera rotation angle $\boldsymbol{\alpha_k}$ to set value α_{kset}. Transient $\boldsymbol{\alpha_k}$ shows that control system works in an excellent manner. There are not any overshoots and $\boldsymbol{\alpha_k}$ is following α_{kset} signal very closely.

As figure 10 presents transient $\boldsymbol{\alpha_k}$ has neither overshoots nor steady state error.
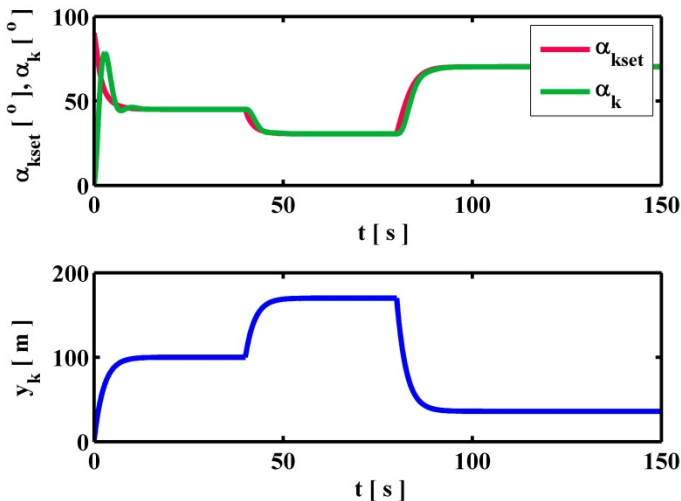
Fig. 10. Transients $\boldsymbol{\alpha_{kset}}$ and $\boldsymbol{\alpha_k}$ in the response to the camera position changes in axis $\boldsymbol{y}$

Figure 11 represents the situation when the helicopter rotation angle is changed after distortion occurs.

Transients $\boldsymbol{\alpha_k}$ and α_{kset} in the response to the helicopter rotation angle α_h are presented in figure 12. The change of the camera rotation $\boldsymbol{\alpha_k}$ is equal to the change of the helicopter rotation α_h which is the result of swirling wind. As figure 12 presents the change of α_h does not cause the change of the required angle of camera rotation α_{kset}. It is caused by the same camera position before and after distortion occurs. The helicopter rotation causes the change of $\boldsymbol{\alpha_k}$. The camera head turns in order to set the camera rotation angle $\boldsymbol{\alpha_k}$ to set value α_{kset}. Transient $\boldsymbol{\alpha_k}$ shows that control system works in a perfect manner. There are overshoots in this moment when the disturbance occurs; however, $\boldsymbol{\alpha_k}$ signal is following α_{kset} signal very quickly.
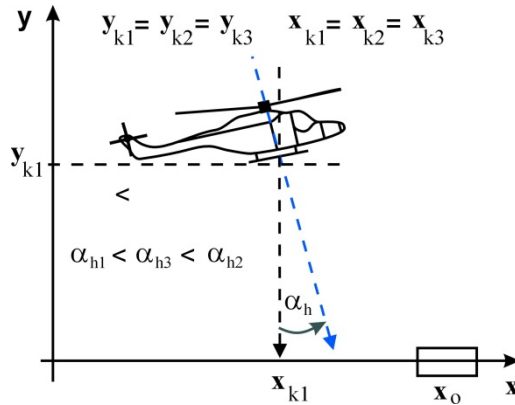
Fig. 11. Disturbance in the form of the helicopter rotation
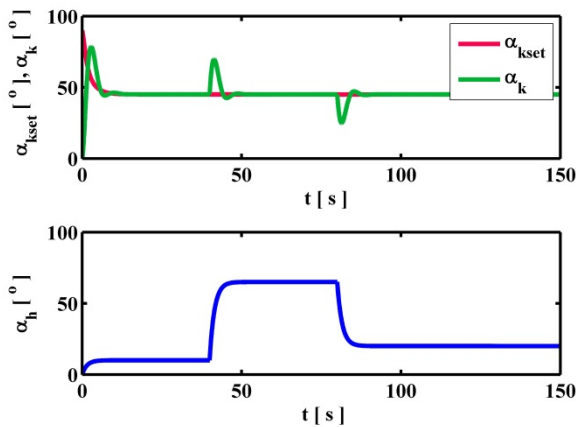
Fig. 12. Transients α_k and α_{kset} in the response to the helicopter rotation angle changes

Responses of signals α_{kset} and α_k in a case of excitations x_k, y_k and α_h which are the same as the above-mentioned, are presented in figure 13.

As figure 13 presents the control system works perfectly in steady states, but incorrectly in transient states. The changes of x_k, y_k and α_h cause the change of the required angle α_{kset} and current value of camera rotation α_kn.

The camera head turns in order to set the camera rotation angle α_k to the set value α_{kset}. There are overshoots in this moment when the disturbance occurs, but in steady state thα_ke signal is following the α_{kset} signal.

The control quality can be improved by means of adding lead compensator PD in close loop, which is presented in figure 6 with signal α_k. The transfer function of this compensator is as follows:
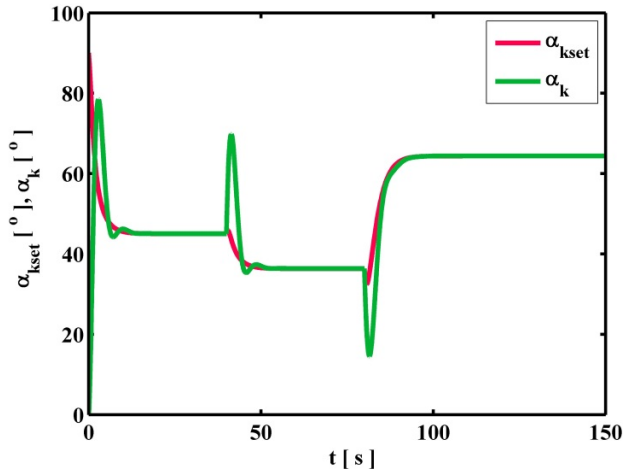
Fig. 13. Responses of signals α_{kset} and α_k in case of excitations x_k, y_k and α_h disturbances
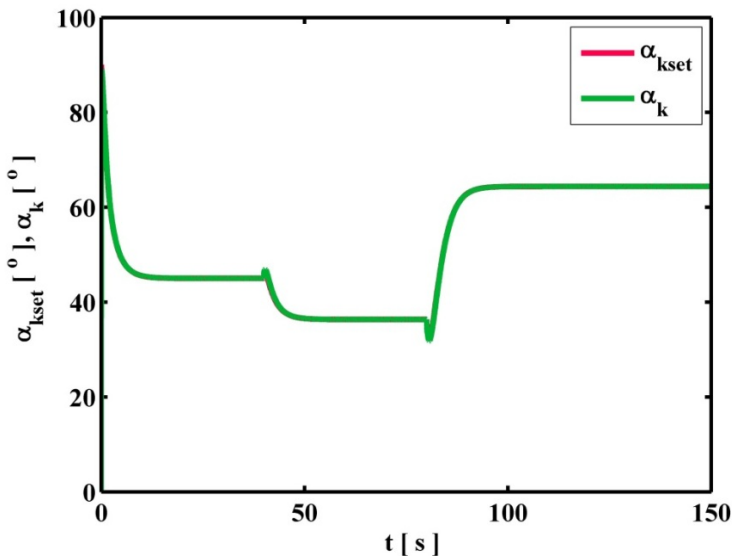
Fig. 14. Responses of signals α_{kset} and α_k in a case of excitation x_k, y_k and α_h disturbances for the system with a lead compensator PD

$$K_c(s) = \frac{30 \cdot (s + 1)}{(1 + s \cdot 0.01)} \tag{8}$$

The compensator was tuned in such way that it is reducing dominant time constant [24]. For system with lead compensator PD the responses of signals α_{kset} and $\boldsymbol{\alpha_k}$ in a case of excitations x_k, y_k and α_h, which are the same as the above-mentioned, are presented in figure 14.

As figure 14 presents the control system works excellent in a steady state and in transients. The change of x_k, y_k and α_h, causes the change of the required angle α_{kset} but current value of camera rotation $\boldsymbol{\alpha_k}$ is following α_{kset} signal very closely. There are not overshoots.

The camera head turns continuously in order to set the camera rotation angle $\boldsymbol{\alpha_k}$ to the set value α_{kset}. This way the camera is all time directed towards the tracked object.

5   Summary

The paper presents camera head control algorithm for Unmanned Aerial Vehicles. What is more, the presented solution is complementary for methods based on image processing. Interestingly, the most important feature of the presented solution is the use of information from IMU (Inertial Measurement Unit) [27] and GPS (Global Positioning System). It is significant enrichment of the range of tools and data which are used. The tracking of the objects, which are located on the ground, was considered in the paper. It was assumed that image processing algorithms are used and produce information about location of the object in the picture. UAV behavior depends on the gusts and rapid changes of the wind. The tracked object can be lost from the camera field of view in the above-mentioned case. Thus it was necessary to seek other sources of data - sources different then image processing system. What was also discussed herein is the case when the object which is located on flat ground is tracked by the helicopter with the camera. The presented solution was based on calculation of the object position in the moment when the object is in the center of the picture. The current camera position, orientation and the calculated object position were indispensable information for the control algorithm.

The examples which were presented herein demonstrate a correct behavior of the camera head control system. The similar thought process could be applied to various different mobile robots [29] and implemented in their navigation systems [31].

References

[1] Davies, Palmer, P.L., Mirmehdi, M.: Detection and tracking of very small low contrast objects. In: Proceedings of the 9th British Machine Vision Conference (September 1998)
[2] Zhang, S., Karim, M.A.: Automatic target tracking for video annotation. Op. Eng. 43, 1867–1873 (2004)

[3]   Irani, M., Peleg, S.: Improving resolution by image registration. CVGIP: Graph.
      Modelsand Image Process. 53, 231–239 (1991)
[4]   Chesnaud, C., Refegier, P., Boulet, V.: Statistical region snake-based segmentation
      adapted to different physical noise models. IEEE Trans. Patt. Anal. Mach. Intell. 21,
      1145–1157 (1999)
[5]   Gordon, N., Ristic, B., Arulampalam, S.: Beyond the Kalman Filter: Particle Filters
      for Tracking Applications. Artech House, Boston (2004)
[6]   Sharp, C., Shakernia, O., Sastry, S.: A Vision System for Landing an Unmanned
      Aerial Vehicle. In: Proceedings of the 2001 IEEE International Conference on Ro-
      botics and Automation, vol. 2, pp. 1720–1727. IEEE, Los Alamitos (2001)
[7]   Casbeer, D., Li, S., Beard, R., Mehra, R., McLain, T.: Forest Fire Monitoring With
      Multiple Small UAVs, Porland, OR (April 2005)
[8]   Kuś, Z., Fraś, S.: Helicopter control algorithms from the set orientation to the set
      geographical location. In: Nawrat, A., Simek, K., Świerniak, A. (eds.) Advanced
      Technologies for Intelligent Systems of National Border Security. SCI, vol. 440, pp.
      3–14. Springer, Heidelberg (2013)
[9]   Nawrat, A.: Modelowanie i sterowanie bezzałogowych obiektów latających. Wy-
      dawnictwo Politechniki Slaskiej, Gliwice (2009)
[10] Valavanis, K.P. (ed.): Advances In Unmanned Aerial Vehicles. Springer (2007)
[11] Castillo, P., Lozano, R., Dzul, A.E.: Modelling and Control of Mini-Flying Ma-
      chines. Springer (2005)
[12] Padfield, G.D.: Helicopter Flight Dynamics. Backwell Science Ltd. (1996)
[13] Manerowski, J.: Identyfikacja modeli dynamiki ruchu sterowanych obiektów lata-
      jaących, WN ASKON, Warszawa (1999)
[14] Kearney, J.K., Thompson, W.B.: Optical flow estimation: An error analysis of gra-
      dient-based methods with local optimization. IEEE Transactions on Pattern Analysis
      and Machine Intelligence 9, 229–243 (1987)
[15] Anandan, P.: A computational framework and an algorithm for the measurement of
      visual motion. International Journal of Computer Vision 2, 283–310 (1989)
[16] Barman, H., Haglund, L., Knutsson, H., Granlund, G.: Estimation of velocity, acce-
      leration, and disparity in time sequences. In: Proc. IEEE Workshop on Visual Mo-
      tion, Princeton, NJ, pp. 44–51 (1991)
[17] Bascle, B., Bouthemy, E., Deriche, N., Meyer, E.: Tracking complex primitives in
      an image sequence. In: Proc. 12th International Conference on Pattern Recognition,
      Jerusalem, pp. 426–431 (1994)
[18] Butt, E.J., Yen, C., Xu, X.: Local correlation measures for motion analysis: A com-
      parativestudy. In: Pattern Recognition and Image Processing Conference, Las Ve-
      gas, pp. 269–274 (1982)
[19] Butt, E.J., Bergen, J.R., Hingorani, R., Kolczynski, R., Lee, W.A., Leung, A., Lubin,
      J., Shvayster, H.: Object tracking with a moving camera. In: Proc. IEEE Workshop
      on Visual Motion, Irving, pp. 2–12 (1989)
[20] Buxton, B.E., Buxton, H.: Computation of optical flow from the motion of edges
      features in image sequences. Image and Vision Computing 2(2), 59–75 (1984)
[21] Campani, M., Verri, A.: Computing optical flow from an overconstrained system of-
      linear algebraic equations. In: Proc. 3rd International Conference on Computer Vi-
      sion, Osaka, pp. 22–26 (1990)
[22] Campani, M., Verri, A.: Motion analysis from firstorder properties of optical flow.
      CVGIP: Image Understanding 56(1), 90–107 (1992)
[23] Carlsson, S.: Information in the geometric structure of retinal flow field. In: Proc.
      2nd International Conference on Computer Vision, pp. 629–633 (1988)
[24] Gessing, R.: Control Fundamentals. Silesian University of Technology, Gliwice
      (2004)

[25] Babiarz, A., Jaskot, K., Koralewicz, P.: The control system for autonomous mobile platform. In: Nawrat, A., Simek, K., Świerniak, A. (eds.) Advanced Technologies for Intelligent Systems. SCI, vol. 440, pp. 15–28. Springer, Heidelberg (2013)

[26] Babiarz, A., Jaskot, K.: The concept of collision-free path planning of UAV objects. In: Nawrat, A., Simek, K., Świerniak, A. (eds.) Advanced Technologies for Intelligent Systems. SCI, vol. 440, pp. 81–94. Springer, Heidelberg (2013)

[27] Jaskot, K., Babiarz, A.: The inertial measurement unit for detection of position. Przegląd Elektrotechniczny 86, 323–333 (2010)

[28] Kostrzewa, D., Josiński, H.: Verification of the search space exploration strategy based on the solutions of the join ordering problem. In: Czachórski, T., Kozielski, S., Stańczyk, U. (eds.) Man-Machine Interactions 2. AISC, vol. 103, pp. 447–455. Springer, Heidelberg (2011)

[29] Demski, P., Mikulski, M., Koteras, R.: Characterization of Hokuyo UTM-30LX laser range finder for an autonomous mobile robot. In: Nawrat, A., Simek, K., Świerniak, A. (eds.) Advanced Technologies for Intelligent Systems. SCI, vol. 440, pp. 143–153. Springer, Heidelberg (2013)

[30] Skorkowski, A., Topor-Kaminski, T.: Analysis of EGNOS-augmented receiver positioning accuracy. Acta Physica Polonica A 122(5), 821–824 (2012)

[31] Daniec, K., Jedrasiak, K., Koteras, R., Nawrat, A.: Embedded micro inertial navigation system. Applied Mechanics and Materials 249-250, 1234–1246 (2013)

[32] Iwaneczko, P., Jędrasiak, K., Daniec, K., Nawrat, A.: A prototype of unmanned aerial vehicle for image acquisition. In: Bolc, L., Tadeusiewicz, R., Chmielewski, L.J., Wojciechowski, K. (eds.) ICCVG 2012. LNCS, vol. 7594, pp. 87–94. Springer, Heidelberg (2012)

[33] Jędrasiak, K., Nawrat, A., Wydmańska, K.: SETh-link the distributed management system for unmanned mobile vehicles. In: Nawrat, A., Simek, K., Świerniak, A. (eds.) Advanced Technologies for Intelligent Systems. SCI, vol. 440, pp. 247–256. Springer, Heidelberg (2013)

Part II
Construction of Image Acquisition Devices Used in UAV Applications

Unmanned Aerial Vehicles are utilized by a variety of uniform services and armed forces. They are also used by search and rescue units. All of the above institutions commonly operate regardless the weather and day/night conditions. This is associated with many challenges to overcome by complex algorithms and innovative video acquisition devices. Combustion engines used in larger UAVs introduce a large amount of high frequency

Additionally during flight in harsh conditions the wind speed is sufficient for unexpected UAV rotation. It has to be compensated by some kind of mechanism capable of 3-DOF rotating camera line of sight. It could be achieved by mechanical construction called gimbal, combination of lenses and optical mechanism or a wide angle of sight e.g. fish eye camera. However operating an UAV is harsh weather conditions can lead to blockage of the mechanical mechanism. In the chapter is also presented an innovative omnidirectional video acquisition device that is composed from multiple cameras with a line of sight covering half of the sphere. There is no mechanical or optical mechanism therefore it is free from the mentioned disadvantages. Additionally due to its multiple camera nature the combined video stream resolution is many times greater than in traditionally used cameras. Moreover it is possible to almost immediately rotate the image by any angle.

Unfortunately traditionally used visible light cameras cover only a small part of the magnetic spectrum and are easily covered by dust, smoke, fog, etc. In order to continue aerial observation thermal imaging cameras have to be used. Such devices can be mounted onboard an UAV and used for observation, target detection, tracking and recognition in challenging weather conditions and low light conditions. Thus providing full day/night observation capability. Thermal imaging cameras along with visible light cameras can be mounted in the single gimbal in order to provide the possibility for image fusion resulting in highlighting the most valuable information from both video sources.

Nowadays, image acquisition devices are mainly used by human operators or large tactical or strategic class UAVs. Therefore there is a need for innovative video sources that are characterized by small weight, low energy consumption and at the same time high resistance to vibrations, shock and temperature. It is a challenging task for developers and difficult compromises have to be made. The chapter presents many of the mentioned challenges along with example solutions and useful and practical suggestions. One of such practical suggestions in an omnidirectional video acquisition device. It is an innovative concept that may find many applications both civilian and military. It can be used to observe areas that may need wide area monitoring such as shops, banks, petrol stations. In military installations OVAD may be used to patrol the area from the ground or from the air. Application allows capturing images from chosen camera. It is possible to immediately switch between cameras or also move around the panorama created from multiple video streams, like in rotating camera. Panorama contains combined view of entire area around device.

Thermal Camera for Autonomous
Mobile Platforms

Grzegorz Bieszczad, Michał Krupiński, Henryk Madura, and Tomasz Sosnowski

Abstract. Unmanned Aerial Vehicles (UAVs) have found many applications, both civilian and military. They can be used by armed forces, police, border guard, customs office, search and rescue units but also in scientific research, power and civil engineering and environmental monitoring. However, regardless of actual application, there is always a requirement for an observation system capable of providing visual data in low light, harsh weather conditions and during nighttime. In the paper the construction of high resolution thermal camera is presented, fitted with microbolometer 640x480 focal plane array operating in 8÷12 μm spectral range. This lightweight and energy efficient device can be mounted onboard an UAV for observation, target detection and recognition in difficult weather and low light conditions and in low visibility situations caused by dust, smoke or fog. The described camera provides full day/night observation capability.

1   Introduction

There are many situations in which UAVs are used as an element of surveillance system, delivering valuable data on actual situation and objects over monitored area. To fulfill such a task, UAVs are usually equipped with various types of sensors and cameras to ensure detection, recognition and identification of phenomena and objects regardless of weather conditions and time of day. A thermal camera with high spatial resolution is a perfect example of an imaging sensor that can significantly enhance the detection, recognition and identification capability of an observation system, which in turn can be simplified and even automated [1, 2, 5, 10, 14]. Simultaneous analysis of image data in two information channels (visual and infrared) gives both the possibility of night operation and increases the

Grzegorz Bieszczad · Michał Krupiński · Henryk Madura · Tomasz Sosnowski
Military University of Technology, Institute of Optoelectronics,
Warsaw, Poland
e-mail:{tsosnowski,hmadura,gbieszczad,mkrupinski}@wat.edu.pl

effectiveness of implemented algorithms for object identification [2, 10, 11]. The application of a thermal camera gives also the possibility to assess the current status and the previous actions of objects by analyzing their thermal signatures (e.g. barrel temperature or engine temperature) [1, 2, 14]. It is also possible to detect concealed, camouflaged objects. It is then possible to mount a high resolution thermal camera with a focal plane array (640x480 pixels, 17 μm pixel pitch, spectral range 8÷12 μm) onboard an UAV. Devices designed for UAVs should be lightweight, small and energy-efficient, so an uncooled microbolometer focal plane array was chosen for the onboard thermal camera. Due to constant progress in microbolometer detector technology its current generation provide high sensitivity, small pixel size and lowered power consumption. Most significant advantage of microbolometer detectors is their ability to work at ambient temperature.

2   General Construction of High Resolution Thermal Camera

High resolution, observation thermal camera is meant for area surveillance and target detection in any time of day, regardless of light conditions and weather (including light fog or smoke) [2]. Cross section and real photo of the designed high resolution thermal camera is presented in Fig. 1.
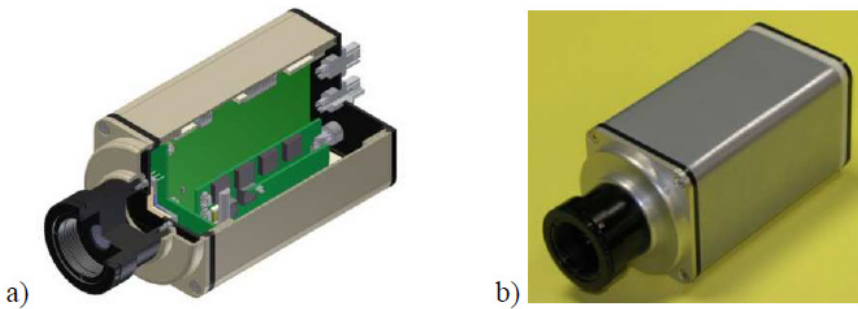
Fig. 1. CAD project (a) and real photo (b) of high resolution thermal camera

The following elements can be distinguished in the construction of a thermal camera: lens (specially designed for infrared spectral range), focal plane array (FPA), digital image processing and control module, power supply and video display module [12, 13]. General block diagram of a thermal camera is presented in Fig. 2.

Power supply must feed the various camera component and meet very strict noise requirements. During the design of power supply for the camera with microbolometer FPA it was necessary to provide several different voltages supplying different camera components. All those voltages are obtained from single external supplying voltage by using switched mode power supplies instead of linear regulated ones. It increased the efficiency and resulted in lower heat dissipation inside
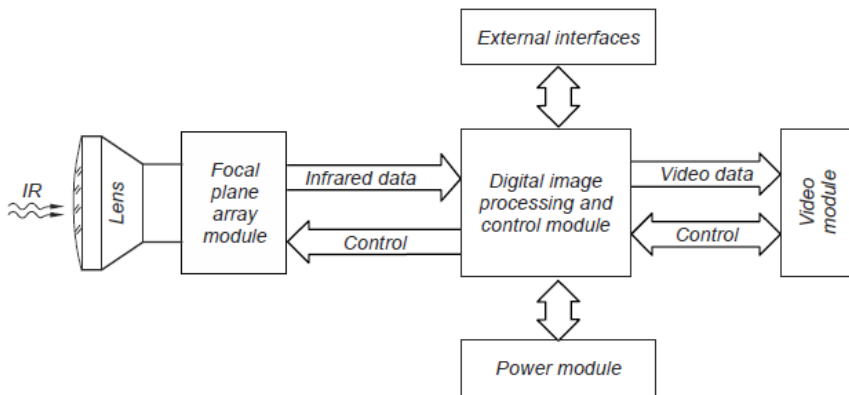
Fig. 2. General block diagram of a thermal camera with all main functional blocks

the camera case. Low power operation and the flexible range of external supplying voltages are also important features of the presented camera. It was assumed, during the design of camera electronic modules, that the camera will accept supplying voltages in the 6V – 12V range. The device can be supplied from typical regular or rechargeable batteries thus allowing the camera to be applied even in mobile systems with autonomous power sources of limited capacity.

2.1   Lens Module

Objective lens for far infrared spectral range is one of the most technologically sophisticated camera components. Its complexity is caused by the requirements for wide field of view, small overall dimensions, wide range of operating temperatures, anti-reflex coatings resistant to environmental conditions and the resolution matching 17 μm pixel pitch of a FPA. Those requirements imposed the application of modern design approach and materials. The lens features aspherical germanium optical elements which reduced the total number of optical elements in the lens design. And due to wide temperature range the passive athermalization of the lens was necessary.

Each optical system is prone to misalignment due to temperature changes. Ambient temperature variations significantly affect the imaging quality of far infrared lens, because of material properties, such as coefficient of thermal expansion and thermal coefficient of refraction. As a result dimensions of mechanical and optical elements as well as optical properties of germanium change with temperature. Usually both those undesired effects do not compensate themselves but they are additive. As a result the focal length is shortened as the temperature rises. Furthermore the FPA itself, due to thermal expansion of the case and mount, is moved away from the reference focal plane.

In order to create the lens operating within 1/4 wave Raleigh criteria in the whole -40C° to +60C° temperature range the particular elements were designed in

such a way to provide compensation of both aforementioned undesired effects. The applied passive athermalization was achieved through certain design solutions and application of materials with appropriate thermal expansion properties, which made it possible to obtain compensation movement of desired magnitude. As a result the optical system was created with the following parameters:

- Focal length 12mm,
- Field of view (for 640 x 480 FPA, 17 um pixel pitch): HFOV~49 VFOW~38
- F-number 1.25,
- weight 29.5g.

It was confirmed during research that the use of a single aspherical lens provides good imaging quality, light weight and simplified mechanical mount of the result-ing obje tive lens. Thus, in spite of complex dual-housing structure the compact unit was obtained and applied athermalization is sufficiently effective in the whole range of operating temperatures. Limiting the number of optical surfaces is also beneficial in terms of transmission losses, which is particularly important in infra-red optical sys-tems made of germanium, a material with high refractive index. The losses can be minimized by lens coatings, but the reduction of the number of optical elements is also important. The resulting objective lens, in spite of a fairy large field of view, provides quite uniform illumination of a focal plane array.

2.2   Focal Plane Array Module

Focal plane array module is the next one of the technologically advanced camera blocks. It is composed of a microbolometer focal plane array and a PCB board with read-out, control and power supply circuits.

   In the presented high resolution thermal camera the FPA made of amorphous silicon was applied. It is an uncooled infrared detector and its spectral range is defined by an optical filter, mounted as an outer cover of a detector case.
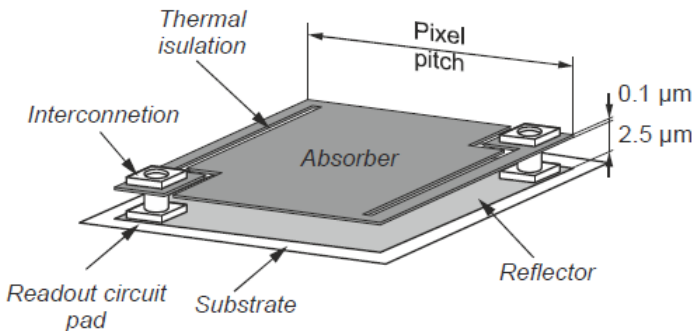
Fig. 3. Single pixel of a microbolometer focal plane array

The applied infrared FPA has 640 by 480 single IR detectors (bolometers) . An active bolometer is made of a silicone membrane covered by an IR absorber. A single detector is a micro electro-mechanical structure. In such structure the detecting element is physically (and thermally) insulated from the rest of the components, including FPA housing. The schematic construction of a single detector in microbolometer array is shown in Fig. 3.
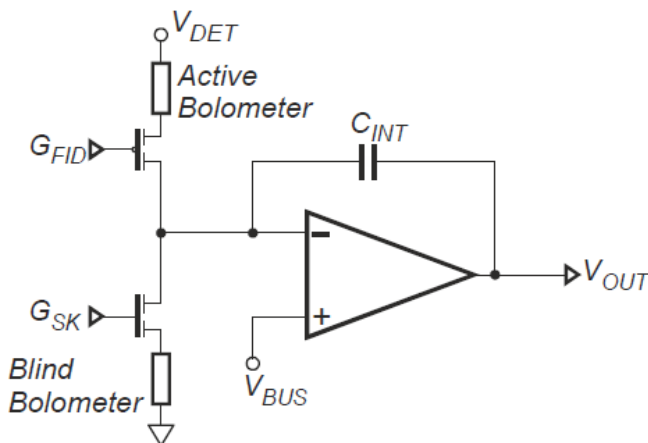
Fig. 4. Simplified diagram of a single pixel read-out circuit

Each individual bolometer is connected to a read-out circuit, which converts the resistance changes into proportional electric signal (voltage). The resistance variations are caused by temperature change of an active bolometer, introduced by total FPA temperature and incident infrared radiation. The conversion of bolometer resistance into voltage signal is performed in a circuit depicted in Fig. 4.

Current-to-voltage converter is applied to obtain electric signal from individual bolometers. The charging current of integrator capacitance C_{INT} is defined by the voltages V_{DET} and V_{BUS} and the resistances of a bolometer and MOSFET transistor. Integration time is set depending on actual frame rate. The portion of total bolometer resistance resulting from bolometer own temperature is also included in the conversion process. To determine its value the "blind" bolometer is applied, covered from incident radiation. Voltages G_{SK}, G_{FID}, V_{DET} and V_{BUS} that directly influence the output signal are shown in Fig. 4. The level of those voltages as well as precision and resolution of their setting determine the dynamic range and the quality of output image. As a result those voltages (values and noise levels) are strictly defined by a FPA manufacturer. Noise parameters of analogue supplying voltages are particularly important and they are defined by manufacturer over specified frequency bands. Allowed values are presented a table 1.

Table 1. Noise requirements for FPS supplying voltages

Voltage	Noise level	Measurement band
V_{BUS}	100 μV	1 Hz ÷ 10 MHz
G_{FID}, V_{DET}, G_{SK}	2 μV	1 Hz ÷ 10 MHz
	5 μV	1 Hz ÷ 10 kHz
	100 μV	1 Hz ÷ 10 MHz

Generally speaking, focal plane array module must provide analogue and digital supplying voltages for an array, analogue control signals for a FPA and buffering of digital control signals. This module should also include analog output stage.
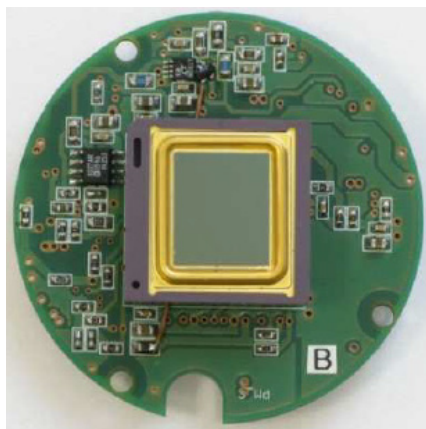
Fig. 5. Photo of a PCB board with FPA array (17 $\boldsymbol{\mu m}$ pixel pitch)

In the presented camera a state-of-the-art array awas applied, with 640x480 pixels and 17 μm pixel pitch. Due to small pixel size (and consequently smaller linear dimesions of an array) the size of objective lens could be reduced, which also contributed to lower weight of the whole camera. In Fig. 5 the printed circuit board is shown with mounted focal plane array.

3 Digital Image Processing and Control Module

In high resolution thermal cameras the fast image processing system has to be applied, which combines significant processing speed with a low power consumption. Additionally modern system has to be flexible, ready to perform different tasks wit out significant hardware modifications. Digital processing in high resolution cameras involves considerable amount of data, which must be processed within defined time window [8, 12, 13]. Data should be processed on the fly (in real time) without introducing excess latencies. For the continuity of data processing the system latencies should be constant, i.e. they cannot cumulate over time. This requires parallelization of image data processing.

Main tasks performed by digital image processing and control module are: controlling the array in order to read-out the values of detector signals, correction of detector non-uniformity (NUC), bad pixel mapping and preparing the data for video display module.
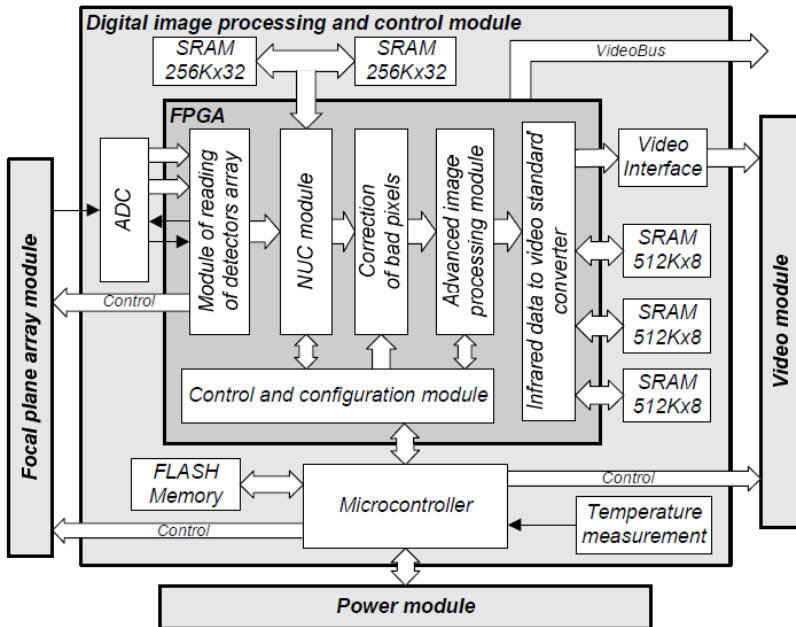
Fig. 6. Functional block diagram of FPGA-based digital image processing and control module

The module was constructed around two main integrated circuits: Field Programmable Gate Array (FPGA) and a microcontroller. Programmable FPGA integrated circuit realizes image processing, which demands considerable processing power. The main tasks of FPGA device are: generating timing signals for infrared array, performing non-uniformity correction, replacement of so-called bad pixels and generation of signals for video display module. Microcontroller is responsible for controlling of all modules in camera and participates in other tasks that do not demand significant processing power. The block diagram of control and image processing module with FPGA device is shown on a Fig. 6, and the photo of the real camera module is presented in Fig. 7.

The main tasks of microcontroller is supervising the image processing chain on every step and communicating with interfaces connected to camera. In particular he microcontroller is responsible for configuring and adjusting biasing voltages for detector array, measuring the FPA and ambient temperatures, controlling the shutter and the process of auto calibration, configuring of video display, modifying and calculating coefficients needed for non-uniformity correction algorithm.

Fig. 7. Printed circuit board of FPGA-based digital image processing and control module

As the microprocessor for the control and image processing module the LPC2292 from NXP was chosen, which is a member of 32-bit ARM7 family. This microcontroller is based on 32-bit CPUs of ARM7TDMI-S type, with 256 kB of internal flash memory. It has 128 bit internal memory interface and unique architecture capable to execute 32-bit program code with high efficiency. It also has low power consumption and rich set of peripherals like 10-bit analog-to-digital converter, 32 timers and communication modules compatible with standards like SPI, I2C, CAN and UART. What is more, a LPC2292 microcontroller has a sufficient number of general purpose input-output (GPIO) ports and external memory interface. The connection between microprocessor and a FPGA circuit by a special communication bus was supported by this last interface.

4   Image Processing Modules Implemented in FPGA

Because of rather high computation power demands and parallelization of image processing, FPGA device EP2C35F672 from ALTERA was applied in control and image processing module . This FPGA integrated circuit provides adequate speed and relatively low power consumption. Applied FPGA device has large number of IO ports, 33 216 logic elements (LEs), 483 840 bits of internal RAM memory, four PLL circuits that allows to generate a series of precision timing signals and 35 hardware multipliers for DSP operations. Hardware multipliers are necessary for building fast and sophisticated digital processing modules consuming low amount of logic resources and with low power demands. In FPGA device the following modules were implemented for the needs of real-time image processing: detector array readout module [12, 13], NUC module [4], bad pixel replacement module, image processing module and image display module.

4.1   VideoBus

In FPGA circuit a special bus was designed to interface image processing modules with each other. All modules implemented in FPGA structure are exchanging image data via VideoBus link, what is schematically illustrated in Fig. 8.
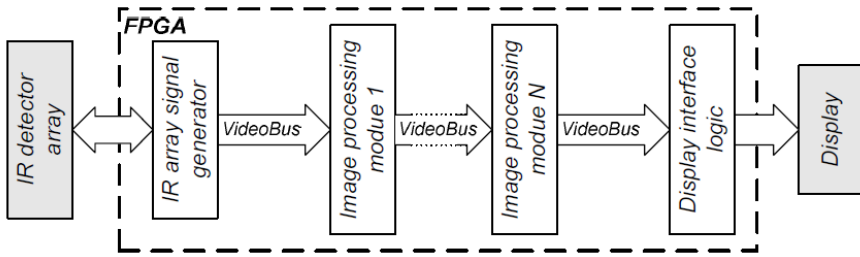
Fig. 8. Block diagram of data processing chain implemented in FPGA

Thanks to uniform VideoBus interface there is a possibility to change the order of executed image processing operations without any need of modifying the modules. The modules are designed in such a way that they can be made transparent to incoming data, passing data through without modification. This feature allows to dynamically control the image data processing.

VideoBus link is composed of 14-bit video data bus (VDATA), vertical synchronization signal (VSYNC), horizontal synchronization signal (HSYNC) and strobe signal (STB). Vertical synchronization signal (VSYNC) is high during transfer of the frame signal. Horizontal synchronization signal (HSYNC) is high during transfer of data related with single line in the frame. The change of strobe signal from low to high state (leading edge) indicates valid data on the Video data (VDATA) bus that is ready to be received. Data on VDATA bus are maintained during the high state of STB signal. VSYNC and HSYNC signals assume high state before the occurrence of first leading edge of STB signal. Timing diagram of signals over VideoBus link are presented in Fig. 9.
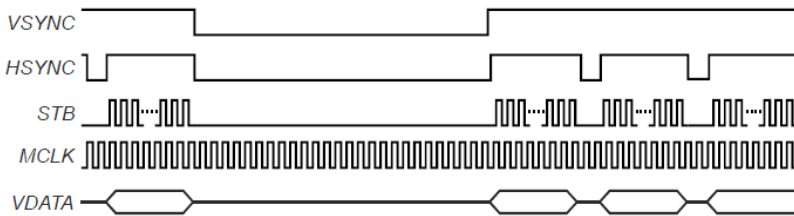
Fig. 9. Timing diagram of signals in VideoBus

4.2   Detector Array Readout Module

The main tasks of detector array readout module is generation of signals driving internal circuitry of detector array to enable reading the signals from all consecutive detectors (pixels). Designed circuit generates the appropriate control signals in a proper sequence, which causes the array output signal to appear at analog or digital output terminal. This signal is a response of the detector and is proportional to the incident infrared radiation.
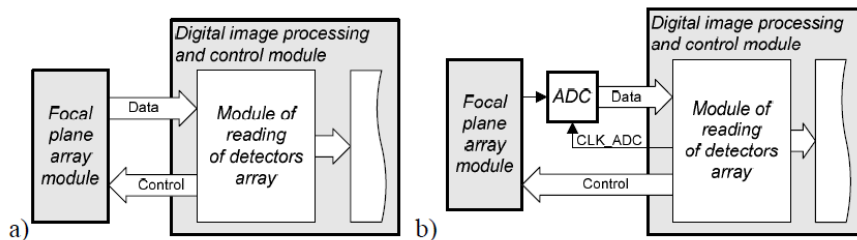
Fig. 10. Read-out circuit for an FPA array with digial (a) and analog (b) output

There are two types of detector array readout interfaces. One is a digital inter-
face, when the array has internal analog-to-digital converter [13]. The block dia-
gram illustrating the connection to such device is presented in Fig. 10a. The main
advantage of that solution is that there is no additional ADC element present in the
device. This can simplify the design, but the use of an internal ADC can some-
times have a negative impact on NETD parameter of the camera.
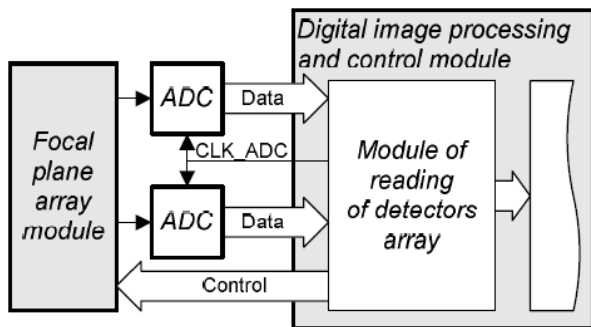
Fig. 11. Read-out circuit for an FPA array with dual analog output

The second interface type is the analog one. In this case an external analog-to-
digital converter is necessary to connect analog array output to digital processing
system. The block diagram of this solution is shown in Fig. 10b. Read-out module
generates control signals not only for an array, but also for ADC converter. Addi-
tionally the input range of a converter must be adjusted to the dynamic range of
array output. This gives the designer full control over the dynamic range of output
signal High resolution infrared arrays (640x480 and higher) have commonly more
than one analog output (usually two or four), providing simultaneous readout from
several detectors. For this type of arrays there is a need to interface to all outputs
using several synchronized analog-to-digital converters. An example readout sys-
tem with two channel analog-to-digital converter is shown in Fig. 11.

In general the readout circuit contains a buffer and ADC converter. On Fig. 10
and Fig. 11 both elements were schematically illustrated as one functional block –
an ADC converter. In fact the analog output of dete tor array has strictly defined

parameters like output impedance and possible output current. That is why it cannot be loaded with resistance lower than nominal (for example 100 kΩ). The majority of fast analog-to-digital converters have low input I pedance, so separate buffer is necessary. Additionally the buffer can be used to adjust the dynamic ranges of both devices – detector array and ADC. The most important parameters of ADC are resolution and speed. Sampling frequency of a converter depends on array design (readout speed and the number of outputs) and on frame rate. The required resolution of ADC is a result of signal to noise ratio (*SNR*) at the output of detector array If the amplitude of the noise in the array is U_N, the amplitude of the signal is U_S, then the *SNR* is given by:

$$SNR = \frac{U_S}{U_N} \tag{1}$$

and the minimal resolution of ADC converter can be then calculated according to the formula:

$$N \geq log_2(SNR), \tag{2}$$

where N is a minimal bit count of ADC converter word.

Digital signals driving detector array, has to be generated for every type of the detector. The task is complex, because different types of detector arrays have different interfaces and demands different signals and timings, even in case of the same manufacturer. A block diagram of UL 04 27 2 detector readout module realized as a FPGA functional block is shown in Fig 12.
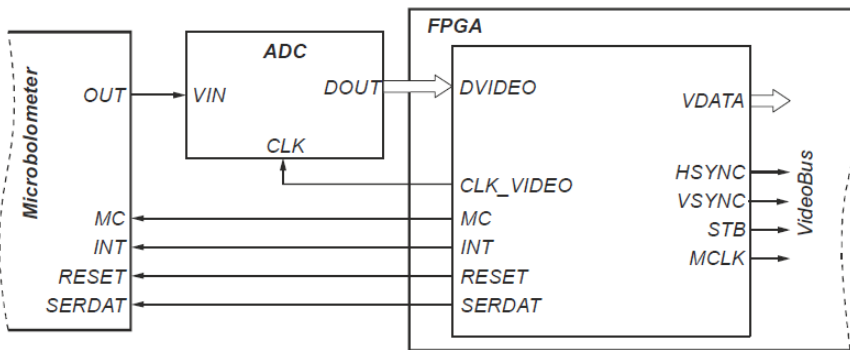
Fig. 12. Block diagram of read-out control module for ULIS' UL 04 27 2 microbolometer FPA

The digital signals for controlling the microbolometer array can be divided into two groups. One is to provide proper timing during readout from detectors whereas the second is used for array configuration. First group includes RESET, INT, MC and CLK_VIDEO. Execution of the module results in reading all the pixel values which are then sent for further processing via image data bus [8, 12, 13]. Example signal diagrams for UL 04 27 2 array are shown on Fig. 13.
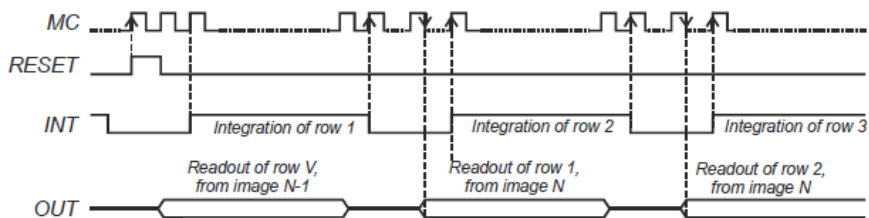
Fig. 13. Timing diagram of control signals for ULIS' UL 04 27 2 microbolometer FPA

A special control circuit was designed to read the signals from the particular detectors in an array. Its purpose is to obtain for of each detector signal proportional to incident IR radiation its digital representation. Data is further sent to other camera blocks by VideoBus link. All analog detector signals (OUT) need to be converted into digital form (DVIDEO). Conversion was performed by ADC converter, which requires clock signal (CLK_VIDEO).
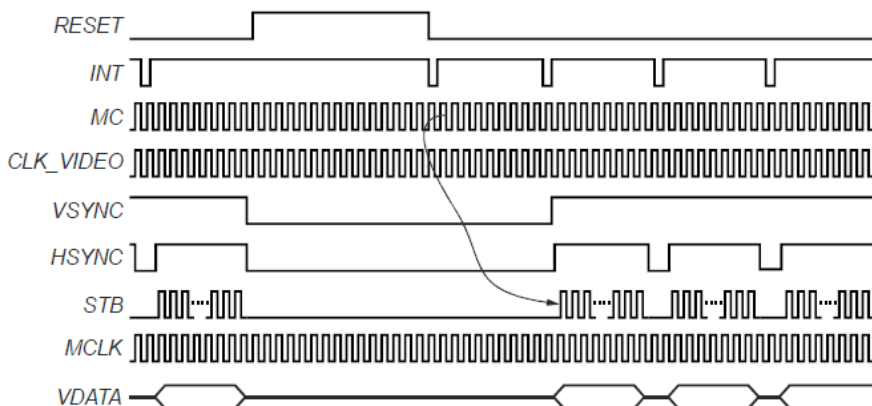
Fig. 14. Timing diagrm of control signals for ULIS' UL 04 27 2 microbolometer FPA

According to array catalogue data all control signal can be generated using single clock signal with MC period. To do this a module was realized with 5-state machine and two synchronous counters. First counter is used to determine the states of RESET signal and for counting clock cycles during the readout of an entire frame. Second counter is used to determine the states of INT and MC signals and performs cycle count during single row readout. On the basis of RESET, INT and MC signals the following VideoBus signals are simultaneously generated: VSYNC, HSYNC, STD, MCLK, VDATA. During the operation of UL 04 27 2 microbolometer array the signals on the output of array are delayed by the time of one row from the integration trigger signal. This is because at the beginning of each frame readout the signals from first row detectors are integrated. Then, during the readout of first row detectors the signals from second row detectors are integrated and the pattern is repeated for the consecutive rows. As a result the total

number of signals for row readout is larger by one than the total number of rows in the array. Example signals generated for microbolometer array are shown on Fig. 14.

The applied ADC converter AD9251 from ANALOG DEVICES has its own latency needed to process incoming analog signal that equals to 9 clock cycles. This means that the result of analog-to-digital conversion is available after tenth measurement is triggered.

4.3 Bad Pixel Replacement Module

Practically in all detector arrays here are some detectors that are not working properly, thus the signal from detected bad pixel has to be eliminated and replaced. During the calibration process the defective pixels are identified when they return incorrect signal value. On this basis the bad pixel map is stored in memory, where every bit corresponds to one detector in an array. If the detector is recognized as bad (meaning its output needs to be corrected) then the corresponding memory value is '1'. In case of good detector (no correction required) the value is '0'. The memory value is used to determinate if the signal from the detector will be displayed. For faulty detector the output value of previous good pixel is substituted instead. The simplified architecture of module realizing this algorithm is shown on Fig. 15.
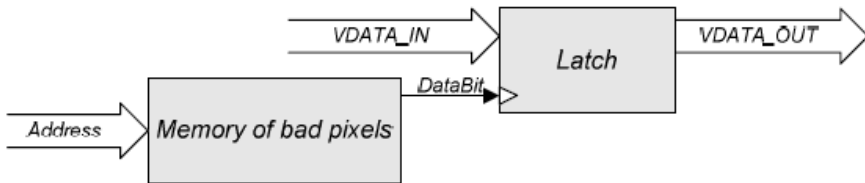
Fig. 15. Operation of bad pixel replacement module

4.4 Video Module

One of the problems encountered in digital image processing is the case when the read-out rate of an array differs from displaying frame rate. And for thermal cameras the displaying frame rate is usually higher. Thus the special module has to be applied, which simplified operation is schematically presented in Fig. 16.

Video module uses two external memories SRAM 1 and SRAM 2. Data from single frame is written to one of the memories (for example SRAM 1). At the same time data to be displayed is being read from second memory (SRAM 2). When whole data from single frame is entirely stored in the first memory, special "Memory select" signal is triggered and the roles of SRAM 1 and SRAM 2 memories are reversed. Now the next frame data is being written to SRAM 2 memory and SRAM 1 data is being read and displayed.
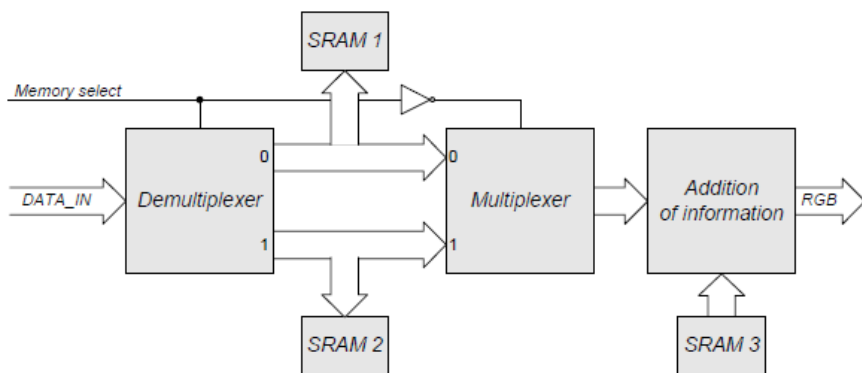
Fig. 16. Operation of module for video displaying and adding additional information to output video data stream

Another function performed by this module is adding additional information to independent video stream. This function is used to implement user interface and to show vital information like e.g. battery level. The video module includes also VGA controller which provides signals for an external display.

4.5 Non-uniformity Correction Module

Infrared detector array always exhibits characteristic non-uniformity of detector responses to uniform incident radiation power [3, 4, 6, 7, 9]. Microbolometer FPA, features unwanted detector gain and offset differences between particular pixel detectors. It is caused by imperfection of individual detectors and readout circuit, characteristic to used technological process as well as array temperature. The effect of non-uniformity of detectors in an array is so called Fixed Pattern Noise (FPN) superimposed on the output image, which decreases the spatial NETD of a thermal imaging camera.

Non-uniformity correction (NUC) consists in digital conversion of output signal from an array in order to eliminate FPN in resulting thermal image. To eliminate non-uniformity effects in the camera, various NUC methods are employed. The most common approach is to process the data from detector digitally. Correction data (NUC correction coefficients) are determined during calibration process where dete tors are exposed to uniform infrared radiation references.

The most principal non-uniformity correction method is so called two-point correction (TPC) algorithm. TPC algorithm is realized according to the formula [4, 7]:

$$Y_{ij}^* = G_{ij}Y_{ij} + O_{ij} \tag{3}$$

where Y_{ij} is a digital value of detector response from *i-th* row and *j-th* column (i, j), G_{ij} and O_{ij} are respectively a gain and offset correction coefficients, and Y_{ij}^* is a corrected value. NUC coefficients for two point correction are calculated during calibration according to formulas [4, 7]:

$$G_{ij} = \frac{Y(T_H) - Y(T_L)}{Y_{ij}(T_H) - Y_{ij}(T_L)}, \tag{4}$$

$$O_{ij} = \frac{Y(T_L)Y_{ij}(T_H) - Y(T_H)Y_{ij}(T_L)}{Y_{ij}(T_H) - Y_{ij}(T_L)}, \tag{5}$$

where $Y_{ij}(T_H)$ and $Y_{ij}(T_L)$ are digital values of detectors response for higher (T_H) and lower (T_L) temperature of uniform reference black body, $Y(T_H)$ and $Y(T_L)$ are mean values of array response for temperatures TH and TL of black body, given by:

$$Y(T) = \frac{1}{MN} \sum_{i=1}^{M} \sum_{j=1}^{N} Y_{ij}(T). \tag{6}$$
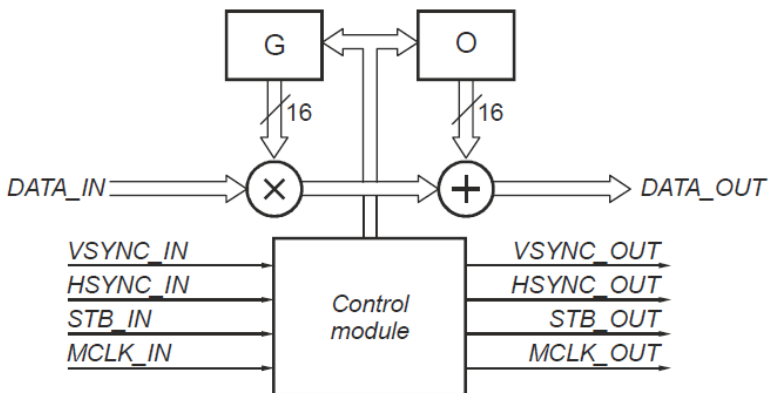
Fig. 17. Block diagram of a hardware NUC correction
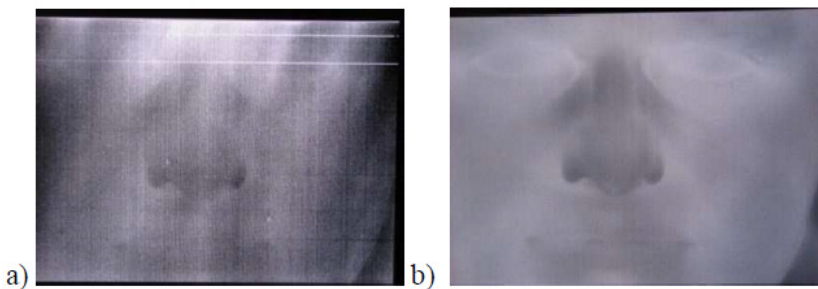
Fig. 18. Sample thermal image before (a) and after (b) NUC correction

On the basis of analysis and simulations the 14-bit resolution of video data (resolution of ADC converter) and 16-bit correction coefficients were adopted [3, 4]. From equation (3) came off that the digital module realizing TPC algorithm

has to make one multiplication and one addition operation. To increase the precision of NUC calculations (which are made on fixed-point digits) the coefficients must be resized accordingly. Block diagram of hardware realization of TPC algorithm for thermal camera is presented on Fig. 17.

In this hardware realization the correction is realized "on the fly". Time of calculation is shorter than the time between reading succeeding detectors. The module is designed to have inputs and outputs compatible with internal VideoBus link. Non-uniformity correction module was described in VHDL language as a parameterized entity. D signer can change (when needed) the parameters of the module like size of actual infrared detector array, length of video data word and length of coefficient data word. Because of that feature this module can be used for any array size. Fig. 18 shows two thermal images: one taken before and one after NUC correction performed by the described module.

5   Calibration, Measurement and Determination of Thermal Camera Parameters

Procedure used to determine the correction coefficients according to TPC algorithm is performed on a test stand [9] with two blackbodies at temperatures TL and TH, respe tively. The stand with mounted camera is kept at constant ambient temperature (e.g. in climate chamber). After switching on the camera, prior to measurements it is ne essary to wait until the array and camera housing temperatures stabilize. Then the calibration procedure may begin. The test stand used for the determination of NUC coefficients is shown in Fig. 19. Averaged array response values for TL and TH temperatures, used for NUC coefficient calculations, are called calibration points. Basic calibration points are the array averaged responses for the temperatures TL = 20°C and TH = 40°C. Calculated correction coefficients Gij i Oij are stored in camera's internal memory. In each detector array a faulty pixels (detectors) can be found, due to manufacturing defects. Those detectors, referred to as "bad pixels" are usually found during calibration. There are several ways to identify bad pixels:

- on the basis of detector gain,
- on the basis of detector offset,
- on the basis of detector noise.

Identification of bad pixels on the basis of detector gain is performed using a threshold value. A pixel is considered bad if its gain coefficient in a NUC table differs from nominal value by more than selected percentage value. For example, if the threshold value is 25% then all the detectors with gain coefficients below 0.75 and above 1.25 are considered bad.

Fig. 19. Test stand for determining NUC correction coefficients and bad pixel identification in microbolometer focal plane array
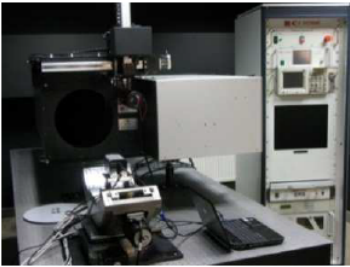
Fig. 20. Test stands for the determination of parameters of thermal cameras (Accredited Laboratory of Institute of Optoelectronics, MUT)

Similarly the identification of bad pixels on the basis of detector offset is carried out. Pixel is considered bad if its offset correction coefficient in NUC table is smaller or greater than defined percentage value (e.g. 30%).

Using detector noise criteria the pixel is marked as bad if its noise level (RMS) exceeds the defined threshold value. For example, for a given noise level (mean value of 5.0 and standard deviation of 1.0) and a threshold set at 3.5, the pixel is considered bad when its RMS noise value exceeds 8.5.

The measurements of basic parameters of the presented thermal camera were performed at the Institute of Optoelectronics on the specialized test stand for the evaluation of thermal cameras [9]. The test stand consists of a collimator, IR radiation standards with control units, rotating test and filter wheels and a computer with video grabber card and specialized software (Fig. 20).

The following camera characteristics were measured on this test stand:

- modulation transfer function MTF,
- signal transfer SiTF,
- minimum resolvable temperature difference (MRTD) characteristics,
- 3D noise model.

MTF function describes the image distortions introduced by a camera. It is defined an a module from normalized to unity FFT transform of luminance distribution in a point source image, for null spatial frequency.

On the basis of derived MRTD characteristics the detection, recognition and identification ranges were calculated for a standard NATO target, according to STANAG 4347. Spatial noise of an imaging system can be calculated using 3D noise model. Each noise component of a system influences the image quality. The analysis of the contribution of each particular noise source is difficult, or rather impossible, as the influence of different noise sources may result in the same type of image degradation. Thus in order to perform noise analysis the 3D noise model was introduced.

In order to determine 3D noise components several images of uniform background were acquired and on this basis the matrix noise model of camera system was created.

6 Summary

The presented high resolution thermal camera with microbolometer focal plane array made of amorphous silicon operates in 8-12 μm spectral range. The applied FPA array, made by ULIS (France), has a size of 640x480 pixels, which amounts to the total number of 307 200 infrared detectors. Thermal resolution is 0.08 degrees Celsius and spatial resolution reaches 1.35 mrad. Such parameters allow for the detection of a human being from over 1300 meters' distance. The camera is equipped with atheromalized lens with single FOV of about 50° and F-number of 1.25. The applied passively athermalized lens can operate in a broad temperature range without the need of man al refocusing.

Fig. 21. Sample image produced by the presented high resolution thermal camera

   High resolution of the applied focal plane array together with relatively high thermal sensitivity allowed to achieve quite long detection, recognition and identification ranges. The observations of real objects were performed during field tests in various visibility conditions. Sample thermal image of a group of persons and passenger cars is shown in Fig. 21.

   The developed camera is a small, lightweight and efficient device with low power consumption. It can be applied in surveillance, reconnaissance and defense systems mounted onboard unmanned aerial vehicles.

References

[1]   Kastek, M., Sosnowski, T., Orzanowski, T., Kopczyński, K., Kwaśny, M.: Multispectral gas detection method. WIT Transactions on Ecology and the Environment 123, 227–236 (2009)

[2]   Madura, H.: Method of signal processing in passive infrared detectors for security systems. Computational Methods and Experimental Measurements, WIT Transactions on Modelling and Simulation 46, 757–768 (2007)

[3]   Bieszczad, G., Orzanowski, T., Sosnowski, T., Kastek, M.: Method of detectors offset correction in thermovision camera with uncooled microbolometric focal plane array. In: Proceedings of SPIE - The International Society for Optical Engineering, vol. 7481, art. no. 748100 (2009)

[4]   Orżanowski, T., Madura, H., Kastek, M., Sosnowski, T.: Nonuniformity correction algorithm for microbolometer infrared focal plane array. In: Advanced Infrared Technology and Applications, AITA 9, Leon, November 8-12 (2007)

[5]   Bieszczad, G., Sosnowski, T., Madura, H.: Improved sum-of-squared-differences tracking algorithm for thermal vision systems. In: Proceedings of SPIE - The International Society for Optical Engineering, vol. 8193, art. no. 81932R (2011)

[6]   Venkateswarlu, R., Er, M.H., Gan, Y.H., Fong, Y.C.: Nonuniformity compensation for IR focal plane array sensors. In: Proc. SPIE, vol. 3061, pp. 915–926 (1997)

[7]   Zhou, B., Wang, Y., Ye, Y., Wu, X., Ying, J.: Realize multi-point method for realtime correction of nonuniformity of uncooled IRFPA. In: Proc. SPIE, vol. 5640, pp. 368–375 (2005); Booth, N., Smith, A.S.: Infrared Detectors, pp. 241–248. Goodwin House Publishers, New York (1997)

[8]   Bieszczad, G., Sosnowski, T., Madura, H., Kastek, M., Barela, J.: Adaptable infrared image processing module implemented in FPGA. In: Proceedings of SPIE - The International Society for Optical Engineering, vol. 7660, art. no. 76603Z (2010)

[9]   Sosnowski, T., Bieszczad, G., Madura, H., Kastek, M., Firmanty, K.: The calibration stand for thermal camera module with cooled infrared focal plane array. In: Proceedings of SPIE - The International Society for Optical Engineering, vol. 7660, art. no. 76603Y (2010)

[10] Madura, H., Kołodziejczyk, M.: Influence of sun radiation on results of non-contact temperature measurements in far infrared range. Opto-electronics Review 13(3), 253–257 (2005)

[11] Krupiński, M., Sosnowski, T., Madura, H., Dabrowski, M.: Infrared and visible im-
      age registration algorithm [Algorytm syntezy obrazu termowizyjnego z obrazem z
      kamery wideo]. Przeglad Elektrotechniczny 88(11 B), 83–86 (2012)
[12] Sosnowski, T., Bieszczad, G., Kastek, M., Madura, H.: Processing of the image from
      infrared focal plane array using FPGA-based system. In: Proceedings of the 17th In-
      ternational Conference - Mixed Design of Integrated Circuits and Systems,
      MIXDES 2010, art. no. 5551280, pp. 581–586 (2010)
[13] Sosnowski, T., Bieszczad, G., Kastek, M., Madura, H.: Digital image processing in
      high resolution infrared camera with use of programmable logic device. In: Proceed-
      ings of SPIE - The International Society for Optical Engineering, vol. 7838, art. no.
      78380U (2010)
[14] Kastek, M., Dulski, R., Trzaskawka, P., Sosnowski, T., Madura, H.: Concept of
      infrared sensor module for sniper detection system. In: IRMMW-THz 2010 - 35th
      International Conference on Infrared, Millimeter, and Terahertz Waves, Conference
      Guide, art. no. 5612447 (2010)

Gyro-Stabilized Platform for Multispectral Image Acquisition

Damian Bereska, Krzysztof Daniec, Karol Jędrasiak, and Aleksander Nawrat

Abstract. This article presents design and implementation of a gyro-stabilized platform for visible light and infrared image acquisition. The process of selection of appropriate vision sensors and their calibration is presented. Additionally there are presented results of conceptual work, design and construction of the working prototype of the device.

1 Introduction

In many technical applications visible light image analysis is insufficient. Often, obtaining the necessary information requires observing the analyzed objects or the entire scene in a different range of electromagnetic waves. Available imaging techniques cover the entire spectrum of electromagnetic waves. However the most commonly analyzed are images acquired at visible light or infrared spectrum. This is the result of the unprecedented progress that has been made in the construction of infrared sensors in recent years. As a result, there is a significant price reduction of cameras working in the range and thus their greater availability.

Damian Bereska · Karol Jędrasiak · Krzysztof Daniec · Aleksander Nawrat
Silesian University of Technology, Institute of Automatic Control,
Akademicka 16, 44-101 Gliwice, Poland
e-mail: {damian.bereska,karol.jedrasiak,
      krzysztof.daniec,aleksander.nawrat}@polsl.pl

Aleksander Nawrat
Ośrodek Badawczo-Rozwojowy Urządzeń Mechanicznych "OBRUM" sp. z o.o.,
ul. Toszecka 102, 44-117 Gliwice, Poland
e-mail: anawrat@obrum.gliwice.pl

Presented in this article opto-electronic gimbal is the result of the first stage of the work carried out over a gyro-stabilized platform for autonomous vehicles. It was designed to enable the installation of optical sensors allowing simultaneous acquisition of images in the visible and infrared bands. At this stage the priority was to create a gyro-stabilized platform for selected optical sensors. The platform enables rotation around two axes.

2   Optical Sensors

Paradoxically, the selection of appropriate optical sensors is not a simple task. Great variety of available solutions and their types requires an analysis of several technical documentations. It is useful to predefine basic criteria such as the availability of equipment, price, native resolution, weight, size, power consumption or operating temperature. In case of a dedicated platform for unmanned ground vehicles (UGVs) a criterion based on dimension of weight is not critical. Important are however image resolution, operating temperature and of course price. During selection of equipment a special attention was paid to the availability of dedicated optical systems, which in case of infrared cameras significantly increase the weight of the device and its price.

As a result of the analysis it was decided to purchase two cameras. The visible light camera was chosen as block camera Sony FCB-EX980 with integrated optics and motorized 26x zoom. The camera is characterized by an extensive automation. As the infrared sensors the Miracle Thermoteknix Systems Ltd. was chosen. It is characterized by a very good price to cost ratio. Technical parameters of both cameras are shown in the tab. 1. It is also sufficient for object detection [7].

3   Camera Calibration

As noted in the introduction the resulting opto-electronic gimbal is ought to allow the installation of optical sensors in such a way that simultaneous acquisition of images from both visible and infrared band are possible.

For many image processing algorithms it is important that both cameras are mutually fit. The desired installation outcome is when both cameras provide consistent output image in terms of size and content of the scene. Such effect can be achieved by adjusting the optical axes of the cameras, their mutual appropriate location and suitable setting of their lenses.

In order to achieve the desired parameters (tab.1) a dedicated test platform was developed and created. A tripod used to enable the measurement of the convergence of optical axes is presented in fig. 1.

Table 1. Technical parameters of the cameras used

	Sony FCB-EX980 [1]	Thermoteknix Systems Ltd. Miracle [2]
Screen resolution [pixels]	380 000	110 592
Operating temperature range [°C]	0 ÷ 50	-20 ÷ 50
Power consumption [W]	1,6/3,6	3,7
Size [mm]	55,3 x 57,5 x 88,5	45 x 52,5 x 57,6
Weight [g]	230	166 (without optics)
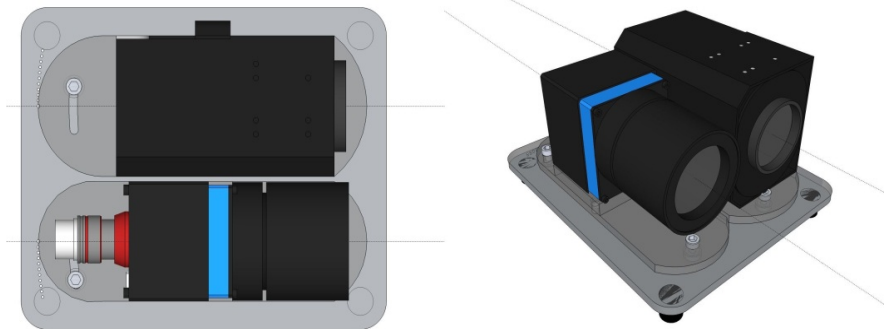
Fig. 1. Schema of a tripod used for measuring the convergence of the optical axes of the visible and infrared spectrum cameras

Fig. 2. presents two images acquired from both cameras. It can be observed that there is a high compliance of the scenes visible in the images.
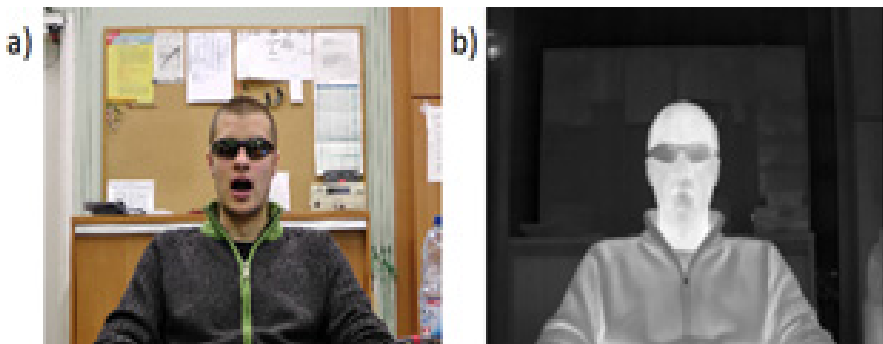
Fig. 2. Images acquired using a prototype platform optimizing mutual position and setting of lenses of both cameras

4 Platform Concept

Before the design of opto-electronic gimbal a review of existing stabilized platforms was carried out. Four devices were selected from all devices meeting the specified criteria and available on the market. Selected devices are presented in tab. 2.

Table 2. Technical comparison of gyro-stabilized platforms

	CloudCapTech TASE300 [3]	HARV ISR Gimbal [4]	Vector 20 [5]	IAI MiniPOP [6]
Pan/ tilt	continuous /(-220° do +40°)	continuous / continuous	continuous / (-90° do +60°)	continuous / (-110° do +40°)
Pan/ tilt	200°/s	600°/s pan 360°/s tilt.	60°/s	65°/s
Size [mm]	176 x 176 x 238	192 x 116 x 267	267 x 213 x 431	260 x 260 x 380
Weight [kg]	2,27	3,17	11,8	16,3

The conceptual work ended with the presentation of two variant of the construction of the platform (fig. 3). Both options took into account the dimensions of the propulsion systems and the required amount of space for mounting control electronics and connectors.
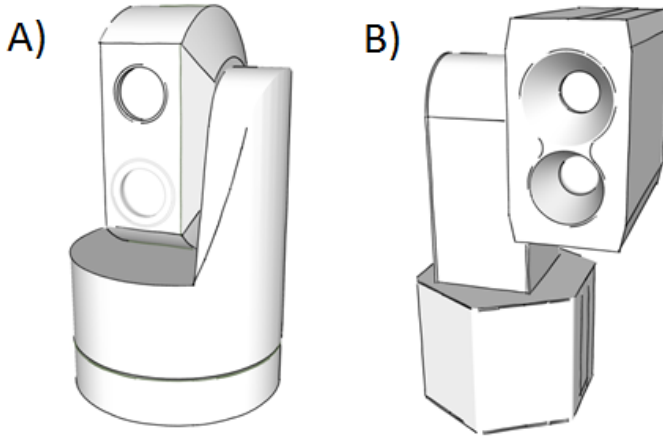
Fig. 3. Two variants of the construction of the platform. Both were considered during conceptual phase of work

For implementation the second variant presented in fig. 3b was chosen. It was characterized by a larger volume of the cassette assembly. Such construction allows convenient installation of cameras according to the designated parameters from section two. Size of the chosen cassette allows precise installation of the inertial measurement unit (IMU) which is used in order to determine the orientation in space. Chosen variant also leaves space for future redevelopment due to additional equipment like e.g. laser range finder.

5 Platform Design and Construction

The concept selected during previous stage of work was developed during design phase into a complete model for CAD/CAM platform (fig. 4). It allowed rapid generation of design documentation. The project was also used during creation of device components using CNC milling machine. Constructed fully functional prototype made of aluminum is shown in fig 5. The main requirement for the design phase of the work was to enable line of sight stabilization during rapid vehicles movements [9].
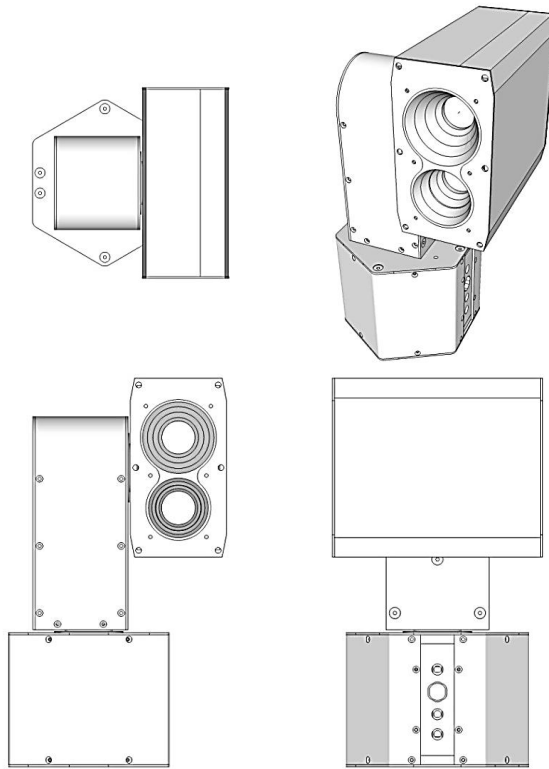
Fig. 4. Orthogonal projections and isometric view of the proposed gimbal
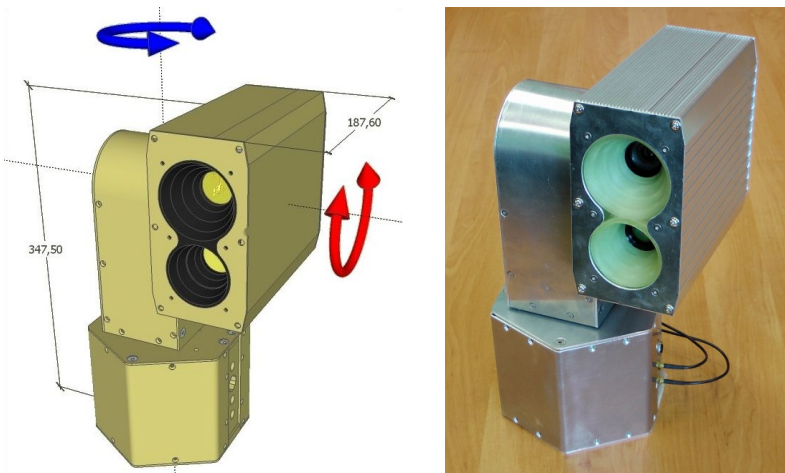
Fig. 5. 3D model of the proposed gimbal with axes of rotation and dimensions marked (left) and a photograph of constructed platform (right)

6   Conclusions

During the first stage of the work carried out over a gyro-stabilized platform a fully functional prototype was constructed. Its design allows for the installation of optical sensors for simultaneous image acquisition in both visible and infrared spectrum. The research team obtained a valuable experience of working with an object that can be installed on any ground vehicle, including unmanned ground vehicles (UGVs). It is worth to mention that it possible to create wing type UAV [10] large enough to carry the presented gimbal. The constructed prototype allowed performing a variety of valuable experiments in the research fields of multispectral image analysis, detection and tracking of objects, mechanical stabilization and digital image stabilization. Regardless the application its control could be previously prototyped in matlab/Simulink [8].

References

[1] Sony Corporation. Products information (2004),
     `http://assets.pro.sony.eu/doc/sesdatasheets/FCB-`
     `EX(Brch).pdf`
[2] Thermoteknix Systems Ltd. Products information (2012),
     `http://www.thermoteknix.com/content/english/thermal_`
     `imaging_ir_products/miricle_thermal_imaging_ir_`
     `cameras/index.html`
[3] Cloud Cap Technology Inc. Products information (2012),
     `http://www.cloudcaptech.com/gimbal_tase300.shtm`
[4] Chatten Associates Inc. Products information (2012),
     `http://www.chattenassociates.com/content/harv-isr-gimbal`
[5] General Dynamics Global Imaging Technologies products information (2012),
     `http://www.gd-imaging.com/index.cfm?acronym=GIT-Vector`
[6] Israel Aerospace Industries (IAI), Tamam Division products lines (2012),
     `http://www.iai.co.il/sip_storage/FILES/6/35596.pdf`
[7] Nawrat, A., Daniec, K., Warmuz, T.: Object Detection Using IR Camera. In: Nawrat, A., Simek, K., Świerniak, A. (eds.) Advanced Technologies for Intelligent Systems of National Border Security. SCI, vol. 440, pp. 129–142. Springer, Heidelberg (2013)
[8] Grygiel, R., Pacholczyk, M.: Prototyping of control algorithms in matlab/Simulink. In: 14th World Multi-Conference on Systemics, Cybernetics and Informatis, WMSCI 2010, vol. 2, pp. 141–145 (2010)
[9] Kuś, Z., Fraś, S.: Helicopter control algorithms from the set orientation to the set geographical location. In: Nawrat, A., Simek, K., Świerniak, A. (eds.) Advanced Technologies for Intelligent Systems of National Border Security. SCI, vol. 440, pp. 3–14. Springer, Heidelberg (2013)
[10] Iwaneczko, P., Jędrasiak, K., Daniec, K., Nawrat, A.: A prototype of unmanned aerial vehicle for image acquisition. In: Bolc, L., Tadeusiewicz, R., Chmielewski, L.J., Wojciechowski, K. (eds.) ICCVG 2012. LNCS, vol. 7594, pp. 87–94. Springer, Heidelberg (2012)

Omnidirectional Video Acquisition Device (OVAD)

Sławomir Fraś, Karol Jędrasiak, Jan Kwiatkowski, Aleksander Nawrat, and Dawid Sobel

Abstract. Omnidirectional video acquisition device (OVAD) is an innovative concept that may find many applications both civilian and military. It can be used to observe areas that may need wide area monitoring such as shops, banks, petrol stations. In military installations OVAD may be used to patrol the area from the ground or from the air. Application allows capturing images from chosen camera. It is possible to immediately switch between cameras or also move around the panorama created from multiple video streams, like in rotating camera. Panorama contains combined view of entire area around device.

Keywords: omnidirectional camera, image processing, undistortion.

1   Introduction

Together with development of technology, optimization of video acquisition becomes more and more complex and challenging problem. Nowadays, cameras are used everywhere, e.g. in film studios, factories, shops, banks, petrol station or CCTV (Closed-circuit Television). Camera is often an extension of human sight, it creates possibility to see more and to look from another perspective. This proves usefulness of cameras in surveying certain locations from the control room,

Sławomir Fraś · Karol Jędrasiak · Jan Kwiatkowski · Aleksander Nawrat · Dawid Sobel
Silesian University of Technology, Institute of Automatic Control,
Akademicka 16, 44-101 Gliwice, Poland
e-mail: {karol.jedrasiak,aleksander.nawrat}@polsl.pl

Aleksander Nawrat
Ośrodek Badawczo-Rozwojowy Urządzeń Mechanicznych "OBRUM" sp. z o.o.,
ul. Toszecka 102, 44-117 Gliwice, Poland
e-mail: anawrat@obrum.gliwice.pl

monitoring parts of the process in factories or in observation of surroundings of unmanned aerial vehicle (UAV) [12]. There are also many other types of video acquisition devices, e.g. stationary or rotating camera. Each type has its pros and cons. The project purpose was to create a device, which combines advantages of other devices and avoids the disadvantages. Basic assumption was that the device has to have possibility to trace all its surroundings and allow instant changes of direction of video acquisition.

2   General Concept of Omnidirectional Video Acquisition

The idea of creating a device with a wide range of view is not something new. Solutions, which offer such video canvassing, already exist. An example of such appliance can be rotating camera (fig. 1). The wide angle of sight of this camera is obtained through the movement of the camera in horizontal or/and in vertical direction. This creates a possibility to direct the camera on the desired area, which is limited only by the range of its movement. When the designated point in space, which is supposed to be captured by camera, is not covered by its current field of view, a latency caused by the time needed to turn rotating camera appears. This solution, theoretically, provides capturing video with 360º of horizontal field of view but at a given instant, operator can observe only a little range of this space. This is why constant operator attention is needed.

Another solution is camera with a "Fisheye" type lens (fig. 1). It allows observation of the whole half-sphere at one moment. The application of such lens with a short focal length, increases the angle of the view of the camera but the result of that operation is considerable image distortion. This "barrel" distortion, is the main disadvantage of cameras based on fisheye lenses. This aberration occurs, when with increasing distance from the middle of captured video stream and approaching the edges of the field of vision, image becomes smaller. It is possible to try to straighten such an image but it is not easy and involves a considerable loss of part of image, and reduction of its quality.

Device, which combines the advantages of the rotating camera as well as the "fisheye" lens is an OVAD (fig. 1). Assembling several cameras enables parallel multidirectional canvassing. The quantity of the cameras depends on the width of their visual field. If the sum of the visual fields of all the cameras is greater or equal than 360º then the image is being registered from all directions. To obtain an image from desired area all that is need to be done is to choose the appropriate camera and operator can immediately get access to it, not having to wait until camera turns to the designated position. Not only does the video stream include the entire 360° horizontal field of view, but it also is not distorted, so it shows no signs of the biggest disadvantage of the fisheye lens. Correction of a small barrel distortion, which appears on video captured by used cameras, can be conducted by a computer program. An application combining the images from all six cameras together into one video panorama is an additional advantage of such a solution.
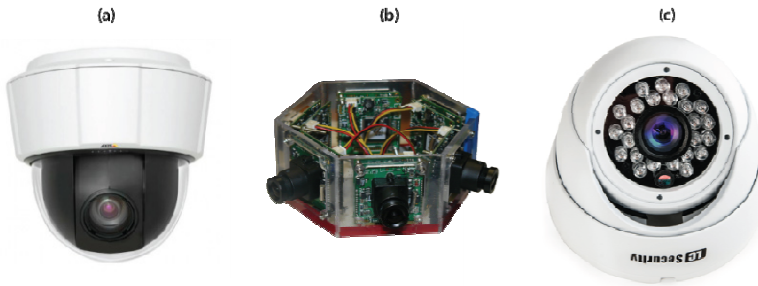
Fig. 1. PTZ camera AXIS P5532-E (a), OVAD (b), LC-1120 FISHEYE Premium (c)

3   Lens Distortion

Distortion is the fifth of Seidel aberrations [1]. This aberration is an effect of non-uniform magnifying over entire field of vision. The bigger incidence angle of rays of light is, the bigger is deviation from primary incidence angle. Distortion does not occur in very thin lenses and in pinhole cameras. However, pinhole camera field of view is narrow in comparison with the one of camera with lens. Increasing field of view of pinhole camera would mean increase of focal plane size. Today focal planes are very small and increasing their size is not reasonable, so increasing its field of view creates necessity to use systems of lenses. The result of that operation is appearing of distortion. There are two main types of optical distortion - tangential distortion and radial distortion. Those two types are describing directions of dislocation of specific points. Radial distortion can be described as displacing of specific points alongside with radiuses diverging from center of lens (radial direction), while tangential distortion appears when points are shift in a direction, which is perpendicular to those radiuses. Tangential distortion may occur when focal plane is not placed in parallel with lens. There are also a few another defined types of distortion, however usually their influence on quality of image is not as important and visible as the one of mentioned radial and tangential distortion. Because of that they are usually omitted during analysis of distorted picture. Radial distortion is displacement of certain points in relation with distance from the middle point of captured image. There are two types of radial distortion:

- barrel distortion (fig. 1.a) – with increasing distance from center of image, there is possibility that image will be curved towards center of image or it can be said that magnification decreases towards edges of image. This aberration is typical for standard lenses. Video streams captured by cameras used in OVAD project are distorted by this type of radial distortion [1].
- pincushion distortion (fig. 1.b) – mostly present in telephoto lenses, with increasing distance from center of focal plane image is curved towards its' edges, magnification increases [1].

There can be found some annotations in literature about moustache distortion (fig 1.c), which is made from both barrel and pincushion distortion. This aberration makes image curved as in pincushion distortion when closer to the edges, while closer to the center it behaves as barrel distortion. Other than moustache distortion this aberration is also named mixed distortion or complex distortion.
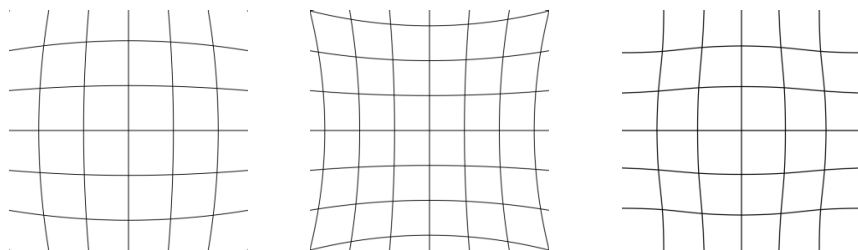
(a) barrel distortion   (b) pincushion distortion   (c) moustache distortion

Fig. 2. Types of radial distortion

Distortion is very common aberration and can be corrected using software methods. Optical systems, which are free of distortion are called orthoscopic.

4   Hardware

Hardware part consist of all parts and elements of OVAD project that are connected with video acquisition and transmission of captured PAL signal to receiver (frame grabber followed by PC). Implementation of hardware required choosing adequate cameras and creating multiplexing unit, used to select two from six incoming PAL signals and forwarding them to transmission line.

4.1   Cameras

Video recorders used in OVAD project are pcb board cameras ACE-S110CHB (fig. 3), which are capturing RGB image with resolution of 480 lines, using Sony 1/3'' Super HAD CCD sensor.
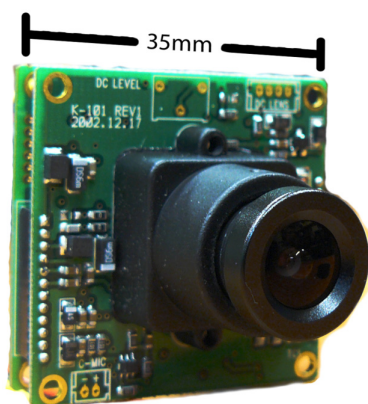
Fig. 3. ACE-S110CHB camera

Table 1. presents selected camera parameters. Choice of these particular cameras is justified by small size of cameras together with relatively high resolution, which stands for quality of captured image. Parameter, which is worth to be considered is angle of camera horizontal view. Required minimum is 60 degrees, because all six cameras shall create a possibility to capture 360° of horizontal field of view. Because of distortion correction, which at most cases means losing some edge parts of image, horizontal field of view of a single camera wider than 60° is highly recommended.

Table 1. Cameras specifications given by manufacturer

TV standard	NTSC/PAL
Sensor	Sony 1/3'' Super HAD CCD
Number of lines	480 TVL
Sensitivity	1 [lux] (F=2.0)
Lens	3.6 [mm] (74° HFOV[1])
Signal-to-Noise Ratio	more than 45 [dB]
Gamma correction	0.45
Video output	composite 1 (vp-p) 75Ω
Supply voltage	12 [V]
Current consumption	140 [mA]
Allowable working temperature	from -10 to +50 [°C]
Dimensions	35x35 [mm]

Orientation of cameras provides 360° horizontal field of vision. Placed in hexagon-shaped Plexiglas® frame cameras are presented in fig. 4.
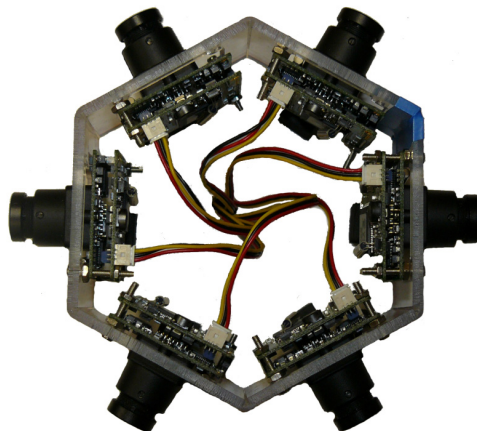
Fig. 4. Orientation of cameras

---

[1] HFOV – horizontal field of view.

4.2   Multiplexing Unit

One of the most important parts of OVAD project was design and implementation of multiplexing unit (fig. 5). From the very first concept this unit was meant to choose two from six incoming PAL signals generated by cameras and to forward those two selected signals to transmitters. Channels, that should be connected to transmission line output, are determined by two analog multiplexers (Texas Instruments CD4051B [3]), which are controlled by STMicroelectronics STM32F103C8T6 [4]. Microcontroller, depending on received information through CAN, sets or resets adequate pins connected to control pins (A, B, C) of multiplexers. By use of Texas Instruments SN65HVD230 [5] (known as VP230), CAN signal is converted to signals, that are accepted by microcontroller.
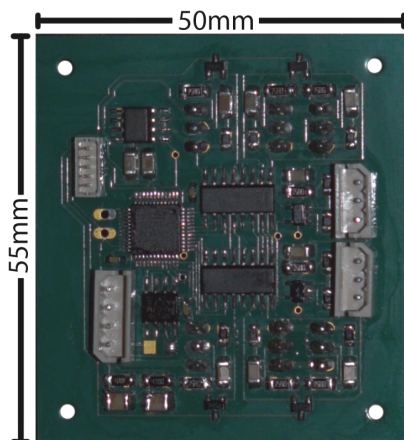
Fig. 5. Multiplexing unit

Properly implemented unit should prevent signal from being reflected back. Solution of that problem is electrical termination of signal by use of 75 [Ω] resistors (terminators). Value of resistance is determined by type of video output used by cameras (composite 75 [Ω] 1Vp-p). However, in a way in which they are used, terminators are creating voltage divider. If not corrected, output signal would have been divided by two. This negative effect is being corrected by operational amplifier Texas Instruments LMV651 [6], with local feedback. Connected as in fig. 7, section C, amplifier proves gain which equals two. Every single one of six input signal is having its offset recovered, which is eliminated when signal leaves multiplexing unit by 10 [μF] capacitor. Value of capacity ensures that every needed frequencies of signal will cross through capacitor – the less capacity is, the higher frequencies would be treat as offset and eliminated by capacitor. Because of that it is very important to maintain both large capacity and small size of capacitors. Whole circuit of multiplexing unit uses 3.3 [V] voltage supply. This voltage is nominal for microcontroller and every single element was selected with consideration of that supply voltage, which is obtained using Texas Instruments LE33CD [7] positive voltage regulator.

4.3   Offset Recovery System

Amplifier output voltage can reach voltage which ranges between 0 and 3.3 [V], which is supply voltage of multiplexing unit, when amplifier becomes saturated. Each input of multiplexing unit is having its offset eliminated by input and output capacitor. This means that 1Vp-p video signal can oscillate between -0.5 [V] and 0.5 [V]. Because of its supply voltage amplifiers could not amplify negative voltages and thus output signal would be damaged. That problem would not occur when input voltage would take values between 0 [V] and 1.65 [V], because in that situation amplified output voltage (considering amplifiers gain G = 2) would take values from 0 [V] to 3.3 [V] range. Applied solution is offset recovery system (fig. 6).
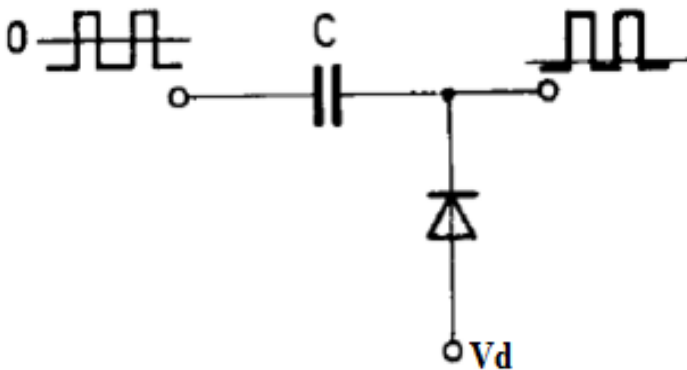
Fig. 6. Offset recovery system [2]

When, after offset elimination, signal voltage ranges from -0.5 [V] to 0.5 [V], capacitor is charged to V_d level by diode, because there exists difference in voltage between signal and V_d and diode BAT54A is connected in forward direction. When input signal turns positive, capacitor is still charged to V_d level and this means that input voltage will add to the current one. Diode is now connected in reverse direction because capacitor voltage is higher than V_d. If signal turns again to negative value capacitor will have lower voltage value than V_d and will be charged again. In conclusion, signal will have its offset recovered and its value will be equal to V_d-U_d, where U_d is value of diode voltage drop.

4.4   Active Branch of Multiplexing Unit

Enabled branch of multiplexing unit, when specified input signal is chosen by multiplexer and forwarded to transmitter, is presented in fig. 7.
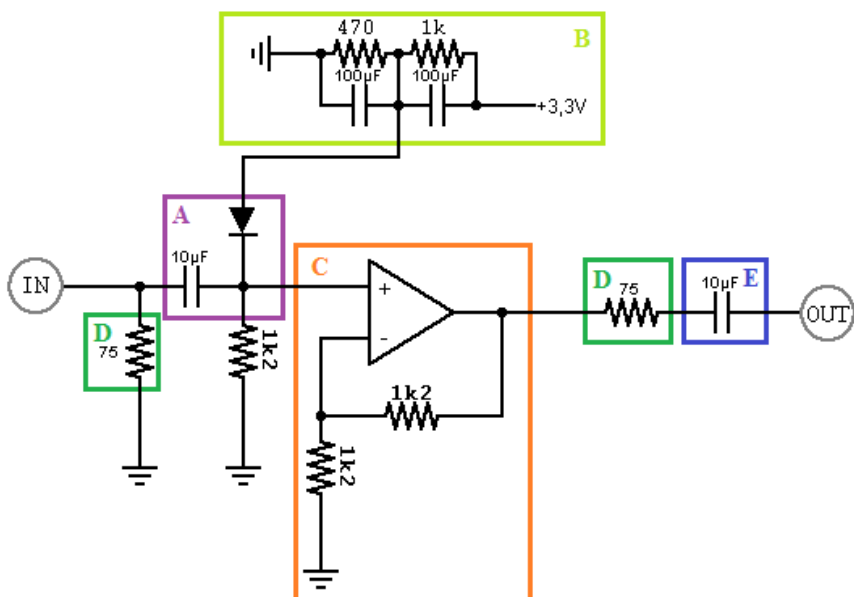
Fig. 7. Active branch of multiplexing unit

Description of sections marked in fig. 7:
A – offset recovery system,
B – voltage divider,
C – operational amplifier, gain G = 2,
D – terminators,
E – offset elimination.

Termination and offset recovery are implemented on each one of six video inputs, before signal would be forwarded through multiplexer. Amplifier, line termination and output capacitor used for offset elimination are placed following multiplexer outputs.

5   Software

Software part of OVAD project consists particularly on creating an application used for real time video processing, which main task is to combine adjacent video streams in a way that prevents spotting fragment of panorama, where those streams are connected, and to provide communication between PC and microcontroller, which is located at multiplexing unit. This communication is used to send information to multiplexer unit about cameras which are currently needed to be transmitted. Second part of software is microcontroller configuration, necessary for proper communication and interpretation of control data acquired through CAN.

5.1   *STMicroelectronics STM32F103C8T6 Configuration*

Implementation of printed circuit that fulfils all needed functionalities and general purposes requires properly programmed microcontroller. The most important parts in STM32 software are configuration of CAN interface, configuration of system interrupts and providing of proper interpretation of acquired control data. CAN configuration can be divided to three main stages:

- initialization and setup of parameters of CAN init structure – implemented CAN interface works asynchronically, in normal mode, in which receiver sends back information about successful receiving of frame. Baud rate equals 500kb/s;
- filter initialization – microcontroller should accept only information, that is addressed to (0x6DF << 5);
- assignment of pins Tx (transmit) and Rx (receive).

Providing of working in asynchronical mode requires configuration of system interrupts. Receiving of properly addressed information enables external interrupt (CAN1_RX1_IRQn). Interrupt handling consists on interpretation of zero byte of data field in CAN frame. Depending on that information microcontroller sets or resets control pins of multiplexers. Adjacent bits in zero byte stand for adjacent cameras, The least significant bit corresponds with zero camera, and each more significant bit stands for next camera as shown in table 2. When bit is set (1), it means that this camera should be forwarded to transmitter. Only byte containing information about forwarding two adjacent cameras are accepted. Each information, whose zero byte differs from the ones shown in table 2 is treated as error, and in that situation nothing will be forwarded to the output of multiplexing unit.

Table 2. Interpretation of control information

Zero byte of data field		Chosen input of multiplexers	
BIN	HEX	MUX1	MUX2
0b00000011	0x03	camera 1	camera 2
0b00000110	0x06	camera 3	camera 2
0b00001100	0x0C	camera 3	camera 4
0b00011000	0x18	camera 5	camera 4
0b00110000	0x30	camera 5	camera 6
0b00100001	0x21	camera 1	camera 6

5.2   *Application*

The application supports the entire process of video acquisition, from the selection of the cameras, through their calibration, to the real time combination of acquired video streams into one panorama (fig. 8). Displaying of the video stream in real time is key feature of the application. This is why the application has to work on

the basis of event handling. A minimum quantity of the code responsible for receiving consecutive frames, processing and showing them to the user in the application window, is located in the main loop of the program. The remaining operations are carried out by pressing one of available buttons or in response to meeting certain conditions specified by programmer himself.
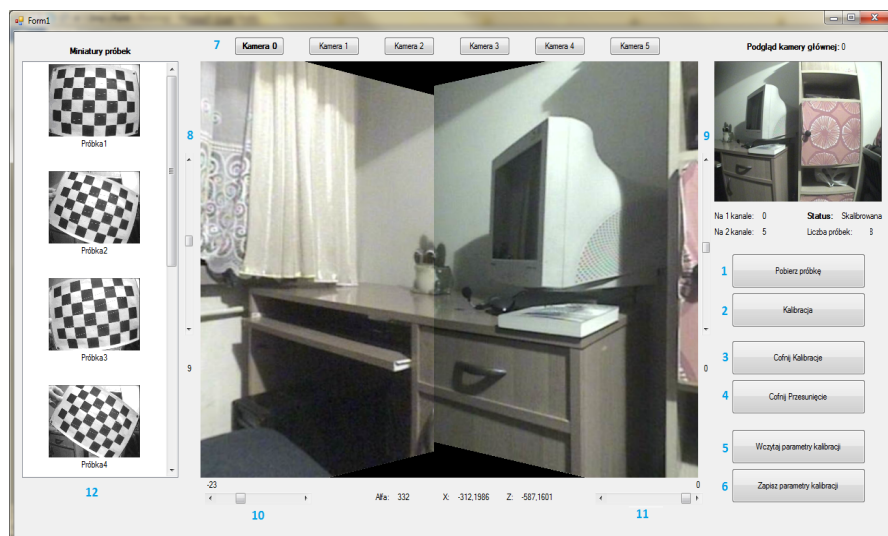
Fig. 8. The application window

A large part of the work was based on exploiting ready-made functions serving the purpose of the image processing. The whole process of the calibration of the cameras is carried out based on the OpenCV [8] library. It provides both, simple to implement functions realising real time video processing, as well as the mechanisms that are used to calibrate the cameras and straightening of distorted images. Since the application is written in C#, EmguCV [9] library has to be used. EmguCV is a cross platform .Net wrapper to the OpenCV image processing library. The calibration requires directing the camera at an object with a known shape and a characteristic pattern, in order to find the calibration of the parameters of distortion by use of certain functions. A pattern of alternating black and white squares (chessboard) was used. Captured samples should contain about thirty images of the chessboard in various positions.

The CameraCalibration.FindChessboardCorners(…) function is used to find coordinates of the chessboard corners in the currently processed frame. Because these points are only approximated, the utilization of CvInvoke.cvFindCorner SubPix(…) function, which computed the exact location of the corners, was necessary.

The next step is the visualisation of achieved results. CameraCalibration. DrawChessboardCorners(…) function was used to draw the chessboard corners on the samples. Those samples can be seen in the list of figures, which is on the left side of the application (Fig. 9). Despite showing samples is not necessary, it can be helpful with determining if the corners were found correctly.
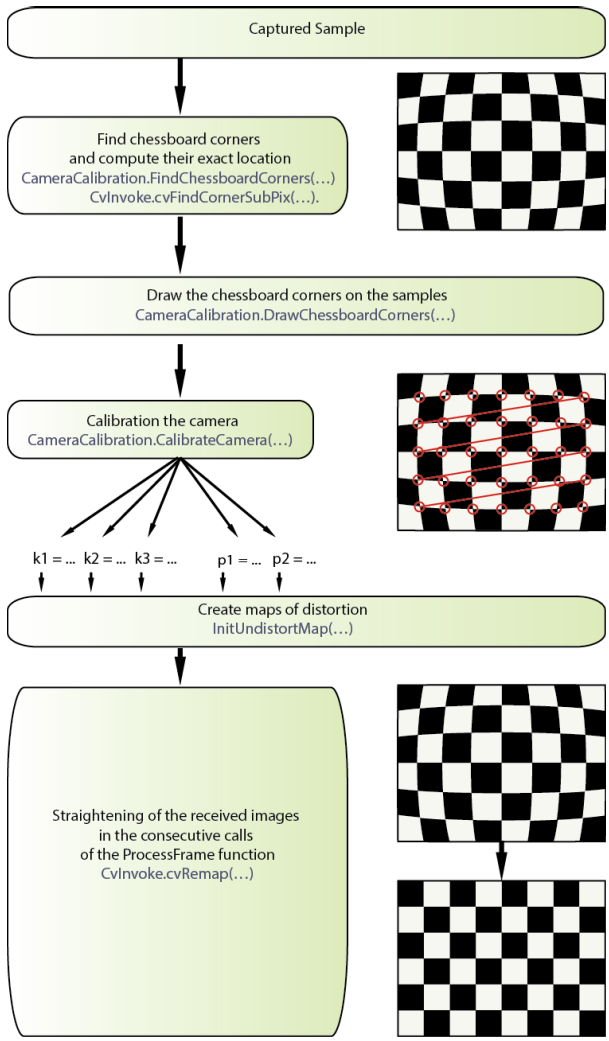
Fig. 9. Process of calibration and undistortion

(a)   (b)

Fig. 10. Distorted (a) and undistorted (b) chessboard

Pressing the *Calibration* button is possible only after capturing specific amount of samples containing the chessboard. It calls a function of camera calibration, which straightens video stream, using determined calibration parameters. The parameters are exploited to create a map of distortion, which serves proper straightening of the received video streams (fig. 10) the corners taken before, determines the external and internal

(a)   (b)

Fig. 11. Combined video streams, in 2D (a) and 3D (b)

The second important library used in the creating of the program was OpenGL, a graphic library well known by people dealing with computer games graphics. The use of this library created a possibility to display acquired video streams in a three-dimensional space, which in turn solved, to a large extent, the problem of joining the streams captured by adjacent cameras. That problem is a result of the fact, that each camera observes its surroundings from different angle, so the same object captured by two adjacent cameras has different shape (Fig. 11). Elements of the library created a possibility of placing an observer inside virtual hexagon-shaped room, and displaying the image registered by the cameras on its walls. This way the angle, at which cameras could see their surroundings, was also the angle of view of the observer. OpenTK [10] library, which is an equivalent of OpenGL library in C# language, was used to implement this mechanism.

Due to the fact, that it is very difficult to flawlessly place cameras in a frame so that they are all perfectly at the same height, a slider, seen at the left side of the displayed image (fig. 8), was implemented, enabling lifting or lowering of the image for each camera separately. Furthermore, below the image, there are sliders providing the possibility of shifting the edge of the image for a selected camera. Their role is to narrow the image from the right or left side. The necessity for such an intrusion in the image arises when parts of the registered objects are doubled in streams captured by two adjacent cameras. It means that the object is as far from the cameras as to fit in the visual fields of both the cameras. There exists only one such distance from both of the cameras, when fields of vision of cameras will intersect and the observed object will be perfectly composed (Fig. 12).
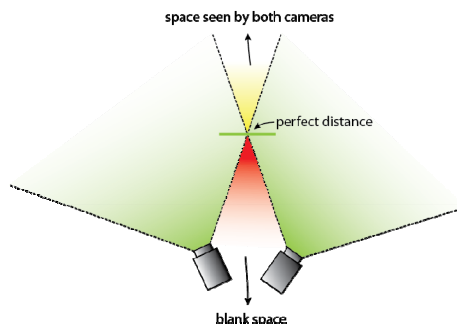
Fig. 12. Cameras visual fields

Use of the above elements and mechanisms fulfilled the functionalities desired to be delivered by application. It is possible to capture real time view in the entire sphere around the device, taking relatively short time to access the video stream from a selected direction. The implementation of the function, collecting the images from adjacent cameras, made it possible to create an uninterrupted video panorama, in which the places, where the successive images join, can hardly be seen.

6   Summary

Implemented device can be found as useful in wide area of contemporary industry. Firstly, because of its small size and weight OVAD can be mount on various unmanned vehicles. General purpose of overall project was creation of device that would be used on UAV (Unmanned Aerial Vehicle), as an alternative to widely used rotating cameras. Another example of utilization may be using OVAD as inspection probe camera, e.g. in supervising of mine shafts or wells. Device may be also useful in all kinds of CCTV (closed-circuit television). OVAD has a few advantages over another solutions like mentioned rotating cameras:

- ability of instant change of looking direction, OVAD, unlike in rotating cameras which are limited by drive time of servo-motor, moreover time of change does not differ
- OVAD can be few times cheaper than rotating cameras dedicated for UAVs,
- absence of moving elements – utilizing of rotating camera may be problematic in difficult weather conditions, such as large pollination, which may cause blockage of moving elements and because of that losing all functionalities of device. Furthermore, blockage might lead to overheating of servo-motor, which eventually may cause irreparable damage,
- huge perspectives on further improvement of device – overall concept is very adaptable and this feature makes a lot of space for innovations , such as extending field of view into half-sphere by utilizing of more cameras or using digital cameras (together with FPGA board) instead of analog ones (that would create a possibility to make device a lot smaller).

References

[1] Jenkins, F., White, H.: Fundamentals of optics. McGraw-Hill Book Company (1957)

[2] Horowitz, P., Hill, W.: Sztuka Elektroniki, WKiŁ, Warsaw, ISBN: 83-206-1128-8

[3] Texas Instruments, CD4051B datasheet, access via Internet: http://www.alldatasheet.com (access: December 2012)

[4] STMicroelectronics, STM32F103x8 datasheet, access via Internet: http://www.alldatasheet.com (access: December 2012)

[5] Texas Instruments, SN65HVD230 datasheet, access via Internet: http://www.alldatasheet.com (access: December 2012)

[6] Texas Instruments, LMV651 datasheet, access via Internet: http://www.alldatasheet.com (access: December 2012)

[7] STMicroelectronics, LE33CD datasheet, access via Internet: http://www.alldatasheet.com (access: December 2012)

[8] Official OpenCV website, access via Internet: http://www.opencv.org (access: December 2012)

[9] Official EmguCV website, access via Internet: http://www.emgu.com (access: December 2012)

[10] Official OpenTK website, access via Internet: http://www.opentk.com (access: December 2012)

[11] Nawrat, A., Daniec, K., Warmuz, T.: Object detection using IR camera. In: Nawrat, A., Simek, K., Świerniak, A. (eds.) Advanced Technologies for Intelligent Systems of National Border Security. SCI, vol. 440, pp. 129–142. Springer, Heidelberg (2013)

[12] Iwaneczko, P., Jędrasiak, K., Daniec, K., Nawrat, A.: A prototype of unmanned aerial vehicle for image acquisition. In: Bolc, L., Tadeusiewicz, R., Chmielewski, L.J., Wojciechowski, K. (eds.) ICCVG 2012. LNCS, vol. 7594, pp. 87–94. Springer, Heidelberg (2012)

Part III
Design of Vision Based Control Algorithms

It is commonly accepted that over 80% of all perceptual information being received by human brain is perceived through eyes. It is natural for control algorithms developers to try to utilize the information as it is done by both human and animal brains. Vision information can be utilized not only for control a single device but also for controlling a group of e.g. mobile robots.

Control algorithm based on vision may allow remote control of an object. One might image a mechanical arm mimicking movements of a human arm basing solely on vision information. Design of such concepts and systems is important for a variety of fields like medicine, military and commercial applications. Recently human-machine interfaces are becoming more and more important of everyday life. Vision based systems are an important part of such systems. When a group of people communicate via each other in harsh weather conditions when there is no possibility to communicate via voice, gestures might be used. Systems recognizing gestures in order to send commands to a group of UAVs might significantly improve the quality of utilization of such systems.

An alternative approach is to use aerial vision information for controlling detected and recognized objects on the ground. Video stream acquired from UAVs has to be stabilized and undistorted in order to acquire precise information sufficient for control. In order to perform distortion compensation some kind of calibration has to be previously done. There are various types of calibration e.g. using planar or non-planar calibration rigs. Different type of calibration might use relative optical flow information in order to establish calibration from motion. After radial and tangential distortion compensation ground objects can be located and their orientation might me estimated. Real applications require to compensate for much more challenging factors like intensity and type of illumination or acquisition noise due to e.g. high temperature of the video acquisition device surroundings.

Another application of vision based control algorithms is navigation of UAV in an unknown dynamically changing environment. One might assume that geodesic terrain map is sufficient for navigation. Unfortunately such maps might be outdated and some tall buildings might not be included. At the same time flora is usually also not taken into consideration during creation of such maps. Finally, there might be some other UAVs or manned flying units in a local environment of UAV that needs to be omitted in order to successfully perform the mission of controlled UAV. Planning a mission using a 3D maps is a challenging problem increasing exponentially with the resolution of the map and the number of waypoints of UAV. Therefore there is a need to simplify the process in order to allow navigation in a dynamically changing environments.

An important part of image processing is image stabilization. It is basically divided into three approaches: mechanical, optical and digital stabilization. Stabilization can be used in optoelectronic gimbal mounted on board of manned objects or unmanned vehicles (UGVs and UAVs). Generally it is desirable to apply stabilization to all cases when deterioration of image quality is perceived due to low and high frequencies.

The chapter includes a number of important challenges in the fields mentioned above. At the same time valuable suggestions and conclusions of authors are presented. Finally, designed algorithms are presented and discussed in detail.

Vision System for Group of Mobile Robots

Artur Babiarz, Robert Bieda, and Krzysztof Jaskot

Abstract. A vision system for group of small mobile robots playing soccer is presented. The whole process of extracting vision information from input images is discussed in detail. The method for correcting radial distortion introduced to the image by camera's lens is presented, then simple adaptive background subtraction algorithm is described. Next, classical flood fill algorithm is presented together with novel optimization giving better results and shorter calculation time. Later, novel method for calculating object's orientation, based on the geometrical moments and special shape of color markers on top of each robot, is presented. Then, the color classifier based on the histogram intersection kernel is discussed. Design of the vision system as a central server providing vision information to many clients simultaneously is presented. Experimental results obtained with use of the algorithm presented are also provided.

1   Introduction

Over 80% of all perceptual information being received by the human's brain comes from his eyes. So it is quite natural that engineers try to add vision to robot systems in order to improve their capabilities. The vision algorithm and its implementation described in this work are part of bigger research project whose goal is to build complete control system able to successfully participate in RoboSoccer tournament. RoboSoccer is an international initiative aimed at research and development of multi-agent systems in complex, dynamic environments. A good example of such multi-agent system is a soccer match of two teams of three robots on small playing field.

Although, at first sight, the RoboSoccer tournament seems to be nothing more than building and playing with toys, practical attempts to participate in it reveal

Artur Babiarz · Robert Bieda · Krzysztof Jaskot
Silesian University of Technology, Institute of Automatic Control,
Akademicka 16, 44-101 Gliwice, Poland
e-mail: {artur.babiarz,krzysztof.jaskot,robert.bieda}@polsl.pl

hundreds of fascinating and challenging problems from the domain of mechanics, electronics, automatic control and artificial intelligence that have to be solved and their solutions implemented. One of these problems is the task of building proper vision system, whose role and importance is briefly discussed in the next section.

The general structure of the complete system for controlling a group of mobile robots is presented on the Figure1. The system consists of playing field (1.5x1.3 m), camera (mounted about 2 m above the playing field), vision system (acquiring images from the camera via frame-grabber card), controller1 which is actually an AI module, responsible for taking all decisions; and radio transmitter, which routes the control decisions made by the AI to the proper robots via radio link. The approach could be extended to multiple types of information and mobile robots [10].
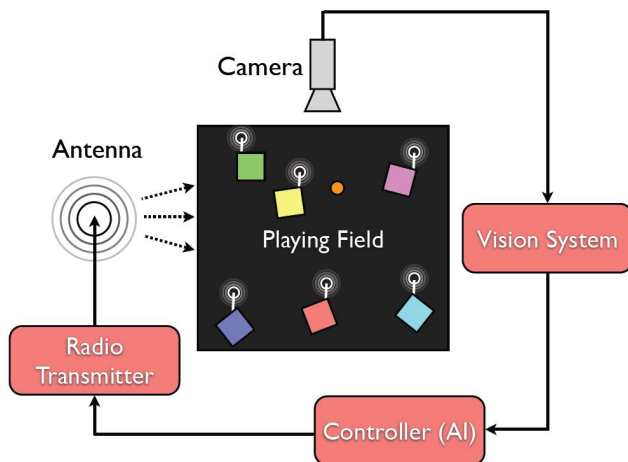
Fig. 1. Placement of vision system in the RoboSoccer control loop

There are two teams with three mobile robots in each. Every robot is a cube having dimension 7.5x7.5x7.5 cm. Teams play with orange golf ball. The robots have black walls and black top cover with colorful marker on it. The black is used because of the simplicity of algorithm removing unneeded parts of the scene during vision processing.

From the control algorithm's point of view, the vision system works as the feedback loop, providing measurements of values being inputs to the controller. Because the vision processing is done on the on the host computer and not on board of a robot, it is possible to develop quite sophisticated and very precise vision algorithm, as the computational power of contemporary PCs is thousands as big as of micro-controllers used on-board the robots.

Vision system could be also used for planning collision free path of other types of robots e.g. UAVs [7], [11]. Such problem is often solved with the methods of A.I [8].

2 Implementation of Vision Algorithm

The algorithm operates in two modes: Learning Mode and Running Mode. This is typical approach in the domain of computer vision, however there are some efforts to get rid of the learning phase and to build an algorithm capable of autonomous online learning [1].

Before the vision algorithm can actually be used it requires short learning phase. The learning is supervised, however there are no very complex tasks that the user have to perform. The algorithm requires user's attention in order to set proper thresholds for shadow removal and background subtraction algorithms and for placing the robots and ball in specific place on the playing field to discover unique color labels denoting every object of interest. As the algorithm is very robust, the threshold values have quite big tolerance and usually default values are sufficient. The block diagram of the steps of learning phase of the algorithm is presented on Figure 2.
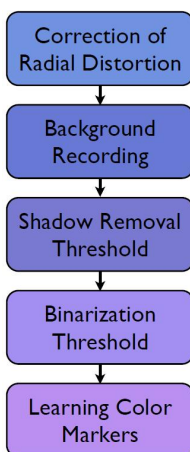
Fig. 2. Schematic diagram of the steps of learning phase of the vision algorithm

After finished learning the algorithm is immediately ready for operation. The block diagram of the running mode of the algorithm is presented on the Figure 3.

The algorithm starts with obtaining RGB image in resolution 320x240. This size comes from the limitations imposed by the frame grabber hardware used during the experiments. Resolution 640x480 is available only in interlaced mode and 640x240 has non-square pixels (twice as tall as wide). The next operation done on the image is shadow removal according to the current background model and selected threshold. Details of this algorithm are described below in separate section.

Improved input image without shadows is then used to extract foreground objects by simple thresholding the difference to the current background model. Obtained binary image is a subject to mathematical morphology operator called dilation, which significantly improves the continuity of foreground objects, which usually become worse when an object is placed over a white line drawn on the black playing field. The dilation operator uses4-neighbourhood and a mask of size 3x3.
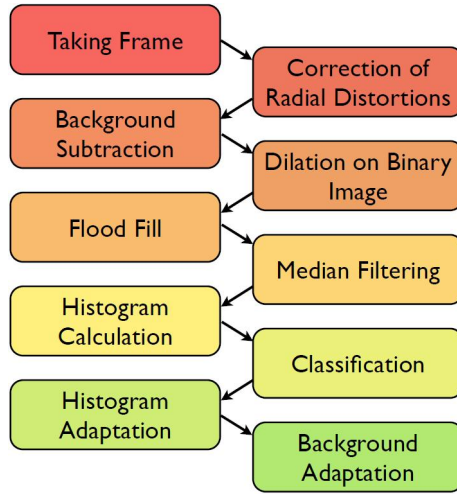
Fig. 3. Schematic diagram of the steps of learning phase of the vision algorithm

The binary image is then a subject to the flood fill algorithm, which marks all distinct objects on the field with distinct labels. It also performs calculations of mass center, main axes of inertia and bounding box for every object. Next the smallest objects are sorted out and only seven biggest ones are taken into account in further processing. As a next step the additional constraint is imposed on these objects - they have to consist of at least 25 pixels. This limit comes from practical measurements showing that the smallest object on a field, the ball, consists of at least 50 pixels, and all typical false objects ("noise") left on binary image consist of at most 10 pixels.

All further processing is done only for pixels being inside of bounding boxes and belonging to the particular object (background pixels are not affected in any way) calculated by flood fill algorithm. The first operation performed on these regions is RGB median filtering. This operation can be described as replacing similar colors with the dominant color, which in turn improves the quality of histogram based classification algorithm. The next step of the algorithm is calculation of color RGB histograms for each region. As usual, in order to speed up the calculations, the colors are quantized from 255 levels per component (R, G, B) to 4 levels. So the number of distinct colors recognized by the histogram is reduced from 16.7 mln to 64 which has proved to be very sufficient.

The histograms obtained are used for classifying objects they represent to 7 classes (ball and 6 unique robots belonging to 2 teams). Classification is done by NN (nearest neighbour) algorithm which compares each histogram with set of reference histograms representing the 7 classes mentioned above (one reference histogram is stored for one particular class). The histogram intersection function [2], [3] serves here as a metric, required by NN method in order to measure a distance between two histograms. Experiments proved that this metric provides quality of classification similar to quadratic cross-distance at the computational cost of bin-to-bin Euclidean metric.

2.1   Camera Setup and Correcting Radial Distortion of Camera's Lens

The only requirement imposed on the camera setup by the vision algorithm is that it should be possible to switch off all features like Auto Gain Control (AGC), Auto White Balance (AWB), etc., in order to provide as constant colors as possible.

Is is also important to set the lens's aperture properly, in order to avoid excessive CCD blooming effect, which, in extreme cases, can distort shape of objects being recognized, thus degrading algorithm's precision. Every consumer-class camera produces images with significant amount of radial distortion which degrades the precision of measurements done on the basis of analysis of acquired image, like estimation of the position and orientation of various objects on the image. Many methods have been developed for the purpose of calibration the camera, which take into account radial and tangential distortion introduced by camera's lenses. The most widely used method is described in [5]. This method however requires precise measurements of coordinates of corresponding points in real world and on image, which would take too much time. So the alternative method is used here which is taken from [6]. It is very simple and quick, however it requires user's attention in choosing proper amount of compensation.

The method uses inverse mapping for finding the color of pixel in output image. Each pair of integer pixel coordinates in output image is mapped to a pair of coordinates in input image, which usually are real numbers rather than integers. Color of the pixel in output image is then calculated either through bilinear, or through nearest neighbour interpolation of the colors of pixels in the neighbourhood of the mapped coordinates. Bilinear interpolation gives much better results than nearest neighbour (NN) interpolation, however it is much slower.

The algorithm performing actual correction can be described as follows. Let $Q_d(x,y)$ be distorted input image and $Q_r(x,y)$ be rectified output image of the same size. Then, for any pair of pixel's coordinates in the output image (x_r, y_r) the pair of corresponding coordinates in the input image (x_d, y_d) can be found from the following formulas:

$$x_d = x(1 - \gamma) + x_c \tag{1}$$

$$y_d = y(1 - \gamma) + y_c \tag{2}$$

where

$$\gamma = \lambda \frac{x^2 + y^2}{x_c y_c} \tag{3}$$

and

$$x = x_r - x_c, y = y_r - y_c \tag{4}$$

and x_c, y_c are coordinates of the center of image. The parameter λ is to be chosen by the user, useful value of it is in the range (0.001, 0.1), depending on the amount of distortion introduced by the particular lens. The color of a pixel in the output

image $Q_r(x_r, y_r)$ corresponding to the input image's pixel at the fractional coordinates (x_d, y_d) can be found in two ways. First is to use a simple NN interpolation:

$$Q_r(x_d, y_d) = Q_d\big(round(x_d), round(y_d)\big), \tag{5}$$

which is very fast method, however some artefacts will be visible on the output image, as shown on the Figure 4. Second method uses bilinear interpolation [15]:

$$\begin{aligned}
Q_r(x_d, y_d) = \ &\frac{Q_d(x_1, y)}{(x_2 - x_1)(y_2 - y_1)}(x_2 - x_d)(y_2 - y_d) \\
&+ \frac{Q_d(x_2, y_1)}{(x_2 - x_1)(y_2 - y_1)}(x_d - x_1)(y_2 - y_d) \\
&+ \frac{Q_d(x_1, y_2)}{(x_2 - x_1)(y_2 - y_1)}(x_2 - x_d)(y_d - y_1) \\
&+ \frac{Q_d(x_2, y_2)}{(x_2 - x_1)(y_2 - y_1)}(x_d - x_1)(y_d - y_1),
\end{aligned} \tag{6}$$

where

$$\begin{aligned}
x_1 &= \lfloor x_d \rfloor \\
y_1 &= \lfloor y_d \rfloor \\
x_2 &= \lceil x_d \rceil \\
y_2 &= \lceil y_d \rceil
\end{aligned} \tag{7}$$

This method gives results of better quality, however its performance very often cannot be accepted. Results obtained with use of this method are shown on the Figure 4(b). Fortunately, quality of corrected image obtained from NN interpolation is sufficient. In case of color images, the above procedures have to be performed for each color channel separately.

(a) (b)
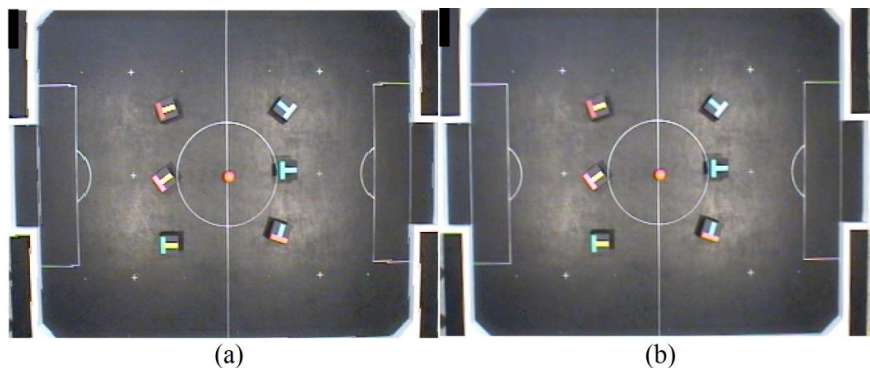
Fig. 4. Results of compensation of the radial distortion with NN (nearest neighbor) (a) and compensation of the radial distortion with bilinear sampling of source image (b)

2.2   *Background Subtraction and Shadow Removal*

The algorithm uses simple RGB (8 bits per channel) background model built by averaging 100 images from camera. Background subtraction is based on a difference image and simple threshold, explicitly set by the user. To calculate the image containing per-pixel differences between corresponding pixels from background model image and input image the Chebyshev metric is used. It operates slightly better than simple Euclidean or City Block (Manhattan) metric. Obtained difference image is then a subject to simple thresholding which results in binary image. The introduction to the problem of background subtraction can be found in [4].

There are four lamps installed over the playing field which not only provide light for camera, but also create quite large shadows. Shadow introduces false colors to the image which degrade the precision of objects positioning. Thus the need for shadow removal algorithm.

Fortunately, in this particular case, shadow removal is trivial task. The background consists mainly of very dark, almost black areas and the shadow is not colored. It is then enough to treat all pixels darker than certain threshold as unconditionally belonging to the background. The algorithm simply checks all pixels of input image and if one is darker than specified threshold, it is replaced by the background pixel. This algorithm is simple and efficient. Result of applying it to the input image is shown on the Figure 5.
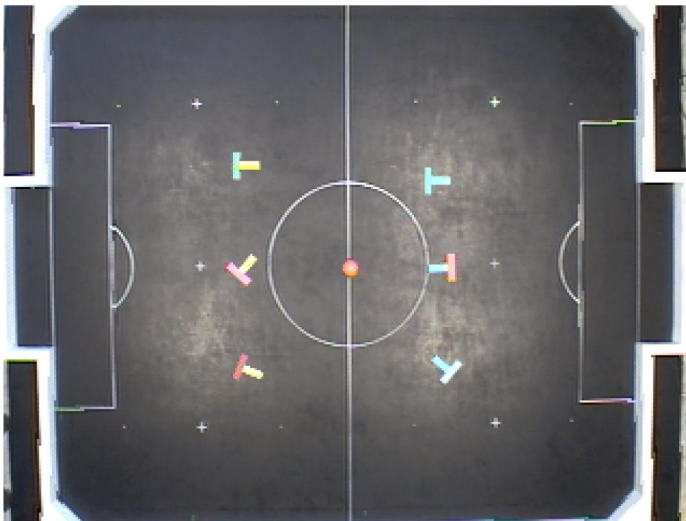
Fig. 5. Results of applying shadow removal algorithm

It is obvious that applying this technique limits the range of colors that can be used as color markers to rather bright ones, however this is not a real problem, as brightness of typical colors used in RoboSoccer is at least twice as high as the threshold value used for shadow removal algorithm.

2.3　Input Image Format

The vision algorithm operates in RGB color space. It has the advantage of being directly available from the frame-grabber hardware, so there is no need for color space conversion. Additionally, working in the RGB color space isintuitive and the visualization and analysis of RGB images and histograms is very easy for human eye. The RGB color space however is not ideal and suffers from nonlinear shift of colors happening after change to the intensity of light. Fortunately, effects of this undesired shift can be easily removed by the adaptation of the algorithm which is described below.

　　In theory, there are other color spaces like HSV or HSL, in which color information is H and S channels should not be vulnerable to changes in the intensity of light. However, experiments proved that although they really are better than RGB color space in preserving the color information unchanged despite of the change of lighting conditions, HSV or HSL histograms also require adaptation, like for RGB. So there is really no significant advantage of using these color spaces.

2.4　Adaptation of Background Model

Although the background subtraction algorithm isn't very sensitive to moderate changes of ambient lighting, it is desirable to give it the ability to update the background model in order to ensure its proper operation during long periods of time.

　　The problem here is not in choosing how to update the background (the moving average algorithm with learning factor α about 0.1 is good enough) but rather in deciding which pixels should be updated. In theory all pixels classified as belonging to the background should be the subject to update, practice however shows that this method leads to pollution of background model with pixels coming from fuzzy edges and from shadow of objects. The solution is to update only pixels lying outside of object's bounding boxes, enlarged twice in order to ensure that no pixels from object's shadow or fuzzy edge will contribute to the update of background model. So the whole procedure of the adaptation of background model can be expressed in the formula:

$$\forall_{(x,y)\in D}[B^{(i+1)}(x,y) = \begin{cases} \alpha B^{(i)}(x,y) + (1-\alpha)I^{(i)}(x,y), & if\,(x,y) \notin X \\ B^{(i)}(x,y), & otherwise \end{cases} \tag{8}$$

where D is a set of pairs (x,y) being coordinates of pixels in the image, B is an image being actual background model, I is input image, X is set of pairs (x,y) being coordinates of all pixels inside two times enlarged bounding boxes, found by flood fill algorithm. Enlargement is done in a way that center of bounding box remains in the same position. Indexes (i) and $(i+1)$ denote previous and current frame, respectively.

2.5   Adaptation of Reference Histograms

The need for continuous adaptation of reference histograms defining the classes of objects comes from the unavoidable nonlinear shift of colors of pixels belonging to every object, which occurs as the object is moving around the playing field. The object has different color in different points on playing field mainly because of the non-uniform lighting provided by four lamps installed over the playing field. This phenomenon is in turn a cause of unpredictable changes in the object's histogram which can lead to recognition errors.

   Fortunately this undesired effect can be compensated by simple moving average algorithm which, after successful recognition, updates the reference histogram with the histogram of an object recognized as belonging to the class defined by this reference histogram. The formula for histogram update is as follows:

$$\forall_{(x)\in X}\left[H_{ref}^{(i+1)}(x) = \alpha H_{in}^{(i)}(x) + (1-\alpha)H_{ref}^{(i)}(x)\right] \tag{9}$$

where X is a set of all possible pixel values x, H_{ref} is a normalized reference histogram being updated and H_{in} is a normalized input histogram. And as above, indexes (i) and $(i+1)$ denote previous and current frame, respectively. For the objects on playing field are able to move really fast (up to $1ms^{-1}$), the learning factor α is quite large here and is equal to 0.2. It is important to notice that histogram obtained by moving average algorithm from two normalized histograms remains normalized as well. The proof is easy and is presented below.

   First, the formula for calculating sum of bins in a histogram created from two normalized histograms according to the moving average algorithm:

$$\sum_{x\in X} H_{ref}^{(i+1)}(x) = \sum_{x\in X}\left(\alpha H_{in}^{(i)}(x) + (1-\alpha)H_{ref}^{(i)}(x)\right) \tag{10}$$

Restructuring right-hand side yields

$$\sum_{x\in X} H_{ref}^{(i+1)}(x) = \sum_{x\in X}\alpha H_{in}^{(i)}(x) + \sum_{x\in X}(1-\alpha)H_{ref}^{(i)}(x) \tag{11}$$

Factors α and $(1-\alpha)$ can be taken outside summing operator yielding

$$\sum_{x\in X} H_{ref}^{(i+1)}(x) = \alpha \sum_{x\in X} H_{in}^{(i)}(x) + (1-\alpha)\sum_{x\in X} H_{ref}^{(i)}(x) \tag{12}$$

Since right-hand side histograms are normalized (sum of bins in each histogram is equal to 1)

$$\sum_{x\in X} H_{ref}^{(i)}(x) = 1 \tag{13}$$

$$\sum_{x\in X} H_{in}^{(i)}(x) = 1 \tag{14}$$

thus the equation 12 becomes

$$\sum_{x \in X} H_{ref}^{(i+1)}(x) = \alpha 1 + (1 - \alpha)1 = 1 \qquad (15)$$

which ends proof.

2.6   Flood Fill Algorithm

Binarized image coming from the background subtraction algorithm contains measures like center of mass, bounding box, geometrical moments etc. can be also calculated, and what's very important, calculating these measures can be done at very small cost. The algorithm used for the labeling purpose (one among others) is called Flood Fill. This algorithm can be described best by the following pseudo code.

```
int currLabel = 0;
stack s;
   for (int y = 1; y < HEIGHT-1; y+=SKIP)
   for (int x = 1; x < WIDTH-1; x+=SKIP)
   if (img.pixel(x, y) == 255) {
      currLabel++;
      s.push(x, y);
      while (!s.empty()) {
         int xx, yy;
         s.pop(xx, yy);
         if (img.pixel(xx, yy) == 255) {
          img.pixel(xx, yy) = currLabel;
          s.push(xx-1, yy-1);
          s.push(xx , yy-1);
          s.push(xx+1, yy-1);
          s.push(xx-1, yy );
          s.push(xx , yy );
          s.push(xx+1, yy );
          s.push(xx+1, yy+1);
          s.push(xx , yy+1);
          s.push(xx+1, yy+1);
         }
   }
}
```

In the above implementation parameters WIDTH and HEIGHT are dimensions of the image img being processed, parameter SKIP is for simple optimization based on the observation that knowing the minimal size occupied on the raster by the objects to be labeled the algorithm does not need to start searching for them from every pixel, it is enough to start searching every n pixels, where n should be a bit

smaller than minimal width or height of objects of interest. The implementation presented above additionally presumes that input image consists of two values only: 0 for background and 255 for foreground objects.

2.7   Estimation of Object's Position and Orientation

Vision algorithm is capable of precise estimation of position of all robots and ball and orientation of robots only. (Quite naturally, orientation is not calculated for a ball). Robots could be interpreted as agents and the approach of planning could be used [9]. However , real time applications requires fast adaptation to changes. Therefore different approach was used. The method used here is described in more detail in [16]. Calculations are done in four stages. First, for each object, the following integrals are calculated:

$$F = \iint_D dxdy \tag{16}$$

$$S_x = \iint_D ydxdy \tag{17}$$

$$S_y = \iint_D xdxdy \tag{18}$$

Where D is a region occupied by the object, F is its area and S_x and S_y are static moments. Next, the position of each object is found from the formulas describing center of the mass:

$$x_0 = \frac{S_y}{F} \tag{19}$$

$$y_0 = \frac{S_x}{F} \tag{20}$$

Then the angle of main axis of inertia is calculated for each robot and finally, the direction of this axis is chosen, as the algorithm for finding the angle of main axis of inertia can't do that automatically and additional heuristics is needed. These two stages are described in more detail in sections below.

2.8   Angle of Main Axis of Inertia

Estimating the orientation of robot on the basis of main axis of inertia is possible thanks to the special shape of the color marker placed on the top of each robot. The shape is presented on Figure 6.
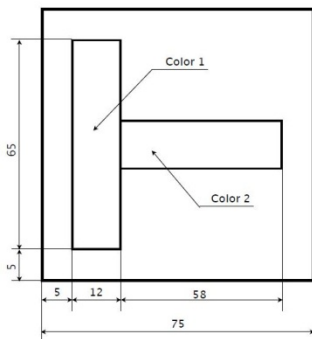
Fig. 6. Design of robots top marker

It was designed with three goals in mind:

- It has to be significantly wider in one dimension, in order to improve precision of estimating the main axis of inertia
- It should be more thick on one end than on the other, to make possible choosing the direction of main inertia axis, according to the algorithm described in the next section
- It has to be small enough, to prevent two or more color markers coming from different robots from being recognized as one object, when being very close to each other.

Estimating the angle of main axis of inertia is done in few steps. First, moments of inertia are calculated:

$$J_x = \iint\limits_D y^2 dx dy \tag{21}$$

$$J_y = \iint\limits_D x^2 dx dy \tag{22}$$

$$J_{xy} = \iint\limits_D xy dx dy \tag{23}$$

Then the elements of tensor of inertia are found:

$$J_{x0} = J_x - F y_0^2 \tag{24}$$

$$J_{y0} = J_y - F x_0^2 \tag{25}$$

$$J_{x0y0} = J_{xy} - F x_0 y_0 \tag{26}$$

Finally, central moments of inertia can be calculated:

$$J_{\xi 0} = \frac{1}{2}(J_{x0} + J_{y0}) + \frac{1}{2}\sqrt{(J_{y0} - J_{x0})^2 + 4Jx_{x_0y_0}^2} \qquad (27)$$

$$J_{\vartheta 0} = \frac{1}{2}(J_{x0} + J_{y0}) - \frac{1}{2}\sqrt{(J_{y0} - J_{x0})^2 + 4Jx_{x_0y_0}^2} \qquad (28)$$

Angles of both axes of inertia are calculated from the following formulas:

$$\alpha_{\xi 0} = arctan\frac{J_{x0y0}}{J_{y0} - J_{\xi 0}} \qquad (29)$$

$$\alpha_{\vartheta 0} = arctan\frac{J_{x0y0}}{J_{y0} - J_{\vartheta 0}} \qquad (30)$$

To calculate the value of arc tangent it is the best to use $atan2$ function from standard math library, as it automatically deals with finding proper sign of result depending on the quadrant of coordinate system. For objects symmetrical with respect to both axes of inertia, the one described by angle $\alpha_{\xi 0}$ is perpendicular to the axis of longest dimension of the object while the axis described by the angle $\alpha_{\vartheta 0}$ is co-linear with the axis of longest dimension, so the vision algorithm uses the second axis of inertia in further calculations.

2.9   Direction of Main Axis of Inertia

The algorithm relies on special design of the shape of color marker on top of each robot described earlier in this chapter. The idea of finding the direction of main axis of inertia is explained on Figure 7 and explained below. Steps taken by the algorithm in order to decide whether the directed angle γ describing direction of main axis of inertia is equal to $\alpha_{\xi 0}$ or $\alpha_{\xi 0} + \pi$ can be described as follows:
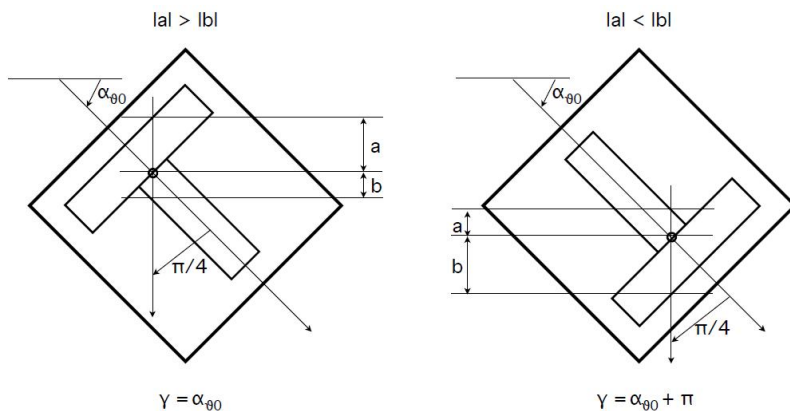
Fig. 7. Idea of finding the direction of orientation axis

- Create two vectors, $\vec{u}$ and $\vec{v}$, with common origin in mass center (x_0, y_0). Initial length of these vectors should be 1. They should be at angle $\frac{\pi}{4}$ and $\frac{\pi}{4} + \pi$ to the main axis of inertia, respectively. Angles are directed and measured clockwise.
- If the vector $\vec{u}$ points to background pixel and vector $\vec{v}$ points to pixel belonging to the object, then $\gamma = \alpha_{v0}$.
- Conversely, if the vector $\vec{v}$ points to background pixel and vector $\vec{u}$ points to pixel belonging to the object, then $\gamma = \alpha_{v0} + \pi$.
- If both vectors point to pixels belonging to the object, the length of these vectors is increased by one and the whole procedure is repeated.

The algorithm is simple and efficient, however it requires that the shape created by background subtraction algorithm should not differ significantly from the reference design presented on Figure 6.

3   Obtained Results

The vision application works under Linux. It is meant to be a centralized vision system providing vision information for all who will ask for it. That goal was achieved by implementing the application as a TCP/IP server, to which clients can connect and ask for vision information (Figure 8 and 9).

The application was tested on a PC computer working under Ubuntu Linux. The computer is equipped with Pentium 4 3.00 GHz Hyper Threading processor, 512 MB DDR RAM and GeForce 5200 FX graphics card. Input images were acquired with Samsung SCC–331 CCD camera equipped with Ernitec lens (f = 6 - 12 mm, ϕ = 35.5 mm, 1:1.4). Images were then digitized by simple BT878-based frame-grabber card. The lighting was provided by four 500W halogen lamps installed 2 m over the corners of the playing field.

The application was compiled by the new GNU C++ compiler in version 4 with use of the following optimization flags: -O3 -funroll-loops. On the test hardware the application uses approximately 50% of CPU time and about 20 MB of RAM. The framerate is constant and is equal to 30 frames per second, which is the limit imposed by the frame-grabber hardware. With better frame-grabber it should be possible to reach about 60 frames per second without any code re-factorization or optimization. Results of precise measurements of time needed for completing particular tasks by the vision algorithm are presented in Table 1. The figures were obtained by averaging 100 measurements. The vision server also responds very quickly, usual response is under 1 ms.

High frame-rate and quick response of the server is crucial for the stability of all control algorithms that use vision information on the feedback loop, so there is always a place for further research here, however the delays introduced by the current version of vision application seem to be acceptable for broad range of control algorithms.
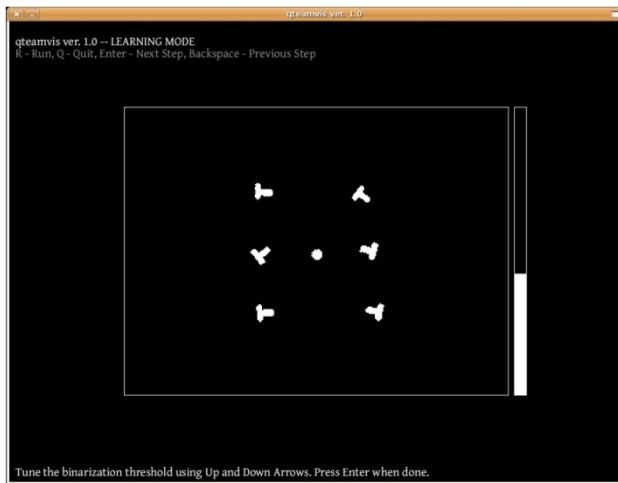
Fig. 8. Proper binarization threshold

Table 1. Processing times of every step of vision algorithm

No.	Operation	Times [ms]
1.	Correction of Radial Distortion	8.4
2.	Shadow Removal	0.98
3.	Image Difference	4.0
4.	Thresholding	0.42
5.	Dilation	0.54
6.	Flood Fill	0.20
7.	Region Sorting and Median Filtering	0.45
8.	Histogram Calculation	0.12
9.	Classification	0.07

The vision algorithm proved to operate reliably. The adaptation of reference histograms works perfectly, which is clearly visible in the corners of the playing field where the lighting conditions are significantly different than near center of the playing field. The background subtraction algorithm is so robust that it works perfectly when the overall lighting conditions were changed by turning on additional lamp, even without adaptation enabled. Size and shape of color markers on top of each robots prevents from the situation where markers of robots being very close to each other are "joined" and constitute one, bigger marker, which of course leads to recognition errors. For this situation is very difficult to deal with, the algorithm assumes that it never happens and the responsibility for assuring that it really wouldn't is in the design of markers.

Fig. 9. Position and size of playing field calibrated properly

The precision of measurements made by vision system is much improved when compared to the previous system and seems to be sufficient to successfully attend the RoboSoccer competition. Measurement errors are presented in the Table 2. The great advantage of the vision system is that it never loses the position of any object on playing field. Orientation axis is also always calculated properly, however the measurement is usually a bit more distorted and there are some oscillations visible. The only measurement that sometimes is done incorrectly is the measurement of direction of orientation axis, fortunately it happens very rarely and in future it should be easy to get rid of this problem by improving the shape of color marker and by switching to higher resolution.

Table 2. Relative errors of measurements of a position and angle

Relative measurement error [%]					
Radial Correction		Robot			Ball
		x	y	γ	x	y
Enabled	0.5	0.6	1.5	0.4	0.5
Disabled	1.0	1.1	2.0	0.9	1.0

Precision of the measurements could possibly be further improved by introducing compensation of cylindrical distortions of camera's lens, this however is left for further research. Switching to the higher resolution should also improve the precision, for the objects will occupy more pixels on raster.

4   Conclusions

The version of vision system presented in this work proved to be very successful and fully operational. Proposed algorithm provides stable vision information i.e. it never losses any objects, they are always tracked properly. Used histogram-based color classifier proved to be very efficient and difficult to mislead, mainly because of the algorithm's ability to adapt stored reference histograms to changing lighting according to the current classification. Color classifier operates properly in the limited colorspace of the NTSC signal coming from cheap industrial camera.

It is very easy to find colors that can be used as markers on top of the robots. The algorithm is sufficiently robust in assumed range of changes in the lighting conditions, both spatial (caused by the nonuniform lighting around the playing field, caused by the fact that there are four lamps above the corners of playing field) and temporal (caused by accidents like turning off one of the lamps or opening the window, which results in increased amount of sunlight coming to the playing field).

Measurement data is precise enough to be used in sophisticated control loops, and the delay introduced to the system is almost constant and in assumed range, guarantying stability of the control algorithms. Relative measurement errors of position coordinates x and y and angle of orientation do not exceed 1.5% and delay is at most 30 ms, being the limitation of the frame-grabber card, which is able to deliver only 30 images each second.

Performance of the application is also very satisfactory - the whole frame is processed in 15 ms. It gives the possibility of obtaining high framerates (at least 60 frames per second) after upgrading the framegrabber card to the model that is able to deliver more than 30 images per second.

The vision data is made available to many other applications via TCP/IP socket. It makes possible building distributed control system for mobile robots, consisting of many computing nodes. Application design is modular, individual components are loosely coupled to each other and are implemented with use of design patterns, which further simplify the design and promote good solutions, so further development should be quite easy. This is particularly important, for the existing code could be used in future industrial-quality vision application.

References

[1]   Sridharan, M., Stone, P.: Autonomous Color Learning on a Mobile Robot. In: The Twentieth National Conference on Artificial Intelligence (AAAI 2005), Pittsburgh, USA (July 2005)

[2]   Jeong, S.: Histogram-Based Color Image Retrieval Psych221/EE362 Project Report. Stanford University (2001)

[3] Lee, S.M., Xin, J.H., Westland, S.: Evaluation of Image Similarity by Histogram Intersection. COLOR Research and Application 30(4), 265–274 (2005)

[4] Piccardi, M.: Background Subtraction Techniques: A Review Lecture Notes. University of Technology Sydney (2004)

[5] Tsai, R.Y.: A Versatile Camera Calibration Techniaue for High-Accuracy 3D Machine Vision Metrology Using off-the-shelf TV Cameras and Lenses. IEEE Journal of Robotics and Automation RA-3(4), 323–344 (1987)

[6] Robinson, J.: CLIP: C++ Template Library for Image Processing (2006),
`http://www.intuac.com/userport/john/clip104.html`

[7] Skrzypczyk, K., Gałuszka, A., Pacholczyk, M., Daniec, K.: Probabilistic approach to planning collision free path of UAV. In: Nawrat, A., Simek, K., Świerniak, A. (eds.) Advanced Technologies for Intelligent Systems of National Border Security. SCI, vol. 440, pp. 59–68. Springer, Heidelberg (2013)

[8] Gałuszka, A., Pacholczyk, M., Bereska, D., Skrzypczyk, K.: Planning as Artifficial Intelligence Problem-short introduction and overview. In: Nawrat, A., Simek, K., Świerniak, A. (eds.) Advanced Technologies for Intelligent Systems of National Border Security. SCI, vol. 440, pp. 95–104. Springer, Heidelberg (2013)

[9] Galuszka, A., Swierniak, A.: Planning in multi-agent environment using strips representation and non-cooperative equilibrium strategy. Journal of Intelligent and Robotic Systems: Theory and Applications 58(3-4), 239–251 (2010)

[10] Jędrasiak, K., Nawrat, A., Wydmańska, K.: SETh-link the distributed management system for unmanned mobile vehicles. In: Nawrat, A., Simek, K., Świerniak, A. (eds.) Advanced Technologies for Intelligent Systems of National Border Security. SCI, vol. 440, pp. 247–256. Springer, Heidelberg (2013)

[11] Iwaneczko, P., Jędrasiak, K., Daniec, K., Nawrat, A.: A prototype of unmanned aerial vehicle for image acquisition. In: Bolc, L., Tadeusiewicz, R., Chmielewski, L.J., Wojciechowski, K. (eds.) ICCVG 2012. LNCS, vol. 7594, pp. 87–94. Springer, Heidelberg (2012)

A Distributed Control Group of Mobile Robots in a Limited Area with a Vision System

Artur Babiarz, Robert Bieda, and Krzysztof Jaskot

Abstract. Digital remote manual control systems are no less complicated than automatic control. Engineers have to overcome number of unique problems. Mechanical parts have to respond to digital signals transferred through wireless connection. Digital control algorithms have to correctly translate the movement of controls at remote station to signals in a way that a operator has a proper feeling of control. The Master Control System presented connects the features of a Drive-By-Wire control system with wireless connection. Main focus is put on the Master controller and its algorithms of input - output translation, that give finer control for an operator. In addition, computer controlled intervention algorithms are proposed that can increase safety of the subject vehicle. All that is done on basis of a small two-wheeled robot and a closed environment of small playground with radio interface allowing wireless connection with the robot, and a vision interface equipped with a camera serving as a visual feedback. Is it a great environment for theoretical considerations, testing and implementation. Modular design of the environment additionally allows the control of whole Mobile Robot Group, not only one robot subject. Moreover sented results can be applied more widely in controllers for cars or other wheeled or tracked vehicles.

1 Introduction

When we think about manual control we often think about things we need to do by hand in our everyday life. Although there are more complicated systems we use, like riding a bicycle or driving a car. Some of us has learned skill to operate those vehicles. After gaining proficiency in such a skill, it is natural for us, we do it

Artur Babiarz · Robert Bieda · Krzysztof Jaskot
Silesian University of Technology, Institute of Automatic Control,
Akademicka 16, 44-101 Gliwice, Poland
e-mail: {artur.babiarz,krzysztof.jaskot,robert.bieda}@polsl.pl

automatically because we have the feeling of controls. Such manual control is a mechanical one. It utilizes a collection of mechanical parts, such as rods or tension cables. Steering wheel in a car directly changes the orientation of wheels, change of gear at the car's gearbox directly changes used gear, etc. This is the most basic method of control, widely used in vehicles around the world, as it successfully accomplishes its goal.

As more complicated vehicles and planes were built, and as rapid growth of technology has allowed, more of the intelligent operations had relied on electronic devices. It has become possible to apply machine intelligence to control. That idea was mainly utilized in flight control, as it has always been a very complicated problem, consisting of vast number of variables [1, 2, 3]. Vision systems are used mainly in mobile robotics for determining the position robot. A very simple way to generate a path with the vision presented in [16]. This method is called *funnel lane*. The coordinates of feature points during the replay phase are compared with those obtained during the teaching phase in order to determine the turning direction. Another problem is the determination of the actual speed of the mobile robot. The authors [14] propose the use of a Kalman filter (KF)-integrated optical flow method to measure the velocity of mobile robots using a downward-looking camera. In [9] the authors present a group of robot motion planning using distributed control and vision system. The control laws are distributed in the sense that they require information only from neighboring robots. Examples of the application of the vision for mobile robot control in a limited area can be found in [6, 11]. The use of vision and Q-learning controller to robust grasping by wheeled mobile robots was presented in [15]. Control law based on sliding-mode theory in order to drive mobile robots to a target location, which is specified by a previously acquired reference image is presented [4]. It is essential to develop new mathematical theories that one day might outperform the mentioned above theories [21, 22, 23].

1.1   Drive-By-Wire

It has come to the point, that some of aircraft whole manual control systems are replaced by electronic interfaces - constructing so called "Fly-By-Wire" systems, in which movement of controls is translated to digital signals, and a computer controller determines how to move the actuators. Example of such a plane is a Boeing 787 Dreamliner [10]. Recent development also applies similar systems to prototype cars in "Drive-By-Wire" systems [5].

Overview of Drive-By-Wire manual control system in comparison to the mechanical manual control is shown on Fig 1. Drive-By-Wire is a basis of creation of remote manual controls, in which signals are sent through wireless connections, and are translated to mechanical actions of its actuators using the controller on subject vehicle. Example of a remotely controlled vehicle is a prototype of
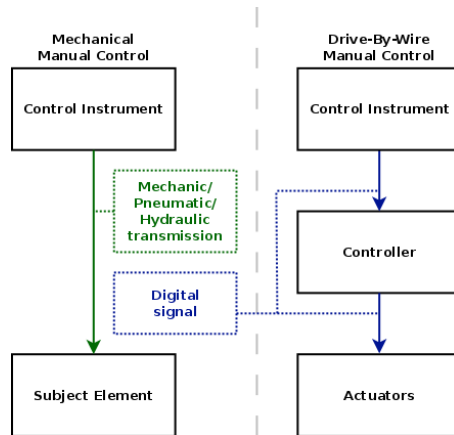
Fig. 1. Overview of Drive-By-Wire manual control system in comparison to the mechanical manual control

"Unmanned Ground Vehicle on BMP II Vehicle Platform", that has been developed by Combat Vehicles Research Development Establishment, Avadi, Chennai, India. The prototype consists of Drive-By-Wire system, which includes electromechanical actuators and drives. This system is controlled by a controller and receives commands through wireless network from the Graphical User Interface located in base station [8]. Modern automotive industry is working on new technologies in order to increase safety of cars. Practical example of successful project in this direction are the assistance systems developed by Volkswagen [13]. They have implemented numerous systems that aid driver in driving the car e.g. front assist or lane assist.

2   Literature Review

Base for construction of the control system is the RoboSoccer project, referred to as an Environment. Its main modules are used in order to reuse the work already done, making possible focusing on the real control algorithms, in turn giving back a great testing and learning facility.

Figure 2 shows the general overview of the RoboSoccer project system.

Its divided into three main parts:

1. Robot subject.
2. Vision system.
3. Radio system.

Each of the parts is described in following sections in details.
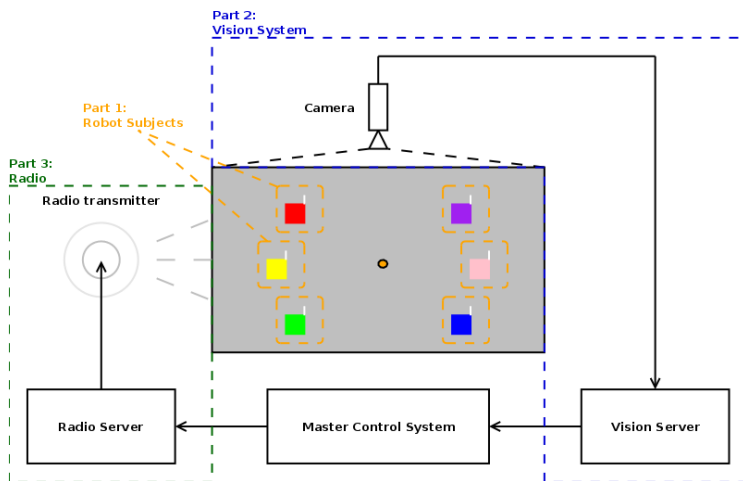
Fig. 2. RoboSoccer system overview

2.1   Robot Subject

The subject to control is a robot, shown at figure 3 with a two-wheeled differential drive, operated by two DC motors. Each of motor has an incremental magnetic encoder, that counts how much a wheel has rotated, and it is the only sensor available at the vessel. It has an on-board micro controller constructed, based on ATMEL microprocessor. It is able to realize simple control procedures, making it possible for Master Control System to focus on more sophisticated algorithms [7]. The wireless connection, serving as input for commands, is provided by the Xbee module, properly interfaced by the software in the on-board controller. The same Xbee module exists at the other end, in Radio system of the project. Therefore robots could be interpreted as agents [19].
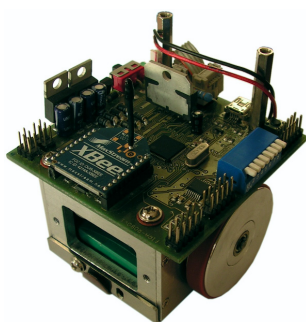
Fig. 3. Robot

The robot provides interface for following actions, which can be commanded through the Radio:

- Change the speed of wheels i.e. set linear velocity of a robot.
- Rotate by given angle, at given angular velocity or at given constant radius.
- Move forward/backward by given distance.
- Go to a given location.

2.2   Skid Limits

Important fact is ensuring that the robot does not slide, as it would input errors to the incremental magnetic encoder, which runs vital part of every algorithm at the robot. That is why the on-board controller avoids skid of wheels, by limiting linear and angular acceleration. It has to be taken into account by the Master Control System, so that the system is cohesive. The limits are calculated in work [7] and are listed in Table 1.

Table 1. Limits

Limit	Value	Unit
Acceleration $\propto_{max}$	1	$\dfrac{m}{s^2}$
Angular acceleration $\propto_{max}$	0.5	$\dfrac{rad}{s^2}$

The α_{max} was obtained experimentally by checking whether a set acceleration causes any sliding and repeating the experiment successively. The value that is used was additionally lowered by 50% in order to minimize the risk of skid, while the α_{max} was calculated from the interaction of wheels with the ground [7].

2.3   Vision System

The vision system provides coordinates and values of angles of robots and ball on the playground. It acquires images from the camera, which is mounted permanently above the playground, via a frame-grabber card. The view from the camera is shown on an exemplary image at Figure 4.
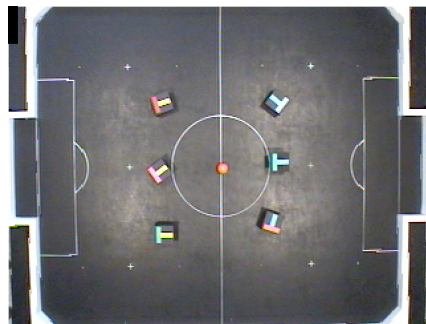
Fig. 4. Playground seen by camera

Acquired images are the only input for vision system, which implements an algorithm, which main goal is to provide precise estimation of position and orientation of objects on field (robots and ball) in different lighting conditions. Vision system not only gives coordinates of objects on the playground, but also field's and robot's dimensions. It was constructed in such a way in order to make vision system more adjustable to changing real environments. Main characteristics of the algorithms are [11]:

- The estimation of orientation has 2° standard deviation and 10° in worst case.
- The estimation of position has $2mm$ standard deviation.
- The speed of processing is 30 frames per second (one frame per $30\ ms$).
- Small differences in lightning of playground does not influence work of the system.
- Algorithm has no problem in recovery from a temporary situation of an object "lost".

We can say that the above features are satisfactory. As it can be seen on Figure 5, the values of orientation and position are very accurate.
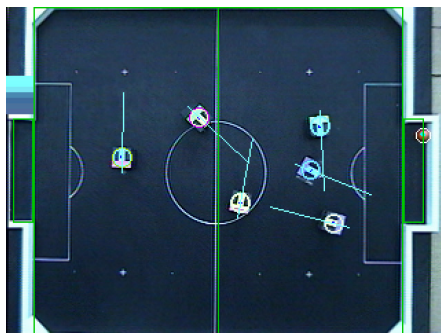
Fig. 5. View from the camera with orientation and position marks sketched on

The application implementing the vision algorithm is a stand-alone server and communicates with clients using the TCP/IP network with use of special Extensible Markup Language (XML) based protocol [12].This XML based communication is implemented in a C++ communication library called libqteam providing interface for programming control algorithms. From the view of control algorithms the vision system works as the feedback loop, providing measurements of values being inputs to the controller. The general way of signal in the vision system is shown on Figure 6.
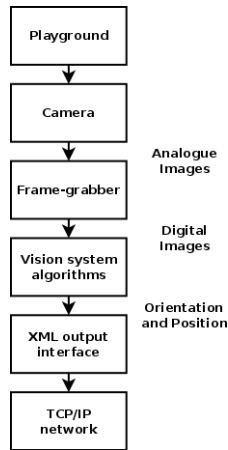
Fig. 6. Signal in vison system

Camera records images of playground, sends it to the computer as an analogue signal, frame-grabber is capturing digital images from that signal. Then vision algorithm basing on this data find orientations and positions of objects, and provides this information in XML format through TCP/IP connection, providing a server for such type of connection. Coordinates given by vision system can be referred to as a global positioning system. It is due to the fact that the robot has internal local positioning system based on his odometers.

Main feature of global positioning, that has to remembered when reading coordinates, is that the point of origin is center of the playground and the chosen team's goal is on the left.

2.4 Radio System

Communication between the master control system and the subject robots is provided by the radio system. It consists of hardware radio module and software for PC that provides output interface. As in the case of vision system, radio system is also implemented as a standalone server, providing interface through TCP/IP connection implemented in the C++ communication library - libqteam. The way of signal in the radio system is shown on Figure 7. The TCP/IP server allows clients to connect and receives commands in simple packet format.
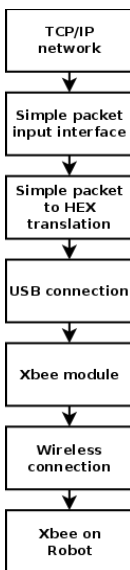
Fig. 7. Signal in radio system

3   System Structure

3.1   Drive-By-Wireless System Overview

The Master Control System presented connects the features of a Drive-By-Wire control system with wireless connection, creating a Drive-By-Wireless system. Its main part is the master controller and control instruments. It utilizes the robot subject, wireless connection and vision feedback provided by the environment. Overview of the system is presented on Figure 8.
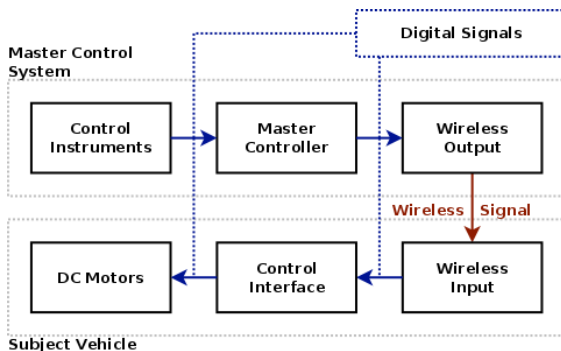
Fig. 8. Drive-By-Wireless system

3.2 Master Control System Structure

The Master Controller is implemented in Java programming language as an application with graphical user interface. It is called **qView** and on Figure 9 can be seen in the middle. Control algorithms are constructed in its basic layer and graphical user interface utilizes them on application layer allowing user interaction and gives the visual feedback. Additional application is the **qPhone**, that is a midlet application for cellphones. Utilizing a bluetooth connection between cellphone and PC computer with qView application installed, it transmits the cellphone's keypad events to qView control algorithms in order to fulfill one of primary goals - possibility to control a robot with a cellphone. Such construction – only transmission of events - makes it able to reuse algorithms, without need of implementing whole new separate controller. However different implementations to planning collision free path [17] are possible e.g. using AI [18], [20].
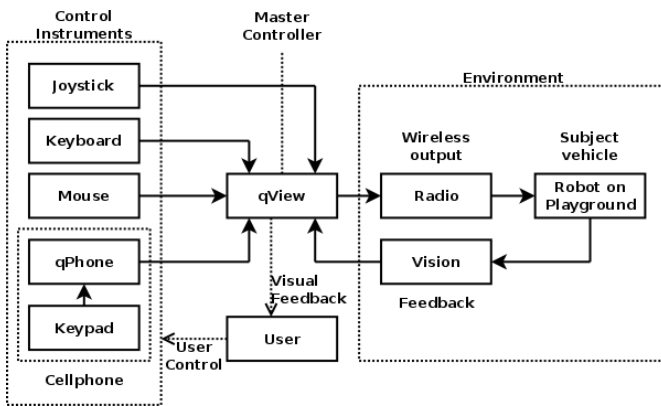
Fig. 9. Master Control System structure

3.3 Visual Feedback

qView application provides the visual feedback of current state of playground. It is rendered using 2D Java graphics library basing on the coordinates gathered from the vision server. In case of successful connection to the vision server, feedback is automatically shown and refreshed at the maximum possible frame rate - i.e. rate at which vision system is processing data from the camera - about 30 frames per second.

3.4 Field Coordinate System

The coordinate system of objects on the field is different from the coordinate system of general 2D graphical rendering1 on screen. Vision system coordinate system point of origin is at the center of playground, while the 2D graphical rendering model point of origin is at the top left point of screen/frame. Also the

vertical dimension is reversed. Both coordinate systems are shown on Figure 10, where red coordinate system is input from vision, and green one is 2D graphical rendering system.
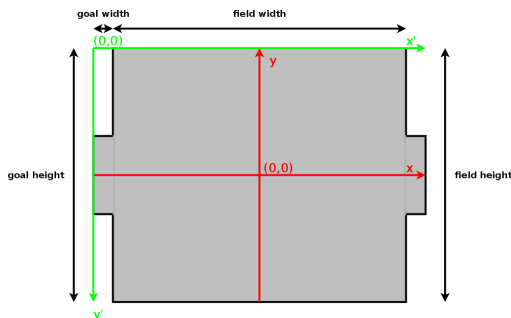
Fig. 10. Coordinate system

In order to correctly display objects on the field, following translation has to be made for every coordinate:

$$x' = x + \frac{fieldwidth}{2} + goalwidth \tag{1}$$

$$y' = -y + \frac{fieldwidth}{2} \tag{2}$$

Both *fieldwidth* and *fieldheight* are downloaded from vision system configuration.

4   Computer Controlled Intervention Experiments

Computer controlled intervention proposed is a playground edge avoidance system. It is composed of two parallel algorithms: speed limiter and trajectory control, that together achieve a successful avoidance system in given environment. In separate though they are also reusable solutions, that could be base for similar considerations in e.g. automotive industry.

4.1   Speed Limiter

The idea of speed limitation is that we want to limit maximum speed, so that the vehicle will not collide with the edge of playground. As we can control the speed, the deceleration can be assumed constant to a maximum possible value of $-1\frac{m}{s^2}$ due to the robot skid limits, we only need the distance of robot from the edge in order to calculate maximal speed the robot can move in order to achieve a condition, that he will be able to stop not colliding with the edge. This speed can be calculated from the following kinematic equation:

$$d = v_0 \cdot t + \frac{1}{2} \cdot at^2 \tag{3}$$

As time is irrelevant in this problem, we can substitute it using following considerations. Having equation for speed with acceleration included:

$$v = v_0 + at \tag{4}$$

We want to have speed equal to $0\frac{m}{s}$ with deceleration equal to $-1\frac{m}{s^2}$ so we get:

$$0 = v_0 - t \tag{5}$$

Which leads to:

$$t = v_0 \tag{6}$$

Substituting this into the (3), assuming $a = -1\frac{m}{s^2}$, and after few simplifications we get:

$$d = \frac{1}{2} \cdot v_0^2 \tag{7}$$

As we control speed, and distance is the parameter, the solution is:

$$v_0 = \sqrt{2 \cdot d} \tag{8}$$

In order to minimize the computer intervention into user's control, we do not want to influence speed directly, that is why in fact we limit the maximum speed:

$$v_{max} = \sqrt{2 \cdot d} \tag{9}$$
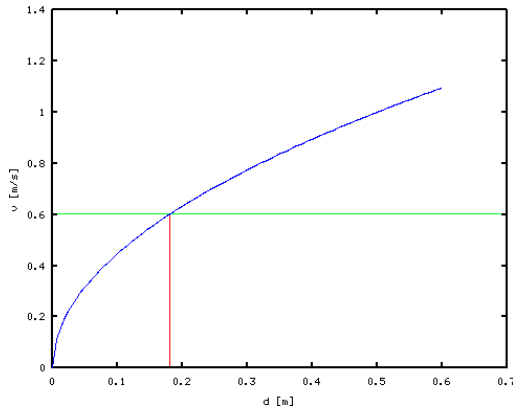
Fig. 11. Speed limitation

This limitation, equation (9) can be interpreted graphically at Figure 12. It has to comply with the global maximal speed of the robot, shown on Figure 11 with a green plot, equal to $0.6\frac{m}{s}$. The meaning of this graph is that the robot maximal

speed is being limited due to the distance of edge at approximately $0.18m$ from the edge in case of $0.6\frac{m}{s}$ global speed limitation.

4.2   Distance Measurements

The speed limit is parameterized by the distance to edge. That value has to be calculated. And in fact we do not want the minimal absolute distance from the edge (see Figure 12, as this could cause a lock down - i.e. the robot speed would be limited to 0 without any chance of further movement.
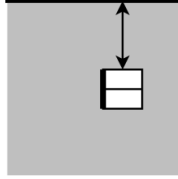
Fig. 12. Minimal absolute distance from the edge

The better choice is to calculate distance to the edge in robot forward and backward orientations (see Figure 13). Even if the speed was limited to 0 at the edge, robot could still turn, making possible the increase of the distance and eventually to move again. This is however harder approach.
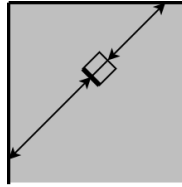
Fig. 13. Distance from the edge in forward and backward orientations

Having coordinates of the robot and size of the playground, we can calculate easily the absolute distances from the edges (see Figure 14):

$$x_1 = \frac{fieldWidth}{2} + x \tag{10}$$

$$x_2 = \frac{fieldWidth}{2} - x \tag{11}$$

$$y_1 = \frac{fieldHeight}{2} + y \tag{12}$$

$$y_1 = \frac{fieldHeight}{2} + y \tag{13}$$

Having such info and the orientation of the robot in angles $0°$ is right, $90°$ is up, $180°$ is right and $270°$ is down), we can calculate distance to the edge in forward and backward orientations using trigonometric formulas, that differ a little in four orientation quadrants: $0° - 90°, 90° - 180°, 180° - 270°, 270° - 360°$; but use the same considerations, thus i present only one quadrant of $0° - 90°$.
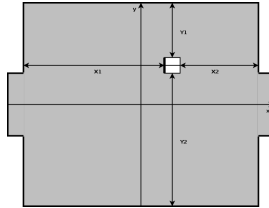
Fig. 14. Minimal distances from the edges

It is most easy to interpret it graphically in the $0° - 90°$quadrant shown at Figure 15. We have two cases. The ray shot forward at angle of robot orientation can either intersect with the top edge at Figure 15(a), or side edge at Figure 15(b). We do not have knowledge about this fact, but when we use the trigonometric functions we do not have to know.

(a) Top edge intersection   (b) Side edge intersection
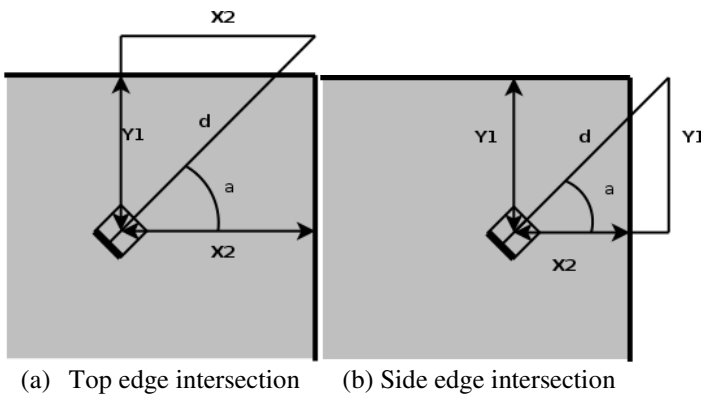
Fig. 15. Forward and backward distance calculation

$$d = min\left(\frac{y_1}{\sin(\alpha)}, \frac{x_2}{\cos(\alpha)}\right) \qquad (14)$$

$$d_{back} = min\left(\frac{y_2}{\sin(\alpha)}, \frac{x_1}{\cos(\alpha)}\right) \qquad (15)$$

This is because when we take the minimum of $\frac{y_1}{\sin(\alpha)}$ or $\frac{x_2}{\cos(\alpha)}$, we always choose the result of cosine as $\frac{y_1}{\sin(\alpha)} > \frac{x_2}{\cos(\alpha)}$ in case 15(b) and the result of sine in case 15(a) otherwise, which are the correct values of distance to the edge in forward

orientation. Similar equations apply to the rest of quadrants and backward distance calculations. Having such distance calculated at real time, we can limit the speed accordingly.

4.3   Control Algorithms

Control instrument signals have to be translated in order to give the user a way to control a given object. Input devices differ from each other in some ways, but also some things may be in common. Best practice is to join the common things together and create one joint controller, then creating more advanced controllers on its basis for each of control instrument. As there can be numerous control instruments connected to qView, in order to provide proper control, only one input device can be allowed to control a given robot. This is done by simple locking mechanism, in which input devices ask for permission to control a robot, and if one is not controlled at a time, permission is granted and lock is activated. In this time no other control instrument can get access to that robot.

Two things in the robot can be controlled - linear and angular speed. Both are accessible directly through functions and this direct approach is most frequently used:

1. Robot::setSpeed(speed).
2. Robot::setTurningSpeed(angSpeed).

Although the on-board controller on the robot also gives another way to control the angular speed, through the Robot::setTurningAngle(radAtan) function. It is a turning radius control algorithm implemented in the robot software and detail description is presented in work [7]. It allows to control turning of the robot at constant radius. The parameter given to this function - atan $\left(\frac{1}{r}\right)$ - can be understood as an angle at which robot would turn if it had third leading wheel. Although in order to keep the turning radius constant, the algorithm has to limit the linear speed accordingly, which could cause that the actions of operator are not natural and not as intended.

5   Experimental Results

This section describes in detail three taken experiments testing the performance of proposed algorithms. The plots of trajectories shown at Figures 16(a) and 19(a) describe position of robot in x and y coordinates, where the edges of playground are at following values:

$$x = \pm 0.75 \tag{16}$$

$$y = \pm 0.65 \tag{17}$$

5.1 Computer Controlled Intervention

The trajectory control successfully executes goals it was given, with the speed limiter working as a helper algorithm. Figure 16 shows the algorithm working as intended. The human operator was controlling the robot using keyboard forward key function, moving the robot towards the edge from left to right. The intervention lowered the speed at the top edge and induced the turn. When the robot got into safe trajectory, it turned off the intervention. Although the current trajectory would make robot hit the right edge, so the speed was eventually limited to 0, because the angle to the edge was too big to change the trajectory.

(a) Trajectory

(b) Speed

(b)   Angular speed
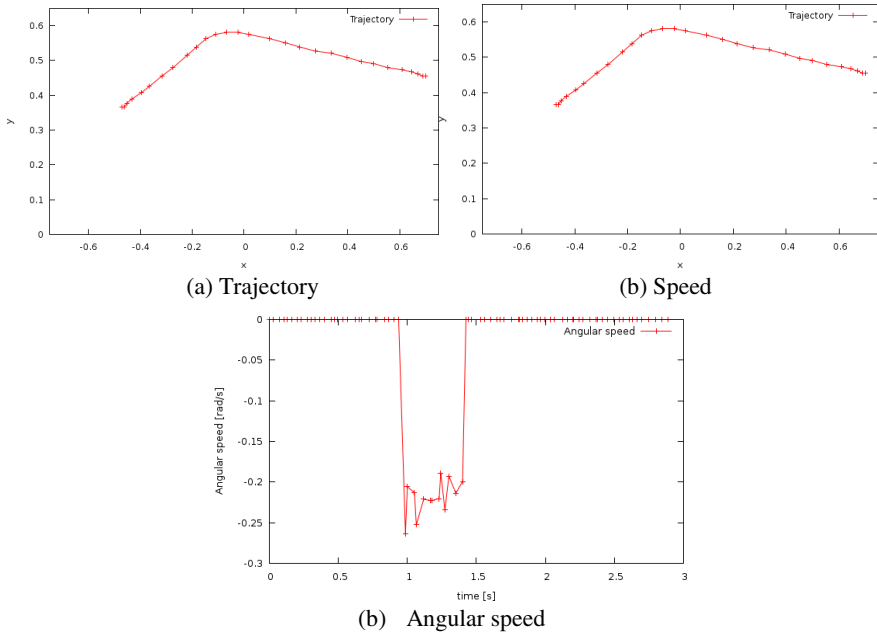
Fig. 16. Computer controlled intervention
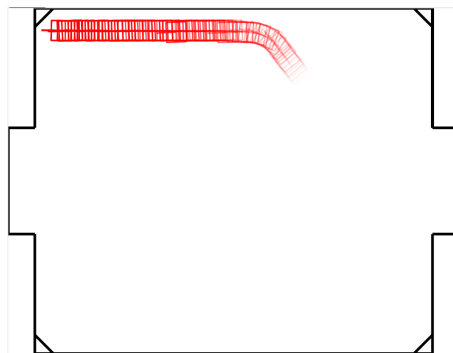
Fig. 17. Trajectory tracked

Trajectory Tracking

Figure 17 shows the trajectory tracked of an experiment similar to the one shown in Section 5.1 i.e. the human operator was inducing only the movement forward. The results are the same: the robot changes the trajectory automatically near the top edge due to the computer intervention and stops at the left edge as intended.

(a) First

(b) Second

(c) Third

(d) Fourth
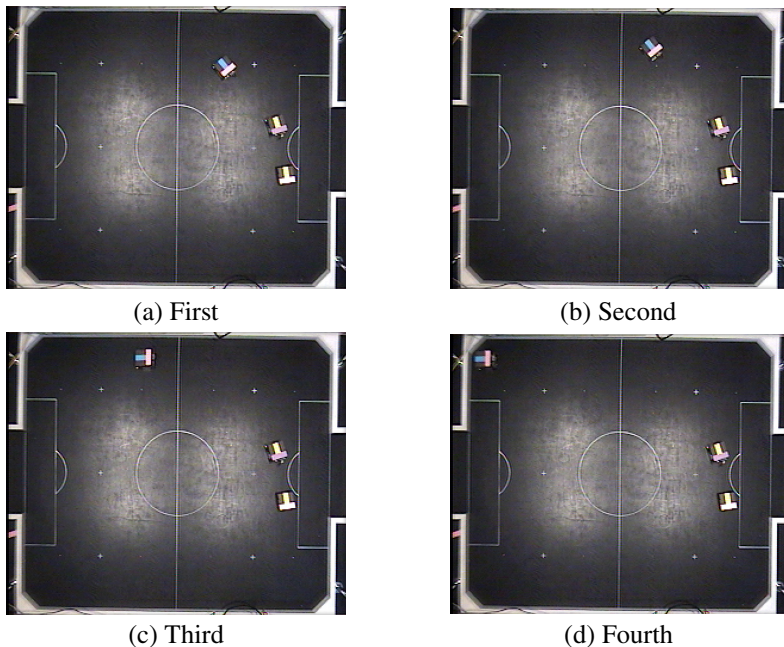
Fig. 18. Photos from the camera

At Figure 18 there are four photo saved from the camera above the playground of the moving robot at the presented trajectory. The last frame 18(d) shows clearly that the robot has stopped before the edge not touching it.

(a) Trajectory

(b) Speed
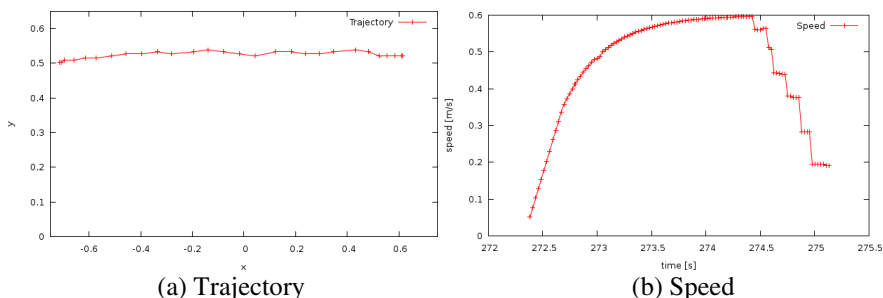
Fig. 19. Computer controlled intervention and human control override
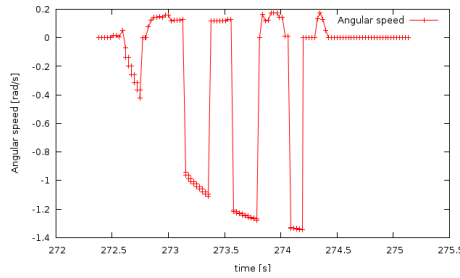
Fig. 19. (*continued*)

6 Summary

The Master Control System achieved all the stated goals. It is a reliable controller for manual control using various control instruments, allows tuning of the parameters of its control algorithms, default values of these are optimized, so that a learning curve of the controls is very steep. Feedback of current state of playground is simple and informative, and the graphical user interface is user friendly - the operator can start controlling robots right away even without reading the manual. Numerous functions can be checked, their effects on each other read and concluded from. Future work on artificial intelligence in the project can utilize this controller in order to teach neural networks.

Most importantly, computer controlled intervention proposed can be reused as a basis in many real world applications, like the example of automotive industry and driving assists on future roads. Algorithms here are working in completely different environment, that imply use of different ways of getting to know the object surrounding, but the idea at the bottom is the same.
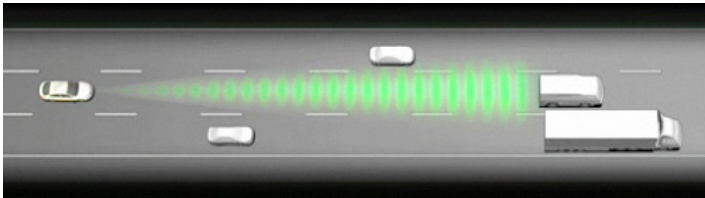
Fig. 20. Front assist [13]
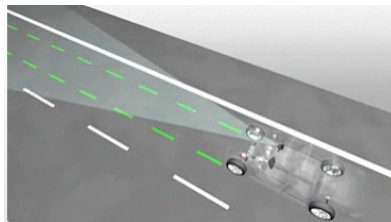
Fig. 21. Lane assist [13]

The speed limiter proposed in this work relates to the front assist proposed by Volkswagen and shown on Figure 20 [13]. While the trajectory control proposed relates to the lane assist shown on Figure 21.

References

[1]   Babiarz, A., Jaskot, K.: Experimental Construction of Walking Robot. Mechanics 27(3), 91–95 (2008)

[2]   Babiarz, A., Jaskot, K.: Ukad inercyjny do pomiaru orientacji obiektw. Przegld Elektrotechniczny 86(11a), 323–333 (2010)

[3]   Babiarz, A., Jaskot, K.: The Concept of Collision-Free Path Planning of UAV Objects. In: Nawrat, A., Simek, K., Świerniak, A. (eds.) Advanced Technologies for Intelligent Systems of National Border Security. SCI, vol. 440, pp. 81–94. Springer, Heidelberg (2013)

[4]   Becerra, H.M., Lopez-Nicolas, G., Sagues, C.: A Sliding-Mode-Control Law for Mobile Robots Based on Epipolar Visual Servoing From Three Views. IEEE Transactions on Robotics 27(1), 175–183 (2011)

[5]   Kosk, P., Balmer, R., Wise, G., Keat, W.: Exploring Engineering: An Introduction to Engneeringand Design. Academic Press (2010)

[6]   Livatino, S., Muscato, G., Privitera, F.: Stereo Viewing and Virtual Reality Technologies in Mobile Robot Teleguide. IEEE Transactions on Robotics 25(6), 1343–1355 (2009)

[7]   Łakota, T.: Design, implementation and programming of mobile robot controller. Masters thesis, Silesian University of Technology, Gliwice (2010)

[8]   Moorthy, A.: Unmanned ground vehicle on bmp ii vehicle platform. A Monthly House Bulletin of Defence Research and Development Organization 29(8), 2 (2009)

[9]   Moshtagh, N., Michael, N., Jadbabaie, A., Daniilidis, K.: Vision-Based, Distributed Control Laws for Motion Coordination of Nonholonomic Robots. IEEE Transactions on Robotics 25(4), 851–860 (2009)

[10] Ramsey, J.W.: Boeing 787: Integrations next step. Avionics Magazine (2005)

[11] Riggs, T.A., Inac, T., Zhang, W.: An Autonomous Mobile Robotics Testbed: Construction, Validation and Experiments. IEEE Transactions on Control Systems Technology 18(3), 757–766 (2010)

[12] Smoliński, M.: Vision system for group of mobile robots. Masters thesis, Silesian Universityof Technology, Gliwice (2006)

[13] Volkswagen: Assistance systems (2010), http://www.volkswagen.com

[14] Song, X., Seneviratne, L.D., Althoefer, K.: A Kalman Filter-Integrated Optical Flow Method for Velocity Sensing of Mobile Robots. IEEE/ASME Transactions on Mechatronics 16(3), 551–563 (2011)

[15] Wang, Y., Lang, H., de Silva, C.W.: A Hybrid Visual Servo Controller for Robust Grasping by Wheeled Mobile Robots. IEEE/ASME Transactions on Mechatronics 15(5), 757–769 (2010)

[16] Chen, Z., Birchfield, S.T.: Qualitative Vision-Based Path Following. IEEE Transactions on Robotics 25(3), 749–754 (2009)

[17] Skrzypczyk, K., Gałuszka, A., Pacholczyk, M., Daniec, K.: Probabilistic approach to planning collision free path of UAV. In: Nawrat, A., Simek, K., Świerniak, A. (eds.) Advanced Technologies for Intelligent Systems of National Border Security. SCI, vol. 440, pp. 59–68. Springer, Heidelberg (2013)

[18] Galuszka, A., Bereska, D., Simek, K., Skrzypczyk, K., Daniec, K.: Application of graphs theory methods to criminal analysis system. Przeglad Elektrotechniczny 86(9), 278–283 (2010)

[19] Galuszka, A., Swierniak, A.: Planning in multi-agent environment using strips representation and non-cooperative equilibrium strategy. Journal of Intelligent and Robotic Systems: Theory and Applications 58(3-4), 239–251 (2010)

[20] Gałuszka, A., Pacholczyk, M., Bereska, D., Skrzypczyk, K.: Planning as artificial intelligence problem - short introduction and overview. In: Nawrat, A., Simek, K., Świerniak, A. (eds.) Advanced Technologies for Intelligent Systems of National Border Security. SCI, vol. 440, pp. 95–104. Springer, Heidelberg (2013)

[21] Czornik, A., Niezabitowski, M.: Lyapunov exponents for systems with unbounded coefficients. Dynamical Systems: An International Journal (2012)

[22] Czornik, A., Nawrat, A., Niezabitowski, M.: On the Lyapunov exponents of a class of second-order discrete time linear systems with bounded perturbations. Dynamical Systems: An International Journal (2012)

[23] Czornik, A., Niezabitowski, M.: On the spectrum of discrete time-varying linear systems. Nonlinear Analysis: Hybrid Systems 9, 27–41 (2013)

System for Multi-axial Mechanical Stabilization of Digital Camera

Damian Bereska, Krzysztof Daniec, Sławomir Fraś, Karol Jędrasiak,
Mateusz Malinowski, and Aleksander Nawrat

Abstract. The article presents designed and implemented system for multi-axial mechanical stabilization. The quality of stabilization using closed-loop control, open-loop control and open-loop control with prediction was experimentally measured. Acquired results are presented and discussed.

1   Introduction

The idea of stabilization of digital camera is to be able to acquire a stable image from camera mounted on any moving platform (e.g. vehicle). The whole stabilization process can be divided into 3 different levels:

1) Mechanical stabilization – adding special servomechanisms or springs to reduce the disturbance and allow camera to independently track objects (mechanics);
2) Optical stabilization – stabilization of system projecting the image on CCD or different converter (micromechanics);
3) Digital stabilization – moving and rotating of the image to compensate the oscillations on pixel level (computing).

Damian Bereska · Krzysztof Daniec · Sławomir Fraś · Karol Jędrasiak ·
Mateusz Malinowski · Aleksander Nawrat
Silesian University of Technology, Institute of Automatic Control,
Akademicka 16, 44-101 Gliwice, Poland
e-mail: {slawomir.fras,damian.bereska,krzysztof.daniec,
     karol.jedrasiak,aleksander.nawrat}@polsl.pl

Aleksander Nawrat
Ośrodek Badawczo-Rozwojowy Urządzeń Mechanicznych "OBRUM" sp. z o.o.,
ul. Toszecka 102, 44-117 Gliwice, Poland
e-mail: anawrat@obrum.gliwice.pl

The aim of this article is to experimentally test and compare a few different control approaches for mechanical stabilization.

To achieve this goal we prepared a special test bench, the pendulum, on which camera can rotate around 2 axes. In order to do the mechanical stabilization, we installed 3 servomechanisms to compensate the rotation (although the pendulum has only 2 freedom degrees, the third rotation can occur as composition of two other). Additionally, to make the necessary measurements we installed two Inertial Measurement Units (IMU). One was placed on the pendulum itself, while the second was placed on the camera. Finally, the proper algorithm controls the mechanical stabilization.

The optical stabilization part is skipped in this article, as most of the modern cameras have it already implemented inside them.

2   Literature Review

Image stabilization is basically divided into three approaches: mechanical, optical and digital stabilization. Mechanical stabilization is performed by mechanically changing the orientation of the image acquisition device. The stabilization in the case of ground-based application can rely on a rigid camera attached, such as using e.g. a tripod, so that the device is constantly looking in one direction. Therefore the device do not carry the vibrations resulting from holding the camera in the hands of the operator. In the case where there is no available substrate property, use free camera mount which does not carry the rotating platform on which it is place, while maintaining the orientation relation to something else – for instance, to the Earth. This problem can be solved in a purely mechanical way using gyroscopes or by using mechanical actuators and inertial measurement sensor [1]. Application of mechanical gyroscopes can get good quality of stabilization however such system is burdened with various constraints such as long boot time caused by the requirement of desired gyro spin speed or long time to set the orientation setting. Second approach involves use of elements capable of inflicting any angle by electronic means. Setting angles of various degrees of freedom can be achieved by using servos, which consists of a power unit, the transmission system, the angle measurement unit and steering motor controller in a way that the predetermined angle is achieved at the output of the servomechanism [2]. This approach is however subject to a rate control problem due to internal closed loop control.

The second approach of angle setting is based on stepper motors that can operate in an open loop. Therefore there is no accumulation of errors in time. Stepper motors allow faster camera orientation which is used for maintaining the direction of viewing of the camera regardless to the rotation of the platform that the camera is mounted. However when the mounting platform is rotating it is required to have the information about the orientation of the platform. It is natural to use acquire such information using inertial measurement unit (IMU). The combination of inertial sensor and a manipulator with three degrees of freedom is therefore sufficient to achieve stabilization of the orientation of the camera in a mobile platform.

At the same time such system is also sufficient for rotating camera line of sight in any direction. In this case the term stabilization covers suppression of low frequencies such as rolling of the platform.

Another approach to image stabilization is optical stabilization. It is similar to the mechanical stabilization. However the correction part does not take place in some kind of gimbal where the whole camera is mounted but only within optics of the camera. Changes in lenses orientations creates a phenomenon that the resulting image is perceived as it would be seen without changes in direction.

The third and last approach in this juxtaposition is digital image processing leading to image stabilization. It is possible to use date acquired from IMU to adjust the higher frequency movements that are beyond the capabilities of the mechanical stabilization part. Digital stabilization can also be performed on the basis of image processing alone. There is no need for IMU data. However using IMU increases the quality of stabilization [4].
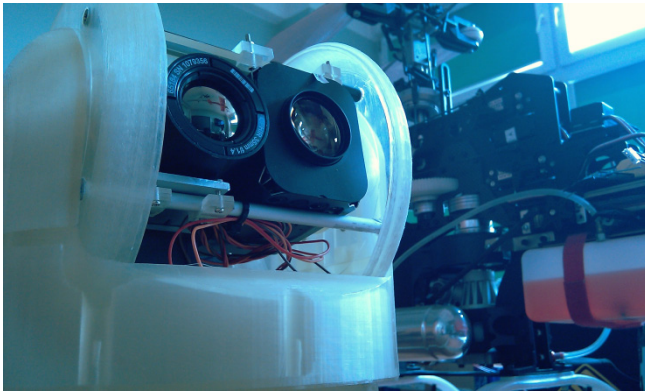
Fig. 1. An example of mechanically stabilized gimbal containing day light camera and thermal imaging camera

Stabilization can be used in optoelectronic gimbal (fig. 1) [5] mounted on board of manned objects or unmanned vehicles (UGVs and UAVs). Generally it is desirable to apply stabilization to all cases when deterioration of image quality is perceived due to low and high frequencies. Similar effect can be observed during performing air maneuvering of the camera platform (e.g. UAV). Stabilized optoelectronic gimbals providing a video stream free from the mentioned negative impacts is basis of vision from multispectral cameras (e.g. IR and visible light)[6] based algorithms like: detection and tracking [7], image rectification [8], VSLAM [9] or object recognition [10]. Especially for UAVs vision information is used for planning collision free trajectory in multi-agent environments [11], [12]. Stabilized video sequence could be also treated as a basis for human recognition based on gait data [13-15].

3   Control Algorithms for Mechanical Stabilization

In order to measure the quality of the mechanical stabilization, the camera was looking at the black shape on white background, so it was possible to calculate the center of the shape's mass at each frame. The lesser is the shift, the better is the stabilization. The axes of the whole system have been picked in the following order: Z axis was turned upward (yaw angle of rotation), X axis was turned to the front (roll) and Y axis was turned to the left (pitch). Possible rotations of test bench (distraction) were allowed on axis X and Y (fig. 2).
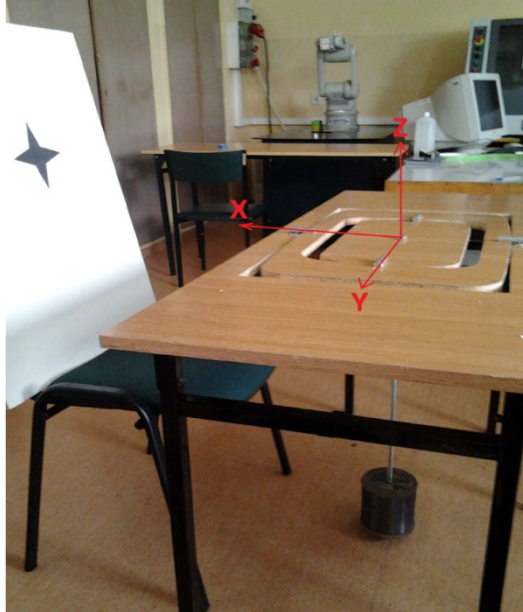
Fig. 2. A photograph of testbed used. Red lines indicates coordinate system axis directions.

Servos are the elements which are able to rotate the element positioned on the axis of rotation by an angle which is proportional to the setpoint. The value can be calculated by the control algorithms which utilizes the available sensory information like orientation from IMU) and setpoints. Control algorithm using those values may be capable of bringing the mechanical system to the state when the camera's line-of-sight is in a given direction. Setpoints for servos may be designate by the control algorithm based on the values selected and sensory information which are not subject of stabilizing. For instance orientation of the testbed which is beyond our manipulation control. Such control system is a control system called open-loop control (fig. 3).
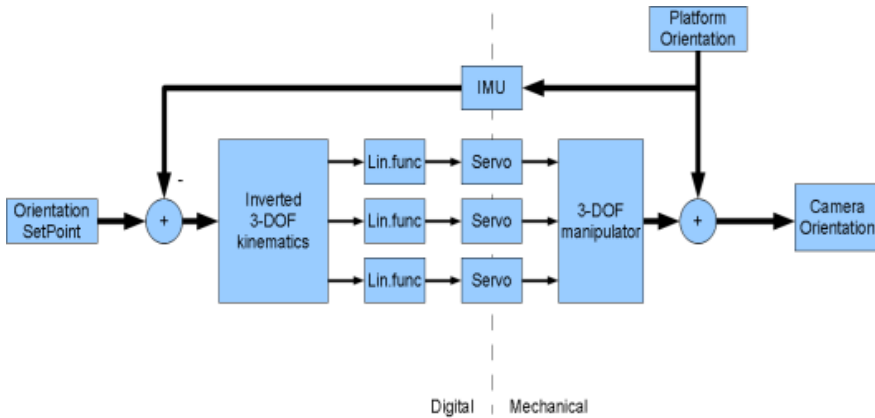
Fig. 3. Schema of the system with open-loop control

A linear function (1) determines the value to be set on the servo in order to turn the next member of the manipulator by a specified angle. Such unit gain allows to transform the Euler angles read from IMU to number of pulses at the output of servomechanisms. The function has the following form:

$$y = 190x + 512 \tag{1}$$
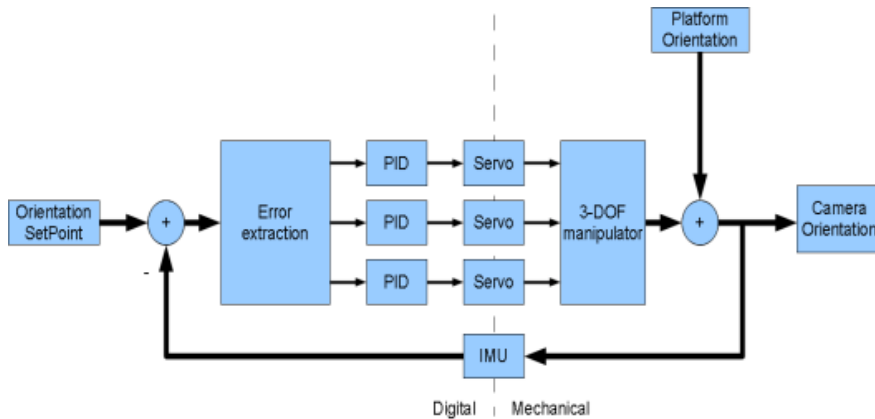
Fig. 4. Schema of closed-loop system with PID controller

The servomechanisms can take input values in the range starting from 0 to 1023. The range represents values from -135° to +135°. Assuming achievement of the immediate set point by the servos the track consists of a linear function and a separate servo gain. Under such assumption the control system is capable of working. The inverse kinematics is responsible for the determination of the angles that need to be used as set points for servos in order to change the orientation of the camera manipulator by a designated value. Orientation of the camera is a
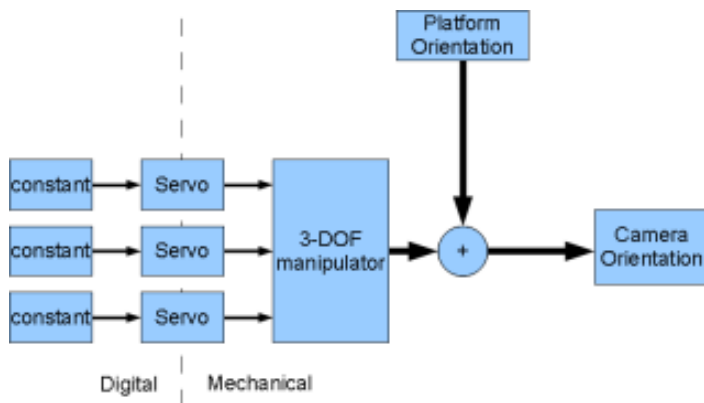
Fig. 5. Schema of the system without stabilization
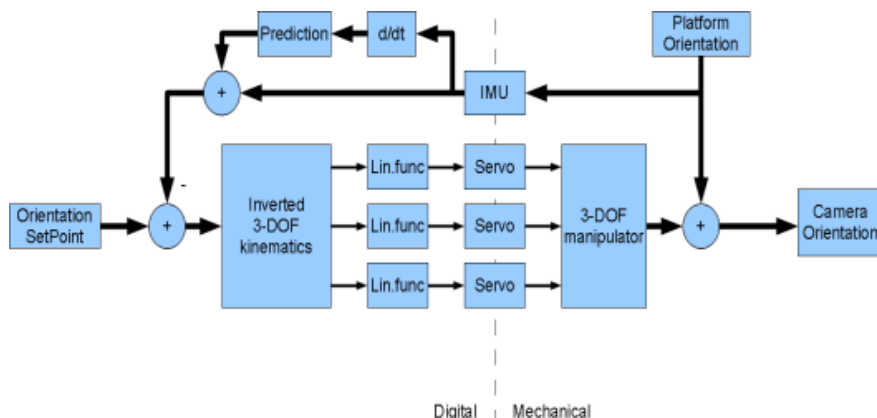
Fig. 6. Schema of the system with open-loop control with prediction

combination of table and manipulator orientations. However the partial orientation of the manipulator is dependent of the current and set point orientation. Manipulator reduces the impact of the current orientation by gradually replacing it with a reference value.

An alternative approach is to use additional information about the state of the object controlled. Such approach is called the closed-loop control because the stabilized state of the object is used to control the set point values of the next time unit (fig. 4).

For the purposes of this publication a variety of algorithms have been developed and implemented in order to test and compare quality of stabilization depending of the algorithm. Tested algorithms were closed-loop control, open-loop control and open-loop control with prediction. As a reference value the offsets of an image from the camera without stabilization (fig. 5).

Perfect open-loop system should provide the perfect stability. However, in reality servos are not infinitely fast. Therefore the control set values have to overtake an ideal set point in order to compensate for the servos delay. The main aim of the prediction is to compensate the servos delays. It is used to improve the speed of servos response. Every servo internally contains closed loop control that introduces regulation delay.

Prediction shown in fig. 6 consists of additional block that uses angular velocities along given axis in order to compensate servo response.

4   Experiments

Aim of the performed experiments was to measure the dispersion of the center of gravity of the image seen by the camera mounted to the manipulator with three degrees of freedom (fig. 7). Manipulator was used to reorient the camera.
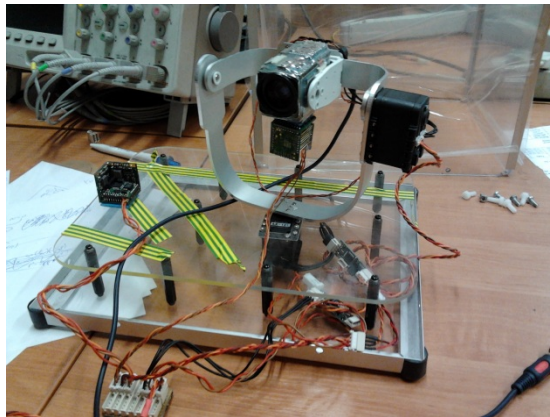
Fig. 7. 3-DOF gimbal used for experiments

The manipulator has been rigidly connected to the movable part of the dedicated testbed allowing infliction of extortion in the two axes of rotation. Measurements of the manipulator base and the orientation of the camera itself were carried out using inertial measurement unit. Used IMUs were connected by the CAN bus. The CAN bus allowed the transfer of data from IMU to the PC via the USB-to-CAN converter. PC was used for recording the data and measuring the center of gravity of the image. The CAN bus was also used for transmitting the data to the controller responsible for stabilization. The throughput of bus was 500 kbps.

Measuring testbed consisted of three parts: a fixed table, helper ring and a movable table. The value of quality of stabilization was computed without stabilization. The quality of stabilization was assumed as ratio of stability angle amplitude of change of the camera angle to change of the angle of the fixed table. The quality index can assume all positive values. However 0 means perfect stability and 1 complete lack of stability.

4.1　Mechanical Stabilization

There were three sets of experiments: rotation over Y axis, rotation over X axis and combined rotation over Y and X axes. Each of the experiments was repeated three times for each control system. To make this article more readable, only the most representative results are presented.

4.1.1　System without Stabilization

System without any stabilization doesn't work at all as it is clearly shown on the Figures 8 and 9. All distractions are being moved on camera, so as a result the camera's shift is big enough to disturb watching images from it, though, presented results may be to compare them with other control systems.
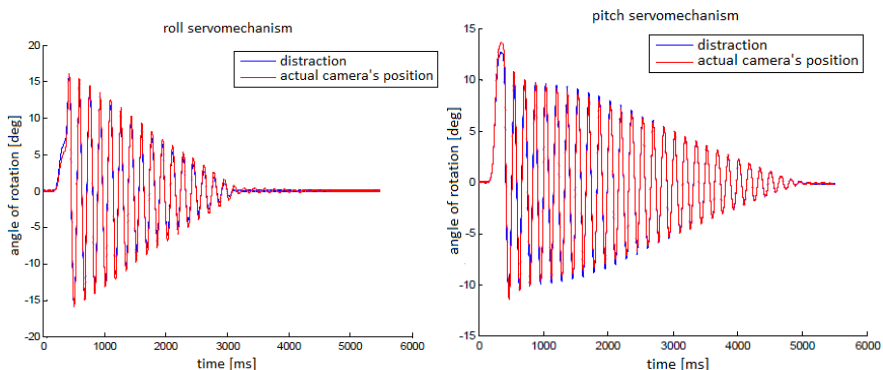
Fig. 8. Output from the roll and pitch servomechanisms in the system without stabilization
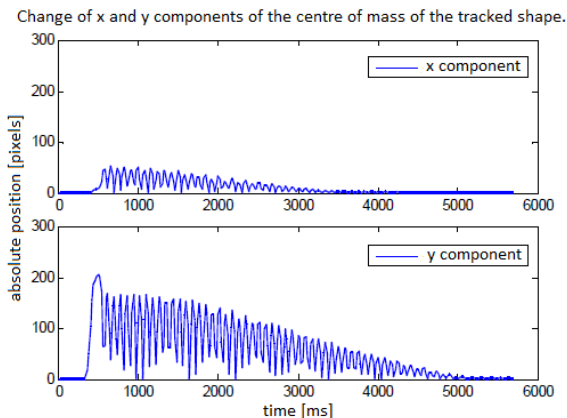
Fig. 9. Shift of x and y components of the center of mass of the tracked shape in the system without any stabilization

4.1.2 Closed-Loop with PID Controller

Measured error ratio was reduced by using closed-loop stabilisation (fig 10,11). The distraction has been reduced almost twice; however, the result isn't something that was expected. The PID controllers are often known as fair good ones, but in the given example the camera was still rotating for about ±5° respectively. An explanation of the results is the fact that the PID controller has to be noted in order to change the offset value for the motor control.
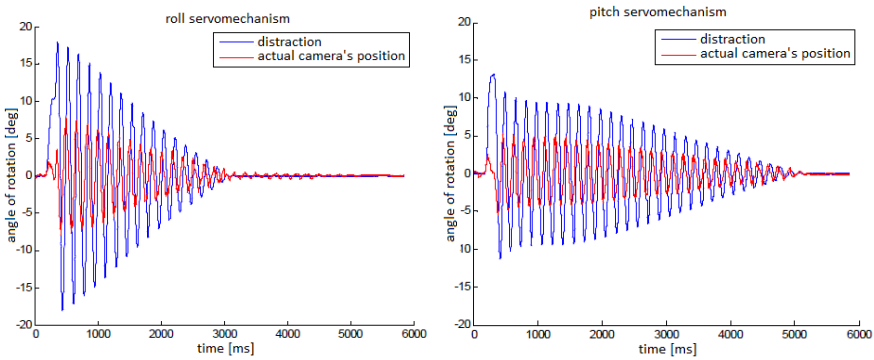
Fig. 10. Output from the roll and pitch servomechanisms in the closed-loop system with PID controller
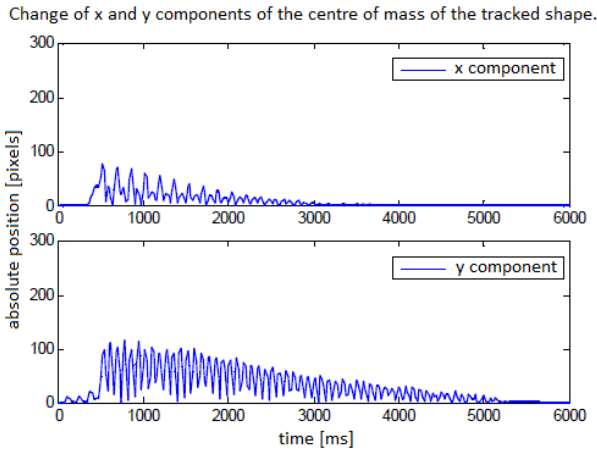
Fig. 11. Shift of x and y components of the center of mass of the tracked shape in the closed-loop system with PID controller

4.1.3 Open-Loop Controller

In the system with open-loop control, the camera rotates with less than 5° in each axis (fig. 12). The result was better than in previous experiment, though, it might be even better with the prediction. Fig. 13 shows, that the shift of the centre of mass from tracked shape is less than 100 pixels on each axis. Although the x component isn't varying much, the y component has been reduced greatly according to Figure 9.
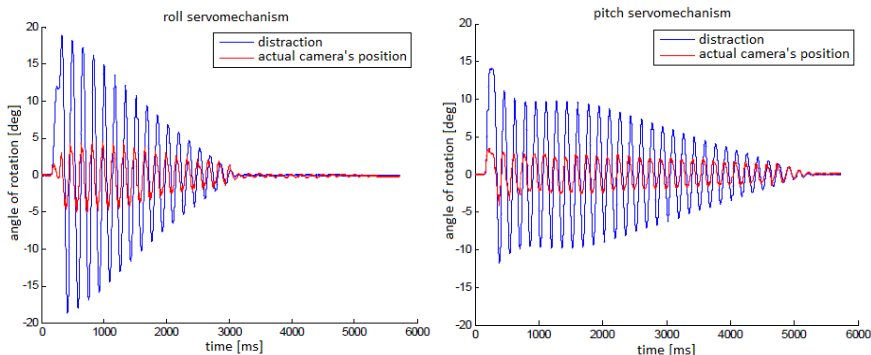
Fig. 12. Output from the roll and pitch servomechanisms in the system with open-loop control
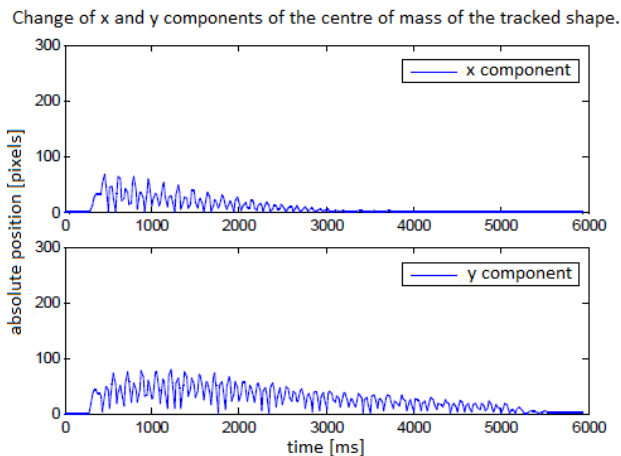
Fig. 13. Shift of x and y components of the center of mass of the tracked shape in the system with open-loop control

4.1.4 Open-Loop Controller with Prediction

The system with open-loop controller with prediction gives the best results. The average camera's rotation is between ±2.5° (Figure 14), which is visually acceptable for human observer. At the same time the centre of mass of the tracked shape shifts on *y* axis on less than 50 pixels, which can be seen on Figure 15.
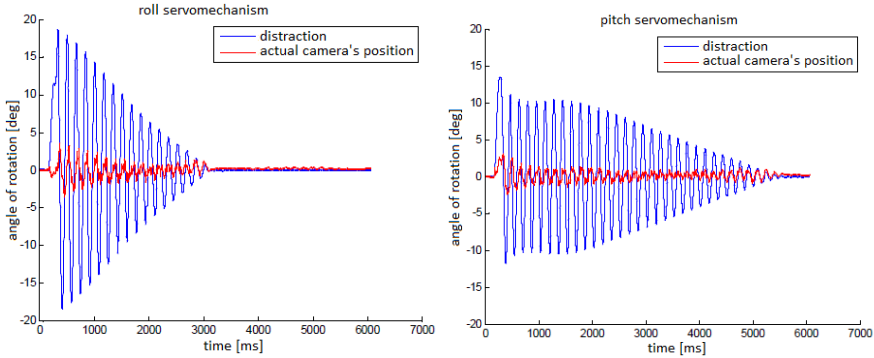
Fig. 14. Output from the roll and pitch servomechanisms in the system with open-loop control with prediction
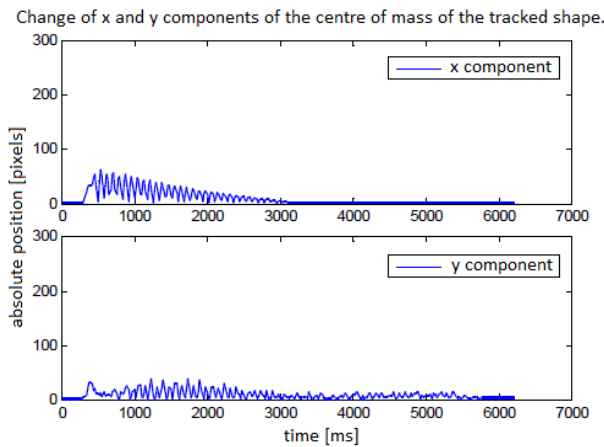
Fig. 15. Shift of x and y components of the center of mass of the tracked shape in the system with open-loop controller with prediction

4.1.5 Test Conclusions

Closed-loop, open-loop and open-loop with prediction stabilization structures were tested. For comparison purposes a test was also carried out without stabilization. The tracked center of gravity of the image observed by the camera without stabilization was sliding around by about 200 pixels. Closed-loop control improved the result. The maximum deflection in the y-axis was reduced to about 125 pixels. Open-loop control yielded better results. The maximum deflection was
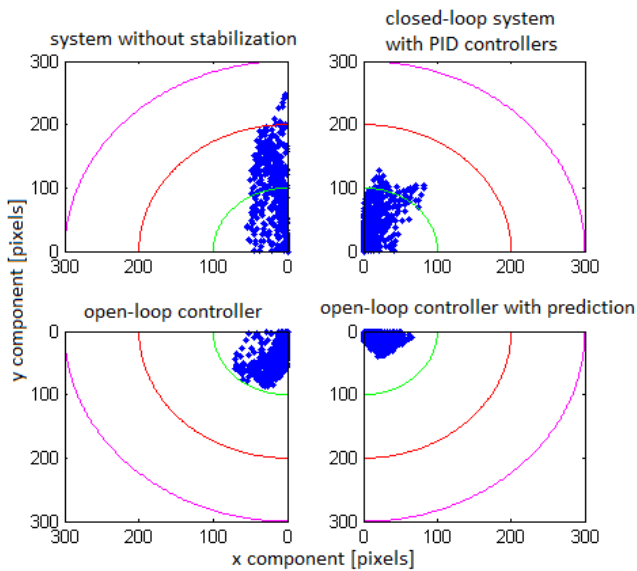
Fig. 16. Comparison of the acquired shift in x and y direction depending on the control type

about 100 pixels. However the best results were obtained for control in an open-loop system with prediction. The acquired experimentally best result was reduction of deviation to about 50 pixels (fig. 16).

5   Conclusions

In the article it was presented developed multi-axial mechanical stabilization system. Quality of the 3-DOF camera stabilisation system was experimentally measured using dedicated 2-DOF platform and two IMUs used for orientation measurements.

The presented experimental results proved that mechanical stabilisation improves low frequency dampening which allows to mount camera on rotary objects like UAV [15].

The image's shift was reduced from more than 250 pixels to less than 50 for open-loop control with prediction. The main conclusions was that open-loop control is better suitable than closed-loop for mechanical stabilisation.

References

[1]   Masten, M.K.: Inertially stabilized platforms for optical imaging systems. IEEE Control Systems 28(1), 47–64 (2008)
[2]   Prakah-Asante, K.O., Islam, A.S., Walczyk, D., Craig, K.: Design, Construction and Testing of a Single-axis Servomechanism for Control Experiments involving Coulumb Friction, Backlash and Joint Compliance. Journal of Engineering Design 4(4), 305–329 (1993)

[3] Hilkert, J.M.: A comparison of inertial line-of-sight stabilization technique using mirrors. In: Proc. SPIE 5430, Acquisition, Tracking and Pointing XVIII, Orlando (July 2004)

[4] Ko, S.J., Sung-Hee, L., Seung-Won, J., Eui-Sung, K.: Fast Digital Image Stabilizer Based On Gray-Coded Bit-Plane Matching. IEEE Transactions on Consumer Electronics 45(3) (1999)

[5] Jędrasiak, K., Bereska, D., Nawrat, A.: The Prototype of Gyro-Stabilized UAV Gimbal for Day-Night Surveillance. In: Nawrat, A., Simek, K., Świerniak, A. (eds.) Advanced Technologies for Intelligent Systems of National Border Security. SCI, vol. 440, pp. 107–116. Springer, Heidelberg (2013)

[6] Świtoński, A., Bieda, R., Wojciechowski, K.: Multispectral imaging for supporting colonoscopy and gastroscopy diagnoses. In: Hippe, Z.S., Kulikowski, J.L., Mroczek, T. (eds.) Human - Computer Systems Interaction. AISC, vol. 99, pp. 131–145. Springer, Heidelberg (2012)

[7] Hurak, Z.: Image-Based Pointing and Tracking for Inertially Stabilized Airborne Camera Platform. IEEE Transactions on Control Systems Technology 20(5), 1146–1159 (2012)

[8] Wenguang, H., Mingyue, D., Nannan, Q., Xudong, L.: Digital deformation model for fishye image rectification. Optics Express 20(20), 22252–22261 (2012)

[9] Xiaodong, L., Aouf, N., Nemra, A.: 3D Mapping Based VSLAM for UAVs. In: Control & Automation 20th Mediterrenean Conference, Barcelona (2012)

[10] Hyuncheol, K., Haehyun, I., Taekyung, K., Jongsue, B., Sanghoon, L., Joonk, P.: Part-template matching-based target detection and identification in UAV videos. In: Proc. SPIE 8360, Airborne Intelligence, Surveillance, Reconnaissance (ISR) Systems and Applications IX, Maryland (April 2012)

[11] Gałuszka, A., Pacholczyk, M., Bereska, D., Skrzypczyk, K.: Planning as Artifficial Intelligence Problem-short introduction and overview. In: Nawrat, A., Simek, K., Świerniak, A. (eds.) Advanced Technologies for Intelligent Systems of National Border Security. SCI, vol. 440, pp. 95–104. Springer, Heidelberg (2013)

[12] Skrzypczyk, K., Gałuszka, A., Pacholczyk, M., Daniec, K.: Probabilistic approach to planning collision free path of UAV. In: Nawrat, A., Simek, K., Świerniak, A. (eds.) Advanced Technologies for Intelligent Systems of National Border Security. SCI, vol. 440, pp. 59–68. Springer, Heidelberg (2013)

[13] Krzeszowski, T., Kwolek, B., Michalczuk, A., Świtoński, A., Josiński, H.: View independent human gait recognition using markerless 3d human motion capture. In: Bolc, L., Tadeusiewicz, R., Chmielewski, L.J., Wojciechowski, K. (eds.) ICCVG 2012. LNCS, vol. 7594, pp. 491–500. Springer, Heidelberg (2012)

[14] Josinski, H., Switonski, A., Jedrasiak, K., Kostrzewa, D.: Human identification based on gait motion capture data. Lecture Notes in Engineering and Computer Science, vol. 1, pp. 507–510 (2012)

[15] Josinski, H., Switonski, A., Michalczuk, A., Wojciechowski, K.: Motion Capture as data source for gait-based human identification. Przegląd Elektrotechniczny 88(12B), 201–204 (2012)

[16] Iwaneczko, P., Jędrasiak, K., Daniec, K., Nawrat, A.: A prototype of unmanned aerial vehicle for image acquisition. In: Bolc, L., Tadeusiewicz, R., Chmielewski, L.J., Wojciechowski, K. (eds.) ICCVG 2012. LNCS, vol. 7594, pp. 87–94. Springer, Heidelberg (2012)

Probabilistic Approach to Planning Collision Free Path of UAV

Dawid Cedrych, Adam Gałuszka, Marcin Pacholczyk, Krzysztof Skrzypczyk, and Aleksander Nawrat

Abstract. In this chapter we present simulation results of an algorithm designed to planning collision free path based on probabilistic search. The aim of this study is to design an algorithm for off-line planning a set of way-points which make the collision free route of an Unmanned Aerial Vehicle (UAV). The planning process is based on the graph that represents the map containing information about altitude of the terrain over which the UAV is intended to perform its mission. The size of the graph increases polynomially with the resolution of the map and the number of way points of UAV. The probabilistic method of making the representative model of the terrain was applied in order to reduce a complexity of planning the collision free path. The functioning and efficiency of the approach proposed was introduced in our previous work, here we use real terrain map and introduce indicators to illustrate properties of the algorithm.

1 Introduction

In this chapter, it is assumed that UAV is intended to perform autonomously the mission assigned by the operator. During the process of the design of UAV control system there are many serious and difficult problems to solve. It is enough to

Adam Gałuszka · Krzysztof Skrzypczyk · Marcin Pacholczyk · Dawid Cedrych · Aleksander Nawrat
Silesian University of Technology, Institute of Automatic Control,
Akademicka 16, 44-101 Gliwice, Poland
e-mail: {adam.galuszka,krzysztof.skrzypczyk,
      marcin.pacholczyk,anawrat}@polsl.pl

Aleksander Nawrat
Ośrodek Badawczo-Rozwojowy Urządzeń Mechanicznych "OBRUM" sp. z o.o.,
ul. Toszecka 102, 44-117 Gliwice, Poland
e-mail: anawrat@obrum.gliwice.pl

mention the collision free path planning, the vehicle stabilizing in changing weather conditions, determining the aerial position and orientation and many others. Due to the a large number of possible applications and benefits related to them, intensive researches have been done in this area. [1, 14, 15, 18, 19, 21, 24].

This paper addresses the first of pointed out issues - the problem of determining the collision free path. Intended application of the developed UAV control system is performing autonomously the patrolling mission over an unstructured terrain. The goal of the planner is determining the set of way points that make the route the vehicle is intended to follow. There are many methods and algorithms of planning collision free paths, derived in a straight-line from mobile robotics [3, 6, 7, 8, 9, 10, 11, 16, 17, 20, 25]. In this work we present simulation results of our algorithm introduced in previous work [22, 4] based on the extensive mathematical research [32, 33, 34] and probabilistic approach [2, 12, 13, 23, 28] to solving the planning problem. The planning process is based on the topological map that contains information about the height of the terrain over which the vehicle is intended to perform its patrol mission. The work of the method is illustrated with an exemplary real map of a fragment of the national border between Poland and Slovakia. This fragment of the border is mountainous and it follows that the border line is complex.

2   Overview of the System

In this section let us recall the conceptual diagram of the UAV control system with the planner module [22]. Figure 1 shows general diagram of the navigation and control system of the UAV. It is created on the base of a typical, known from mobile robotics hierarchical, hybrid architecture.
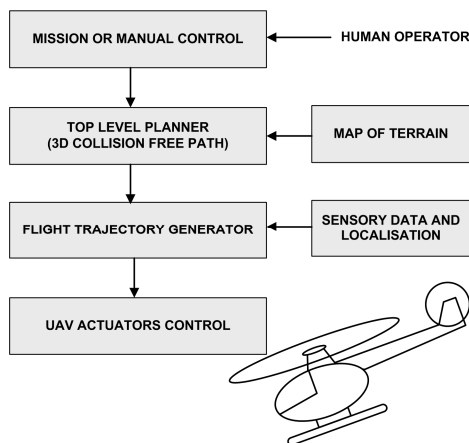
Fig. 1. The conceptual diagram of the UAV control system with the planner module being the point of the work presented

At the top level of the system, there is a module called *planner* which is the point of this study. The human operator assigns mission by specifying the places (points) the vehicle is intended to fly over. The role of the planner is to generate the set of way-points that determine the collision free path. The planner module is also provided with data about topology of the terrain. Using this data the model which is used further in the planning process is created. The next module is responsible for generating the collision free trajectory which enables the flight between the way-points.

The navigation module has to be also provided with information about the position and orientation in space. Determining the coordinates, and orientation is performed by the localization subsystem. The plan created by the planner does not take into account the dynamics of the space inside of which the vehicle operates. Therefore the navigation system has to be also provided with data about existence of objects that can appear in the surrounding of the vehicle. This information is collected by the sensory system. The bottom level of this architecture is the motion control system which is to execute the trajectory generated by the navigation system like in [29]. As it was mentioned before the core of this article is just the design and simulation evaluation of the algorithm dedicated to work with the planner module. The process of the design is presented and described in the rest part of this paper. In real application GPS [30] and an opto-electronic gimbal for image stabilization would be required [27].

2.1   Assumptions

The planning system presented here is designed for the UAV which purpose is patrolling the border of the state. However it is created to satisfy a number of conditions and assumptions. They make some limitations for possible application and the framework in which the system work properly. So it is important to clearly point them out and discus. The following are the main assumptions that were followed during the design process:

- The patrol mission is performed on the given, priory stated height H_0.
- There is a map that provides information about height of the terrain points.
- The maneuver of avoiding obstacles is preferred to the flying over them.
- The UAV cannot cross the state border during its mission.

The assumptions pointed out, are the main limitations of the planning method presented. However they are realistic and justified and they do not limit the system to only simulation studies, and make the method applicable in real systems.

2.2   Problem Statement

Let us first define the mission to be performed by the UAV [31]. The mission in fact is the collection of locations defined by human operator the vehicle is intended to fly over as well as the altitude H_0 of the flight. Let us denote the mission as the set:

$$M = \{m_1, m_2, ..., m_p\} \quad m_1 = (x_i, y_i), \qquad i = 1,2, ..., P \tag{1}$$

The goal of the planner module is to calculate in the 3D space a set of points that lay between the locations defined by operator. Therefore for each pair of points:

$$(m_i, m_{i+1}), \quad i = 1,2, ..., P-1 \tag{2}$$

the module is intended to find a set of way points that determine the collision free path defined in 3D space:

$$S_i = \{s_{i1}, s_{i2}, ..., s_{iQ}\}, \quad s_{i,k} = (x_{i,k}, y_{i,k}, z_{i,k}), \quad i = 1,2, ..., P-1 \tag{3}$$

As it was mentioned before the overall process of calculating the path in 3D space is split on two stages. First one is determination the path in 2D space and second - extension the original path on the 3D space. All further discussion will be made, without the loss of generality, for a single pair of points defined in (2), and denoted hereafter as: m_1, m_2. Of course all the process can be repeated for any pair of the points.

2.3 Map of the Terrain

The process of planning the collision free path is based on the assumption that the system is provided with the map that contains data about height of each point of the terrain. In this chapter the map is adopted from the map database that also includes the surface details [26]. We chose surroundings of the border line between Poland and Slovakia shown in the Figure 2. The Matlab model of the terrain is shown in the Figure 3.
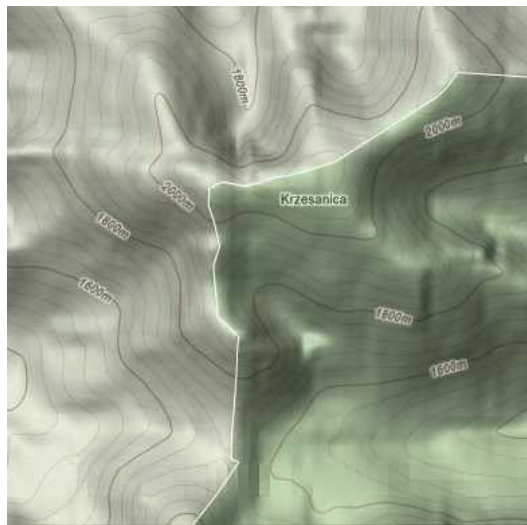
Fig. 2. Real map of the terrain. The gray color is the terrain of Poland, green – of Slovakia.
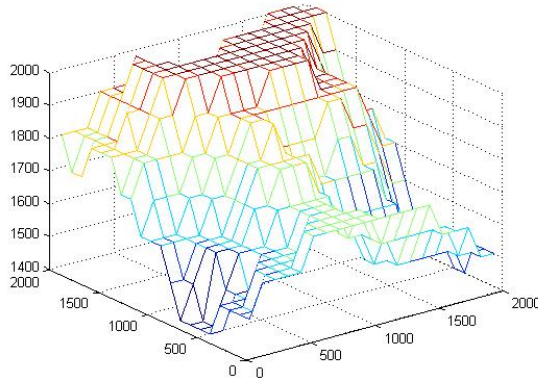
Fig. 3. 3D MATLAB model of the real map

2.4   *Probabilistic Approach*

Since the search space in 3D models is large that implies hard computations have to be performed in order to find the solution. The probabilistic approach allows to simplify the problem. Instead of searching through entire space a number of representative elements are selected. For instance if the map has a resolution 100x100 in the process of searching the solution requires 10000 elements to be processed. The planner searches the optimal solution using the reduced space. Let us denote the randomly selected set of representative samples of the original model as:

$$R = \{r_1, r_2, \dots, r_Z\} \tag{4}$$

where

$$r_i = \{k, l\}, \qquad k = \langle 1, N \rangle \ and \ l = \langle 1, M \rangle \tag{5}$$

In (5) the elements k, l are integer values selected in a random way from the given range. An exemplary containing 25 elements, random realization of the subspace is presented in fig. 3. Using representative elements contained in (4) the process of search the collision free path is performed. If the size of the (4) is not large enough or the distribution of points does not allow to find admissible solution, the process of selecting the representative subspace is repeated or the size of the set (4) is increased.

2.5   *Graph Model*

The next stage of the process of finding the solution is creating the model that will be a base for the planning process. Here in this study the graph representation of the random subspace is proposed. Hence the model has a form of weighted graph defined as:

$$W = (V, E) \tag{6}$$

where

$$V = \{v_1, \dots, v_{Z+2}\}, \qquad E = \{v_i, v_j, w_{i,j}\},$$
$$w_{i,j} \neq \infty, \quad i, j = 1, 2, \dots, Z+2 \tag{7}$$

In (7) v_1 and v_{Z+2} are equal to m_1 and m_2 correspondingly which are defined in (2). This set defines the vertices of the graph (6). Second part of the graph model is the set of edges E. It defines mutual, spatial relations between elements defined by V as well as costs of transitions between any given pair of vertices. Calculation of costs is a crucial part of the model creation. All the process of planning is based on the graph representation so the quality of the model is critical for this process. In this the cost between two elements of the set V is calculated as:

$$w_{i,j} = \|v_i - v_j\|(1 + S_{i,j}) \tag{8}$$

where $\|v_i - v_j\|$ denotes Euclidean distance between ith and jth vertex, and:

$$S_{i,j} = \sum_{k=1}^{K} L_k \Big|_{v_i}^{v_j} \tag{9}$$

is a sum of altitudes read from the map (\ref{fig:2}) along the line that connects vertex ith with vertex jth. This mapping is done according the following rule:

$$L_k = \begin{cases} 0 \; for \; altitude < H_0 \\ H_{m,n} \; for \; altitude \geq H_0 \end{cases} \tag{10}$$

If the line that connects vertex ith with vertex jth crossed the state border line (9), the sum is set to a relatively big number to prevent the algorithm for searching paths that crosses the border lines. As a result of determining costs of transitions between all pairs of vertices the cost matrix is created. It is denoted as:

$$D = \{S_{i,j}\} \; i, j = 1, 2, \dots, Z+2 \tag{11}$$

2.6   Solution

For the representation given by (11) searching the path of minimal cost is performed. There are many effective algorithms for minimal path search [5] but in this study the Dijkstra's algorithm was chosen. Since the graph defined by (11) is the complete one, always exists the path connecting vertices v_1 and v_{Z+2}. As a result of the graph search the path that connects those vertices is found:

$$P^* = \{p_1, \dots, p_p\}, \qquad p_1 = v_1, p_p = v_{Z+2}, \qquad 2 \leq P \leq Z+2 \tag{12}$$

each element of the set (12) is a point in a 2D space. Next stage consists of transforming this solution into 3D space. This process is done by attributing each point of the (12) with appropriate altitude. This is done in the following way: For each

pair p_k, p_l of points from the set (12) it is checked if for any point p_i that lays on the line between p_k, p_l the height is lower than H_0. If yes, the point is attributed with the coordinate $z_i = H_0 + \Delta H$ and this point is added to the solution. As a result of this iterative procedure the final solution defined in 3D space is determined:

$$P_F^* = \{p_{F1}, p_{F2}, \dots, p_{FR}\}, \qquad P \leq R \tag{13}$$

where each element $p_{Fi}, i = 1,2, \dots R$ defines a point in 3D space that has coordinates $((x_i, y_i, z_i))$.

2.7 Indices of the Quality of Generated Solution

Here we introduce three indices for rating founded solution. It is reasonable to assume that UAV energy consumption increases with the incease of trajectory. It also increases for frequent changes of the altitude of UAV during the mission. The following are three proposed indices:

- S_2- is the length of the path in 2D space.
- S_2- is the length of the path in 3D space.
- d_S - is the sum of changes of absolute values of UAV altitudes.

3   Simulations

In this chapter we present simulation results. The following are the main assumptions that were followed during the simulation process:

- The reference altitude (priory stated height H_0) of UAV is set to H_0= 1500 m, 1600 m and 1700 m.
- The minimal distance between UAV and the terrain surface ('safety margin') is set to $dH = 50$ m.
- The number of randomly generated points is set to $z = 30$.

Below three sets of figures are shown for different altitudes. For readers convenience in these figures the state border lines are represented by canyons. Figures 4 and 5 are for $H_0 = 1500$ m, figures 6 and 7 for $H_0 = 1600$ m, figures 8 and 9 for $H_0 = 1700$ m.

In the following tables the indices values are presented. For each altitude 5 solutions were generated. Table 1 shows the values of indices for H_0= 1500 m, table 2 is for $H_0 = 1600$ m and finally, table 3 is for $H_0 = 1700$ m. It is observed, that the values of indices are decreasing with increase of H_0.
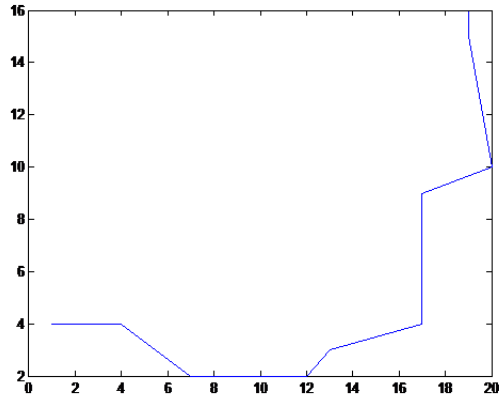
Fig. 4. Path of UAV for $H_0 = 1500m$
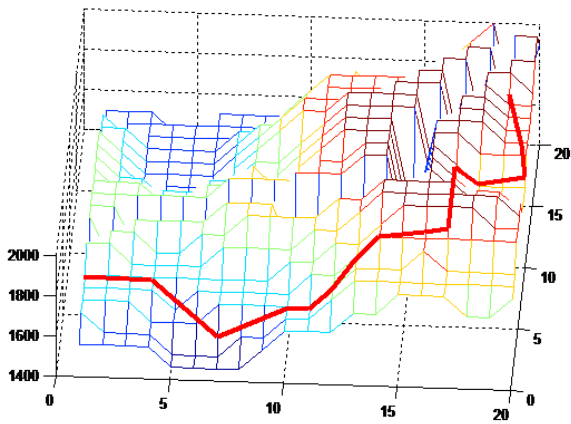
Fig. 5. 3D Matlab model of UAV path for $H_0 = 1500m$
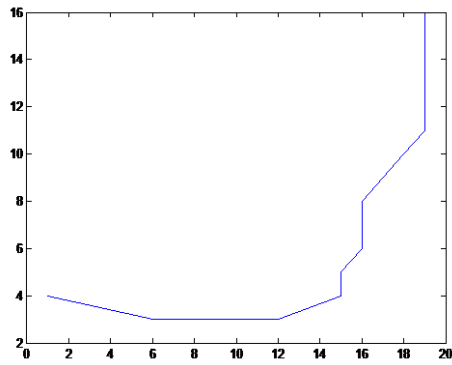
Fig. 6. Path of UAV for $H_0 = 1600m$
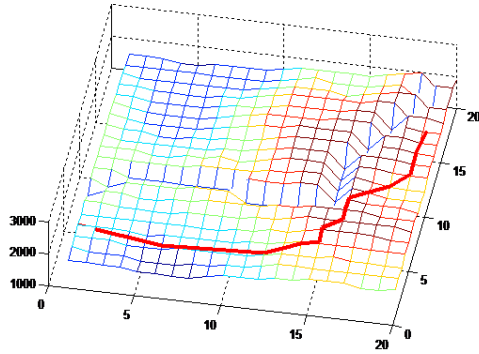
Fig. 7. 3D Matlab model of UAV path for $H_0 = 1600m$
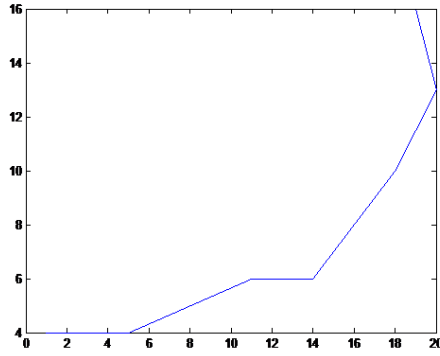
Fig. 8. Path of UAV for $H_0 = 1700m$
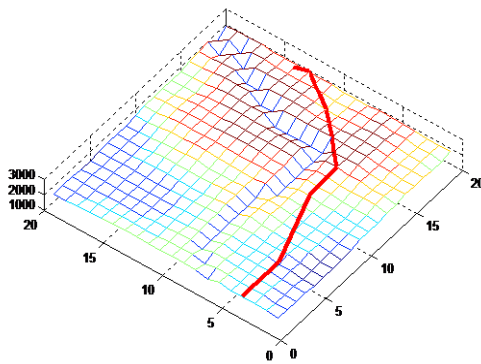
Fig. 9. 3D Matlab model of UAV path for $H_0 = 1700m$

Table 1. Indices values of UAV path for $H_0 = 1500m$

Simulation number	$S_2[m]$	$S_3[m]$	$dS[m]$
1	2722	3602	800
2	3900	4983	1500
3	3293	4241	1150
4	3530	4616	1300
5	3140	3761	800
Average value	3317	4240	1100

Table 2. Indices values of UAV path for $H_0 = 1600m$

Simulation number	$S_2[m]$	$S_3[m]$	$dS[m]$
1	2791	3187	750
2	3743	4170	850
3	2574	3021	750
4	3131	3921	950
5	2991	3381	750
Average value	3046	3536	810

Table 3. Indices values of UAV path for $H_0 = 1700m$

Simulation number	$S_2[m]$	$S_3[m]$	$dS[m]$
1	3219	3500	750
2	2700	3057	750
3	2661	2837	550
4	3055	3491	650
5	3054	2520	950
Average value	2937.8	3281	730

4   Conclusions

In this chapter set of simulations that generates solution of the problem of collision free path planning in 3D space was presented. The target application of the discussed method is determination of the way points of the flight of the UAV. Presented approach allows to find feasible path in 3D space simultaneously reducing the computations. Thanks to the simplification that consists in splitting the process on two stages the method is both effective and simple (in terms of computation costs). The simplicity was the one of the most important assumptions taken for the design of the UAV control system. Since the method is not deterministic it generates different solutions. After a number of simulations it was checked that all the generated solutions are also feasible ones and they are satisfactory for the overall UAV control system.

References

[1]   Adolf, F.M., Hirschmuller, H.: Meshing and Simplification of High Resolution Urban Surface Data for UAV Path Planning. Journal of Intelligent and Robotic Systems 61, 169–180 (2011)

[2]   Barraquand, J., Kavraki, L., Latombe, J.C., Motwani, R., Li, T.Y., Raghavan, P.: A random sampling scheme for path planning. International Journal of Robotics Research 16, 759–774 (1997)

[3]   Barraquand, J., Langlois, B., Latombe, J.C.: Numerical Potential-Field Techniques for Robot Path Planning. IEEE Transactions on Systems Man and Cybernetics 22, 224–241 (1992)

[4]   Cedrych, D.: Poszukiwanie trajektorii bezzaogowego obiektu latającego w przestrzeni 3D z wykorzystaniem elementów teorii grafów. Unpublished engineer project, Silesian University of Technology (2011) (in polish)

[5]   Deo, N.: Graph Theory with Applications to Engineering and Computer Science. Prentice Hall Series in Automatic Computation (1974)

[6]   Fujimura, K., Samet, H.: A Hierarchical Strategy for Path Planning Among Moving Obstacles. IEEE Transactions on Robotics and Automation 5, 61–69 (1989)

[7]   Ge, S.S., Cui, Y.J.: New Potential Functions for Mobile Robot Path Planning. IEEE Transactions on Robotics and Automation 16, 615–620 (2000)

[8]   Hsu, D., Latombe, J.C., Motwani, R.: Path Planning in Expansive configuration spaces. International Journal of Computational Geometry and Applications 9, 495–512 (1999)

[9]   Hwang, Y.K., Ahuja, N.: A Potential-Field Approach to Path Planning. IEEE Transactions on Robotics and Automation 8, 23–32 (1992)

[10] Kambhampati, S., Davis, L.S.: Multiresolution Path Planning for Mobile Robots. IEEE Journal of Robotics and Automation 2, 135–145 (1986)

[11] Kant, K., Zucker, S.W.: Toward Efficient Trajectory Planning - the Path-Velocity Decomposition. International Journal of Robotics Research 5, 72–89 (1986)

[12] Kavraki, L.E., Kolountzakis, M.N., Latombe, J.C.: Analysis of Probabilistic Roadmaps for Path Planning. IEEE Transactions on Robotics and Automation 14, 166–171 (1998)

[13] Kavraki, L.E., Svestka, P., Latombe, J.C., Overmars, M.H.: Probabilistic Roadmaps for Path Planning in High-Dimensional Configuration spaces. IEEE Transactions on Robotics and Automation 12, 566–580 (1996)

[14] LaValle, S.M.: Planning Algorithms. Cambridge University Press (2006)

[15] Lumelsky, V.J., Mukhopadhyay, S., Sun, K.: Dynamic Path Planning in Sensor-Based Terrain Acquisition. IEEE Transactions on Robotics and Automation 6, 462–472 (1990)

[16] Lumelsky, V.J., Stepanov, A.A.: Dynamic Path Planning for a Mobile Automaton with Limited Information on the Environment. IEEE Transactions on Automatic Control 31, 1058–1063 (1986)

[17] Lumelsky, V.J., Stepanov, A.A.: Path-Planning Strategies for a Point Mobile Automaton Moving Amidst Unknown Obstacles of Arbitrary Shape. Algorithmica 2, 403–430 (1987)

[18] Nakamura, Y., Mukherjee, R.: Nonholonomic Path Planning of Space Robots Via a Bidirectional Approach. IEEE Transactions on Robotics and Automation 7, 500–514 (1991)

[19] Nikolos, I.K., Valavanis, K.P., Tsourveloudis, N.C., Kostaras, A.N.: Evolutionary Algorithm Based Offline/Online Path Planner for Uav Navigation. IEEE Transactions on Systems Man and Cybernetics Part B-Cybernetics 33, 898–912 (2003)

[20] Paik, D.S., Beaulieu, C.F., Jeffrey, R.B., Rubin, G.D., Napel, S.: Automated Flight Path Planning for Virtual Endoscopy. Medical Physics 25, 629–637 (1998)

[21] Pehlivanoglu, Y.V., Baysal, O., Hacioglu, A.: Path Planning for Autonomous Uav Via Vibrational Genetic Algorithm. Aircraft Engineering and Aerospace Technology 79, 352–359 (2007)

[22] Skrzypczyk, K., Gałuszka, A., Pacholczyk, M., Daniec, K.: Probabilistic Approach to Planning Collision Free Path of UAV. In: Nawrat, A., Simek, K., Świerniak, A. (eds.) Advanced Technologies for Intelligent Systems of National Border Security. SCI, vol. 440, pp. 59–68. Springer, Heidelberg (2013)

[23] Thrun, S., Burgard, W., Fox, D.: Probabilistic Robotics. MIT Press (2005)

[24] Tisdale, J., Kim, Z., Hedrick, J.K.: Autonomous UAV Path Planning and Estimation an Online Path Planning Framework for Cooperative Search and Localization. IEEE Robotics and Automation Magazine 16, 35–42 (2009)

[25] Zhu, D., Latombe, J.C.: New Heuristic Algorithms for Efficient Hierarchical Path Planning. IEEE Transactions on Robotics and Automation 7, 9–26 (1991)

[26] Maps with terrain details (2012), http://wysokosc.mapa.info.pl/

[27] Jędrasiak, K., Bereska, D., Nawrat, A.: The Prototype of Gyro-Stabilized UAV Gimbal for Day-Night Surveillance. In: Nawrat, A., Simek, K., Świerniak, A. (eds.) Advanced Technologies for Intelligent Systems of National Border Security. SCI, vol. 440, pp. 107–116. Springer, Heidelberg (2013)

[28] Galuszka, A., Bereska, D., Simek, K., Skrzypczyk, K., Daniec, K.: Application of graphs theory methods to criminal analysis system. Przeglad Elektrotechniczny 86(9), 278–283 (2010)

[29] Skrzypczyk, K.: Behaviour activity based maps applied to mobile robot navigation. In: Proceedings of the 13th WSEAS International Conference on Systems, pp. 295–300 (2009)

[30] Skorkowski, A., Topor-Kaminski, T.: Analysis of EGNOS-augmented receiver positioning accuracy. Acta Physica Polonica A 122(5), 821–824 (2012)

[31] Iwaneczko, P., Jędrasiak, K., Daniec, K., Nawrat, A.: A prototype of unmanned aerial vehicle for image acquisition. In: Bolc, L., Tadeusiewicz, R., Chmielewski, L.J., Wojciechowski, K. (eds.) ICCVG 2012. LNCS, vol. 7594, pp. 87–94. Springer, Heidelberg (2012)

[32]   Czornik, A., Niezabitowski, M.: Lyapunov exponents for systems with unbounded coefficients. Dynamical Systems: An International Journal (2012)

[33]   Czornik, A., Nawrat, A., Niezabitowski, M.: On the Lyapunov exponents of a class of second-order discrete time linear systems with bounded perturbations. Dynamical Systems: An International Journal (2012)

[34]   Czornik, A., Niezabitowski, M.: On the spectrum of discrete time-varying linear systems. Nonlinear Analysis: Hybrid Systems 9, 27–41 (2013)

Part IV
Practical Applications of Classification Algorithms Used in Video Streams for UAV

Main aim of design and construction of UAVs is their practical application. A matter of great importance for real life solutions is utilization of them as a part of complex high level systems. An essential feature of such systems is a great deal of automation achieved often by using classification algorithms. They provide the basis for such advanced systems. However, their design is a lengthy process and requires intensive evaluation using both simulation and experimental data. Even then, it is often necessary to apply amendments based on the actual real life experience of the application.

The first stage of testing such systems is utilization of data acquired using advanced simulation environments. Characteristic feature of recent simulators are their advanced physics engines. It is possible to implement an UAV navigation algorithm following established trajectory and at the same time observe video streams acquired from virtual cameras mounted under UAV models implemented in the simulation environment. Obtained positive results using simulation is often considered as a first step of development detection and classification algorithms.

Misrecognition can sometimes lead to irreversible consequences therefore in order to improve the quality of recognition frequently fusion of data from multiple sources of information is used. Unfortunately increased amount of information often becomes impossible for real time processing using current hardware. It is therefore necessary to use dimensional reduction and clustering algorithms in order to reduce the amount of processed data.

An example of using aerial vision from unmanned aerial vehicles is recognition of people based on their gait features. It is a complex problem that might be solved using already hinted dimensionality reduction algorithms both in linear version like PCA, as well as non-linear, such as MPCA.

However it is worth mentioning that before the video stream from a camera mounted on an UAV it is necessary to wirelessly transmit to human operator using ground base station. This process has to be reliable in order to allow UAV practical application. At the same time due to safety considerations it has to be encrypted because of due to the high risk of wireless data capture. In addition, video data transmission requires a significant network bandwidth. Communication over long distances is charged a considerable limitation in this regard. Therefore it is necessary to use a dedicated image and sound compression algorithms.

Another challenge is to design and implement dedicated communication devices. They allow autonomous communication between the miniature unmanned vehicles in a group without the need for continuous ground control. The chapter presents such device. There is described physical layer and software layer as well as tests with a group of UAV's.

All of the above issues have been included in the chapter. In addition, for each issue a current challenges are presented. Finally, solutions developed by research teams are also presented. Results, thoroughly discussed examples and valuable advices might be found within them.

Information Fusion in Multi-agent System Based on Reliability Criterion

Martin Mellado and Krzysztof Skrzypczyk

Abstract. The paper addresses the problem of information fusion in Multi-Agent System. Since the knowledge of the process state is distributed between agents, the efficiency of the task performance depends on a proper information fusion technique applied to the agents. In this paper we study the case in which each agent has its own sensing device and is able to collect information with some certainty. Since the same information can be detected by multiple agents, the global certainty about the given fact derives from the fusion of information exchanged by interconnecting agents. The key issue in the method proposed, is an assumption that each agent is able to asses its own reliability during the task performance. The method is illustrated by the pick-up-and-collection task example. The effectiveness of the method proposed is evaluated using relevant simulation experiments.

1   Introduction

In Multi-Agent Systems (MAS), a primary task the system is intended to perform is distributed between a number of entities (agents). The beginnings of this branch of science were inspired by Artificial Intelligence in the 1950's. It was recognized that there are a number of tasks that MAS can perform more efficiently than centralized, single unit systems. Thanks to one of the features of MAS - modularity, even the domain of complex problems which are sometimes unpredictable can be solved by a number of simple entities, specialized in solving a particular part of the primary problem [12]. The benefits that these systems can offer are obvious

Martin Mellado
Instituto de Automatica e Informatica Industrial, Universidad Politecnica de Valencia
e-mail: krzysztof.skrzypczyk@polsl.pl, martin@ai2.upv.es

Krzysztof Skrzypczyk
Silesian University of Technology, Institute of Computer Science,
Akademicka 16, 44-101 Gliwice, Poland

and compelling. On the other hand, there are a lot of challenges that must be met in order to design effective and robust systems that are able to solve problems or execute tasks. These challenges were discussed in [12] and it is enough to point out the problems like   coordination [2], [4],[5], [13], [14] task division [3], [7], [10],[17], cooperation [1], [7], [8], [15] etc. The potential advantages of MAS were quickly noticed by researchers who deal with problems related to Robotics. They have discovered that some specific tasks whose execution requires building and operating complex, powerful robotic units, can be performed more effectively by simpler, highly specialized robots. There are a number of problems that have become benchmarks and test-beds for the quality assessment and analysis of Multi-Robot Systems (MRS) functioning. This paper addresses one of the most important issues related to MAS which is fusion of information provided by multiple agents. The knowledge of the process state is distributed between agents, the efficiency of the task performance depends on a proper information fusion technique applied to the agents. In this paper we study the case in which each agent has its own sensing device and is able to collect information with some certainty. Since the same information can be detected by multiple agents, the global certainty about the given fact derives from the fusion of information exchanged by interconnecting agents. The key issue in the method proposed, is an assumption that each agent is able to assess its own reliability during the task performance. The method is illustrated by the pick-up-and-collection task example. However an application of the fusion technique discussed in this paper is not narrowed down only to the problem defined. It can be used in any system that is able to assess its own performance quality. A good example is the system of detecting and recognition objects by a number of cameras observing the same scene. Each of camera is usually mounted in an opto-electronic gimbal [16]. The effectiveness of the method proposed is evaluated using relevant simulation experiments.

2   System Description

The subject of this paper is the information fusion method in MAS. In order to present our approach we use the framework of the system dedicated for performing pick-up-and-collection task which consists of collecting a number of objects scattered inside a workspace of limited area. Figure 1 illustrates the principal idea of organizing the system. As was mentioned, there is an unknown number of objects to be collected, scattered over an area being the workspace of the system. The system consists of a specified number of robotic-units also called agents. Each agent can be defined by the following features [12]:

- limited sensing abilities,
- possibility of communication with limited number of other agents,
- a set of actions that an agent is able to take,
- reasoning about those actions based on its own knowledge.

Since agents can communicate with each other they can exchange information about objects that are detected by their sensing devices and this way increase their knowledge of the number and location of objects sensed by other team mates. The subject of the paper is the method of agents sensing fusion which results in improvement of the process global knowledge.
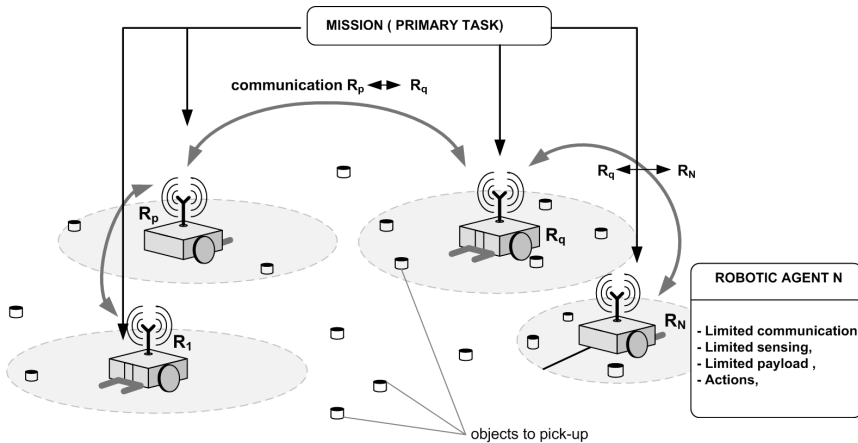
Fig. 1. Diagram that illustrated organization of the MAS being the subject of the discussion

2.1 *Workspace*

The workspace is a constrained, unstructured, flat area where a number of objects the robots are intended to collect are scattered. The objects are defined by a set of indices:

$$O = \{i\}, \qquad i = 1, 2, \ldots, M \tag{1}$$

where M is the total number of objects located inside the workspace. It has to be stressed that this number is not known to any agent. The location of each object is defined by a pair of coordinates $o_i = (x_{0,i}, y_{0,i})$ $i \in O$. No data of these positions are provided to particular agents.

2.2 *Agents Description*

The system consists of N robotic agents that are equipped with a sensory system that allows them to detect objects O and determine the location of detected objects. Let us define the team of the robotic agents as a set:

$$R = \{i\}, \qquad i = 1, 2, \ldots, N \tag{2}$$

a pose r_i of each agent is determined by a triple $(x_{r,i}, y_{r,i}, \Theta_{r,i})$, where the elements denote coordinates of the center and heading of the agent defined in the workspace coordinate frame.

2.3 Sensing Abilities

Each robotic agent is provided with perception devices that allow it to detect objects in its vicinity. Therefore, let us define a set of objects detected by the ith agent as a set of indices:

$$O_i = \{j\}, \qquad i \in R, \qquad j \in O \wedge O_i \subseteq O \tag{3}$$

The perception of the agent is limited by the range of its sensors. The range of the sensors is denoted by $s_{r,i}$, which means that only those objects can be detected by the agents satisfying the following:

$$k \in O_i \Leftrightarrow d_{i,k}^o = \sqrt{\left(x_{r,i} - x_{o,k}\right)^2 + \left(y_{r,i} - y_{o,k}\right)^2} \le s_{r,i} \tag{4}$$

Each agent is able to assess its detection quality. It is defined by certainty factor which varies in range from 0 to 1. The design of detection model and certainty evaluation is not the subject of this paper. For the purpose of the study we assume that detection certainty of the agent is influenced by two factors. The first one is related to its perception abilities which (it this study) decreases with the distance $d_{i,k}^o$ between the ith agent and kth object. The second factor influencing the certainty is a random process related to the sensing devices inaccuracy, noise etc. The influence level of particular factors is weighted by coefficients w_d and w_n the sum of which is equal to one. Using those coefficients we can simulate the sensing reliability of the given agent. In the study presented the detection certainty of the kth object by the ith agent is modeled as:

$$\hat{p}_{i,k} = f_{i,k}^d + w_n\left(-f_{i,k}^d + \left(1 - 2f_{i,k}^d\right)\delta_i\right) \tag{5}$$

where $w_n = 1 - w_d$ and $\delta_i \in [0,1]$ is a random number that characterize the influence of inaccuracy and uncertainty. The component $f_{i,k}^d$ is related to perception abilities of the ith agent and is defined as:

$$f_{i,k}^d = w_d\left(1 - \frac{1}{1 + e^{-\alpha\left(d_{i,k}^o - s_{r,i}\right)}}\right) \tag{6}$$

Balancing the influence of the random and detection part of the model we can simulate reliability of particular agents.

2.4 Communication

Agents are provided with communication devices that allow the exchange of information and coordination of mutual actions. It is also assumed that the

communication abilities of agents are limited. The limitations for the purpose of this study are narrowed down to the range of the communication devices. That means the given agent is able to communicate only with those agents that are closer than some threshold value. Let us define the set, which determines the those agents that ith agent is able to communicate with:

$$\Phi_i = \{j\}, \qquad j \in R \wedge j \neq i \tag{7}$$

It must be stressed that two agents are in communication only when the transmission of data can be made in both directions. The agent can receive information and its transmission can be received by the other one. This happens only if the following is satisfied:

$$j \in \Phi_i \iff d_{i,j}^r < b_i \wedge d_{i,j}^r < b_j \tag{8}$$

where $b_{i/j}$ denotes the range of communication devices of the ith and jth agent, while the value $d_{i,j}^r$ in (8) is the distance between the ith and jth agent.

3   Agent Reliability Assessment

As was mentioned before, the information fusion idea is based on the assumption that each agent is able to evaluate (during the task performance) its reliability related to the acquired sensory data correctness. In this section the method of reliability assessment will be presented. Let us first distinguish the discrete moment in the MAS operation and let us denote it by $n = 0,1,2, \ldots$ .In the beginning of the MAS operation ($n = 0$) the reliability of ith agent is equal to some predefined value:

$$c_i(n = 0) = c_{i0} \in [0,1] \tag{9}$$

Let us assume that ith agent in the moment n detects the set of objects defined by (3). We will refer to this set hereafter as:

$$O_i(n) = \{j\}, \qquad i \in R, j \in O \wedge O_i \subseteq O \tag{10}$$

After detecting the objects defined by (10), the certainty factor is determined for each object detected according to the function (5), let us denote this estimated value as:

$$\hat{p}_{i,j}, j \epsilon O_i(n) \tag{11}$$

While performing the task and picking up the objects (10) the agent is able to confront the real state of the process with its predictions. Let us introduce the factor that defines an error of the certainty assessment done by the ith agent with respect to the jth object detected:

$$e_{i,j} = \left| \hat{p}_{i,j} - p_{i,j} \right| \tag{12}$$

where $p_{i,j} \in \{0,1\}$ in (12) denotes a detection correctness of the jth object. If the object was detected correctly $p_{i,j}$ takes the value 1 and 0 otherwise. Using the value of (12) we can determine the agent reliability based on a single picking up operation. The reliability value is calculated as a function of the (12). In this research an sigmoid function was applied to assign the value of reliability on the basis of the detection correctness error. Hence the reliability factor defined for ith agent using the jth picking up experiment is defined as:

$$c_{i,j} = 1 - \frac{1}{1 + e^{-\beta(e_{i,j}-e_{i0})}} \tag{13}$$

where β parameter tunes the steepness of the curve around the threshold e_{i0}. This parameter defines the maximal acceptable error (12), by which it is possible to set the agent reliability at the level of 1. Applying the equation (13) to each object from the set (10) it is possible to determine the reliability of the agent at the nth stage of the system operation. In this study it is obtained by averaging results:

$$c_i^{O_{i(n)}} = \frac{1}{k}\sum_{k=1}^{K} c_{i,k}, \quad K = \bar{\bar{O}}_i(n) \tag{14}$$

The detection and recognition process is performed on the basis of the data collected in the single operation cycle of the sensory system. Therefore calculating the agent reliability as the average given by (14) seems to be valid approach. Finally, the reliability of the ith agent at the nth stage of the process can be evaluated as an exponential moving average with a time window of length Z. It can be determined recursively using the following formula:

$$c_i(0) = c_i^{O_i(0)}$$
$$c_i(n) = \lambda c_i^{O_i(n)} + (1-\lambda)c_i(n-1), \quad for\ n > 0 \tag{15}$$

where λ is a constant smoothing factor which value can be from 0 to 1. It represents the weighting factors applied to the values calculated in the past. The higher value of λ the faster discounting older values is. In this study this coefficient is expressed in terms of the time window length:

$$\lambda = \frac{2}{Z+1} \tag{16}$$

Applying the above reasoning to every agent, we can assess their reliability at each stage of the process.

4   Data Fusion

As was stated in the previous sections in the MAS information about the process performed is distributed among multiple agents. Due to different perception

abilities, location and possible malfunctions of the sensory devices, the informa-
tion about the same part of the process (in the case of this study - objects) can be
different. Since agents are able to communicate each other and exchange data, the
information fusion can be made. Various information about the same part of the
process can be used to increase the agents certainty. In the case discussed, agents
exchange information about the objects detected as well as the certainty of the
detection fact. Since they share the common resources, the same object can be
detected by multiple agents. So the question arises how make a fusion of informa-
tion collected by different agents. In this study an application of the reliability
factor was applied. It was assumed that each agent is able to assess its reliability
by confronting its certainty estimation with the real state of the process. Let us
define the set R_k of agents, and their certainties related to the fact of detecting the
object k:

$$\hat{P}_k = \{\hat{p}_{i,k}\}, \qquad i \in R_k \tag{17}$$

Using the reliability notion, it is possible to make fusion of certainty by weighted
averaging the data provided by the agents. Hence the common certainty of agents
defined in R_k, about the object kth is calculated as:

$$p_{R_k,k}(n) = \frac{1}{\sum_{i \in R_k} c_{i,k}} \sum_{i \in R_k} c_{i,k}(n)\hat{p}_{i,k} \tag{18}$$

The reliability of each agent is a function of the weighting coefficient. The higher
reliability the greater influence of the information collected by the agent on the
final certainty value.

5   Simulation

In order to verify and evaluate the quality of the method presented, a simulation
experiment was arranged. Two robotic-agents are placed inside an rectangular
workspace of size 500x500[m]. Each agent is equipped with a sensory system
which is able to detect objects in the area defined by the angle of view and the
range of the sensors. The values of the range and angle are set to (90[m],75[deg])
and (110[m],95[deg]) for the first and second agent correspondingly. Inside the
workspace there are 100 objects placed on locations selected in a random way.
Figure 2 presents the experiment arrangement. The goal of the agents is efficient
collecting objects. The agents are able to communicate each other and exchange
information about the objects detected. Moreover it is assumed that agents ex-
change information about their reliability self-assessment.
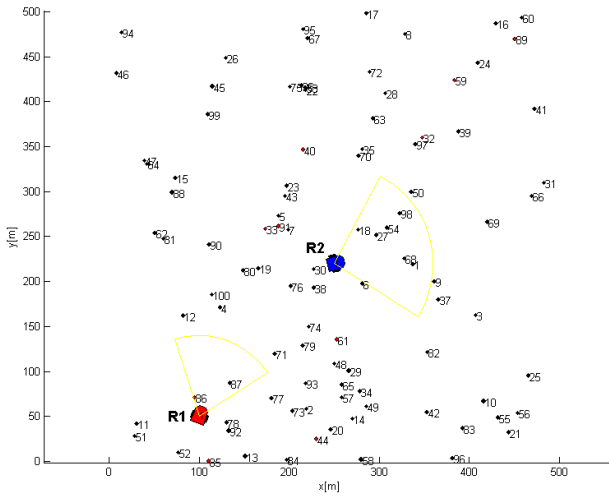
Fig. 2. The simulation experiment arrangement

The aim of the first part of the simulation experiment was to verify the procedure quality of the reliability assessment. The experiment was as follows. The agent was repeating the procedure detect-collect 15 times. The reliability of the agent was modeled according to the (5) by changing the influence of the random component. The simulation was performed for three values of $w_d = 0.7, 0.5, 0.05$. The results of the experiment are presented in the fig.3.
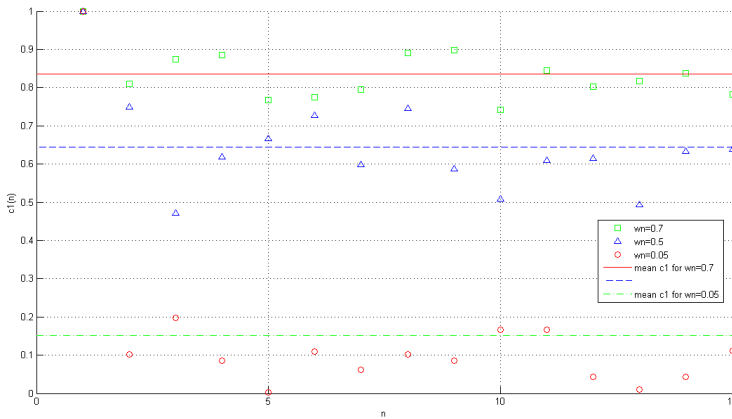
Fig. 3. The agent reliability assessment

We can observe that with the decrease of w_n (what corresponds to increasing the random component) the reliability assessment decrease what means the evaluation method works correctly.

Next part of experiment was arranged to evaluate an reliability influence on the effectiveness of the pick up collection task performance. The first agent was performing 15 detect-collect cycles. The number of objects collected N_{col} was counted. The procedure was repeated 5 times. The average number of objects collected in 5 simulation runs was the measure of the method effectiveness. The procedure described above was done for three different values of parameter w_n. The results are gathered in the tabular (fig.4).

No.	N=10, RP=5	
	$w_{n,1}$	N_{col}
1	1	42
2	0.5	31
3	0	9

Fig. 4. Results of the second experiment

As can be seen the quality of the sensing, which is related to the reliability has a direct influence on the effectiveness of the task performed. The last part of simulation research was to asses influence of exchanging information on the agent effectiveness improvement. In this experiment two agents were performing the task simultaneously. The agents were in permanent communication. The first agent was modeled as the one of high reliability. The reliability of the second one was set by the parameter w_n to values 0.5 and 0. We can see that thanks to the communication and information fusion effectiveness of performing the task was improved (compare fig.4 and fig.5).

No.	N=10, RP=5		
	$w_{n,1}$	$w_{n,2}$	$N_{col,1}$
1	0.5	1	36
2	0	1	13

Fig. 5. Results of the third experiment

That proves that proper data fusion in MAS can improve the quality of the system operation.

6   Conclusion

This paper addressed the problem of information fusion in MAS. The method of combining data provided by intercommunicated agents is discussed. The approach presented is based on reliability of particular agents. The level of reliability is evaluated by each agent while performing the task by confronting its data collected with the real state of the process. This approach is very simple to implement what is its great advantage. The functioning of the data fusion algorithm is illustrated using an example of pick up and collection task. Nevertheless the method is flexible and can be applied to any MAS in which agents are able to assess its reliability using different sensory systems, the vision systems for instance. Some relevant simulation examples are presented to prove the effectiveness of the approach presented.

References

[1]   Cheng, X., Shen, J., Liu, H., Gu, G.: Multi-robot Cooperation Based on Hierarchical Reinforcement Learning. In: Shi, Y., van Albada, G.D., Dongarra, J., Sloot, P.M.A. (eds.) ICCS 2007, Part III. LNCS, vol. 4489, pp. 90–97. Springer, Heidelberg (2007)

[2]   Harmati, I., Skrzypczyk, K.: Robot team coordination for target tracking using fuzzy logic controller in game theoretic framework. Robotics and Autonomous Systems 57(1) (2009)

[3]   Jones, C., Mataric, M.: Adaptive Division of Labor in Large-Scale Minimalist Multi-Robot Systems. In: Proc. of IEEE/RSJ International Conference on Intelligent Robots and Systems, Las Vegas, pp. 1969–1974 (2003)

[4]   Kaminka, G.A., Erusalimchik, D., Kraus, S.: Adaptive Multi-Robot Coordination: A Game-Theoretic Perspective. In: Proc. of IEEE International Conference on Robotics and Automation, Anchorage Convention District, Anchorage, Alaska, USA (2002)

[5]   Kok, J.R., Spaan, M.T.J., Vlassis, N.: Non-communicative multi-robot coordination in dynamic environments. Robotics and Autonomous Systems 50(2-3), 99–114 (2005)

[6]   Klusch, M., Gerber, A.: Dynamic coalition formation among rational agents. IEEE Intelligent Systems 17(3), 42–47 (2002)

[7]   Kraus, S., Winkfeld, J., Zlotkin, G.: Multiagent negotiation under time constraints. Artificial Intelligence 75, 297–345 (1995)

[8]   Kraus, S.: Negotiation and cooperation in multiagent environments. Artificial Intelligence 94(1-2), 79–98 (1997)

[9]   Mataric, M., Sukhatme, G., Ostergaard, E.: Multi-Robot Task Allocation in Uncertain Environments. Autonomous Robots 14, 255–263 (2003)

[10]   Schneider-Fontan, M., Mataric, M.J.: Territorial Multi-Robot Task Division. IEEE Transactionson Robotics and Automation 14(5), 815–822 (1998)

[11]   Winkfeld, K.J., Zlotkin, G.: Multiagent negotiation under time constraints. Artificial Intelligence (75), 297–345 (1995)

[12] Wooldridge, M.: An Introduction to Multiagent Systems. Johnn Wiley and Sons Ltd., UK (2009) ISBN:978-0-470-51946-2

[13] Vail, D., Veloso, M.: Dynamic Multi-Robot Coordination. In: Schultz, A., et al. (eds.) Multi Robot Systems: From Swarms to Intelligent Automata, vol. II, pp. 87–98. Kluwer Academic Publishers, The Netherlands (2003)

[14] Cheng, X., Shen, J., Liu, H., Gu, G.: Multi-robot Cooperation Based on Hierarchical Reinforcement Learning. In: Shi, Y., van Albada, G.D., Dongarra, J., Sloot, P.M.A. (eds.) ICCS 2007, Part III. LNCS, vol. 4489, pp. 90–97. Springer, Heidelberg (2007)

[15] Gałuszka, A., Pacholczyk, M., Bereska, D., Skrzypczyk, K.: Planning as Artificial Intelligence Problem-short introduction and overview. In: Nawrat, A., Simek, K., Świerniak, A. (eds.) Advanced Technologies for Intelligent Systems of National Border Security. SCI, vol. 440, pp. 95–104. Springer, Heidelberg (2013)

[16] Jędrasiak, K., Bereska, D., Nawrat, A.: The Prototype of Gyro-Stabilized UAV Gimbal for Day-Night Surveillance. In: Nawrat, A., Simek, K., Świerniak, A. (eds.) Advanced Technologies for Intelligent Systems of National Border Security. SCI, vol. 440, pp. 107–116. Springer, Heidelberg (2013)

[17] Galuszka, A., Bereska, D., Simek, K., Skrzypczyk, K., Daniec, K.: Application of graphs theory methods to criminal analysis system. Przeglad Elektrotechniczny 86(9), 278–283 (2010)

Prototyping the Autonomous Flight Algorithms Using the Prepar3D® Simulator

Krzysztof Daniec, Paweł Iwaneczko, Karol Jędrasiak, and Aleksander Nawrat

Abstract. This article concerns prototyping of the control algorithms for unmanned flying objects using the virtual reality. More specifically, there is discussed an integration between simulation environment and unmanned aerial vehicle (UAV) control software. This integration is based on software in the loop simulation. The control software uses PI controllers cascade, which stabilize the aircraft in the simulated air. Used simulator is Prepar3D® from Lockheed Martin corporation. Implemented algorithms that are used to control the UAV in simulation environment can be used to future prototype of vision based algorithms. All implemented algorithms are presented along with the developed software, which we are using to navigate the flying object on real map.

1 Introduction

Nowadays, more and more military and government organizations are supplying in the unmanned flying objects. Since they can be used in difficult and dangerous circumstances, they are becoming more popular. UAV (Unmanned Aerial Vehicles) objects have a wide range of possible uses: they can be used by emergency services to search for missing people, can be used for patrolling and monitoring a specific area and as well are applied as a means of transport a various types of cargo, in the particular case these dangerous, such as radioactive wastes and unexploded ordnance. Most of these aircraft are equipped with advanced devices for image acquisition.

Krzysztof Daniec · Paweł Iwaneczko · Karol Jędrasiak · Aleksander Nawrat
Silesian University of Technology, Institute of Automatic Control,
Akademicka 16, 44-101 Gliwice, Poland
e-mail: {pawel.iwaneczko,karol.jedrasiak,krzysztof.daniec,
        anawrat}@polsl.pl

The construction and service for unmanned aircraft is fairly expensive and it should be added that the cameras are usually the most expensive part of the aircraft. Furthermore, prototyping autonomous flight algorithms and vision based algorithms is time consuming and requires multiple tests and a priori assumptions. In prototyping the algorithms helpful appear to be a real-world simulators. Therein can be tested the control algorithms including the dynamics of flying object, GPS system simulation and among others earth model WGS-84. Using the simulator allows to run the tests without fear of destruction of the real object, and what goes with it, from possible accidents and exposure to the risk of third parties. Using a simulation of the real world we are making a large financial savings resulting from no need for rebuilding the model in the case of (undesirable) breakdown. We also save the time that we could spend much more, during the design of mechanisms for autonomous flight. Using a simulation environment Prepar3D® Lockheed Martin, we are able to get data from all kinds of sensors and also to control the flying object model. This environment has mapped physics, not only in the air, but also on land and in the water. Importantly, the simulation allows us to change the weather, which greatly influences the dynamics of moving objects in it. The simulation includes, for example, buildings and artificial traffic, which can be used to prototype the vision based algorithms. In addition, it should be mentioned, that realistic is also a terrain, as well as locations of all airports and cities.

Main contribution of this paper are control algorithms for UAV on the set trajectory. This trajectory can overlap with the existing highway network, waterways and air routes. Thanks to this, it is possible to use a video stream from the onboard virtual camera for prototyping vision based algorithms.

2   Literature Review

The Control of the unmanned objects based on vision is an active area of research. In many publications we met with topics devoted just to control of flying objects using a flight simulators. One of them, worth mentioning is the work of Eric R. Mueller [1], which was based on the studies carried out with Hardware-in-the-Loop simulation. Simulation was based there on Matlab/Simulink® mathematic model, while the control values was calculated by using LQR controllers [2]. Another important publication is the work of Eric N. Johnson and Sumit'a Mishra [3], which uses simulation both in SIL (Software In the Loop) and HIL (Hardware In the Loop) and the simulation visualization. In the will of the explanation, the SIL-loop simulation controls a physical process model (the simulator) using the software, which is a model of the regulator, which was run on the same hardware platform. In the HIL-simulation process is involved a real regulator, which communicates with the simulator through the appropriate interfaces. In the articles [4] and [5] the authors use a simulation environment implemented in the "Matlab/Simulink® 6-DOF", and visualization, "FlightGear". The simulator that was used there is characterized by a greater reality, because it includes the basic model of atmospheric, gravity and magnetic field.
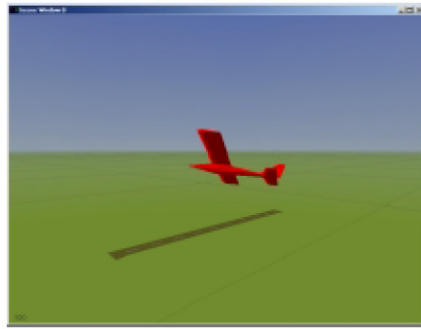
Fig. 1. Simulator implemented in "C" language

In the work [6] the flight simulator was implemented in "C" language and taking into account an airplane model servos and simulated GPS (fig. 1). Procerus Technologies [7] developed even its own electronic system (autopilot), which allows to control both the real object as well as testing the HIL-simulation. Kestrel Autopilot is designed to control the UAV objects of flying wing type, where the control system is based on a PID controllers cascade. In closing we can mention the work of the Institute of Aviation [8],which uses the Kestrel autopilot system for designing robust optimal control based on H-infinity and μ-Synthesis method. The articles mentioned above describe only control algorithms, and the simulators characterized by them are not so advanced to support the image data processing from on-board cameras.

Based on the experience of C. Kownacki [9], at the beginning we have performed autonomous flight control algorithms, that allowed us to get better results with prototyping the vision based algorithms. It is important, that this article describes the use of images from simulation to road tracking algorithms. Image which was taken from a camera (fig. 2), was processed by the Sobel operator followed by linear Hough algorithm. Similar assumptions and conclusions are described in derivative works [10] and [11].

Fig. 2. Example of road edge detection [9]

3   Lockheed Martin Prepar3D

Prepar3D® was mostly implemented by Lockheed Martin™, but it was created on Microsoft ESP (*Enterprise Simulation Platform*), which was designed for the purpose of Microsoft Flight Simulator. Microsoft's program has been widely used, but it was limited only to control the flying objects, which also proved to be insufficient for current military purposes. To ensure the possibility of further product development, Lockheed employed several members of the ACES studio. In the future, Lockheed Martin is going to modify the Microsoft ESP to allow its use for military and civil services training in the event of any type of disasters.

Prepar3D® flight simulator has a wide range of functionality. Three of them appear to be necessary and sufficient for prototyping control algorithms. The first of functionalities is object model configuration. Configuration of the model allows us for example to change many of the physical and geometrical parameters such as weight, size and wingspan. It also allows us to change dynamic parameters such as engine power, effectiveness and stability of ailerons or elevator deflection. Those allows us to parameterize object model, whose behaviour resembles the real object.

There can be configured the sea, air and road traffic, that proves to be useful for prototyping the vision based algorithms, for example, for vehicle and ships tracking purpose. The simulation allows to create on-board cameras, which can be moved or zoomed both by an operator and also as well as an appropriate autonomous algorithm. It is possible to run multiple cameras at one time, not only in vision system, but also in thermo-vision, night-vision (fig. 3) and infrared vision systems. These virtual cameras can be placed (configured) in areas that correspond to the location of cameras in real UAV. Optionally it could be possible to acquire multispectral images [12]. This gives a wide possibilities to create different types of algorithms for object detection and obstacle avoidance. These algorithms can be further moved to the real aircraft electronic module.
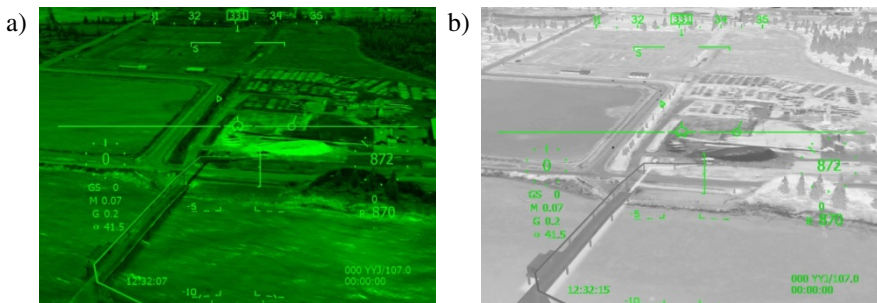
Fig. 3. Vision systems: a) night vision, and b) thermo-vision

4   Flying Model Description

Flying object model should receive control data and returns the sensory variables. Another example of the Prepar3D® functionalities is reading the variables from the simulation environment. Being used by us data returned by the virtual sensors from the simulator are as follows:

- LLA geodetic position: latitude (φ), longitude (λ), altitude above sea-level (h),
- object orientation: roll (rotation around the x axis, α), pitch (rotation around the y axis, β) and yaw (rotation around the z axis, γ),
- airspeed (v).

The third, and the mostly useful functionality, which is used, is controlling the aircraft. To control an object in the Prepar3D® environment algorithm uses four variables: rudder, elevator, ailerons and throttle. The main airplane axes and the three main control elements are illustrated in the fig. 4.
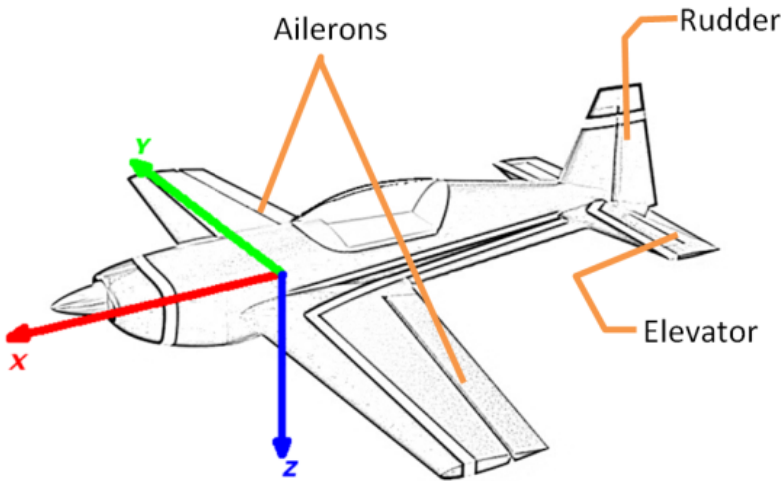
Fig. 4. Airplane model with axes description

5   Controllers Cascade

Object control and stabilization is based on PI controllers.[12] Algorithm uses the discrete PI controller, that is described by formula (1).

$$u_i = k_p * \left(e_i + \frac{h}{T_I} * \sum_i \left(\frac{e_i + e_{i-1}}{2} \right) \right) \tag{1}$$

where: u_i – controller output at the moment i, e_i – error, controller input at the moment i, k_p – controller proportional gain, T_I – controller integrator gain, h – delay time.

In the control algorithm was implemented 4 basic and 2 master PI controllers. The basic regulators are responsible for the calculation of the control values, while the master regulators are responsible for elaborate the setpoints for the basic PI controllers. PI controllers cascade used in the stabilization algorithm are described in the fig. 5.
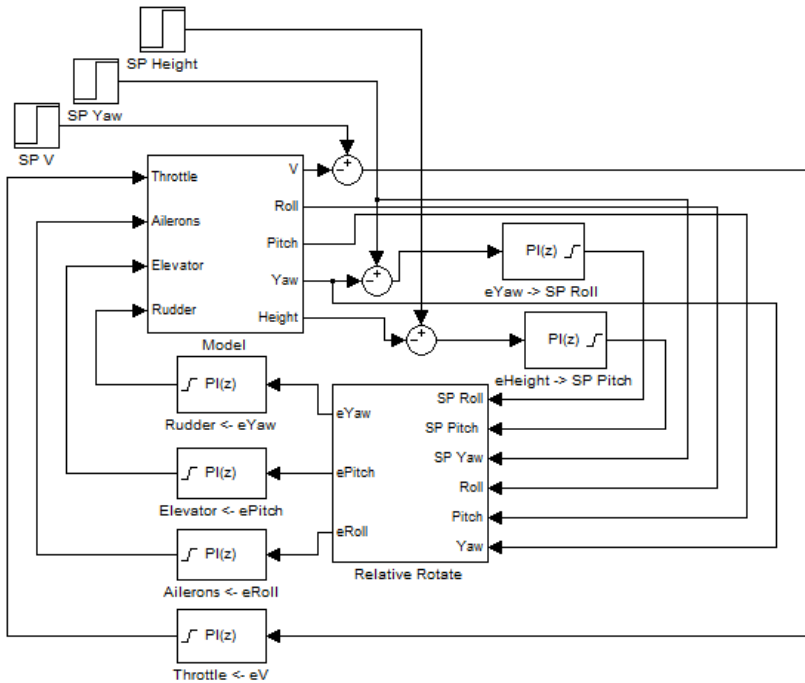
Fig. 5. PI controllers cascade

Basic controllers visible in the schema (fig. 5) are: airspeed controller – throttle control based on speed error ($eV \rightarrow Throttle$), pitch controller – elevator control based on pitch error ($ePitch \rightarrow Elevator$), roll controller – ailerons control based on roll error ($eRoll \rightarrow Ailerons$) and yaw controller – ruder control based on yaw error ($eYaw \rightarrow Rudder$). Master controllers are: height controller – elaborate pitch setpoint value based on height error ($eHeight \rightarrow SP\ Pitch$), heading controller – elaborate roll setpoint value based on yaw error ($eYaw \rightarrow SP\ Roll$).

Basic controllers are active all the time, but the heading regulator has a variable parameters depending on the operation mode. In the case of object angular stabilization the master regulators are inactive because setpoints are given by the operator. During the automatic flight, which means a flight on a given height, with predefined velocity, and on the set azimuth, there are active all of the six controllers. It should also be mentioned that the error of all rotation angles

$(\alpha_e, \beta_e, \gamma_e)$ is calculated relative to the object, not to the earth, and it is presented in fig. 5 in a block "Relative Rotate". The mechanism of functioning of the block "Relative Rotate" is also described by the equation (2).

$$\mathbb{R}_e = \mathbb{R}_{sp} * \left(\mathbb{R}_{ypr}\right)^{-1} \tag{2}$$

where: $\mathbb{R}_{ypr}$ – rotate matrix created from actual values of Euler angles (α, β, γ), $\mathbb{R}_{sp}$– rotate matrix created from setpoint values of Euler angles $(\alpha_{sp}, \beta_{sp}, \gamma_{sp})$, $\mathbb{R}_e$– rotate matrix with Euler angles error $(\alpha_e, \beta_e, \gamma_e)$. The angles error can be calculated from three trigonometric formulas (3).

$$\alpha_e = \text{atan2}\left(\mathbb{R}_{e\,23}, \mathbb{R}_{e\,33}\right)$$
$$\beta_e = \text{asin}\left(-\mathbb{R}_{e\,13}\right) \tag{3}$$
$$\gamma_e = \text{atan2}\left(\mathbb{R}_{e\,12}, \mathbb{R}_{e\,11}\right)$$

where: $\boldsymbol{\alpha_e}$ – roll angle, $\boldsymbol{\beta_e}$ – pitch angle, $\boldsymbol{\gamma_e}$ – yaw angle.

6   Autonomous Flight Algorithm

To get a fully autonomous object, PI controllers are not enough. They are responsible only for the stabilization, what means that the plane can fly at the required height and setpoint orientation relative to the ground. Flying object should store in the memory the planned route with the takeoff and landing positions. The route consists of a sequence of points, described as a geographic coordinates LLA, the Latitude (φ), Longitude (λ) and Altitude (height above sea level, h). Each of the commands performed during the flight must be properly interpreted and converted to setpoints for the PI controllers.

To navigate an unmanned object, algorithm uses the transformation from the geodetic position (LLA) to ENU coordinates (East, North, Up) [13], which are formed from a plane tangent to the Earth's surface fixed to a specific location. Units are converted to meters.

The presented autonomous flight algorithm consists of four partial algorithms responsible for taking-off, landing, taking waypoints and circling.

6.1   *Taking-Off and Landing Algorithm*

The basic requirement for the autonomous take-off are accurate measurements of geographical coordinates and the altitude, of start and end of the runway. Take-off algorithm consists of only a few simple instructions. After launching the engine algorithm maintain the orientation of the runway and it accelerate the aircraft to the desired speed. Next, the algorithm change the setpoint pitch angle of the aircraft, and then there are determined the ENU coordinates for the destination

height. The next step is to achieve an initial height that is equal to $^1/_5$ of the destination altitude. When this happens, there are activated height and heading controllers, which effects the stabilization of the take-off destination altitude.

The autonomous landing algorithm proved to be quite difficult to implement, and despite all the efforts, it is not perfect. The landing process is divided into two parts, the first concerns the approach to land and set the plane on of the glide path (fig. 6), while the second concerns the landing curve. To determine the coordinates of the approach for landing, important information is: where (relative to airport) is a plane.
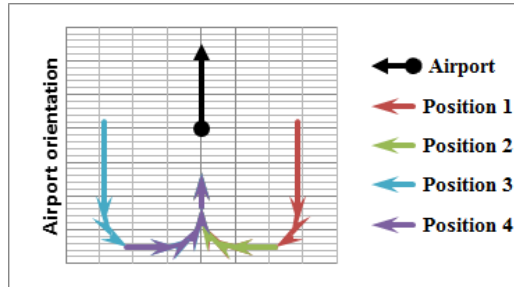
Fig. 6. Approach for landing

Depending on the location aircraft, the algorithm determines from 6 (purple and green colors) to 9 (blue and red colors) coordinates. The first coordinate is not always at the beginning of the first arrow in the fig. 6. It can be located for example in the middle of this arrow. The method for determining whether a coordinate is reached, is to compare the absolute values of all three ENU coordinates, with predefined precision value (4).

$$ACK = |E| \leq p \cap |N| \leq p \cap |U| \leq p, \tag{4}$$

where: ACK − confirm the position is reached, E, N, U − ENU coordinate components, p − redefined precision value in meters.

When the airplane reaches the beginning of the glide path, algorithm starts to determine the landing curve. The function of the curve is described by the formula (5), but it is scaled to the left and right side of the x-axis. Each part contains 10 coordinates, and the whole left side concerns only for the airport. Navigation during landing is fairly complicated, and therefore, when determining achieved position algorithm checks only the height of the airplane. Using the following ENU coordinates there is determined the pitch angle from the formula (6), and the orientation of the plane is set towards the end of the runway. When the height relative to the airport will be sufficiently low (i.e. the plane will be about $5m$ above the runway), the setpoint speed is reduced to the landing speed, and finally when airplane reaches this speed the engine is turned off.

$$y = 1,2^x \qquad (5) \qquad \beta_{sp} = \text{atan2}\left(u, \sqrt{e^2 + n^2}\right) \qquad (6)$$

where: x – maps the landing path in the East-North plane, β_{sp} – setpoint pitch angle, u, e, n – ENU coordinates components.

6.2   Circling and Taking Waypoints

Circling command is an additional option, which starts automatically, when the airplane is in the air, has already completed a flight along the waypoint path, and when the user doesn't manage to give any new commands in the specified time period. Executing this command, the algorithm is still changing the aircraft azimuth by some angle α after passing a certain given distance d. The whole air movement is obviously on a preset height h. Positions of the circular path are calculated from the ENU conversion and then they are converted to setpoints for the PI controllers.

During the flight along the desired path, which consists of a sequence of points in LLA form algorithm uses the stabilization of the setpoint height and stabilization of the orientation, which are calculated from designated ENU coordinates. With this option ENU coordinates are calculated in real time, which is based only on current and destination GPS position. Arbitration method for achieve destination position is the same as for other commands formula (4).

7   Tests

This paper presents four test of unmanned aircraft flights in simulation environment Prepar3D®. These tests were performed on a single PC with running Microsoft Windows 7. This computer is running two applications: simulation environment Prepar3D® and control application which. These applications communicate with each other using a dedicated SimConnect library shared by Lockheed Martin (fig. 7).

Fig. 7. Connection between Prepar3D® and control application

The first two tests were performed to show the results of the completed PI controllers tuning, and the UAV flight stabilization. Both the third and fourth test describes the pseudo autonomous flight which is based on a sequence of geographic coordinates. The purpose of the last test is flight over the artificial traffic on the highway, which is the first step to create a tracking algorithms.

7.1 Control Algorithm

First test is the stabilization of the aircraft azimuth and it is shown in the fig. 8. Plot in the part A shows the aileron control, while the plot in part B represents the setpoint values of the angles: setpoint yaw (γ_{sp}), setpoint roll (α_{sp}) and current values of angles: yaw (γ) and roll (α). Setpoint yaw variable $\left(\gamma_{sp}\right)$ was changed four times by the operator, while the other variables including ailerons control on the plot in part A were calculated by the PI controllers formula (1). The value of the current roll angle (α) is keeping up with its setpoint value (α_{sp}) in less than one second. The value of the airplane azimuth is changed at a constant speed, so the settling time depends on the error value. With an yaw error (γ_e) equal to 15° settling time is about 5 seconds and the control is without overregulation. It is worth noting that the maximum aileron control in this case does not exceed 20% of the control range.
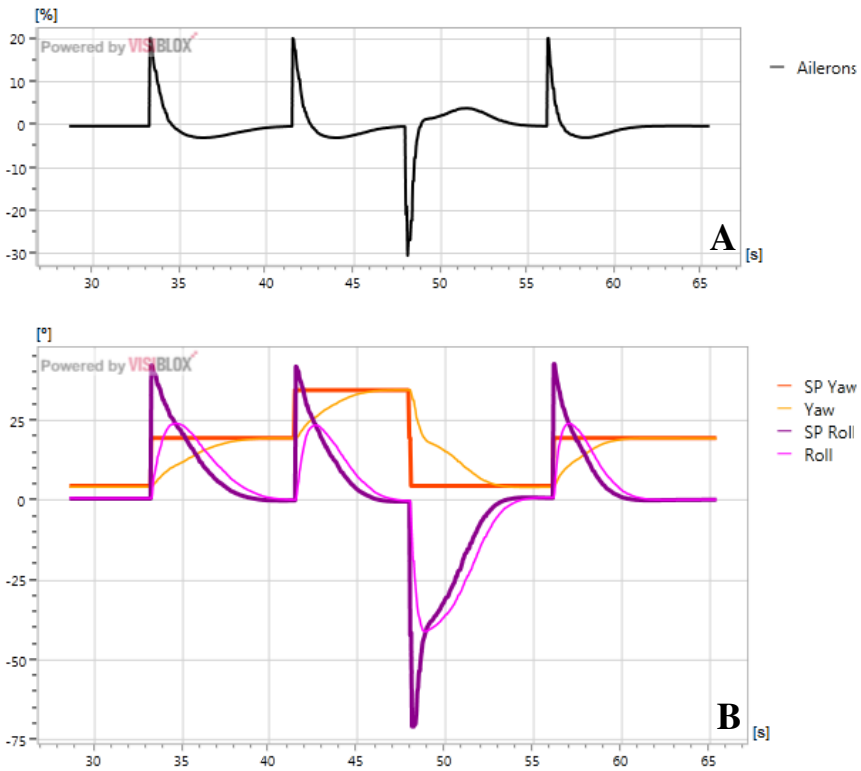
Fig. 8. Azimuth and roll stabilization plots

The next test is similar to previous, but it describes the stabilization of the air-craft altitude above sea level (fig. 9). Plot A shows the elevator control and the plot B shows the setpoint value of the altitude (h_{sp}) and current value of altitude (h). In this case value of the setpoint height variable (h_{sp}) was changed two times by steps by the operator. The settling time and the magnitude of the overregulation depends on the height error value. Overregulation reaches a higher value when the airplane is reducing altitude. Overregulation is much lower when airplane has to increase its altitude. Reduction of the altitude of the aircraft with a value of 100 m takes about 20 seconds.
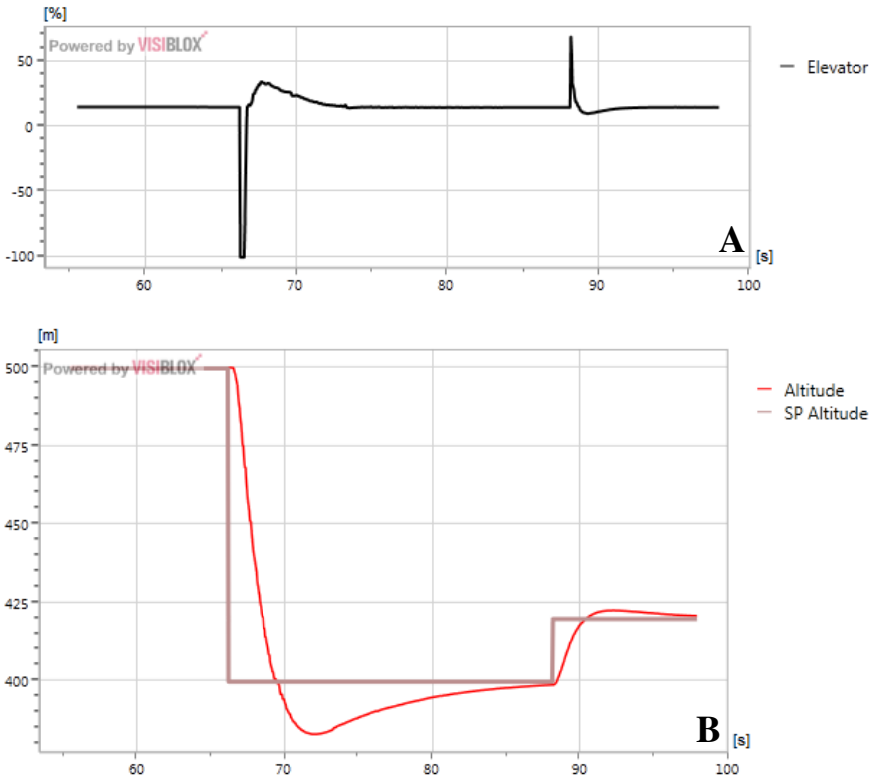
Fig. 9. Height stabilization charts

Waypoints flight, which is one of the commands described in section 6.2, was presented in the fig. 10. It shows an example of a flight along the sequence of two geographic coordinates. Presented figure has two elements, a visualization from the Prepar3D® simulation environment (fig. 10a), and the control application (fig. 10b). Map [14], that is included in the control application is a real representation of the object's position in the simulator. The buildings, which are located behind
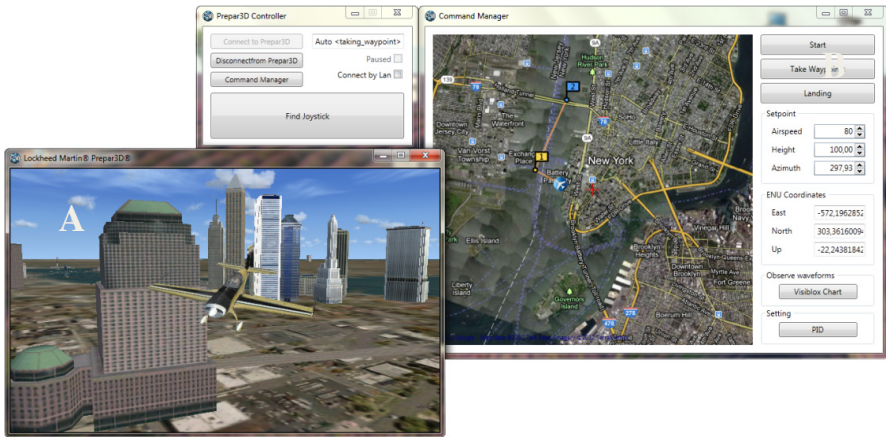
Fig. 10. Control application and Prepar3D® screenshot – waypoints flight

the airplane are a regular part of the simulation created by Lockheed Martin corporation, and also are in a position corresponding to reality.

Presented algorithms were implemented in C# language using WPF graphics engine. The application allows to connect to a simulation environment Prepar3D® on the same computer, and via TCP/IP protocol. Control application allows to control in autonomous mode, and as well in the stabilization mode. An interesting option is to control object with a USB device in manual mode. There is an ability to create a route on the real map. Map module allows also to add take-off and landing commands. An important feature in this software is the ability to view charts and change all the parameters of the PI controllers, which is fully sufficient for testing and prototyping algorithms for autonomous flight in the simulation environment Prepar3D®.

7.2 Artificial Traffic in Prepar3D®

Prepar3D® simulator includes artificial traffic on the highways. Vehicles moving along such roads may be, for example, detected by the detection algorithms implemented in the control application. To zoom in more precisely in possibilities, that Prepar3D® gives for the vision processing purpose, there was prepared a situation (fig. 11b) where the aerial object have to pass the previously prepared route. The plane have to take two waypoints at the height of 100 m above sea and with setpoint speed 50 km/h. Camera, that is configured under the flying object (fig. 11a) can be moved in three ways (yaw, pitch and roll) and it can be zoomed up to 20 times.
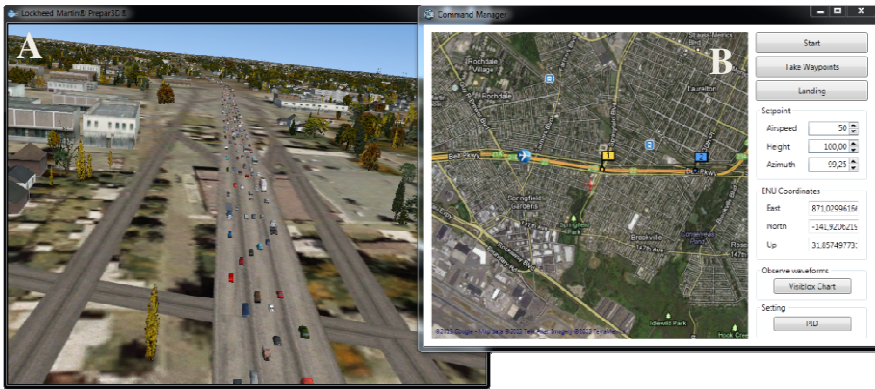
Fig. 11. Airplane flight above the highway: a) Prepar3D®, b) Control application

8   Conclusions

The performed tests in the SIL simulation were ended successfully. The plane can fly autonomously in a virtual reality. Therefore it can be supposed that the regulators cascade can be successfully used in the real world and can be implemented in a hardware of a real unmanned aerial vehicle (UAV) [16]. The quality of the presented solution is promising and will be verified during test flights. It was proved that it is possible to prototype control algorithms in a virtual reality simulation software. Having a working flight algorithm the next step could be to an implementation of vision based algorithms in virtual reality, that could analyze artificial traffic and could affect aircraft control algorithm in order to follow the selected object on the ground. Furthermore, it is also possible to begin work on algorithms responsible for avoiding obstacles such as tall buildings or other aircrafts.

References

[1]   Mueller Eric, R.: Hardware-in-the-loop Simulation Design for Evaluation of Unmanned Aerial Vehicle Control Systems. NASA Ames Research Center, Moffett Field, CA, 94035

[2]   Gessing, R.: About Optimality of Discrete-Time LQ Observer Based Regulator, Silesian University of Technical, Institute of Automation

[3]   Johnson, E.N., Mishra, S.: Flight simulation for the development of an experimental UAV. School of Aerospace Engineering, Georgia Institute of Technology, Atlanta, GA, 30332-015

[4]   Jung, D., Tsiotras, P.: Modeling and Hardware-in-the-Loop Simulation for a Small Unmanned Aerial Vehicle, Georgia Institute of Technology, Atlanta, GA, 30332-0150

[5]   Sorton, E.F., Hammaker, S.: Simulated Flight Testing of an Autonomous Unmanned Aerial Vehicle Using Flight-Gear, Infotech@Aerospace, Arlington, VA, AIAA 2005-7083 (September 2005)

[6]   Johnson, E.N., Fontaine, S.: Use of Flight Simulation to Complement Flight Testing of Low-cost UAVs. In: AIAA Modeling and Simulation Technologies Conference and Exhibit, Montreal, Canada, AIAA 2001-4059 (August 2001)

[7]   Procerus Technologies: Kestrel Autopilot System, Autonomous Autopilot and Ground Control for Small Unmanned Aerial Vehicles, UAV Flight Guide, Version 1.8 (December 10, 2012),
      `http://www.procerusuav.com/Downloads/Manuals/UAV_`
      `Flight_Guide.pdf`

[8]   Mystkowski, A.: Robust control of unmanned aerial vehicle - simulation investigations, Białystok Technical University, Prace Instytutu Lotnictwa, Warsaw, pp. s.82–s.102 (2011) ISSN 0509-6669 216

[9]   Konwacji, C.: Control algorithm of micro aerial vehicle flight in streets' canyons based on vision system 4(3), s.76–s.86 (2010)

[10] He, Z., VenkataramanIyer, R., Chandler, P.R.: Vision based UAV flight control and obstacle avoidance. In: American Control Conference (2006)

[11] Rathinam, S., Kim, Z., Sengupta, R.: Vision-Based Monitoring of Locally Linear Structures Using an Unmanned Aerial Vehicle1. J. Infrastruct. Syst. Special Issue: New Sensors, Instrumentation, and Signal Interpretation 14, 52–63 (2008)

[12] Świtoński, A., Bieda, R., Wojciechowski, K.: Multispectral imaging for supporting colonoscopy and gastroscopy diagnoses. In: Hippe, Z.S., Kulikowski, J.L., Mroczek, T. (eds.) Human - Computer Systems Interaction. AISC, vol. 99, pp. 131–145. Springer, Heidelberg (2012)

[13] Ruszewski, A.: Stabilization of discrete-time systems by PID controllers, Zeszyty Naukowe. Silesian University of Technical, Institute of Automation, z. 145, pp. 171—176 (2006)

[14] Drake, S.P.: Converting GPS Coordinates ($\varphi\lambda$h) to Navigation Coordinates (ENU), Surveillance Systems Division Electronics and Surveillance Research Laboratory (December 10, 2012),
      `http://dspace.dsto.defence.gov.au/dspace/bitstream/`
      `1947/3538/1/DSTO-TN-0432.pdf`

[15] GMap.NET – Great Maps for Windows (December 10, 2012),
      `http://greatmaps.codeplex.com/`

[16] Iwaneczko, P., Jędrasiak, K., Daniec, K., Nawrat, A.: A prototype of unmanned aerial vehicle for image acquisition. In: Bolc, L., Tadeusiewicz, R., Chmielewski, L.J., Wojciechowski, K. (eds.) ICCVG 2012. LNCS, vol. 7594, pp. 87–94. Springer, Heidelberg (2012)

Feature Extraction and HMM-Based Classification of Gait Video Sequences for the Purpose of Human Identification

Henryk Josiński, Daniel Kostrzewa, Agnieszka Michalczuk, Adam Świtoński, and Konrad Wojciechowski

Abstract. The authors present results of the research on human recognition based on the video gait sequences from the CASIA Gait Database. Both linear (principal component analysis; PCA) and non-linear (isometric features mapping; Isomap and locally linear embedding; LLE) methods were applied in order to reduce data dimensionality, whereas a concept of hidden Markov model (HMM) was used for the purpose of data classification. The results of the conducted experiments formed the main subject of analysis of classification accuracy expressed by means of the Correct Classification Rate (CCR).

Keywords: dimensionality reduction, gait-based human identification, Hidden Markov model, manifold learning.

1   Introduction

Gait is defined as coordinated, cyclic combination of movements which results in human locomotion [1]. Gait is considered as one of behavioral biometric features. A unique advantage of gait as a biometric is that it offers potential for recognition at a distance or at low resolution or when other biometrics might not be perceivable [2] especially from UAVs [26]. Gait can be captured by two-dimensional video cameras of surveillance systems or by much accurate motion capture (*mocap*) systems which acquire motion data as a time sequence of poses.

Henryk Josiński · Daniel Kostrzewa · Agnieszka Michalczuk · Adam Świtoński ·
Konrad Wojciechowski
Silesian University of Technology, Institute of Computer Science,
Akademicka 16, 44-101 Gliwice, Poland
e-mail: {henryk.josinski,adam.switonski,agnieszka.michalczuk,
        daniel.kostrzewa,konrad.wojciechowski}@polsl.pl

However, in a development phase of a human identification system gait databases, such as CASIA, CMU MoBo, NIST/USF, Soton, UMD, can be also used as data sources for classification purposes.

Motion data lie in high-dimensional space. It is stated in [3] that many classifiers perform poorly in high-dimensional spaces given a small number of training samples. Thus, feature extraction or dimensionality reduction is an attempt to transform a high-dimensional data into a low-dimensional equivalent representation while retaining most of the information regarding the underlying structure or the actual physical phenomenon [4].

The research was aimed at verification of the hidden Markov model (HMM) accuracy as a gait video data classifier as well as at comparative analysis of quality of linear and non-linear methods of dimensionality reduction with regard to classification of reduced gait data.

Generally, gait-based identification approaches can be divided into two categories: *model-free* and *model-based*. The former category can be split into approaches based on a moving shape and those which use integrate shape and motion within the description [2]. In the first example of the model-free approach silhouettes of walking human beings were extracted from individual frames using background subtraction, their morphological skeletons were computed and the modified independent component analysis (MICA) was proposed to project the original gait features from a high-dimensional measurement space to a lower-dimensional eigenspace. Subsequently, the L2 norm was used to measure the similarity between transformed gaits [5]. The principal components analysis (PCA) was also used for the purpose of human recognition [6], [7]. In the latter case three types of motion: slow walking, fast walking and walking with a ball were taken into consideration. In [8] the recognition process was based on temporal correlation of silhouettes, whereas a spatio-temporal gait representation, called *gait energy image* (GEI), was proposed in [9]. The application of the *Procrustes* shape analysis method and the *Procrustes* distance measure in gait signature extraction and classification was shown in [10]. Numerous studies, *inter alia* [11], [12], present frameworks developed for recognition of walking persons based on the dynamic time warping technique (DTW).

The model-based approaches use information about the gait, determined either by known structure or by modeling [2]. The Acclaim ASF/AMC format is often applied as the skeleton model of the observed walking person. Numerous methods aim to estimate the model directly from two-dimensional images. In [13] the particle swarm optimization algorithm (PSO) is used to shift the particles toward more promising configurations of the human model. In [14] 2D motion sequences taken from different viewpoints are approximated by the Fourier expansion. Next, the PCA is used to construct the 3D linear model. Coefficients derived from projecting 2D Fourier representation onto the 3D model form a gait signature. Another set of features used for human identification is extracted from spatial trajectories of selected body points of a walking person (root of the skeleton, head, hands, and feet), named as *gait paths* [15].

Methods based on the concept of the hidden Markov model [16] play also an important role in research on gait-based human identification, starting from application of the generic HMM [17], [18], where the width of the outer contour of the binarized silhouette of a walking person was chosen as the feature vector. Different variants of the HMM, such as, *inter alia*, population HMM [19], factorial and parallel HMMs [20] found also applications in the considered research area. The method proposed in [21] is very close to the topic of the present paper – it transforms sequences of silhouettes into low-dimensional embedding by manifold learning using the Gaussian Process Latent Variable Model (GP-LVM) before modeling their dynamics by means of the HMM.

The organization of the paper is as follows. Important components of the research procedure, including a brief description of the methods used for the purpose of dimensionality reduction as well as aspects of HMM adaptation to gait-based recognition are discussed in section 2. Results of the conducted experiments are presented and analyzed in section 3. The conclusions are formulated in section 4.

2   Research Procedure

A collection of silhouettes, extracted from the consecutive frames of a single gait sequence, was used as a feature vector on which linear (PCA) or non-linear method (isometric features mapping (Isomap) or locally linear embedding (LLE)) was applied in order to reduce data dimensionality. Subsequently, HMM was utilized as a classifier of the reduced data.

2.1   Data Source

Similar to the research described in the chapter "Selection of individual gait features extracted by MPCA applied to video recordings data" 80 sequences from the dataset A of the CASIA Gait Database (only those recorded from the parallel view, in case of need reflected in order to unify the direction of motion) were used for the purpose of gait-based human recognition. Contrary to the requirements of the MPCA algorithm, the sequences didn't need to be normalized in spite of their different length. The average length of a single sequence is about 90 frames and the bounding box of every video frame was determined with a fixed resolution 100×180. Hence, average number of features characterizing a single gait sequence comes to 1620000 ($100 \times 180 \times 90$).

2.2   Dimensionality Reduction Methods

Both linear and non-linear dimensionality reduction methods were applied to prepare gait data for classification.

Principal component analysis is one of the classic linear methods of dimensionality reduction. Given a set of high-dimensional feature vectors, PCA projects them onto low-dimensional subspace spanned by principal components. The first principal component is the direction which maximizes variance. The second principal component maximizes variance in a direction orthogonal to (i.e., uncorrelated with) the first component. Generally, the k-th principal component ($k > 1$) indicates the direction along which variance is maximum among all directions orthogonal to the preceding k-1 components. PCA is most useful in the case when data lie on or close to a linear subspace of the data set [22].

Isometric features mapping and locally linear embedding are algorithms proposed for manifold learning which is an approach to non-linear dimensionality reduction. Manifold learning is the process of estimating a low-dimensional structure which underlies a collection of high-dimensional data [23]. In other words, manifold learning algorithms essentially attempt to duplicate the behavior of PCA but on manifolds instead of linear subspaces [22].

The Isomap algorithm [24] comprises the following stages:

1. Estimate pairwise the geodesic distances (distances along a manifold) between all data points. To perform this estimation, first construct a k-nearest neighbor graph weighted by the Euclidean distances. Then compute the shortest-path distances using Dijkstra's or Floyd-Warshall's algorithm. As the number of data points increases, this estimate converges to the true geodesic distances.
2. Use the Multidimensional Scaling (MDS) [23] to find points in low-dimensional Euclidean space whose interpoint distances match the distances estimated in the previous step.

A D-dimensional manifold can be arbitrarily well-approximated by a d-dimensional linear subspace by taking a sufficiently small region about any point. Consequently, the LLE algorithm finds a local representation of each point based on its k nearest neighbors (measured by Euclidean distance) assuming that within the neighborhood the manifold is approximately flat and then reconstructs a low-dimensional representation with a similar configuration (see Fig. 1 – an often cited illustration from Saul and Roweis [25]).

The LLE algorithm consists of the following three steps:

1. Assign k nearest neighbors to each data point X_i, $1 \leq i \leq n$ in D-dimensional space.
2. Compute the weights W_{ij} in order to reconstruct linearly each data point from its k nearest neighbors. The weights are chosen to minimize the reconstruction error:

$$\varepsilon(W) = \sum_i \left| X_i - \sum_{j \in N(i)} W_{ij} X_j \right|^2, \tag{1}$$

where $N(i)$ denotes the set of k nearest neighbors of the data point X_i. The reconstruction weights sum to 1 and $W_{ij} = 0$ if $j \notin N(i)$.

3. Under assumption that the same weights W_{ij} that reconstruct the data point X_i in D dimensions should also reconstruct its embedded manifold coordinates in d dimensions, compute the outputs Y_i which are best reconstructed by the weights W_{ij} in d-dimensional space ($d \ll D$). The d-dimensional configuration is found by minimizing the cost function:

$$\Phi(Y) = \sum_i \left| Y_i - \sum_j W_{ij} Y_j \right|^2 . \tag{2}$$

with respect to $Y_1, \ldots, Y_n$ and subject to the constraints that for each j

$$\sum_i Y_{ij} = 0 , \tag{3}$$

and that

$$Y^T Y = I . \tag{4}$$

The value of d must be specified *a priori*.
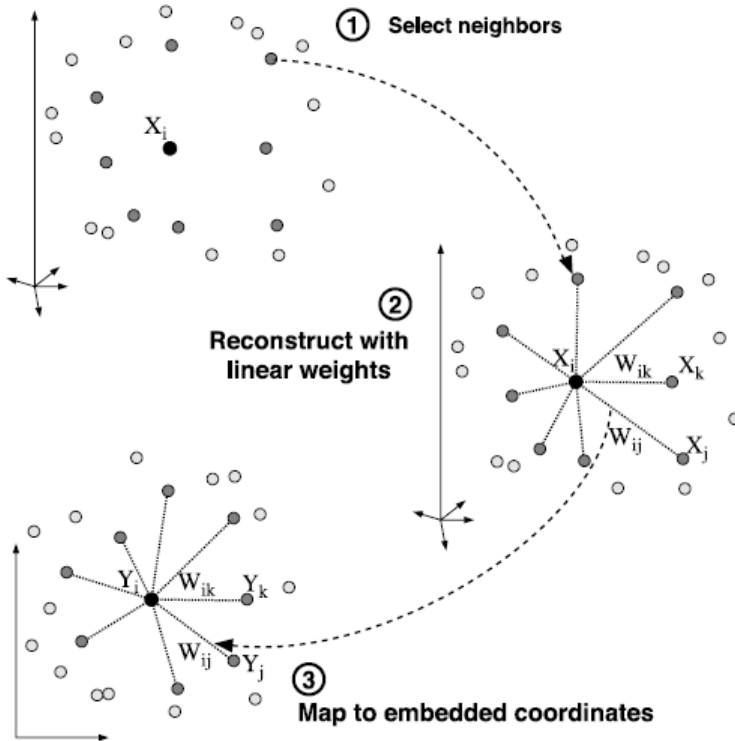
Fig. 1. Steps of the LLE algorithm [25]

2.3   Hidden Markov Model

A Hidden Markov Model (HMM) is a statistical tool used for modeling generative sequences characterized by a set of observable sequences [16].

An HMM of a system is defined as a triple $\lambda = (\pi, A, B)$, where A is the state transition probability matrix, B is the observation probability matrix and π is the initial state distribution [2]. The system has N states (s_1, s_2, …, s_N), M observation symbols (v_1, v_2, …, v_M), q_t denotes the state of the system at time t and O_t represents the observation symbol of the system at time t.

The initial state distribution is described by $\pi = \{\pi_i\}$, where $\pi_i = P(q_1 = s_i)$, $1 \le i \le N$. The state transition probability matrix is defined as $A = \{a_{ij}\}$, where $a_{ij} = P(q_{t+1} = s_j \mid q_t = s_i)$, $1 \le i, j \le N$. The observation matrix is specified as $B = \{b_j(k)\}$, where $b_j(k) = P(O_t = v_k \mid q_t = s_j)$, $1 \le j \le N$, $1 \le k \le M$.

Modeling human gait using HMM essentially involves identifying the N characteristic stances (poses) of an individual, which correspond to the N states of the system, and modeling the dynamics between the N such stances [2].

The "parallel-oriented" sequences from the dataset A with reduced dimensionality were divided evenly into training set and test set according to the schema presented in Fig. 2. During the training phase separate model λ_j was constructed for every actor j, $1 \le j \le 20$ for the given number N of states. Subsequently, in the testing phase the probability $P(O \mid \lambda_j)$, that the considered sequence O from the test set was produced by the individual j, was computed for all estimated models λ_j. Finally, the unknown actor X in the sequence O was determined by the largest value of the probability $P(O \mid \lambda_j)$:

$$X = \arg \max_j \log(P(O \mid \lambda_j)) \cdot \tag{5}$$
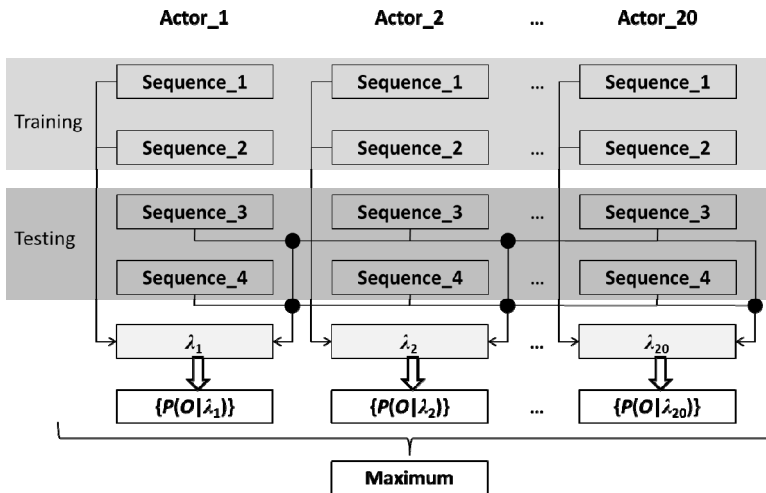
Fig. 2. Phases of the HMM-based classification

The HMM applied in experiments is ergodic, i.e. it allows for transitions from any state to every other state. Probabilistic allocation of the observations to the states is described by the continuous multivariate Gaussian distribution.

3   Experimental Results

Adapted versions of the procedures from the Matlab Toolbox for Dimensionality Reduction   (*http://homepage.tudelft.nl/19j49/Matlab_Toolbox_for_Dimensionality_Reduction.html*) were used in the phase of data preparation, whereas the process of the HMM-based data classification was programmed in C# using the Statistics library of Accord .Net framework (*http://code.google.com/p/accord/*).

Accuracy of data classification was measured by means of the Correct Classification Rate (CCR).

The main goal of the numerical experiments was to determine the dependency between CCR and number N of system states varying from 2 to 8 for a different values of resultant dimensionality d. However, because of computational expensiveness of the Dijkstra's algorithm constructing the shortest path for the Isomap, maximum value of d used for this method was equal to 5. Results of classification received in case of $d = 5$ for all three reduction methods (PCA, Isomap, LLE) are presented in Fig. 3 (the number k of nearest neighbors was set to 20).
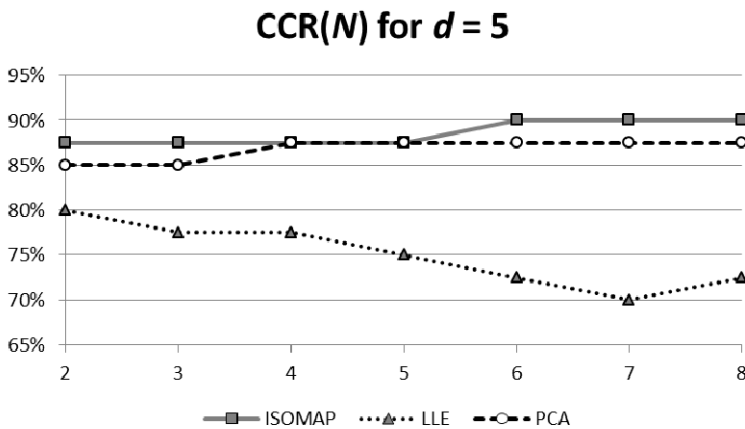
Fig. 3. Dependency between CCR and number N of states for all three methods using $d = 5$

The whole set of experiments was performed for PCA and LLE using a set of resultant dimensionalities d including successive powers of 2 from 1 to 512. Such a dependency obtained for the PCA is depicted in Fig. 4, but it is necessary to mention that sets of results related to $d = 1$, 2 as well as $d = 512$ are not presented

graphically for the clarity of figures. In the former case the experimental results were remarkably worse than for greater values of *d*. On the other hand, classification accuracy in the latter case was equal to 100 % without exception.
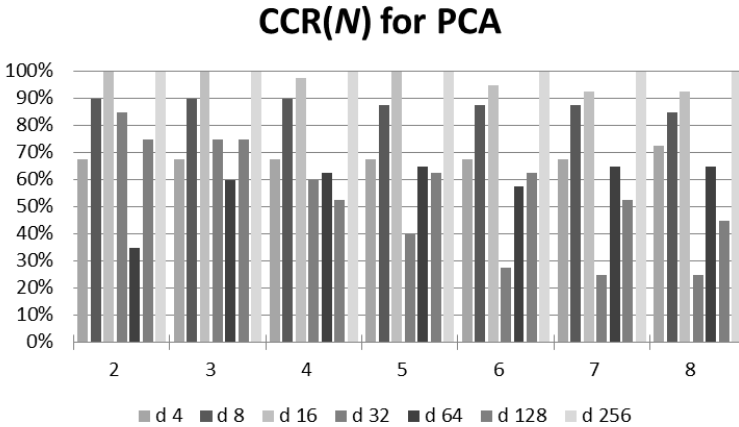
Fig. 4. Dependency between CCR and number *N* of states for PCA

Analogical results received in case of the LLE for *k* = 20, 40, 80, 160 are presented in Fig. 5, 6, 7, 8, respectively.
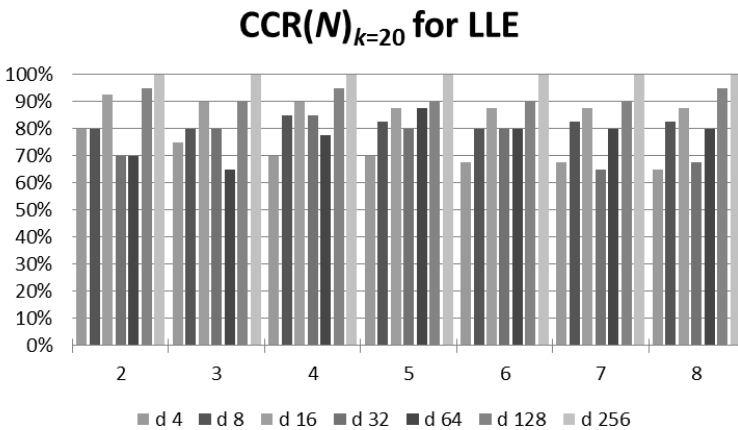
Fig. 5. Dependency between CCR and number *N* of states for LLE using 20 neighbors
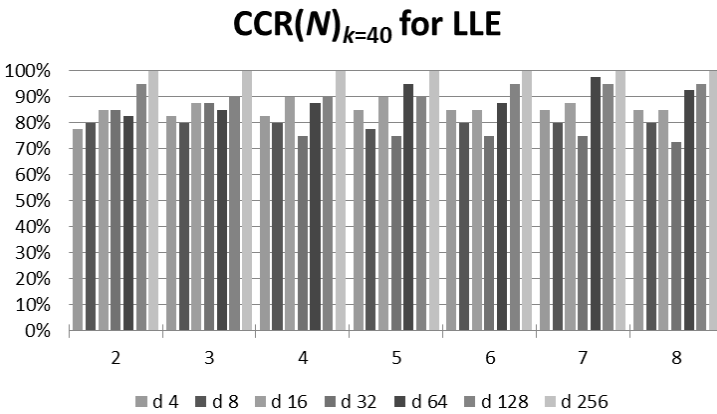
Fig. 6. Dependency between CCR and number *N* of states for LLE using 40 neighbors
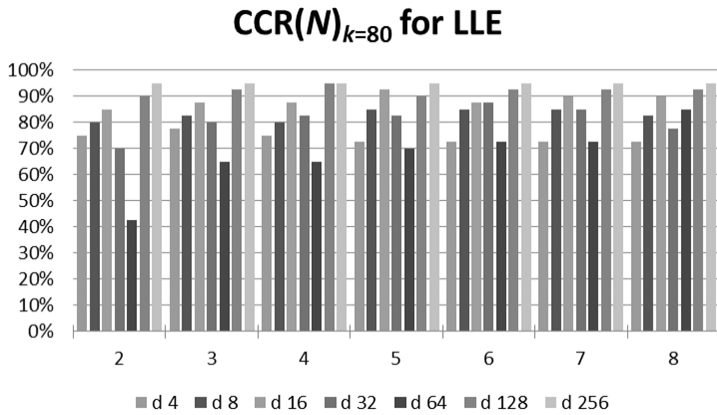
Fig. 7. Dependency between CCR and number *N* of states for LLE using 80 neighbors
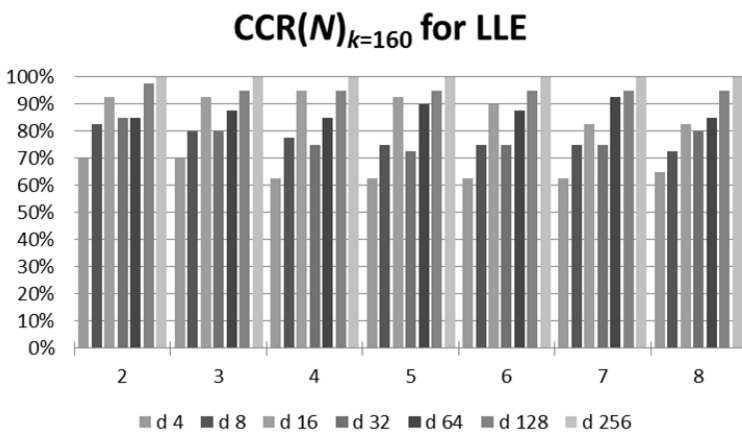
Fig. 8. Dependency between CCR and number *N* of states for LLE using 160 neighbors

The previously computed CCR values were averaged for PCA as well as for each LLE variant separately, with regard to the given value of d (see Fig. 9) and to the given value of N (see Fig. 10). The complete range of N was taken into account, whereas the set of dimensionalities was limited to powers of 2 from 4 to 256.
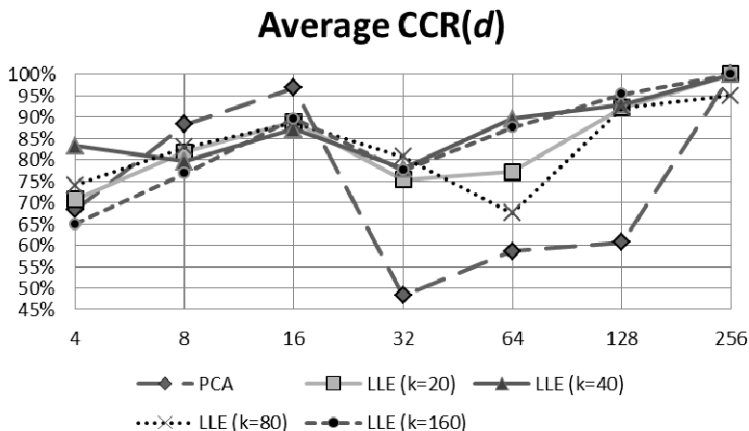
Fig. 9. Dependency between average CCR and dimensionality d for PCA and all LLE variants

Fig. 9 shows that the 100 % accuracy was obtained for the reduced dimensionality $d = 256$ for both methods with the exception of the LLE variant using $k = 80$ nearest neighbors (avg(CCR) = 95 %). As it was aforementioned, according to expectations the accuracy remained equal to 100 % for $d = 512$ regardless of the variant of dimensionality reduction. It is worthwhile mentioning that the accuracy of the GP-LVM and HMM-based classification of the CASIA gait sequences, reported in [21] was equal to 86 %. However, in this case the analyzed sequences were not limited to the "parallel-oriented" subset. Although in the 3 following cases: $N = 2, 3, 5$ accuracy obtained by the PCA was equal to 100 % already for $d = 16$, but taking the average accuracy into consideration the LLE outperforms the PCA.

In particular, the maximum average value of the CCR equal to 88.57 % was achieved for $N = 7$ states by means of the LLE using $k = 40$ nearest neighbors.

Admittedly, it was mentioned in [25] that the LLE algorithm can only be expected to recover embeddings whose dimensionality is strictly less than the number of neighbors ($d < k$), but the results of classification of the CASIA gait sequences show that in opposite case the reconstruction error is small enough to obtain acceptable classification accuracy. This observation confirms the remark that the exact relation between k and the faithfulness of the resulting embedding remains an important open question [25].
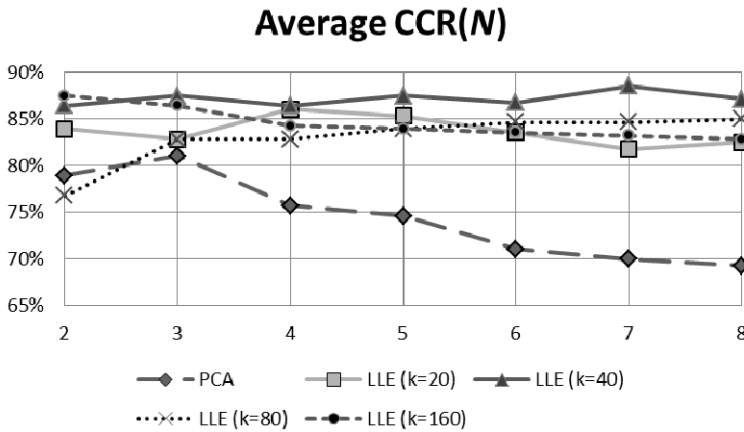
Fig. 10. Dependency between average CCR and number N of states for PCA and LLE variants

4   Conclusion

The average values presented in Fig. 9 and Fig. 10 suggest that the non-linear dimensionality reduction method (LLE) is superior to the linear technique (PCA) in application for classification of gait sequences. Generally, first of all just video and image data sets are supposed to exhibit low-dimensional manifold structures [22].

Application of the HMM as classifier of gait sequences was successful, particularly in view of the fact that the classification accuracy equal to 100 % was obtained.

Conclusions drawn from experiments with video sequences taken from the CASIA Gait Database will be helpful during the next stage of the research which will be based on video material from the municipal surveillance system.

Future research will also explore the influence of the feature selection methods on the accuracy of the gait-based identification process. The promising Invasive Weed Optimization (IWO) metaheuristic will be adapted to the searching the feature space for an adequate subset of features.

References

[1]   Boyd, J.E., Little, J.J.: Biometric Gait Recognition. In: Tistarelli, M., Bigun, J., Grosso, E. (eds.) Advanced Studies in Biometrics. LNCS, vol. 3161, pp. 19–42. Springer, Heidelberg (2005)
[2]   Nixon, M.S., Tan, T.N., Chellappa, R.: Human Identification Based on Gait. Springer (2006)

[3] Lu, H., Plataniotis, K.N., Venetsanopoulos, A.N.: MPCA: Multilinear Principal Component Analysis of Tensor Objects. IEEE Transactions on Neural Networks 19(1), 18–39 (2008)

[4] Law, M.H.C., Jain, A.K.: Incremental nonlinear dimensionality reduction by manifold learning. IEEE Transactions on Pattern Analysis and Machine Intelligence 28(3), 377–391 (2006)

[5] Pushpa Rani, M., Arumugam, G.: An Efficient Gait Recognition System for Human Identification Using Modified ICA. International Journal of Computer Science & Information Technology 2(1), 55–67 (2010)

[6] Wang, L., Tan, T., Ning, H., Hu, W.: Silhouette Analysis-Based Gait Recognition for Human Identification. IEEE Transactions on Pattern Analysis and Machine Intelligence 25(12), 1505–1518 (2003)

[7] Ali, H., Dargham, J., Ali, C., Moung, E.G.: Gait Recognition using Principal Component Analysis. In: Proceedings of the 3rd International Conference on Machine Vision, pp. 539–543 (2010)

[8] Sarkar, S., Phillips, P.J., Liu, Z., Vega, I.R., Grother, P., Bowyer, K.W.: The HumanID Gait Challenge Problem: Data Sets, Performance, and Analysis. IEEE Transactions on Pattern Analysis and Machine Intelligence 27(12), 162–177 (2005)

[9] Han, J., Bhanu, B.: Individual Recognition Using Gait Energy Image. IEEE Transactions on Pattern Analysis and Machine Intelligence 28(2), 316–322 (2006)

[10] Wang, L., Ning, H., Hu, W., Tan, T.: Gait Recognition Based on Procrustes Shape Analysis. In: Proceedings of the 9th International Conference on Image Processing, pp. III-433–III436 (2002)

[11] Hong, S., Lee, H., Nizami, I.F., An, S.-J., Kim, E.: Human Identification Based on Gait Analysis. In: Proceedings of the International Conference on Control, Automation and Systems, pp. 2234–2237 (2007)

[12] Kale, A., Cuntoor, N., Yegnanarayana, B., Rajagopalan, A.N., Chellappa, R.: Gait Analysis for Human Identification. In: Proceedings of the 4th International Conference on Audio- and Video-Based Biometric Person Authentication, pp. 706–714 (2003)

[13] Krzeszowski, T., Kwolek, B., Wojciechowski, K.: Articulated Body Motion Tracking by Combined Particle Swarm Optimization and Particle Filtering. In: Bolc, L., Tadeusiewicz, R., Chmielewski, L.J., Wojciechowski, K. (eds.) ICCVG 2010, Part I. LNCS, vol. 6374, pp. 147–154. Springer, Heidelberg (2010)

[14] Zhang, Z., Troje, N.F.: View-independent person identification from human gait. Neurocomputing 69, 250–256 (2005)

[15] Świtoński, A., Polański, A., Wojciechowski, K.: Human Identification Based on Gait Paths. In: Blanc-Talon, J., Kleihorst, R., Philips, W., Popescu, D., Scheunders, P. (eds.) ACIVS 2011. LNCS, vol. 6915, pp. 531–542. Springer, Heidelberg (2011)

[16] Rabiner, L.R., Juang, H.: An Introduction to Hidden Markov Models. IEEE ASSP Magazine, 4–16 (1986)

[17] Kale, A., Rajagopalan, A.N., Cuntoor, N., Krüger, V.: Gait-based Recognition of Humans Using Continuous HMMs. In: Proceedings of the 5th IEEE International Conference on Automatic Face and Gesture Recognition, pp. 336–341 (2002)

[18] Sundaresan, A., Roy-Chowdhury, A., Chellappa, R.: A Hidden Markov Model Based Framework for Recognition of Humans from Gait Sequences. In: Proceedings of the 2003 IEEE International Conference on Image Processing, pp. II-93–II-96 (2003)

[19] Liu, Z., Sarkar, S.: Improved Gait Recognition by Gait Dynamics Normalization. IEEE Transactions on Pattern Analysis and Machine Intelligence 28(6), 863–876 (2006)

[20] Chen, C., Liang, J., Zhao, H., Hu, H., Tian, J.: Factorial HMM and Parallel HMM for Gait Recognition. IEEE Transactions on Systems, Man, and Cybernetics – Part C: Applications and Review*s* 39(1), 114–123 (2009)

[21] Cheng, M.-H., Ho, M.-F., Huang, C.-L.: Gait analysis for human identification through manifold learning and HMM. Pattern Recognition 41(8), 2541–2553 (2008)

[22] Cayton, L.: Algorithms for manifold learning. Technical Report CS2008-0923, University of California (2005)

[23] Ihler, A.: Nonlinear Manifold Learning 6.454 Summary. MIT (2003)

[24] Tenenbaum, J.B., de Silva, V., Langford, J.C.: A Global Geometric Framework for Nonlinear Dimensionality Reduction. Science 290, 2319–2323 (2000)

[25] Saul, L.K., Roweis, S.T.: Think Globally, Fit Locally: Unsupervised Learning of low Dimensional Manifolds. Journal of Machine Learning Research 4, 119–155 (2003)

[26] Iwaneczko, P., Jędrasiak, K., Daniec, K., Nawrat, A.: A prototype of unmanned aerial vehicle for image acquisition. In: Bolc, L., Tadeusiewicz, R., Chmielewski, L.J., Wojciechowski, K. (eds.) ICCVG 2012. LNCS, vol. 7594, pp. 87–94. Springer, Heidelberg (2012)

The Dedicated Wireless Communication Device for Group of Unmanned Vehicles

Krzysztof Daniec, Karol Jędrasiak, Roman Koteras, Aleksander Nawrat, and Tadeusz Topór-Kamiński

Abstract. This article describes communication system designed and implemented on Silesian University of Technology based on experience acquired in previews projects. Communication system was designed for micro UAVs. First part of this work describes physical layer and second part describes software layer such as data encryption, establishing and maintaining connection. Proposed devices was tested on group of UAVs and acquired results are very promising.

1 Introduction

Communication is one of the most important aspects of monitoring, managing and remote controlling various types of unmanned vehicles. Currently most of the unmanned vehicles are controlled remotely by a trained operator. Such approach is sufficient and efficient only for the small scale operations. In case of need of application of a large group of unmanned vehicles at the same time another approach is required. One of the commonly used solutions is partial autonomy of the object. The role of the operator is changed from continuously controlling to simple issuing orders to the vehicle . A significant amount of unmanned vehicles are large enough to carry some type of dedicated computer that is responsible for communication and autonomous navigation. However the size and especially the weight of the computer is not small enough for application in miniature, flying objects. Therefore new dedicated miniature communication device was required to develop.

Krzysztof Daniec · Karol Jędrasiak · Roman Koteras · Aleksander Nawrat ·
Tadeusz Topór-Kamiński
Silesian University of Technology, Institute of Automatic Control,
Akademicka 16, 44-101 Gliwice, Poland
e-mail: {krzysztof.daniec,karol.jedrasiak,
        roman.koteras,aleksander.nawrat}@polsl.pl

In this article we present a developed miniature radio communication device that is dedicated for application in unmanned vehicles. It allows autonomous communication between the miniature unmanned vehicles in a group without the need for continuous ground control. The implementation is based on the results of the previous work in the field of wireless transmissions [1] and consists of two layers: the physical layer and secure communication layer. The main contribution of the article is presentation of the secure, miniature communication device that allows creation of groups of miniature autonomous unmanned vehicles. Application of the presented in the article device allows for autonomous communication without any PC class devices onboard and therefore improves the stability and reliability of the SETh [2] like systems.

2   Literature Review

Developing a new kind of dedicated software is always preceded by a thoughtful literature review. There are not many projects aimed for developing a new dedicated hardware. Most of the literature discussion is center around final application. Authors in the work [3] present an infrared communication device. It is based on pulse modulation technique and PWM in order to increase the communication distance. Recently the main stream of research in the area of wireless communication has been divided into two main parts. Scientists centered around the first part are attempting to solve the problems of cooperation of multiple mobile robots over wireless embedded transmission devices [4] or creation of pervasive sensor networks [5]. Aim of the research in the second part is to increase the throughput and communication delays in the LTE networks [6].

A matter of great importance is security of the wireless transmission. There are numerous approaches based on encryption. However there are also approaches trying to improve the safety of the data by changing the physical way of transmission [7] or introducing a new way of authorization and authentication of packets.

3   Communication Model

The act of communication between the vehicles within the group is essential for implementation of cooperation algorithms allowing partial autonomy of the vehicle. At the same time the link between the mobile vehicles can be interpreted as e.g. Ethernet network and apply one of existing routing algorithms in order to send the information from object A (e.g. UAV [9]) to object C with help of an object B in the middle when there is no direct link between A and C. Reliable communication is necessary for navigation purposes [10]. Traditionally used communication models are presented in the fig. 1. In the fig.1a a centralized communication model is presented. In the model each of the objects is communicating via cable or radio by universal radio modem with central computer. Such approach allows cooperation of the objects only within the area covered by the main computer. In

case of the connection failure there is no possibility for cooperation therefore such model is usually only used for monitoring of the vehicles parameters. In the fig1.b a model allowing vehicles cooperation is presented. Each of the vehicles is communicating via each other using universal radio modem and PC class computer responsible for data encryption and implementation of the secure communication protocol. Such approach does not require central computer therefore its maximum range of operation is not limited as long as the cooperating objects are within reach of its own radio modems.
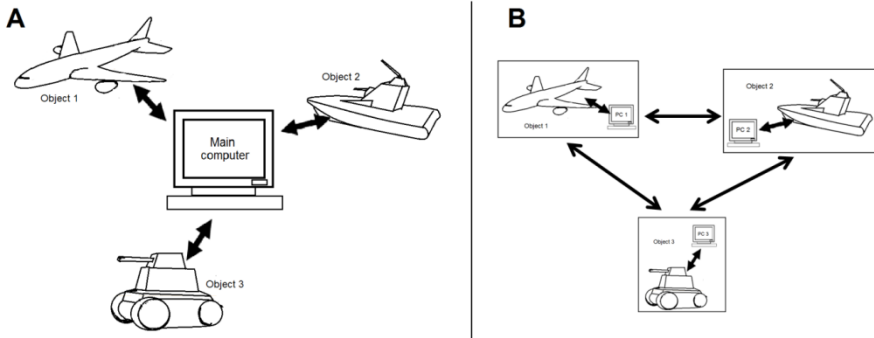
Fig. 1. The idea of communication in the groups of unmanned vehicles. A) communication with the use of central ground base station. B) communication with use of local computers responsible for communication.

The main disadvantage of such solution is the obligation of carrying the relatively heavy PC class computer only for communication purposes. It is well known that the PC computers are not as reliable as dedicated solutions therefore it was decided to design a communication device that allows unmanned vehicles transparent communication without the need for installing PC. A schema of such model is presented in the fig. 2.

During design phase of the dedicated secure radio communication device presented in the article some assumptions about the application scenarios were made. First assumption is that a pair of devices that are willing to communicate with each other are required to have a common symmetric key used during authorization and attempting connection processes. It is allowed that more devices, in some cases even the whole group are using the same symmetric key during the process of authorization. Single communication device can store multiple keys. However only one key per remote connection link is stored. The limitation's origin is the fact that before application the communication devices are configured using cable connection. During configuration an authorization key is installed along with information about the devices that belong to the group and common group authorization key.
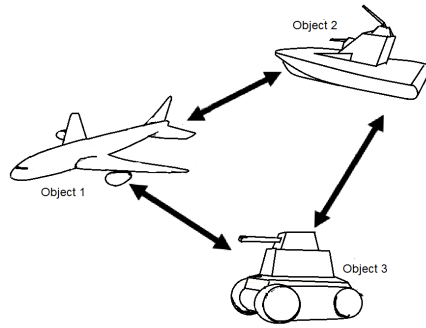
Fig. 2. Application of the presented miniature communication device allows for communication without any PC class devices onboard which allows significant miniaturization of the vehicles and improves the reliability of the solution at the same time

It was assumed that the communication device has to encrypt all of the exchanged data. Each of the packets should be numbered in order to eliminate the situation that due to attacker's actions some of the packets changed their order or were multiplied.

4   Physical Layer

During design phase of the development of the presented in the article device a set of requirements were made. One of the main requirements about physical layer were miniature size and weight and transmission channel for exchange telemetry and sending orders. The channel has to be characterized by a wide range but not necessary high throughput.

In order to satisfy the requirements there was designed a miniature radio frequency emitter presented in the fig. 3. It consists of transceiver designed for frequencies up to 1 GHz supported by a . The final frequency of the device was set to 869.525 MHz, right in the middle of the unlicensed ISM 869 MHz. The modulation is GFSK with frequency deviation plus/minus 30 kHz. The throughput of the channel was defined as 64kBaud It is a compromise between long range with the maximum 500mW power and high throughput. An additional limitation on throughput was the requirement of two way communication. The device is working in the Listen-Before-Talk (LBT) mode therefore it is possible to send data even when the channel is occupied in more than 10%.

GFSK modulation is based on probing the receiver frequency. However the change is not a step change but rather mild. Therefore the signal spectrum is narrower. Transmission of the '0' symbol is acquired by sending a signal at the frequency Fc-Fdev (middle frequency minus deviation), while the '1' signal is the opposite Fc+Fdev. Transmitted data is divided into packets. Each packets length is a multiple of one byte.
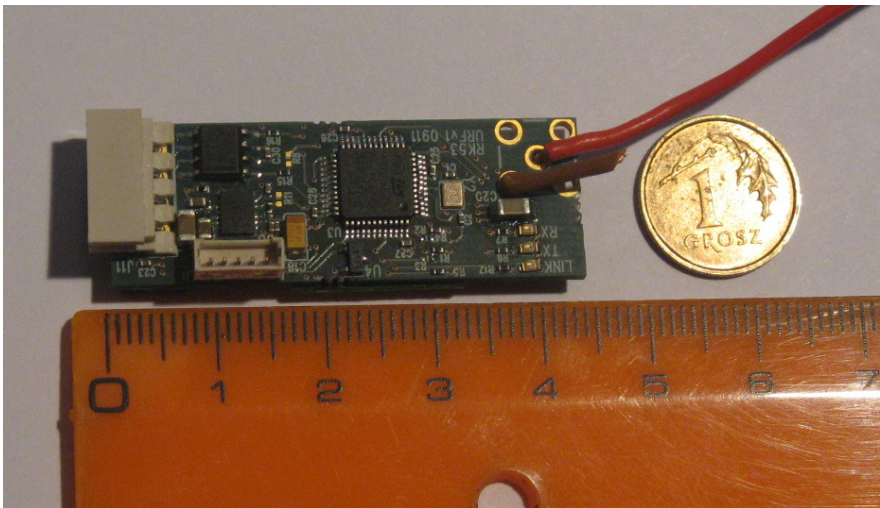
Fig. 3 The miniature dedicated secure radio communication device described in the article compared to the polish smallest coin and the ruler in cm

The sending frame starts with preamble consisting of six bytes with a same hexadecimal value 0xAA. The value is used for receiver and sender devices synchronization. After preamble there are two bytes with values 0xD3 and 0x91 signalizing the start of the data section. Besides it, those bytes are also used for bit synchronization of the receiver.

After the synchronization word there is a single byte specifying the number of data bytes in the frame. Allowed values are from 1 to 255. After described byte there is a sequence of data bytes. Length of the sequence is equal to the value of the data number byte.

There are no control sums or mechanisms of bleaching the data at the physical layer. Resignation of such mechanisms is due to implementation at the communication layer cryptographic algorithms which naturally hide all the feature of the data and detect damaged or erroneous packets.

5   Data Encryption

In order to maintain the confidentiality of the data transmitted between devices, AES encryption algorithm is used. It enables encryption and decryption the data blocks with length of 16 bytes. The key may have 16, 24 or 32 bytes (128, 192, 256 bits). Along with the encryption algorithm the hash function and a protocol of exchanging keys is ued.

The encryption algorithm itself does not describe how the amount of data of any length is to be converted to cipher text – it only describes the transformation of a single block. Therefore, the algorithm must be used in one of cipher block modes of operation. Encryption mode used is CTR (Counter) mode. This mode is characterized

by the ability to generate arbitrarily long string of blocks (keystream). In order to generate it, it is required a key and a nonce value (the value for a single call). The resultant sequence of blocks is used to convert non-confidential data to an encrypted form by a simple transformation of the XOR between the plaintext block and the block of keystream. In the case of a length not a multiple of the block, one can leave the appropriate number of bytes in the stream key, because it does not interfere with the possibility to decrypt the data. Due to the advantages of CTR: No need for a decoding function, no need for padding, and a large freedom in the implementation, it was decided that other modes are no needed.

Due to the symmetry of the encoding and decoding operations in the CTR mode a single crypto_encproc function was implemented in the hardware. The function parameters are block of data of any length, the encryption key, the size of the header and the unique value NOONCE. Inside the function crypto_encproc a key stream is generated. The input to the cipher are 16-byte blocks in which the first 4 bytes of a given nonce value stored in the byte order from the youngest, then it is from 0 to 8 bytes of the packet header, completed to 8 bytes of zeros followed by four bytes describing the shift of the first byte in the packet, which will be covered by the block. By design, the header is no longer than 8 bytes. All cryptographic keys used by the hardware are 256 bits (32 bytes).

The second most important function in the whole system is a hash function. It is necessary because of the need to generate and verify the HMAC authorizing the values for all packages, and for the separation of certain parts of the system.

The hash function used was SHA-256. It maps a block of data of any length in a short fixed length of 256 bits (32 bytes). Function selection was dictated by the current state of knowledge about the safety of different hash function, the size of the hash has been chosen to equal the length of the key in the encryption algorithm, making it possible to easily implement certain procedures for the compilation of the connection between the devices.

The primary use of the hash function is to determine the value of authorizing for packages. The authorization allows to detect falsification of data and prevents an attacker to set own packages without knowing the correct keys.

Computation of the value of an authorizing mechanism was implemented within the function crypto_authproc:

HMAC (key, nonce, msg): = H (key || H (key || nonce || msg) || NOONCE)

Where H () represents a single calculation using the hash function, || means concatenation of data blocks. Using the key in the HMAC function ensures that the attacker is not able to generate the correct value of an authorizing, because they do not have complete information required to calculate the correct hash function value.

Dual use of hash function is to eliminate certain defects, which derives from the hash function SHA-256. In case of single call, the attacker would have not access to the authorizing value, but he would be able to generate the correct value for the extended package on the basis of acquired basic package. In order to prevent this, the result of the internal hash function is additionally mixed with a key. This

removes the security gap resulting from the use of an iterative hash functions. The HMAC value is calculated for each package separately and sent along with it.

In order to assure safety of keys exchange between the devices it was decide to use the Diffie-Hellman key-exchange protocol. It allows to establish a common secret between two devices with the use of an unprotected channel. In order to run the DH protocol it is required to select group used for executing operations of exponentiation of large numbers. During experiments nine numbers were chosen. Each of them is a safe prime number p. It means that both p and number p_2 computed by the equation:

$$p_2 = \frac{p-1}{2},$$
(1)

are prime numbers.

6 Data Encryption

The communication protocol consists of two main parts: establishing and maintaining the connection. It is assumed that the addresses of the devices are in the range from 0 to 16 383 (within 14 bits).

6.1 Establishing Connection

The process of establishing connection was divided into two phases. During first phase the device initiating the communication sends the PING packet to the receiver which replies with the PONG packet. Both packets are time and quantity secured by using counters of number of starts and time of execution. After receiving the PONG packet, the sender is assured about the existence of the receiver. Then the synchronizing SYN packet is send. The last 16 bytes of the SYN packet contains random value used as an aid during generating random temp keys. The response for the synchronizing packet is SYNACK with the same structure as the SYN packet. After exchanging those two packets both devices generate common temporary key using the function:

```
  tk  :=  SHA256(AddrA  ||  RunCntA  ||  RndA  ||  AddB  ||
RunCntB  ||  RndB  ||  AuthKey)
```

6.2 Maintaining the Connection

During proper communication between the devices a smaller packet is used. The header's length is 4 bytes and authorization value's length is 8 bytes. Transferred data is encoded by estimated channel. Its number is in the range from 0 to 32767 and is written in first two bytes of the data. Third and fourth bytes contain the sequential number of the packet. Due to the low throughput of the transmission there are no other protocol limitations.

The idea of using channels was introduced in order to reduce the device addressing overhead. However, it also improves the security of the data by hiding the information about the receiver. It is known only for a short period of time during opening channel. Each communication device can have active 4 sending and 4 receiving channels at the same time.

In order to maintain the connection a single packet with 12 bytes of data is send. First two bytes contains the same value 0xFF, next two bytes are equal to two oldest bytes of the sequential number counter, rest of the bytes are the number of four channels. In case of lost channel transmission continues with the next channel. The set of channels is recovered with incoming maintaining connection packets. Sending those packet also forces movement within the network which prevents from losing connection.

7   Conclusions and Future Work

The article presents the dedicated secure miniature radio communication device for group of unmanned vehicles. The device is capable of establishing and maintaining a secure connection on its own, which releases the resources of the vehicles CPU for more advanced control and navigation algorithms. Therefore by using the presented device it is possible to implement cooperation schemes in vehicles in the same group.

The device was designed on basis of previous tests [1],[8] and already tested using a group of unmanned aerial vehicles. Acquired results prove the possibility of a secure communication in a range depending of the used antenna but starting from 2 km. During the performed tests regardless the application in the forest the connection was stable and reliable which is very promising for future implementations within project ideas like [11].

References

[1]   Topor-Kaminski, T., Żurkowski, R., Grygiel, M.: Selected methods of measuring the delay in data transmission systems with wireless network interfaces. Acta Phys. Pol. A 120(3), 182 (2011)
[2]   Nawrat, A., Jędrasiak, K.: SETh system spatio-temporal object tracking using combined color and motion features. In: Chen, S., Li, Q., Hangzhou, C. (eds.) Proc. of ROCOM 2009, 9th WSEAS International Conference on Robotics, Control and Manufacturing Technology, WSEAS, May 20-22, p. 67 (2009)
[3]   Cheng, C., Hong, L.: Electric Power Automation Equipment (2009)
[4]   Srovnal Jr., V., Machacek, Z., Srovnal, V.: Proc. of ICN 2009, 8th International Conference on Networks, March 1-6, IARIA, Cancun, Mexico, p. 253 (2009)
[5]   Dohler, M., Li, Y.: Cooperative Communications: Hardware, Channel and PHY. John Wiley & Sons, United Kingdom (2010)
[6]   Doppler, K., Rinne, M., Wijting, C., Riberio, C., Hugl, K.: IEEE Communications Magazine 47(12), 42 (2009)

[7]   Reising, D.R., Temple, M.A., Mendenhall, M.J.: 3, no, vol. 3(1), p. 41. Inderscience Publishers (2010)

[8]   Topór-Kamiñski, T., Krupanek, B., Homa, J.: Delays Models of Measurement and Control Data Transmission Network. In: Nawrat, A., Simek, K., Świerniak, A. (eds.) Advanced Technologies for Intelligent Systems of National Border Security. SCI, vol. 440, pp. 257–278. Springer, Heidelberg (2013)

[9]   Iwaneczko, P., Jędrasiak, K., Daniec, K., Nawrat, A.: A prototype of unmanned aerial vehicle for image acquisition. In: Bolc, L., Tadeusiewicz, R., Chmielewski, L.J., Wojciechowski, K. (eds.) ICCVG 2012. LNCS, vol. 7594, pp. 87–94. Springer, Heidelberg (2012)

[10] Nawrat, N., Kozak, K., Daniec, K., Koteras, R.: Differential navigation for UAV platforms with mobile reference station. In: Proceedings of the International Conference on Applied Computer Science, pp. 465–471 (2010)

[11] Kozak, K., Koteras, R., Daniec, K., Nawrat, A.: qB-Distributed real time control system in UAV design. In: Proceedings of the 13th WSEAS International Conference on Systems, pp. 185– 189 (2009)

Selection of Individual Gait Features Extracted by MPCA Applied to Video Recordings Data

Henryk Josiński, Agnieszka Michalczuk, Andrzej Polański, Adam Świtoński, and Konrad Wojciechowski

Abstract. The scope of this article is selection of individual gait features of video recordings data. The gait sequences are considered to be the 3rd-order tensors and their features are extracted by Multilinear Principal Component Analysis. Obtained gait descriptors are reduced by the supervised selection with greedy hill climbing and genetics search methods. To evaluate the explored individual feature sets, classification is carried out and CFS correlation based measure is utilized. The experimental phase is based on the CASIA Gait Database 'dataset A'. The obtained results are promising. Feature selection gives much more compact gait descriptors and causes significant improvement of human identification.

1 Introduction

Gait is defined as coordinated cyclic combination of movements which results in human locomotion [5]. There are strong individual gait features which allows for efficient identification. Such a biometric technique does not require awareness of identified human, which is a great advantage in comparing to other methods. Most simple and most often used gait acquisition is carried out by traditional video cameras. The gait is usually represented by a sequence of binary silhouettes determined by background subtraction.

The classification of a motion data can be performed on the basis of extracted feature sets of the time sequences. For instance in [8] the first two lowest Fourier components are chosen and in [20] four types of features are proposed for gait

Henryk Josiński · Agnieszka Michalczuk · Andrzej Polański · Adam Świtoński ·
Konrad Wojciechowski
Silesian University of Technology, Institute of Computer Science,
Akademicka 16, 44-101 Gliwice, Poland
e-mail: {adam.switonski,henryk.josinski,andrzej.polanski,
    konrad.wojciechowski}@polsl.pl

paths classification: statistical, histogram, Fourier transform and timeline. The features can be calculated by using dimensionality reduction techniques [24]. The classical approaches of dimensionality reduction of motion data do the work at the level of the pose descriptors. In [19] on the basis of distances between the selected body parts, the feature vectors of binary silhouettes are extracted and the first two principal components are chosen. In [10] linear PCA and in [15] nonlinear manifold learning is applied prior to the classification with HMM. In [21] and [19] DTW follows by the reduction of pose descriptors by PCA of feature vectors calculated for video and motion capture data, respectively. In [18] a modified ICA is used for skeletons of binary silhouettes. Other examples can be found in [12], [8] and [11].

Recently the multilinear reduction methods for tensor objects have gained more attention. They allow to reduce multi-dimensional objects indexed by multiple indices. The motion sequences are addressed by the frame number and spatial coordinates, which means that the entire sequences can be reduced, not only the pose descriptors. In [16] the MPCA method is used for the detected cycles of binary silhouettes and the classification is performed by selected distance functions. The MPCA reduction is also extended by LDA method. The application of MPCA to the classification of motion capture data by supervised learning can be found in [22]. In [14] mutlilinear ICA and in [17] uncorrelated MPCA are applied to face recognitions.

It is very challenging task to propose small number of features without loss of individual data. Thus, feature vectors are usually defined in high dimensional spaces, which makes the classification more difficult and less reliable. However, it is still possible to discover a feature subset sufficient for precise motion data classification by a proper search method. That is main contribution of presented research. We apply supervised feature selection for extracted features of video sequences. The effectiveness of selection is evaluated by obtained compression rate and accuracy of a classification.

On the basis of our previous work [6] we decided to extract features of video recordings data by MPCA technique and classify them by supervised machine learning. To reduce the dimensionality of feature space and discover most informative ones the selection is carried out, prior to classification phase. Similar as in [6] CASIA gait database is used to examine proposed identification method.

2   Gait Data Representation

Portions of the research in this paper use the CASIA Gait Database collected by the Institute of Automation, Chinese Academy of Sciences. The database contains raw video recordings as well as extracted binary silhouettes by background subtraction (see Fig. 1). The data could be used as a basis for markerless motion capture [23].
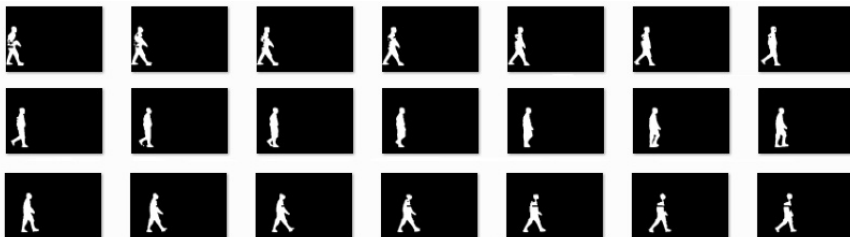
Fig. 1. Gait sequence from the CASIA database – actor "ljg"

CASIA dataset A is chosen. It contains 240 sequences of gaits coming from 20 subjects, recorded from three different camera perspectives: i.e. parallel, 45 degrees and 90 degrees to the image planes.

Subjects walk forward in two opposite directions. To improve the reduction and obtain directly comparable MPCA components, which simplifies classification, gaits are unified. We select only the parallel view and reflected horizontally gaits of opposite direction. To make classification independent from gait location and to remove useless data, a bounding box of every video frame is determined. It has fixed 100x180 resolution, adjusted to the tallest subject, and is centered to silhouette geometric centroid.

Gait sequences are considered to be the 3rd-order tensors with modes determined by spatial coordinates and time domain. The MPCA requires the same mode dimensionality of all tensors which is satisfied for spatial coordinates, but because of a different number of frames of video recordings the time domain mode has to be normalized. We applied linear scaling with a number of frames determined by an average video size.

3 Gait Identification Performed by Human

To prove the thesis of human ability to identify persons on the basis of visual gait analysis, the experiment was carried out. The disjoint training and test sets, containing gaits of four different persons were selected from CASIA dataset A. We asked the group of ten volunteers to recognize gaits. At the first stage, the volunteers tried to notice and remember individual gait features on the basis of a prepared training set. After the training phase, the recognition was performed. The test set consisted of four gaits, exactly one sample of every actor which are different than the ones of the training set. The gaits visualizations in training and testing phases are repeated depending on the necessity of the volunteers. The visualization is done on the basis of determined binary silhouettes as shown in Fig. 2.

Fig. 2. Training set visualization

Detailed results are presented in Tab. 1. The total average precision in the meaning of percentage of correctly identified gaits is 45%. It is noticeably better than random guessing which has only 25% in case of four actors. Most of the volunteers properly classified two gaits and missclassified other two ones, beside volunteers V7 and V8 which have worse precision with only single correctly identified gait. The standard deviation calculated for subsequent volunteers is 11% and for subsequent gaits is 26%.

Table 1. Identification performed by human, experiment 1

	V1	V2	V3	V4	V5	V6	V7	V8	V9	V10	**AVG**
FYC	1	0	1	1	1	0	1	1	1	1	**80%**
HY	0	1	1	1	0	0	0	0	0	0	**30%**
LJG	0	0	0	0	0	1	0	0	1	0	**20%**
LQF	1	1	0	0	1	1	0	0	0	1	**50%**
AVG	50%	50%	50%	50%	50%	50%	25%	25%	50%	50%	**45%**

To examine gait discrimination of the following actors separately - maybe some of them are very easy to recognize but others are difficult, we determine confusion matrix and split the task into four two class problems, similar as in authorization challenges. We calculate true positives (TP), true negatives (TN), false positives (FP), false negatives, precision, specificity and sensitivity [13]. The results are presented in Tab. 2 and Tab. 3. In most cases the actor FYC is properly identified, it has noticeably the greatest precision, sensitivity and sensibility. His distinctiveness is probably caused by his long hairs, which are easy for human to recognize. The missclassification of remaining actors HY, LJG and LQF is very similar, they are confused quit randomly. Greater specificity values are mainly the result of more negative samples in the test set.

Table 2. Confusion matrix, experiment 1

	FYC	HY	LJG	LQF
FYC	8	1	1	0
HY	1	3	5	1
LJG	1	3	2	4
LQF	0	3	2	5

Table 3. Two class problems, experiment 1

	TP	TN	FP	FN	Precision	Sensitivity	Sensibility
FYC	8	28	2	2	90%	93%	80%
HY	3	23	7	7	65%	77%	30%
LJG	2	22	8	8	60%	73%	20%
LQF	5	25	5	5	75%	83%	50%

The obtained average identification precision is definitely better in comparing to random guessing, however it seems that selected gaits are very discriminative and should allow for more accurate identification. That is a reason we repeated experiment with simultaneous presentation of the training and test sets. It means, that volunteers observed and analyzed all gaits in the same moment and their task was only to match samples of the training and test sets. In such a case, the identification is independent on human abilities to memorize noticed individual gait features and relies only the observed gait similarities.

Table 4. Identification performed by human, experiment 2

	V1	V2	V3	V4	V5	V6	V7	V8	V9	V10	AVG
FYC	1	1	1	1	1	1	1	1	1	1	100%
HY	1	1	1	1	1	1	1	1	1	1	100%
LJG	1	0	1	1	1	1	1	1	1	1	90%
LQF	1	0	1	1	1	1	1	1	1	1	90%
AVG	100%	50%	100%	100%	100%	100%	100%	100%	100%	100%	95%

The results of identification with simultaneous presentation of the training and test sets are presented in Tab. 4, Tab. 5 and Tab. 6. This time they are very close to the ideal case of 100% of classification accuracy, only single volunteer V2 mistook actors LJG and LQF. As we supposed humans are easily able to recognize persons on the basis of their gait inspection, but more challenging task is to keep in mind discovered individual gait features. Probably longer teaching phase would improve the results of the experiment 1. The number of persons to identify by human is obviously limited, because of restriction of simultaneous presentation and observation.

On the basis of the experiment performed we can state the thesis that gait allows to high precision human identification.

Table 5. Confusion matrix, experiment 2

	FYC	HY	LJH	LQF
FYC	10	0	0	0
HY	0	9	1	0
LJG	0	1	9	0
LQF	0	0	0	10

Table 6. Two class problems, experiment 2

	TP	TN	FP	FN	Precision	Sensitivity	Sensibility
FYC	10	30	0	0	100%	100%	100%
HY	9	29	1	1	95%	97%	90%
LJG	9	29	1	1	95%	97%	90%
LQF	10	30	0	0	100%	100%	100%

4   Multilinear Principal Component Analysis

Multilinear principal component analysis, proposed in [16] is the multilinear extension of classical PCA method. The input and output data are considered to be tensor objects and contrary to PCA dimensionality reduction operates directly on tensors rather than its vectorized form.

A tensor is a multidimensional object, whose elements are addressed by indices. The number of indices determines the order of the tensor, where each index defines one of the tensor modes [16]. In MPCA an elementary matrix algebra is extended by two operations: tensor unfolding and the product of a tensor and matrix. The unfolding transforms a tensor into a matrix according to a specified mode. The tensor is decomposed into column vectors, taken from the perspective of a specified mode, see Fig. 3.

The tensor X multiplication by the matrix U according to mode n $\widetilde{X_m} \times {}_nU$ is obtained by the product of the unfolded tensor and the matrix U. To go back to a tensor space, an inverse unfolding operation is applied. In other words, the mode n of the tensor X is projected into the matrix U.
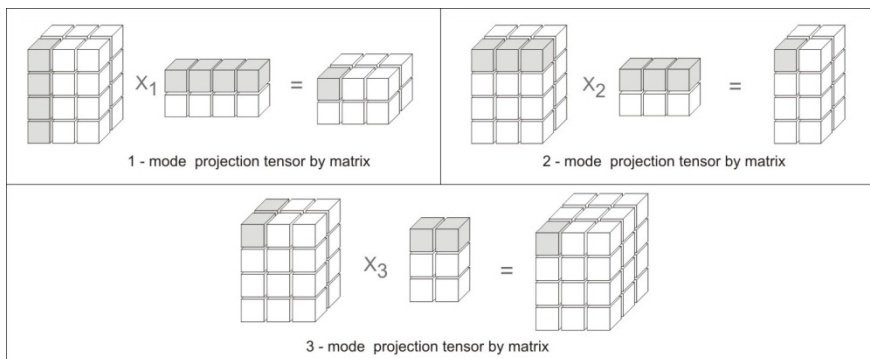
Fig. 3. 1,2 and 3-mode tensor matrix product

The MPCA algorithm consists of the following steps:

1. Preprocessing - the normalization of input tenor samples to zero mean value.
2. Learning phase of MPCA - a loop with specified number of iterations,

- Initialization - for each mode k:
  - o set matrix: $\Phi^{(k)*} = \sum_{m=1}^{M} \tilde{X}_{m(k)} X_{m(k)}^T$, where $\Phi^{(k)*}$ denotes the desired matrix and $X_{m(k)}$ is the mth input tensor sample in the k-node vector subspace, determined by unfolding operation.
  - o Eigen-decomposition of the matrix $\Phi^{(k)*}$,
  - o Selection of P^k most significant eigenvectors which form a projection matrix $U^{(k)}$ .Eigenvectors are evaluated by corresponding eigenvalues and the number of selected eigenvectors is determined by the variation cover $Q = \frac{\sum_{i_k=1}^{P_k} \lambda_{i_k}^{(k)*}}{\sum_{i_k=1}^{I_k} \lambda_{i_k}^{(k)*}}$, where I_k specifies the dimensionality of mode k and λ_{i_k} is i-th eigenvalue of matrix $\Phi^{(k)}$.
- Local optimization - for each mode update tensors: $\tilde{Y}_m = \tilde{X}_m \times_1 U^{(1)} \times_2 U^{(2)} \times_3 \cdots \times_{(k-1)} U^{(k-1)} \times_{(k+1)} U^{(k+1)} \times \dots \times_n U^{(n)}$

3. Reduction phase of MPCA - calculate the output tensors by their projection on the determined matrices $U^{(k)}$.

Our implementation of MPCA is based on Jama-1.0.2 library, supporting matrix operations and eigen decomposition.

5   Previous Work

In [6] we proposed and examined method of gait identification based on the MPCA reduction and supervised learning. The experimental phase was carried out on the basis of dataset A of CASIA Gait Database. We considered two approaches of MPCA reduction called "Single dataset" and "train set and test set". In the first one all gait sequences are involved in learning phase of MPCA - determining the eigenvalues and eigenvectors. In the train set and test set approach, the gait database is divided into the training and test sets - two sequences of each actor are included in the training set and the remaining two in the test set. Similarly to the supervised classifiers, MPCA uses only the training set in the learning phase. In Fig. 4 the relationship between variation cover Q and obtained number of MPCA components is presented. For the maximum considered parameter Q = 0.99, each of gait sequences is reduced approximately twice from the initial size of 900 to about 500 thousands of attributes in both cases. A single attribute is obtained when Q is less than 0.08. The compression rate is very similar for both analyzed train datasets.
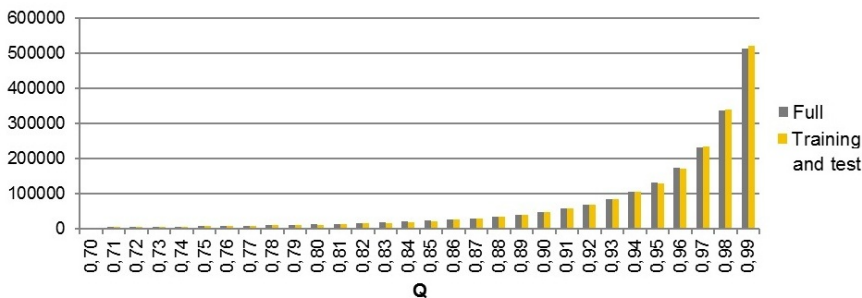
Fig. 4. Dimensionality reduction after applying MPCA algorithm

The reduced data was classified by two statistical WEKA classifiers. It is a Naive Bayes (NB) and the 1-nearest neighbor (1NN) classifier. The classification was repeated twice for both proposed reduction approaches. In case of the "single dataset", 10-fold cross-validation is used to split data into the training and test parts. The classification accuracy is evaluated by percentage of correctly classified gaits out of the test set.

The detailed classification results for the "single dataset" approach are shown in Fig. 5. The mean classification accuracy for all considered Q values of 1NN classifier is 42.94% and the best result is 73.75% obtained by Q = 0.19 and Q = 0.20. There is a noticeable downward trend for the increasing Q parameter. More MPCA components undoubtedly contain more individual data, but also more noise.

The situation is quite different for Naive Bayes, which has a higher average score: 53.32% Beside the cases of strongly reduced gaits, ranging to Q = 0.48 with 358 MPCA components, it is much more precise. There is a very clear extreme for Q = 0.78 and 9064 attributes, in which the best classification accuracy of 86.25% is obtained. More MPCA components not only do not improve classification, but very strongly decrease it, to the worst performance of 16.25% for Q = 0.99.
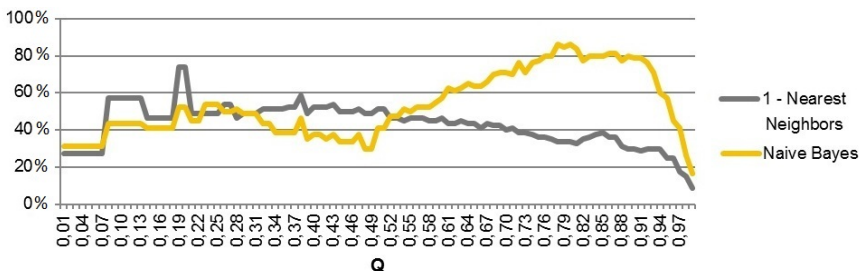
Fig. 5. 1NN and NB classification results for the single dataset approach

When the training set of MPCA and the supervised classification contain only half the data in case of "train set and test set" approach, the results are much worse as shown in Fig. 6. The performance does not exceed 30% and 43% of classification accuracy for Naive Bayes and 1NN classifiers, respectively. It is much better than random guessing, which gives only 5%, but still very poor. It is probably caused by the weak representativeness of input and reduced spaces because of the small size of the training set. Only two gait instances of each class are insufficient for effective probability estimation of high dimensional continuous spaces, necessary in statistical classification.
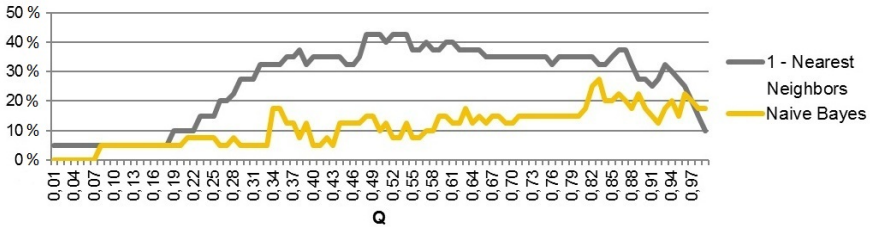
Fig. 6. Naïve Bayes classification results for continuous and discretized spaces for train set and test set approach

To improve the classification we applied supervised discretization of reduced feature spaces, which should make statistical estimation easier. Because calculating distances in discrete spaces seems to be much less accurate than in the continuous ones, which is a crucial step of 1NN, we repeated the tests only for Naive Bayes classifier. In discretization we applied MDL method proposed by Fayyad and Irani [7]. The results shown in Fig. 7 are even better than we expected. Regardless of the poor representativeness of the training set, the maximum accuracy is 92.50% for Q=0.67 and 0.85, which means only three misclassified gaits. We can locate extreme once again. However the influence of noise in high dimensional spaces is weaker, for Q=0.99 accuracy is still greater than 60%.
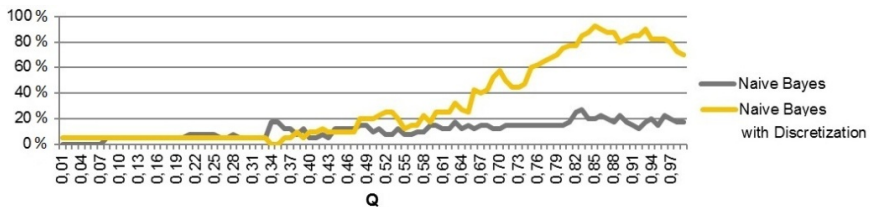
Fig. 7. Naïve Bayes classification results for continuous and discretized spaces for train set and test set approach

Because of such promising results obtained by the classification based on discretized spaces for the "train set and test set" approach, we evaluated the influence of discretization on classification performance for the single dataset approach. As

seen in Fig. 8, the results have once again improved noticeably. The maximum precision is 98.75% for a wide range Q values starting from 0.76. It is always the same gait of the same subject, which is wrongly misclassified.
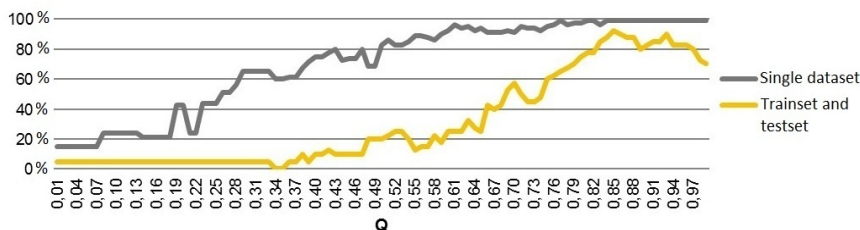
Fig. 8. Naïve Bayes classification results for discretized spaces

6   Feature Selection

The separate challenge is the automatic feature selection task, the choice of the most remarkable features from the point of view of the given classification problem.

The exhaustive search of the all possible combinations of the features subsets is unworkable because of the computation complexity, the problem is NP complete. For the simple case of 50 features there are 1.1259e+015 possible combinations to test. That is the reason why the approximate methods have to be used.

There are two main approaches in feature selection: attributes rankings and search strategies based on the evaluation of the whole subsets [13]. In the ranking approach we evaluate each of the attribute separately by the some kind of the quality index and select the highest scored ones. The number of attributes to select could be specified or could be determined based on the scores obtained. The crucial problem is the way attributes are evaluated. The most well-known rankers are based on the calculated statistics as for instance GINI index, chi square test, Fisher ratio or depend on the determined entropy as for instance information gain and gain ratio.

However the assumption of existence only simple relations between single attributes and class values is very naive. In many cases the worth of the attribute can be noticed only if considered with others. That is a reason why the methods with evaluation of whole feature subsets are gaining more attention. They are more reliable and usually give more compact representation, with greater predictive abilities.

In approach with whole subset evaluation there are two crucial issues. It is the search method which specifies how the feature space is explored and the way subset are evaluated.

In most cases the greedy hill climbing and genetic algorithms are used as search methods. In the hill climbing exploration [13], we start with empty subset and in the subsequent steps choose that attribute added to the currently determined subset

which causes the best subset evaluation score. The loop is iterated till the total evaluation score is improving. In backward direction strategy, we start with complete feature set and in the following steps remove single attributes. The search also can be bidirectional. To minimize the probability of termination in local extreme, we can apply greater number of non-improving nodes to consider before finishing search. In genetic search strategy [1] candidate solutions represented feature subsets are coded by binary strings. The subsequent generations of feature subsets are inherited from previous ones with usage of basic genetic operators as selection, crossover and mutation.

The most obvious way of subset evaluation can be performed by the precision of a subsequent classification [4]. Such an evaluator is called wrapper. Its main disadvantages are associated with great computational complexity and its dependency on a classifier and its parameters choices. More simple, consistency evaluator determines the level of consistency in the class values when the training instances are projected onto the subset of attributes [3]. The are also correlation based subset evaluators. Proposed in [2], CFS evaluator estimates the individual predictive ability of each feature along with the degree of redundancy between them. Subsets of features that are highly correlated with the class while having low intercorrelation are preferred.

7   Experiments and Results

We extend the work presented in [6] by supervised feature selection carried out prior to classification. It allows to obtain more compact gait description with lower dimensionality. The assessment of selected subsets of features corresponds to obtained compression rate and classification accuracy.

Supervised selection requires to supply a training set to be able to discover most remarkable attributes. This is a reason why the approach called "train and test set" [6] is utilized. The single training set is used to determine MPCA projection matrix, select most valuable MPCA components and teach classifier.

Greedy hill climbing with forward direction and genetic search methods and wrapper with nearest neighbor classification and CFS subsets evaluators are chosen to perform selection. To classify gait descriptors similar as in [6] statistical nearest neighbor and Naive Bayes classifiers are applied. At the current stage, discretized MPCA spaces, which obtained best accuracy in classification ([6], Fig. 8) are not taken into consideration in feature selection. Both utilized subset evaluation approaches based on nearest neighbor classification scheme and estimation of correlation seems to be more precise if carried out for continuous spaces rather than corresponding them discrete ones.

In Fig. 9 the obtained compression rates for successive variation covers Q of MPCA and for every combination of considered search method and evaluator are presented. The relation of number of MPCA components and variation cover Q is presented in Fig. 4. Compression rate is calculated to be a ratio of number of

selected attributes to number of attributes in an input space. It can be noticed that greedy hill climbing gives much more compact descriptors with lower number of features in comparison to genetic search. For instance in case of variation cover Q=0.50 which gives 504 MPCA components, greedy hill climbing selects 7 and 34 features with wrapper and CFS evaluators respectively and genetic search selects 194 and 78 components. The difference rises with increasing variation cover Q. In case of Q=0.80 and 10773 MPCA components greedy hill climbing selects 10 and 240 features and genetic search selects 1746 and 1903 components. It is so because of the complexity of considered selection problem. The input set is very high dimensional and discriminative properties are scattered across MPCA components. It is extremely difficult to improve the classification accuracy by adding a single attribute, because only specified subsets of features have distinctive abilities. It is a reason why greedy hill climbing with wrapper subset evaluator terminates at first local extreme and it not able to discover efficiently individual gait features.
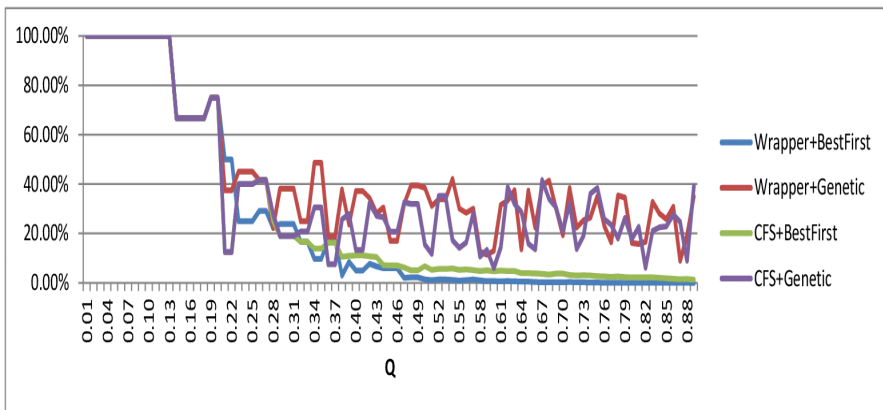
Fig. 9. Compression rates

However much more important assessment of selected MPCA components gives classification accuracy presented in Fig. 10. It shows percentage of correctly classified gaits of a test set in respect to MPCA variation cover Q and applied selection strategy. Globally best precision is 95%, obtained by 449 attributes selected from the input set containing 29400 MPCA components for Q=0.87, which means 0.03% of compression rate, by hill climbing search and CFS evaluator. Genetic search with CFS evaluator is very similar. It has 92.5% of classification precision and it has very similar dependency on a number of features of an input space. Much worse results gives wrapper evaluator, especially if combined with hill climbing search, which is caused by the same reason as explained in compression rates analysis.
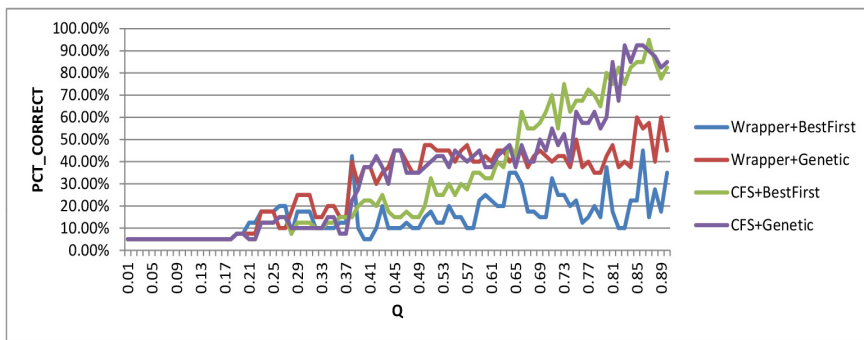
Fig. 10. Selection rates

8 Conclusions

The general conclusion are consistent with those presented in [6]. Multliinear principal component analysis is an effective method of feature extraction of a motion data, which allows to identify humans precisely. However individual gait features are scattered across numerous MPCA components. Thus attribute selection simplifies gait description, discovers most discriminative features and allows for more efficient classification.

The identification performed on the basis of reduced MPCA space, as presented in Fig. 10 is improved significantly in comparing to raw MPCA space as presented in Fig. 6. What is more, although strong dimensionality reduction, selected attributes preserve most of individual gait features.

The obtained features subsets strongly depends on utilized subset evaluation strategy. Wrapper evaluation approach which in general is considered to be more precise, in our problem gives significantly worse results. It can be explained by scattering of individual gait features across MPCA components, so correlation based measures as for instance CFS evaluator, are more efficient in the input space exploration.

References

[1] Goldberg, D.E.: Genetic algorithms in search, optimization and machine learning. Addison-Wesley (1989)
[2] Hall, M.A.: Correlation-based Feature Subset Selection for Machine Learning. Hamilton, New Zealand (1998)

[3] Liu, H., Setiono, R.: A probabilistic approach to feature selection - A filter solution. In: 13th International Conference on Machine Learning, pp. 319–327 (1996)

[4] Kohavi, R., John, G.H.: Wrappers for feature subset selection. Artificial Intelligence 97(1-2), 273–324 (1997)

[5] Boyd, J.E., Little, J.J.: Biometric Gait Recognition. In: Tistarelli, M., Bigun, J., Grosso, E. (eds.) Biometrics School 2003. LNCS, vol. 3161, pp. 19–42. Springer, Heidelberg (2005)

[6] Michalczuk, A., Świtoński, A., Josiński, H., Polański, A., Wojciechowski, K.: Gait identification based on MPCA reduction of a video recordings data. In: Bolc, L., Tadeusiewicz, R., Chmielewski, L.J., Wojciechowski, K. (eds.) ICCVG 2012. LNCS, vol. 7594, pp. 525–532. Springer, Heidelberg (2012)

[7] Fayyad, U.M., Irani, K.B.: Multi-interval discretization of continuous valued attributes for classification learning. In: Thirteenth International Joint Conference on Artificial Intelligence, pp. 1022–1027

[8] Tacoob, Y.: Parameterized Modeling and Recognition of Activities. Computer Vision and Image Understanding 73(2), 232–247

[9] Kulbacki, M., Segen, J., Bak, A.: Unsupervised learning motion models using dynamic time warping. In: Proc. Symp. Intell. Inf. Syst., pp. 217–226

[10] Iwamoto, K., Sonobe, K., Komatsu, N.: A Gait Recognition Method using HMM. In: Proceedings of the 9th European Conference on Computer Vision, pp. 1936–1941. IEEE

[11] Liang, W., Tieniu, T., Huazhong, N., Weiming, H.: Silhouette Analysis-Based Gait Recognition for Human Identification. IEEE Transactions on Pattern Analysis and Machine Intelligence 25(12)

[12] Sminchisescu, C., Jepson, A.: Generative Modeling for Continuous Non-Linearly EmbeddedVisual Inference. In: ICML

[13] Witten, I.H., Frank, E.: Data Mining: Practical Machnine Learning Tool and Techniques

[14] Vasilescu, M., Terzopoulos, D.: Multilinear Independent Components Analysis. In: Proceedings of the IEEE Computer Vision and Pattern Recognition Conference

[15] Cheng, M.-H., Hoa, M.-F., Huanga, C.-L.: Gait analysis for human identification through manifold learning and HMM. Pattern Recognition 41(8), 2541–2553

[16] Lu, H., Plataniotis, K.N., Venetsanopoulos, A.N.: MPCA: Multilinear Principal Component Analysis of Tensor Objects. IEEE Transactions on Neural Networks 19(1), 18–39

[17] Lu, H., Plataniotis, K.N., Venetsanopoulos, A.N.: Uncorrelated Multilinear Principal Component Analysis through Successive Variance Maximization. IEEE Transactions on Neural Networks 20(11), 1820–1836

[18] Pushpa, R.M., Arumugam, G.: An efficient gait recognition system for human identification using modified ICA. International Journal of Computer Science & Information Technology 2(1)

[19] Benbakreti, S., Benyettou, M.: Recognition Human by gait using PCA and DTW. In: 3th International Conference on Computer Science and its Applications

[20] Josinski, H., Switonski, A., Michalczuk, A., Wojciechowski, K.: Motion Capture as data source for gait-based human identification. Przegląd Elektrotechniczny 88(12B), 201–204 (2012)

[21] Świtoński, A., Polański, A., Wojciechowski, K.: Human Identification Based on the Reduced Kinematic Data of the Gait. In: ISPA 2011 - 7th International Symposium on Image and Signal Processing and Analysis, pp. 650–655, art. no. 6046684 (2011)

[22] Josinski, H., Switonski, A., Jedrasiak, K., Kostrzewa, D.: Human identification based on gait motion capture data. Lecture Notes in Engineering and Computer Science, vol. 1, pp. 507–510 (2012)

[23] Krzeszowski, T., Kwolek, B., Michalczuk, A., Świtoński, A., Josiński, H.: View independent human gait recognition using markerless 3d human motion capture. In: Bolc, L., Tadeusiewicz, R., Chmielewski, L.J., Wojciechowski, K. (eds.) ICCVG 2012. LNCS, vol. 7594, pp. 491–500. Springer, Heidelberg (2012)

Comparative Analysis of Power Loses in Selected Measurement Devices Used in SMART GRID Systems

Aleksander Nawrat, Anna Piaskowy, Artur Skórkowski,
and Tadeusz Topór-Kamiński

Abstract. This article provides information on smart grid and smart measurement systems with a special focus on the advantages of their implementation as well as concerns present at the stage of design and component selection. The tests conducted on a selected group of measurement devices used in smart grid systems made it possible to compare power losses characteristic for these devices. In the analysis presented below, both classic inductive meters and electronic meters with various communication modems were used.

1   Introduction

The name "smart grid" is used in reference to modern power grids featuring a two-way digital communication system connecting the supplier and the consumer and equipped with smart measurement and monitoring systems. Smart measurement systems [1, 6, 7, 8] constitute an integral part of all smart grids.

   In particular, development of the idea of intelligent measuring and monitoring can be applied in the case of autonomous flying objects. These objects are usually equipped with a system of sensors and actuators supervised by a microprocessor system (fig. 1). In case of electric powered and assisted by solar energy UAVs [14] it is extremely important to monitor and efficiently manage power consumption. Aim of such unmanned vehicles is the longest time of operation. It is worth to mention that energy consumption in UAVs is determined by many factors inter

Aleksander Nawrat · Anna Piaskowy · Artur Skórkowski · Tadeusz Topór-Kamiński
Silesian University of Technology, Institute of Automatic Control,
Akademicka 16, 44-101 Gliwice, Poland
e-mail: {anna.piaskowy,artur.skorkowski,
       aleksander.nawrat}@polsl.pl

alia weather conditions. Therefore, it is important that both the autonomous surveillance systems embedded in the UAV as well as ground-based systems have full information about the energy level of the object in order to correctly determine further actions of the vehicle. The information has to be processed using the algorithms developed on the basis of extensive mathematical research [32, 33, 34].
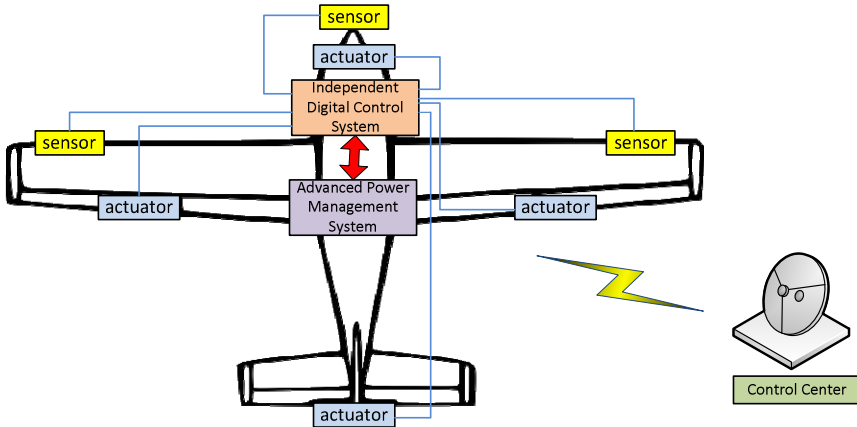
Fig. 1. Autonomous flying object measurement and control systems diagram

Legal regulations concerning the issue of smart grid implementation can be found in the Attachment I.2 to the Directive 2009/72/EC concerning common rules for the internal market in electricity which obliges the Member States to assess implementation of smart measurement systems as an important step towards launching smart grids [2].

Additionally, the Directive 2006/32/EC on energy end-use efficiency and energy services highlights the necessity to utilize measurement systems which precisely gauge the factual energy consumed by the end user and provide information on usage times[1].

The advantages of smart grids include [3]:

- capability to influence the consumers' behaviour, e.g. to encourage them to use energy in a fashion that decreases energy consumption and levels power usage peaks, by introducing appropriate lists of prices;
- ability to better manage the grid, which ensures improved supply safety and cheaper operations;
- ability to smoothly integrate multiple small energy sources (in particular the renewable energy), which will contribute to reduction in fossil fuel usage and carbon dioxide emissions;
- formation of a market where innovative companies can flourish; the number of jobs is expected to increase; all these factors will beneficially influence the economic growth.

When weighing up the advantages of smart grids, one may not disregard potential hazards, such as high investment costs and possible threats to consumers' privacy. There are also some concerns regarding the utilization of "smart meters". An analysis of selected electrical energy meters' power losses which significantly influence the utilization costs will be presented later in this work.

Implementation of smart grid systems along with smart meters is mostly aimed at optimization of power grid operation. Also communication with energy end users will be more efficient, mostly being focused on increasing their awareness about the possibilities of energy conservation. Execution of the last goal is dependent on development of a so-called HAN (Home Area Networks) concept, which provides communication between home equipment and its electronic meters [6, 7, 8, 9].

Implementation of HAN-based smart grid systems will provide the consumers with:

- ability to check the current power consumption data,
- ability to track power consumption over 24h periods,
- ability to choose optimal times of operation for energy-intensive equipment, depending on the tariff used,
- access to information on changes in the tariff,
- ability to change the tariff,
- ability to join discount programmes.
- In addition, users who will consciously manage their energy consumption make a contribution to environmental protection. On the other hand, by taking advantage of smart grid systems and two-way communication with end users electric energy suppliers will be able to:
- streamline the process of reading data from energy meters,
- improve management of vast amounts of data from energy meters,
- set up load profiles which will make it possible to charge consumers more precisely,
- improve network resource management,
- optimize operations in production facilities on the basis of data about the factual energy demand,
- react to big network load in order to avoid blackouts,
- detect and check power failure reports,
- respond faster to blackouts.

In the simplest scenario, data will be transmitted within a home network from an electronic meter to a touchscreen-equipped minicomputer where all the information about energy consumed by the equipment will be presented. On this basis the user will be able to manually switch off the most energy-intensive devices. Additionally, in the future some more advanced solutions will be available. For instance, through a home network integrated panel the user will be able to control various devices by e.g. switching them on/off or changing their settings so that they consume less energy [7]. It is expected that most devices in the future will

have an embedded capability to communicate across home networks, especially these devices with high power consumption levels, such as lighting, heating, ventilation and air conditioning equipment, tap and swimming pool water heaters, swimming pool pumps, electrical home appliances, such as washing machines, refrigerators and electric car charging sockets.

While the aim of HAN network has already been precisely defined, it remains undecided what kind of communication interface or interfaces will be used in the future to provide the necessary functionality. Communication interface developers vie with each other to create the state-of-the-art interfaces that will meet HAN energy management requirements, trying to lure smart meter manufacturers to implement their technologies.

Wireless communication has dominated the home computer network market mostly through popularization of Wi-Fi networks based on IEEE 802.11 specification. The advantages of this type of networking are e.g. high reliability as well as capability to reach high data transmission speeds. It has been decided, though, that Wi-Fi networking should not be considered for a potential HAN standard as the specification has grown too complex. This, in turn, benefited other cheaper and slower wireless standards, such as ZigBee which is presently considered to be the most serious candidate for domination of HAN networking market [11]. Recently, ZigBee Alliance, which brings together the companies that work on the development of ZigBee specification, has presented the latest version of its product - Smart Energy 2.0. The most important functions are: support for utility meters (electric energy, gas, water, heating), ability to present results in different units of measurement and show prices in different currencies, both of which make it easier to use the technology in different parts of the world. As for communication, support is provided for transmitting text messages in different languages along with read receipts. The profile makes it possible to work with battery or network powered meters, conduct different kinds of measurements (e.g. load profile, power factor), access real-time information about energy used/generated and record all this data. Smart Energy 2.0 supports multiple methods of interacting with HAN-enabled devices, e.g. by setting values to particular parameters and triggering alarms in case they are exceeded, recording attempts to modify meters and setting up network access protections, including the necessity to sign in with an installation key or standard public key cryptological methods. ZigBee Smart Energy 2.0 is already being supported by some smart energy meters manufacturers.

A competitor to ZigBee standard is Z-Wave specification. It was created to remotely control various electronic home devices and support simple commands, such as switch on/off and turn up/down commands. As these operations do not require high transmission speeds, Z-Wave networks work at the maximum speed of 9600 b/s. Contrary to its main competitor, Z-Wave network do not work on 2.4 GHz broadband and therefore its transmission cannot be interrupted by interferences with signals from e.g. Wi-Fi networks. Depending on the region, Z-Wave specification provides transmission on various frequencies. In Europe, for instance, this is 868 MHz band and in the USA - 908 MHz. Not unlike ZigBee network, Z-Wave has the ability to work in mesh topology.

In order to evaluate the possibility of utilizing the popular Bluetooth standard in HAN networks and prepare adequate technical solutions, a group called Smart Energy Study Group was created. The advantages of leveraging Bluetooth technology in smart grid are e.g. its identifiability and low power consumption, which are important in case multiple devices are to be used. As growth potential for smart grid market is high, concrete results of Smart Energy Study Group work are expected.

Wireless data transmission across long distances which makes it possible to integrate multiple smart home systems may be currently implemented using GSM mobile communication and GPRS data transmission technologies [10].

When it comes to wired transmission, the most serious contender for domination of home networks is PLC technology, i.e. data transmission through power grid. One of the leaders in this group, well-known for 10 years and holding an estimated market share of at least 80%, is HomePlug standard. Its creators, brought together in HomePlug Powerline Alliance since the work on smart grid concept started, have wooed industry representatives to choose HomePlug to be an alternative to wireless communication. As the interest in the technology was reciprocated, the energy sector approached HomePlug Powerline Alliance to prepare a new version of this specification, taking into account costs and power consumption required by HAN networks. As a result, on the basis of HomePlug AV specification, HomePlug Green PHY (HomePlug GP) was developed. Transmission in HomePlug AV occurs in a band with frequency ranging from 2 to 30 Mhz. OFDM modulation with subcarriers interval of 24.414 kHz was used (1155 subcarriers). In order to obtain the best signal quality possible, especially in channels where selective fading occurs as a consequence of multipath, adaptive transmission is used in HomePlug AV which consists in modulating sub-carriers   by means of various methods, including BPSK, QPSK, 16QAM, 64 QAM, 256 QAM, 1024 QAM - the choice of method dependent on the transmission channel properties. In order to examine them, test signal is sent which is then retransmitted to an emitter where based on the measurement of its amplitude correct modulation pattern is selected. Thanks to adaptive transmission application, transmission speeds of 20-200 Mb/s can be achieved. In addition, HomePlug AV uses CSMA access as the primary mechanism and TDMA as secondary alternative. On the basis of HomePlug AV, HomePlug GP was developed. For this very reason, there exist many similarities between the two, e.g. the frequency remains unchanged (from 2 to 30 MHz), just like OFDM modulation method does. At the same time, due to HAN requirement, some things were simplified. The key difference consists in reduction of the maximum transmission speed, which in HomePlug GP networks is equal to 10Mb/s. In addition, the only modulation technique is QPSK. That means that adaptive transmission is not utilized, thus there is no need to transmit test signals or store information on channel properties. Thanks to these modifications, emitter and receiver structures were significantly simplified and their energy efficiency increased. As a consequence, these changes brought reductions in costs. Adaptive transmission was replaced in HomePlug GP by ROBO technique (Robust OFDM), i.e. coding with repetition which consists in transmitting the same information on multiple subcarriers. Thus, the signal will be restored in the receiver, even if in a

particular channel some subcarriers are dampened or distorted, e.g. as a result of interference or selective fading. This increases transmission reliability but at the same time makes it impossible to achieve high speeds, which in case of HAN does not pose a problem. Contrary to HomePlug AV, the GP version does not provide TDMA access. A novelty in HomePlug GP, though, is an additional work mode with a limitation on power consumption as well as a so-called DBC (Distributed Bandwidth Control) mechanism introduced so as to prevent possible transmission interferences in HomePlug AV coming from devices supporting HomePlug AV standard. HomePlug GP is also compatible with ZigBee wireless technology, more precisely – with ZigBee Smart Energy 2.0 profile.

Although HomePlug GP currently holds the leading position in the competition for domination over HAN market when it comes to the PLC communication standards, this does not mean the technology is free from challengers. Recently, in particular in Europe, two specifications have been gaining popularity: PRIME (Powerline Related Intelligent Metering Evolution) and G3. PRIME standard was written from a scratch as a specification intended to support communication in intelligent energy systems, especially in HAN networks. It takes advantage of OFDM modulation and 9-95 kHz frequency. Transmission speed in PRIME standard ranges from 16 to 130 kb/s. G3 networks, on the other hand, work in band from 10 to 490 kHz. This standard also uses OFDM modulation. Maximum transmission speed for G3 is 250 kb/s, and transferred data can be encrypted using AES-128 algorithm. This standard enables transmission in both low-power and middle-power networks. Therefore G3 is named as one of the candidates for connecting HAN to the public power grid. By means of this connection, a meter with a two-way communication capability will send to the energy supplier the data about the energy consumption and at the same time receive from them various commands, control signals and also e.g. information about the scale of prices which will be sent further within HAN network.

Another competitor of PLC is the G.hn standard. Work on its development has been conducted by HomeGrid Forum for some time now under the patronage of ITU-T. Originally G.hn is expected to be used to transmit multimedia data, mostly HD video signals, by means of wires used in households (coaxial, electric and phone cables). So far three types of the standard have been developed: broadband version which provides transmission at a speed of up to 200 Mb/s, profile for smart grid application, especially as a HAN connection with public power grid - therefore the maximum speed is expected to reach 25 Mb/s and a narrowband version, so-called G.hnem, optimized for HAN application. G.hnem is a simplified version of the basic specification, which enables transmission at speeds below 500 kb/s.

It must be remembered that measurement data transmission in data acquisition systems which smart grid networks undoubtedly are requires that selected measurement data transmission network's influence on the measurement results is examined. It is crucial to determine parameters of teletransmission network which affect the final measurement result and which of them may be view as not exerting any influence. Among them one can include e.g. various delays which transmission lines introduce and which must be identified and first of all measured [12]. In

order to that, data transmission line models are built which determine quantities that are crucial for the transmission, on the basis of which it is possible to prepare a final interpretation of measurement data received from network detectors [13].

The most demanding of the European electrical energy, gas, water and heat suppliers set requirements for horizontal compatibility. Manufacturers prepared solutions which meet the above requirements. Companies: Iskraemeco, Landys & Gyr, Itron in April 2010 started the IDIS (Interoperable Device Interface Specification) association.

Obtaining IDIS certificate by a manufacturer of a system or its elements lets energy companies invest safely, as they can change the supplier of any of the system parts in the future. The most important qualities of IDIS certificate are: open interfaces for meter and network management, low investment risk and future-proofness, being based on international DLMS standard, supporting EU standardization mandate and meter management directive, supporting application for multiple energy companies, scalability for mass meter replacement and adjustability for future applications.

While the smart grid specification is well documented, there still is not unified definition for a "smart meter". It is assumed that a smart meter is an electric energy meter which has additional functionalities. The functions that are most often mentioned are: remote reading, remote switch for energy supply (on/off), capability to register energy consumption in given periods, remote tariff change (the method of determining the costs of energy).

As noted earlier, the name smart meter refers to an electric energy meter which has additional functionalities. From metrological point of view, such a meter does not differ in any way from a typical meter: the part responsible for measurement continues to be of interest for legal metrology - this part should meet all the requirements that a typical meter satisfies. The part of the meter responsible for additional functionalities is relevant to metrology in a respect that it must not exert any undesirable influence on the measuring part or the transmitted data [3]. Undesirable influence on a measurement part refers to e.g. loss power, e.g. power needed to keep the electronic part of the meter running which should not be included in the payments for the energy consumed, i.e. it should be borne by energy supplier alone. In the analysis shown below, "classic meter" will be represented by a commonly used induction meter, whereas meters intended for smart grid systems will be electronic meters equipped with various communication modems which take advantage of both wired and wireless interfaces for data transmission.

2   Power Loss Measurement for Various Electric Energy Meters

The subject of this work is the comparative analysis of power losses in selected electrical energy measurement devices. The study was conducted on various types of electric energy meters, including:

- 1-phase electronic meters with GSM/GPRS modems
- 3-phase electronic meters with GSM/GPRS modems

- 1-phase electronic meters with PLC modems
- 3-phase electronic meters with PLC modems
- 1-phase electronic meters without modems
- 3-phase electronic meters without modems
- 1-phase inductive meters
- 3-phase inductive meters

The scope of the study covered multiple meters of a single type at all times so that repeatability of the results obtained could be ascertained. Typical meters that are commonly used were chosen for the research. Intentionally, however, type markings were changed.

During measurements the meters were powered by rated voltage, and measurements of electrical currents were conducted independently in voltage circuits of each phase. Current circuits of particular phases were not loaded during the measurements, and therefore powers obtained during the measurements come from power loss only. All the results were obtained on the basis of representative measurement series for which both typical and maximum values were defined. To demonstrate the differences in measurement results fragments from measurement series for selected 1-phase meters with various communication modems are shown below.

2.1   Measuring Circuit Used for 1-Phase Meters

Fig. 2 shows a circuit intended for indirect measurements of currents 1-phase meter voltage circuits, including inductive and electronic meters. In the circuit, a current/voltage converter was used in the form of a shunt R3, on which voltage components (active and passive) are measured by means of vector nanovoltmeter (LIA). Referential voltage Uref is taken from a resistor R2 within a resistance divider of the voltage supplied from the examined phase feeding the electrical energy meter. Current circuits were not loaded during loss power measurements, $Z_{io} = \infty$. Meter power loss (real power P1h, reactive power Q1h and apparent power S1h) for feeding phases were calculated on the basis of measured current components in meter's input voltage circuits.
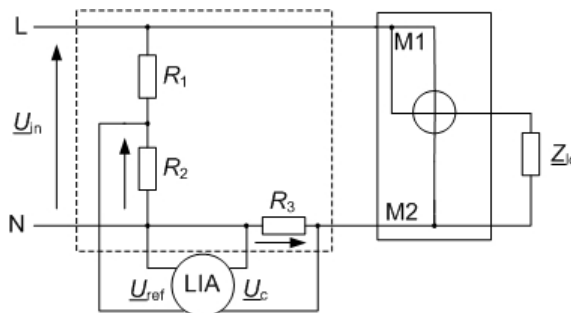
Fig. 2. Circuit intended for indirect measurements of currents in 1-phase meter voltage circuits

Measurements consisted in recording changes in currents components. Afterwards, based on the series of measurement results typical and maximum values were determined, which made it possible to determine typical and maximum values for meters' power losses. All the calculations were made for the basic harmonic of the measured signals.

2.2   Measuring Circuit Used for 3-Phase Meters

As shown in fig. 3, the circuit intended for indirect measurements of currents in 3-phase meter voltage circuits works similarly to the circuit shown in fig. 2 with a single difference - the role of current/voltage converter is taken here by measuring transformer with resistance R 3. The figure shows also the basic layout of internal connections of the calibrator supplying the circuit as well as a scheme of connection between the circuit and the meter.

The circuit shown in fig. 2 could not be used, as the phase current intensity must be measured in the phase conductor on the calibrator's output. The conductor has phase voltage.
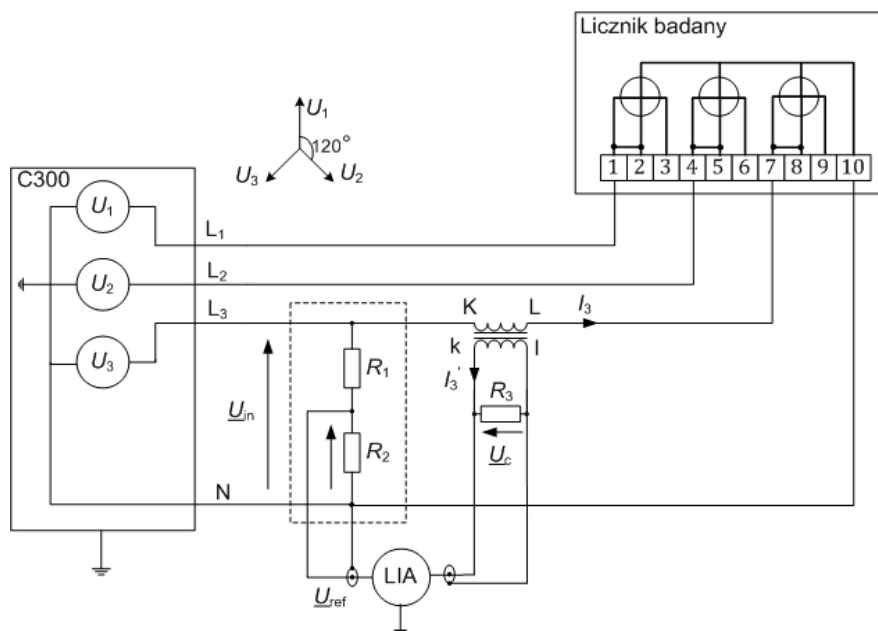
Fig. 3. Circuit used for indirect measurement of currents in 3-phase meter voltage circuits

The phase conductor on the side of joint powering point could not be used as the calibrator does not provide access to the joint point from the phase conductors' side. Neutral conductor could not be used as it conducts a sum of all phase currents. Therefore, current transformer with 1:1 ratio whose secondary winding is shorted by a resistor with small value was applied. This transformer galvanically isolates milivoltmeter measuring circuit from the phase conductor. At the same time the voltage drop on the resistor is proportional to phase current intensity, as in system from fig. 2.

In case of tests on 3-phase meters, the measuring circuit is connected consecutively to each phase of input voltage circuits of a 3-phase supply meter.

All results included in the tables below are averaged results from multiple measurements. The necessity to average the results was a consequence of higher harmonic background in the measured current flows.

3 Measurements of Electronic Meters

Measurements of energy losses in 1-phase electronic meters were conducted in a circuit whose scheme is shown in fig. 2. In tables 1 and 2 typical and maximum energy loss values are shown for 1-phase electronic meters equipped with GSM/GPRS and PLC modems as well as the ones without modems.

On the other hand, power loss measurements for 3-phase electronic meters were conducted in a circuit whose scheme is shown in fig. 3. In tables 3 and 4, compared are the typical and maximum values of power losses obtained for the 3-phase electronic meters with GSM/GPRS and PLC modems and without modems. In the tables below both values of power loss for meters with connected and disconnected (values in brackets) GSM/GPRS modems are shown.

3.1 *Results from 1-Phase Electronic Meter Measurements*

The diagrams shown in fig. 4 shows fragments of measurement series registered to determine the typical and maximum power loss values for various electronic meters. The number of samples taken for each series ranges from a few hundred to a few thousand, depending on the meter type. Necessity to use such long series in the study stems from energy demand volatility during meters' operation as well as the necessity to account for various work modes of communication modems which smart grid systems are equipped with.
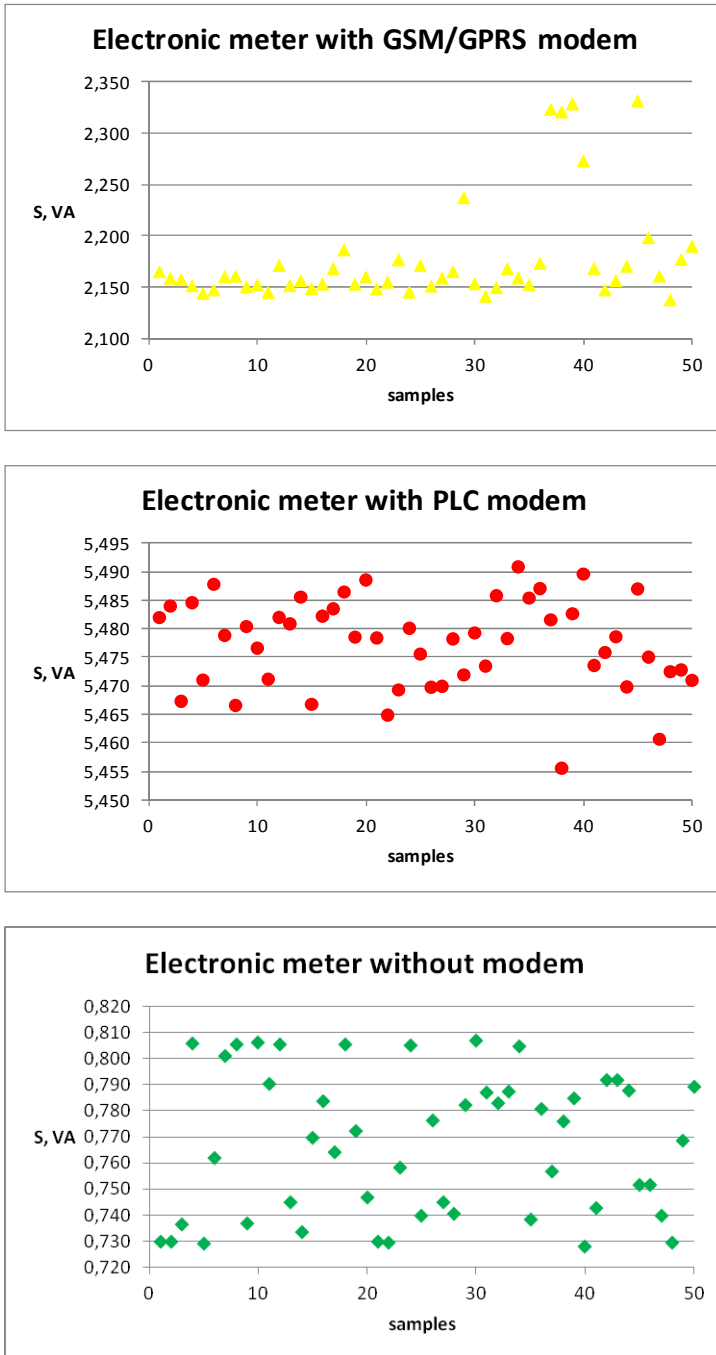
Fig. 4. Fragments of measurement series registered for various 1-phase electronic meters

Table 1. Comparison of typical power loss values for 1-phase electronic meters

1-phase electronic meters			Power loss (typical values)		
Meter type	Number	Modem type	P1h, W	Q1h, Var	S1h, VA
L1GSM	1	GSM/GPRS	2.17 (1.02)	-0.04 (-0.04)	2.17 (1.02)
L1GSM	2	GSM/GPRS	2.13 (1.01)	-0.15 (-0.04)	2.14 (1.01)
L1GSM	3	GSM/GPRS	2.15 (1.00)	-0.15 (-0.04)	2.15 (1.00)
L1PLC	1	PLC:IEC61334-5-1	2.08	4.93	5.35
L1PLC	2	PLC:IEC61334-5-1	2.13	5.05	5.48
L1PLC	3	PLC:IEC61334-5-1	2.12	4.97	5.40
P1	1	-	0.40	-0.65	0.77
P1	2	-	0.36	-0.55	0.65
P1	3	-	0.39	-0.64	0.75

(...) - power loss values for a meter with a disconnected GSM/GPRS modem

Table 2. Comparison of maximum power loss values for 1-phase electronic meters

1-phase electronic meters			Power loss (maximum values)		
Meter type	Number	Modem type	P1h, W	Q1h, Var	S1h, VA
L1GSM	1	GSM/GPRS	2.34 (1.06)	-0.06 (-0.09)	2.34 (1.07)
L1GSM	2	GSM/GPRS	2.89 (1.05)	-0.15 (-0.08)	2.89 (1.05)
L1GSM	3	GSM/GPRS	2.34 (1.05)	-0.15 (-0.08)	2.35 (1.05)
L1PLC	1	PLC:IEC61334-5-1	2.11	5.06	5.48
L1PLC	2	PLC:IEC61334-5-1	2.15	5.06	5.50
L1PLC	3	PLC:IEC61334-5-1	2.13	5.00	5.43
P1	1	-	0.44	-0.69	0.82
P1	2	-	0.39	-0.59	0.71
P1	3	-	0.43	-0.68	0.80

(...) - power loss values for a meter with a disconnected GSM/GPRS modem

The results presented in the tables account for: real power P1h, reactive power Q1h and apparent power S1h, obtained for the basic harmonic of the measured current. The tables present only some selected but representative measurement results for various types of meters. Measurements were conducted for multiple meters of one type and only results from three meters of one type are shown in the tables so as to present the characteristic result repeatability.

3.2   Results from 1-Phase Electronic Meter Measurements

The results presented in the tables account for: real power P1h, reactive power Q3h, and apparent power S1h, obtained for each phase, for basic harmonic of currents, measured consecutively in all three input voltage circuits of a 3-phase supply meter.

Table 3. Comparison of typical power loss values for 3-phase electronic meters

3-phase electronic meters				Power loss (typical values)		
Meter type	Number	Modem type	Phase	P_{1h}, W	Q_{1h}, Var	S_{1h}, VA
L3GSM	12552303	GSM/GPRS	L1	0.65 (0.27)	0.30 (0.16)	0.71 (0.32)
			L2	0.62 (0.26)	0.28 (0.13)	0.68 (0.29)
			L3	0.65 (0.25)	0.26 (0.14)	0.71 (0.29)
L3GSM	12634810	GSM/GPRS	L1	0.70 (0.25)	0.29 (0.14)	0.76 (0.29)
			L2	0.68 (0.25)	0.28 (0.15)	0.74 (0.29)
			L3	0.66 (0.25)	0.26 (0.15)	0.71 (0.29)
L3GSM	12634937	GSM/GPRS	L1	0.65 (0.27)	0.29 (0.13)	0.71 (0.30)
			L2	0.65 (0.26)	0.27 (0.13)	0.71 (0.29)
			L3	0.65 (0.27)	0.28 (0.13)	0.70 (0.30)
L3PLC	12585401	PLC:IEC61334-5-1	L1	-0.54	4.35	4.38
			L2	-0.55	4.26	4.29
			L3	-0.51	4.21	4.24
L3PLC	12537801	PLC:IEC61334-5-1	L1	-0.52	4.34	4.37
			L2	-0.47	4.28	4.31
			L3	-0.56	4.21	4.24
L3PLC	12585090	PLC:IEC61334-5-1	L1	-0.49	4.30	4.32
			L2	-0.41	4.06	4.08
			L3	-0.51	4.04	4.07

Table 3. (*continued*)

P3	711016 74	-	L1	0.39	-0.08	0.40
			L2	0.38	-0.07	0.39
			L3	0.40	-0.07	0.40
P3	711016 78	-	L1	0.40	-0.07	0.40
			L2	0.41	-0.09	0.42
			L3	0.36	-0.05	0.36
P3	711052 22	-	L1	0.36	-0.05	0.36
			L2	0.35	-0.06	0.35
			L3	0.38	-0.09	0.39

(...) - power loss values for a meter with a disconnected GSM/GPRS modem.

Table 4. Comparison of maximum power loss values for 3-phase electronic meters

3-phase electronic meters				Power loss (maximum values)		
Meter type	Number	Modem type	Phase	P_{1h}, W	Q_{1h}, Var	S_{1h}, VA
L3GSM	12552303	GSM/GPRS	L1	1.04 (0.67)	0.66 (0.55)	1.23 (0.87)
			L2	1.22 (0.67)	0.69 (0.55)	1.40 (0.87)
			L3	1.21 (0.68)	0.71 (0.56)	1.40 (0.88)
L3GSM	12634810	GSM/GPRS	L1	1.21 (0.65)	0.78 (0.54)	1.43 (0.84)
			L2	1.03 (0.64)	0.70 (0.53)	1.24 (0.83)
			L3	1.03 (0.64)	0.72 (0.53)	1.25 (0.83)
L3GSM	12634937	GSM/GPRS	L1	1.06 (0.65)	0.68 (0.53)	1.26 (0.84)
			L2	1.30 (0.64)	0.76 (0.53)	1.51 (0.83)
			L3	1.20 (0.65)	0.72 (0.53)	1.40 (0.84)
L3PLC	12585401	PLC:IEC6133 4-5-1	L1	-0.69	4.42	4.47
			L2	-0.58	4.30	4.34
			L3	-0.67	4.28	4.33

Table 4. (*continued*)

L3PLC	12537801	PLC:IEC61334-5-1	L1	-0.57	4.39	4.42
			L2	-0.52	4.33	4.36
			L3	-0.61	4.26	4.30
L3PLC	12585090	PLC:IEC61334-5-1	L1	-0.54	4.35	4.38
			L2	-0.46	4.11	4.14
			L3	-0.56	4.08	4.12
P3	71101674	-	L1	0.77	-0.46	0.90
			L2	0.76	-0.45	0.88
			L3	0.77	-0.46	0.90
P3	71101678	-	L1	0.82	-0.50	0.96
			L2	0.81	-0.50	0.95
			L3	0.77	-0.45	0.90
P3	71105222	-	L1	0.77	-0.45	0.90
			L2	0.76	-0.46	0.89
			L3	0.79	-0.51	0.94

(...) - power loss values for a meter with a disconnected GSM/GPRS modem.

4   Inductive Meter Measurements

Measurements of energy losses in 1-phase inductive meters were conducted in a circuit whose scheme is shown in fig. 2. In tables 5 and 6 compared are the typical and maximum power loss values for 1-phase inductive meters.

Measurements of energy losses in 3-phase inductive meters were conducted in a circuit whose scheme is shown in fig. 3. In tables 7 and 8 compared are the typical and maximum power loss values obtained for 3-phase inductive meters.

Inductive meters were examined in order to compare power loss results obtained for meters with results characteristic for electronic meters used in smart grid systems. Such comparison is expected to answer the question whether or not electronic meters, in particular meters with communication modems, are characterized by greater energy demand required for their operation.

4.1   Results from 1-Phase Inductive Meter Measurements

Figure 5 shows fragments of measurement series registered to determine the typical and maximum power loss values for 1-phase inductive meter. Not unlike the electronic meters, the number of all samples in the measurement series registered to determine the typical and maximum power loss values were significantly greater than what is presented in figure 5.
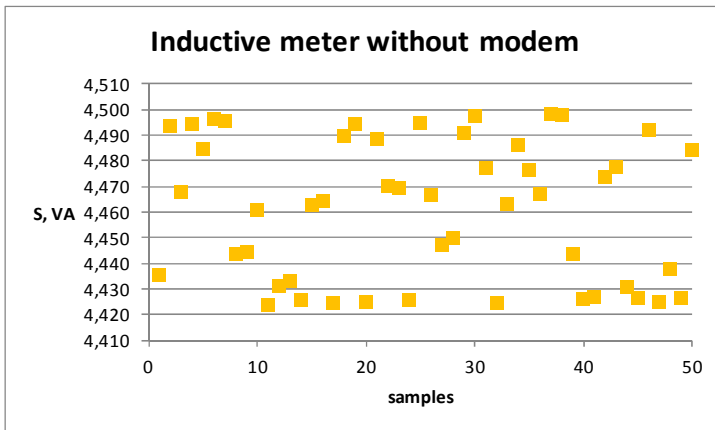
Fig. 5. Fragment of measurement series registered for a 1-phase inductive meter

The results presented below account for: real power P1h, reactive power Q1h and apparent power S1h, obtained for the basic harmonic of the measured current.

Table 5. Comparison of typical power loss values for 1-phase inductive meters

1-phase inductive meters		Power loss (typical values)		
Meter type	Number	P_{1h}, W	Q_{1h}, Var	S_{1h}, VA
PI1	1	1.22	-4.84	4.99
PI1	2	1.19	-4.73	4.87
PI1	3	1.12	-4.32	4.46

Table 6. Comparison of maximum power loss values for 1-phase inductive meters

1-phase inductive meters		Power loss (maximum values)		
Meter type	Number	P_{1h}, W	Q_{1h}, Var	S_{1h}, VA
PI1	1	1.25	-4.88	5.04
PI1	2	1.23	-4.77	4.93
PI1	3	1.15	-4.38	4.53

4.2   Results from 3-Phase Inductive Meter Measurements

The results presented below account for: real power P1h, reactive power Q1h and apparent power S1h of each phase, obtained for the basic harmonic of currents measured consecutively in all three input voltage circuits of a 3-phase supply meter.

Table 7. Comparison of typical power loss values for 3-phase inductive meters

3-phase inductive meters			Power loss (typical values)		
Meter type	Number	Phase	P1h, W	Q1h, Var	S1h, VA
PI3	1	L1	1.93	-2.90	3.48
		L2	1.96	-2.89	3.49
		L3	1.93	-2.98	3.55
PI3	2	L1	2.00	-2.86	3.49
		L2	2.09	-2.96	3.63
		L3	1.97	-3.01	3.60
PI3	3	L1	2.05	-2.81	3.48
		L2	2.12	-2.97	3.65
		L3	2.01	-3.07	3.67

Table 8. Comparison of maximum power loss values for 3-phase inductive meters.

3-phase inductive meters			Power loss (maximum values)		
Meter type	Number	Phase	P1h, W	Q1h, Var	S1h, VA
PI3	1	L1	2.31	-3.28	4.01
		L2	2.32	-3.26	4.00
		L3	2.33	-3.40	4.12
PI3	2	L1	2.39	-3.25	4.04
		L2	2.47	-3.35	4.16
		L3	2.36	-3.36	4.11
PI3	3	L1	2.41	-3.21	4.01
		L2	2.49	-3.37	4.19
		L3	2.38	-3.44	4.18

Measurement results for inductive meters as "classic meters" constituted the point of reference for the analysis of power loss for various types of electronic meters used in smart grid systems.

5 Summary and Conclusions

It seems that there is no turning back from smart power networks. Their operation will certainly be regulated by European standards to a greater extent than by "hard" law regulations which will be used in more sensitive areas, such as measurement accuracy and electrical energy users' personal data safety [3]. In this work, various power loss measurement results were presented, both for "classic meters" and electronic ones that used in smart grid systems, in order to carry out a comparative analysis of power required for their correct operation.

Maximum power loss values registered for 1-phase meters, both electronic and inductive, differs insignificantly from typical values, which means that for this type of meters power loss values for meters of the same kind exhibit small spread, and are constant in time, too (fig. 6).
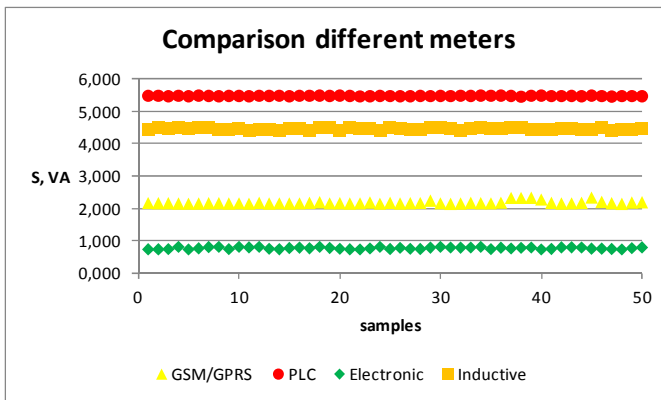
Fig. 6. Comparison of maximum power loss values registered for various 1-phase meters

The greatest differences in power loss values, observed in longer operation time, appear for 3-phase electronic meters with GSM/GPRS modems. For this type of meters, the ratio between maximum power loss values and corresponding typical values is often close to 2.

Comparing power losses for meters with GSM/GPRS and PLC modems, one may notice that, be it 1-phase or 3-phase meters, devices with PLC modems are characterized by significantly greater power loss, even greater than analogous inductive meters.

In addition, it has been ascertained that current flows in voltage circuits of electronic meters include a harmonic series which are generated and introduced into the supply network by the meter circuit. Examination of these flows and determination of functional dependencies require additional analyses which are not included in the scope of this study.

Analysing the data, one can easily notice that power loss for electronic meters with different communication modems do not differ considerably from the powers required to feed inductive meters. This corroborates the fact that utilization costs of electronic and classic inductive meters are similar, which means that cost cannot constitute an argument against their implementation in smart grid concepts.

References

[1]   European Commission: Communication from the European Commission to the European Parliament, the Council, the European Economic and Social Committee and the Committee of Regions: Smart Grids: from innovation to deployment, COM/2011/0202, Brussels (April 12, 2011)

[2]   Directive 2009/72/EC of the European Parliament and of the Council of 13 July 2009 concerning common rules for the internal market in electricity and repealing Directive 2003/54/EC Text with EEA relevance. Official Journal L 211 (September 14, 2009)

[3] Krzysztof, P.: International legal instruments and recommendations concerning smart grid area. In: Materials for 9th Science and Technology Conference, PPM 2012, Krynica-Zdrój (2012)

[4] Waldemar, N.: Rozproszone systemy pomiarowe. Transport and Communication Publishers, Warszawa (2006)

[5] Wiesław, W.: Organizacja komputerowych systemów pomiarowych. Warsaw Technical University Publishing House, Warsaw (1997)

[6] Jacek, Ś., Marcin, T.: Technika smart meteringu, Warsaw (2010)

[7] Ryszard, M.: Integracja inteligentnych pomiar pomiarów zużycia energii elektrycznej, gazu, ciepła i wody. Polish Federation of Engineering Associations NOT, Warsaw (2009)

[8] Studium wdrożenia inteligentnego pomiaru energii elektrycznej w Polsce. Institute of Power Engineering, Branch in Gdansk, R&D Unit, Gdansk (2010)

[9] Suchanek, J.: Automatyzacja odczytów wskazań liczników energii elektrycznejw gospodarstwach domowych. Wiadomości Elektrotechniczne Magazine (4) (2004)

[10] Maćkowski, M.: The packet transmission in the GPRS, EDGE, UMTS networks in Real-Time measuring systems. Pomiary Automatyka Kontrola Magazine (06), 362–364 (2008)

[11] Kocot, M., Olszyna, J., Winiecki, W.: Remotely configurable distributed measurement system. Pomiary Automatyka Kontrola Magazine (09), 792–794 (2012)

[12] Topór-Kamiński, T., Żurkowski, R., Grygiel, M.: Selected methods of measuring the delay in data transmission systems with wireless network interfaces. Acta Phys. Pol. A 120(4), s.748–s.754 (2011)

[13] Topór-Kamiński, T., Krupanek, B., Homa, J.: Delays models of measurement and control data transmission network. In: Nawrat, A., Simek, K., Świerniak, A. (eds.) Advanced Technologies for Intelligent Systems of National Border Security. SCI, vol. 440, pp. 257–278. Springer, Heidelberg (2013)

[14] Iwaneczko, P., Jędrasiak, K., Daniec, K., Nawrat, A.: A prototype of unmanned aerial vehicle for image acquisition. In: Bolc, L., Tadeusiewicz, R., Chmielewski, L.J., Wojciechowski, K. (eds.) ICCVG 2012. LNCS, vol. 7594, pp. 87–94. Springer, Heidelberg (2012)

[15] Czornik, A., Niezabitowski, M.: Lyapunov exponents for systems with unbounded coefficients. Dynamical Systems: An International Journal (2012)

[16] Czornik, A., Nawrat, A., Niezabitowski, M.: On the Lyapunov exponents of a class of second-order discrete time linear systems with bounded perturbations. Dynamical Systems: An International Journal (2012)

[17] Czornik, A., Niezabitowski, M.: On the spectrum of discrete time-varying linear systems. Nonlinear Analysis: Hybrid Systems 9, 27–41 (2013)

Technology Development of Military Applications of Unmanned Ground Vehicles

Tomasz Czapla and Józef Wrona

Abstract. The paper presents history, current state of knowledge and future perspectives of unmanned technology application for military ground vehicles. As the first, the beginning and evolution of unmanned technology from on remote control based solutions to autonomous ones is described. Then classification and overview of systems currently manufactured and developed. At the end of the paper perspectives and directions of unmanned ground vehicles development is presented.

1   Introduction

The first military applications of unmanned ground vehicles appeared in nineteenth century. Just now they assists the commander and the warriors during execution of dangerous tasks at the more and more complex battlefield. The field of abilities of the unmanned military systems is very wide. They are able to transport equipment, carry some weapons, collect intelligence information, detect the threats, etc. Technology development has an great impact on these abilities and thus possibilities of usage of these systems.

   We can observe incremental innovations in the area of these systems rather than radical or even revolutionary (Arditi, D., Kale, S., and Tangkar M., 1997). Theirs development is depended on some factors such as technology development and needs to achieve new capabilities that are able to fight against threats of the

Tomasz Czapla
Silesian University of Technology, Faculty of Mechanical Engineering, Division of
Theoretical and Applied Mechanics, ul. Konarskiego 18A, 44-100 Gliwice, Poland
e-mail: `jwrona@wat.edu.pl`, `tomasz.czapla@polsl.pl`

Józef Wrona
Military University of Technology,
ul. gen. Sylwestra Kaliskiego 2, 00-908 Warsaw, Poland
Industrial Research Institute for Automation and Measurements,
Aleje Jerozolimskie 2022, 02-486 Warsaw, Poland

current battlefield. It is very difficult to discuss with the military budgets impact on these area because in this case the main issue is soldier protection.

Asymmetric character of contemporary warfare causes imbalance in the means of power, resources and costs resulted from this asymmetry. In consequence, armed forces need to develop complex and expensive operational capabilities and their application methods in order to fight against relatively simple and inexpensive techniques used by irregular enemy troops or terrorists.

The efforts focused on unmanned military vehicles had been taken up far before the IEDs threat occurred, what is described in the paper (Saska, Krzystała, Mężyk., 2011). There are several projects on military unmanned vehicles also performed in Poland (Mężyk, Nawrat, 2011).

2   History and Classification

The first success in the field of unmanned vehicles technology was achieved by Nicolae Tesla, Serbian inventor living in USA. In 1898 Tesla has built two remotely controlled boats. Six feet long vehicles were built of steel and equipped with electromechanical radio receiver with actuators connected to the steering system. Boats were called "teleautomatons" and had electric propulsion system (Fig. 1a). Despite the fact that inventor tried to offer the vehicle to the military authorities in USA and Great Britain, they shown no interest in using new technology. Over 30 years later German navy was using radio controlled boats developed from cable-controlled boats FL-7 from 1917 (Tesla, 1898).

Tesla predicted further development of unmanned vehicles and described it in his diary: **„Telautomata will be ultimately produced, capable of acting as if possessed of their own intelligence, and their advent will create a revolution"** (Tesla, 1898). Modern unmanned vehicles are becoming to resemble Tesla's vision.
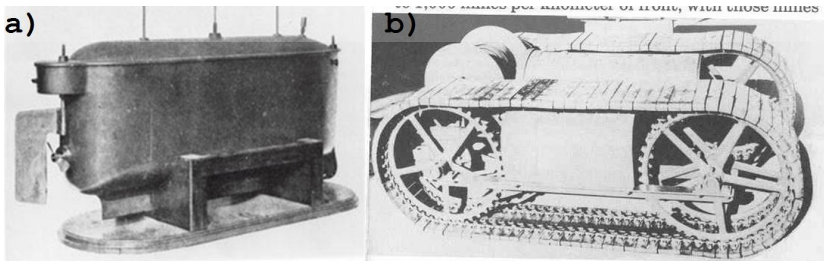
Fig. 1. The first two unmanned vehicles: a) Teleautomaton – Tesla's unmanned boat, b) Wikesham's land torpedo (sources: Tesla, 1921, Wikersham 1922)

In 1928 Elmer E. Wikersham (1922) has patented unmanned ground vehicle that was intended to provide explosives to the target (Fig. 1b). Vehicle remained a prototype but it should be mentioned that idea of the landmine was an answer for position warfare and "trench to trench" tactics.

The experience gained from position warfare (First World War in Europe 1914-1918 and Russian-Japanese or Chinese-Japanese wars in Asia) have led to development of remotely controlled ground vehicles intended to provide explosives to the enemy fortifications as a main purpose.

The idea of creation the first advanced Japanese unmanned ground vehicle had origin on 22th of February 1932 in the battle for Miaohangchen near Shanghai. During the battle, three Japanese soldiers crawled towards the Chinese fortifications and detonated explosives carried on themselves. The suicide attack allowed to break through the enemy positions but was criticized by General Reikichi Tada as the waste of live the Japanese soldiers. As a supervisor of secret new technologies testing division he started the program that effected with building a series of unmanned military ground vehicles including Yi-Go as the first of them. The first and smallest vehicle carried 35 kg of explosives in front compartment. Two electric motors, 2hp each with were mounted in rear section of the vehicle. Total weight was 200 kgs and top speed in off-road conditions was 4 kph (Jabłoński J.).
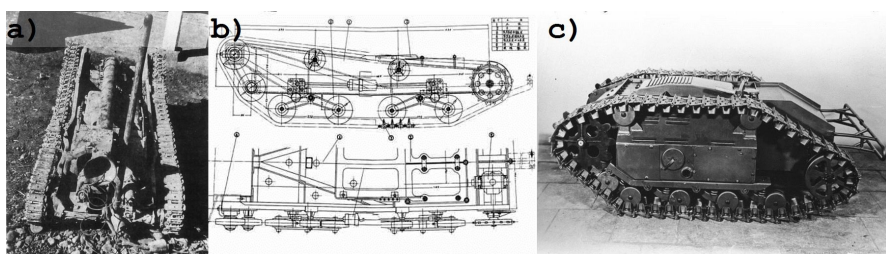
Fig. 2. Japanese and German self-propelled landmines: a) Mobile mine Yi-Go in version Ko, b) The scheme of mobile mine in version Ko, c) SdKfz. 302 Goliath (sources: Jabłoński, Wikimedia)

Similar vehicle, SdKfz. 302 Goliath, was built by Germans and militarily used in Second World War. The vehicle was based on the project of French engineer Adolphe Kegresse. Total mass of carried explosives was 100 kg with total weight 430 kgs. Vehicle was cable-controlled from maximum distance 650 m.

Fig. 3. Teletank TT-26 (sources: Бронетехника в Фотографиях, Военный Альбом)

The front section contained explosives, middle section engines and propulsion system, rear one cable drum. First versions of the vehicle were equipped with electric motors, later were replaced (SdKfz. 303) with internal combustion engine. High manufacturing cost, low armor protection, high control-cable vulnerability and low top speed (11.5 km/h) caused that the vehicle was not used for destroying tanks as it was originally intended to (Skotnicki M.). That is why it is very important to determine in the beginning of the designing process the Concept of Operations (CONOPS) with the requirements that should fulfill the system.

In The Soviet Army unmanned ground platforms were build basing on modified T-26 tanks. Radio controlled tanks were renamed to TT-26. Vehicles are shown in Fig.3. Tanks were equipped with lamp radio receiver and pneumatic actuators. Despite installing remotely controlled steering system, manned operation remained available for modified tanks. The main purpose of the vehicle was carrying chemical weapons system towards enemy positions without exposing own personnel for risk. There was also version carrying explosives as payload.

Two battalions were equipped with TT-26 "Teletanks", first one was destroyed during first months of war. Second one was engaged in battle of Moscow but remote control equipment was unmounted and tanks were manned operated (Широкорад, 2005).

Described above "Teletank" TT-26 was an universal military platform equipped with modern technology that allowed to extend the application area by unmanned operation mode ability with preserving full functionality as a manned vehicle.

The research on unmanned autonomous vehicles was started in late 60's of 20 century. As a part of artificial intelligence application for controlling the vehicles, a mobile robot SHAKEY fig. 4 was funded by Defense Advanced Research Projects Agency (DARPA) and developed at Stanford Research Institute. SHAKEY was equipped with a TV camera, ultrasonic range sensors and touch sensors connected by radio link with central computer performing navigation and exploration tasks.

Fig. 4. SHAKEY (source: Hoggett R., 2005)

SHAKEY was able to perform simple operations like route following or navigation and also advanced missions provided by user (Hoggett, 2005).

The overview of the unmanned vehicles show their evolution from simple cable-controlled or radio-controlled machines to the robot with some level of autonomy. The variety of unmanned vehicles used in military application caused the need of classification for different categories.

Examples of different types Unmanned Ground Vehicles used to perform specific tasks in military operations include: UGVs used as a support of dismounted soldiers by performing tasks like: reconnaissance, surveillance, door breach, smoke generation, etc. These UGVs can be carried by soldiers themselves. Next type of UGV is dedicated for use as transporters for supplying distant posts or carrying equipment during troops movement or as armed reconnaissance vehicles that are able to fire their weapon via C4ISR network with the man in-the-loop. These vehicles are larger in size and could not be carried by soldiers. Third group can be described as unmanned ground combat vehicles that are able to use their weapon in autonomous mode (Munk, 2003).

More detailed classification of Unmanned Ground Vehicles was proposed by U.S. Army Developmental Test Command (2009). There are three categories of UGVs based upon size (Fig. 5), mode of operation(Fig. 6), and weapon type (Fig. 7).

Category	Sub-category	Description
Mode of Operation	Tethered	Mode with direct, wired connection demanding line of sight (LOS) maintenance (except certain applications - tunnel, pipe operations). Human operator controls 100% actions performed by the vehicle
	Remote Controlled	Mode with human operator fully controlling the vehicle without gaining information from UGV's sensors thus LOS has to be maintained. Human operator controls 100% actions performed by the vehicle
	Tele-operated	Mode with human operator fully controlling the vehicle with feedback provided by UGV's sensors (i.e. video, audio, laser). Human operator controls 100% actions performed by the vehicle. Does not demand LOS
	Autonomous	Mode of control that does not demand human operator interaction during the mission. Operator can program the mission before an action
	Semi-autonomous	Mode with at least one autonomously controlled function. Level of autonomy could vary for different UGVs. Usually operator interaction is used to control weapon
	Manned	Mode with direct human control with operator onboard

Fig. 5. Unmanned Ground Vehicles classification based on mode of operation
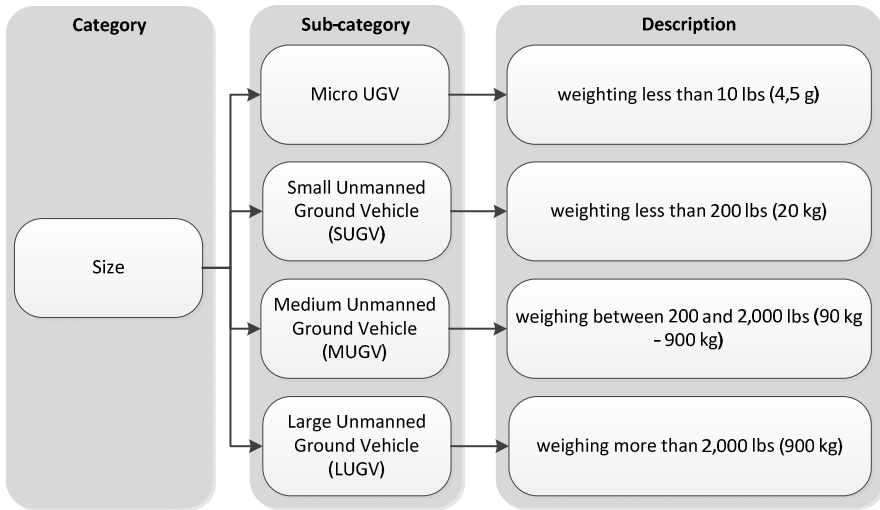
Fig. 6. Unmanned Ground Vehicles classification based on size
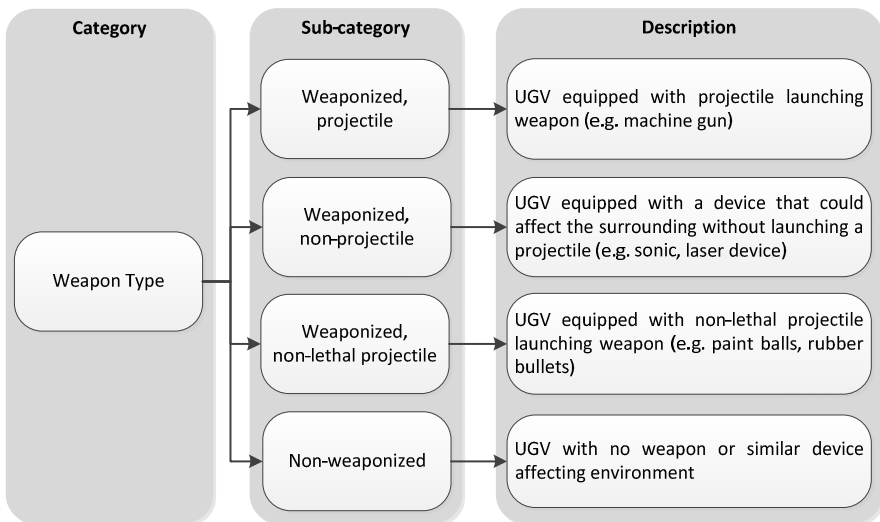
Fig. 7. Unmanned Ground Vehicles classification based on weapon type

3   Unmanned Ground Vehicles Overview

There are several types of unmanned vehicles currently used and developed. First group described below consists of mine clearing and multipurpose engineering vehicles. Panther, Dok-Ing, Digger and ARTS could be remotely controlled or tele-operated without advanced autonomous control systems onboard. Second group contains mainly autonomous vehicles at various stage of development.

3.1 Panther

The M1 Panther II was based on modified hull of M1 Abrams main battle tank (Fig. 8a). The vehicle destination is breaching minefields in combat conditions. The Panther II is capable to clear 4600 m2 of minefield in an hour. Panther II can be equipped with mine rollers exploding mines without causing a damage for the vehicle or mine plough pushing mines to the direction of motion. Vehicle can be operated in manned mode and tele-operated. The maximum tele-operation with using CCTV control system distance is 780 m. Vehicle is armed with 7.62 mm machine gun for self-defense (Military-Today). Summarized technical data of Panther II UGV are shown in Table 1.

Table 1. Panther II technical data

Weight	43700 kg
Length x Width x Height	~8 x ~3.8 x ~1.85 m
Engine power	1500 hp
Max speed	~72 km/h
Range	~500 km
Gradient/side slope	60/40 %
Vertical step	1.2 m
Trench	2.75 m
Fording	~1.5m
Mode of operation	Manned, tele-operated

3.2 Dok-Ing

Dok – Ing mine clearing vehicles are tracked, remotely controlled with no visual sensor feedback from the vehicle (Fig. 8b). Machines are able to clear anti-personnel and withstand explosion of anti-tank mines. There are two types of vehicle: MV-4 and larger MV-10. Platforms could be remotely controlled from an armored vehicles or from the ground. Smaller machine can clear house yards, forest paths, river banks and other types of the terrain inaccessible for larger vehicles. MV-4 has 944 – 2184 m²/hour mine clearing capacity, MV-10 is able clear 5000 m² per hour.

The MV-10 uses two kinds of equipment: rotating flail tool for activating the anti-personnel and anti-tank mines and rotating tiller for secondary clearance and also for maintaining the digging depth on a constant level. Both tools can operate simultaneously or independently (Dok-Ing). The technical data of Dok-Ing MV-4 and MV-10 are shown in Table 2.

Table 2. Technical data of Dok-Ing vehicles

Vehicle model	MV-4	MV-10
Weight	55600 kg	189600 kg
Length x Width x Height	4455 x 2015 x 1470 mm	4606 x 2240 x 2100 mm
	5145 x 2015 x 1470 mm (with pulled in and extended clearing arm)	7226 x 2975 x 2129 mm (prime mover without and with tool)
Engine power	129kW (173,82HP)	571kW (760HP)
Max speed	5 km/h	10 km/h
Endurance	2.8 – 4.6 h	9.5 – 19 h
Gradient/side slope		37deg/25deg
Vertical step		
Trench		
Fording		
Mode of operation	Remotely controlled	Remotely controlled

3.3 Digger D-3

The Digger D-3 demining vehicle is designated for mine clearance and also for land preparation, vegetation clearance and area reduction (Fig. 8c). It can be equipped with flail and tiller in mine clearing configuration or standard tools like shovel, fork etc. Vehicle is dedicated to use in heavy conditions: ambient temperature up to 50 degrees. Platform is dedicated to clear the anti-personnel mines but it's hull can withstand an explosion of anti-tank mine. Maximum mine clearing capability is 2000 m2/h at 13 cm depth. The vehicle can be remotely controlled from maximum distance of 500 m (Digger DTR). Technical data of Digger D-3 vehicles are collected in Table 3.

Table 3. Technical data of Digger D-3 vehicle

Weight	8760/9225 kg (with flail/tiller)
Length x Width x Height	5730 x 1690 (2320 with tool) x 1890 mm
Engine power	129 kW/173HP
Max speed	7 km/h
Endurance	3.4 – 4.1 h
Gradient/side slope	35/30 degrees
Vertical step	
Trench	
Fording	
Mode of operation	Remotely controlled
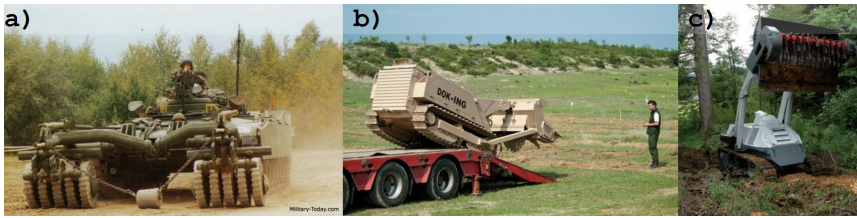
Fig. 8. Unmanned mine clearing vehicles: a) Panther II, b) Dok-Ing, c) Digger D3 (sources: Military-Today, Dok-Ing, Digger DTR)

3.4 All-Purpose Remote Transport System (ARTS)

ARTS is a remotely controlled tracked platform that could be used for mine clearing, hazardous material handling and removing of unexploded ordinance (Fig. 9a). As the vehicle is tele-operated, there is no risk for the personnel during its operation. System contains a prime mover which is a Posi-Track™ MD70 tractor, the Operator Control Unit and attachable tools including a brush cutter, a bucket, pallet forks, a backhoes, plow, a range clearance blade, and a water cannon (Fig. 9a). Operator gains an information from the vehicle through two cameras installed on the tractor directing forward and reward. The maximum distance between the operator and the vehicle is 3.2 km (All-Purpose Remote Transport System (ARTS) Capabilities Demonstration, 2002). Technical data of ARTS UGV are listed in Table 4.

Table 4. Technical data of ARTS vehicle

Weight	2948 kg
Length x Width x Height	2890 x 1670 x 1980 mm
Engine power	-
Max speed	12.9 km/h
Endurance	
Gradient/side slope	
Vertical step	
Trench	
Fording	
Mode of operation	Remotely controlled, teloperated

3.5 Crusher

The Crusher is a combat UGV currently developed at Carnegie Mellon University (National Robotics Engineering Center, Crusher). It is designed to comply the Armed Reconnaissance Vehicle program of Future Combat System (Fig. 9b). It can be armed with small weapon mounted on stabilized platform equipped with

FLIR and daylight camera for target acquisition. Surveillance system is mounted on a mast. The vehicle is equipped with series hybrid electric drive system with power station containing 60 kW diesel engine charging lithium-ion batteries and electric propulsion motors. Vehicles operation modes could vary from tele-operated to autonomous. Technical data are summarized in Table 5.

Table 5. Technical data of Crusher vehicle

|	
Weight	5987 kg
Length x Width x Height	5.1 x 2.59 x 1.52 m
Engine power	60 kW
Max speed	42 km/h
Endurance	
Gradient/side slope	40°/-
Vertical step	>1,22 m
Trench	>2.03 m
Fording	
Mode of operation	Tele-operated, autonomous

3.6 Gladiator

Gladiator is a wheeled multipurpose unmanned ground vehicle currently developed at Carnegie Mellon University (National Robotics Engineering Center, Gladiator). It is designated to perform combat, logistic, mine clearing and reconnaissance missions. Platform is supposed to accomplish its missions with using various sensors: daylight and infrared cameras, laser rangefinder, acoustic sensors and GPS. Vehicle will be able to use M240G 7.63 machine gun and M249 5.56 mm squad automatic weapon for direct fire. As a transport platform it will carry weapons, ammunition, supplies and wounded personnel. Technical data of the Gladiator vehicle are shown in Table 7.

Table 6. Technical data of Gladiator vehicle

Weight	1270 kg
Length x Width x Height	2.03 x 1.29 x 1.52 m
Engine power	
Max speed	33 km/h
Endurance	24 h including 8 h travel and 16 h stationary surveillance
Gradient/side slope	
Vertical step	
Trench	
Fording	
Mode of operation	Tele-operated, autonomous

3.7   MDARS

Mobile Detection Assessment Response System (MDARS) was developed by General Dynamics Robotic Systems. The platform remains in service with the U.S. Department of Energy and the U.S. Army. MDARS can be tele-operated and work in autonomous mode, up to 16 vehicles can be controlled by a single operator. The vehicle is equipped with all-around obstacle avoiding system (General Dynamics Robotic Systems). Technical data of the vehicle are provided in Table 7.
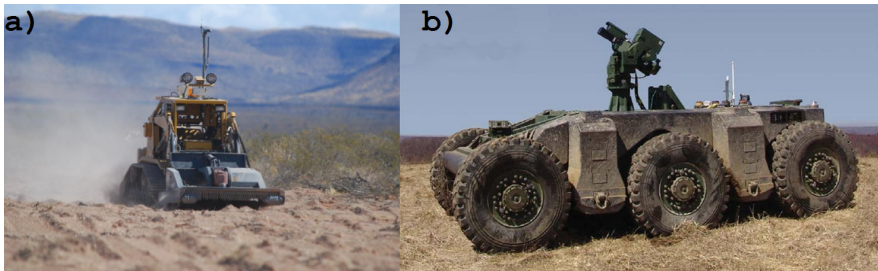
Fig. 9. Unmanned ground vehicles: a) ARTS, b) Crusher (sources: U.S. Army, Hightech-Edge)

Table 7. Technical data of MDARS vehicle

|	
Weight	1360 kg
Length x Width x Height	2.92 x 1.64 x 2.62 m
Engine power	
Max speed	32.1 km/h
Endurance	16 h
Gradient/side slope	
Vertical step	
Trench	
Fording	
Mode of operation	Tele-operated, autonomous

3.8   MULE

Multifunctional Utility/Logistics & Equipment Armed Robotic Vehicle - Assault (Light) (MULE ARV-A(L)) is a multipurpose UGV currently developed by Lockheed Martin Missiles and Fire Control Systems (Global Security). The MULE complies with Future Combat System and has three variants: transport version (MULE-T), an Armed Robotic Vehicle - Assault (Light) (MULE ARV-A(L)), and a counter-mine vehicle (MULE-C). Since the FCS program was canceled in 2009, only the MULE ARV-A(L) is under development. Vehicle has in-hub mounted propulsion electric motors on each of six wheels. MULE can be equipped with an

M240 machine gun, Javelin missiles, and a sensor platform (with an electro-optical/infrared sensor). Technical data of described vehicle are shown in Table 8.

Fig. 10. Unmanned multi-purpose ground vehicles: a) Gladiator, b) MDARS, c) MULE (sources: Newton, 2011, Spawar Systems Center Pacific, Global Security)
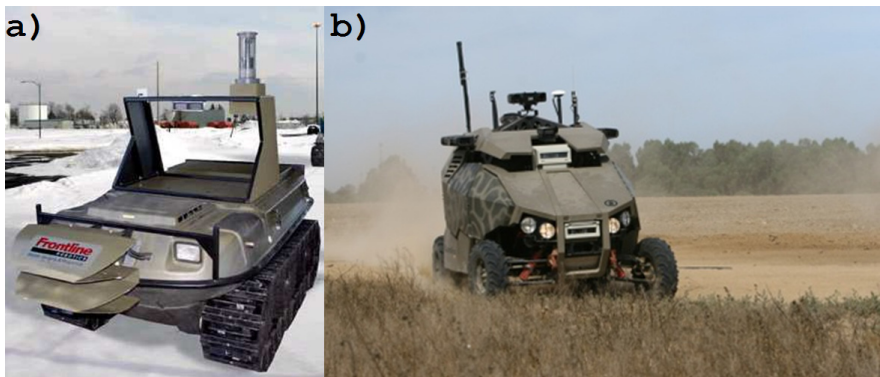
Fig. 11. Unmanned ground vehicles: a) GRUNT, b) Guardium (source: Frontline Robotics, G-NIUS Unmanned Ground Systems LTD)

3.9   GRUNT

The GRUNT (GRoundUniTs) wheeled vehicle was developed by Frontline Robotics. The platform is based on Argo All-Terrain-Vehicle using commercial solutions of sensors and PC-104 industrial computer. The vehicle works in autonomous mode and has radio communication systems. The GRUNT is equipped with all-around imaging cameras, night-vision sensors, radar, and a continuous navigation system. Technical data are listed in Table 9.The vehicle is shown in Fig. 11a.

Table 8. Technical data of MULE vehicle

Weight	2500 kg
Length x Width x Height	4.34 x 2.24 x 2.56 m
Engine power	
Max speed	32.1 km/h
Endurance	16 h
Gradient/side slope	40%/-
Vertical step	
Trench	
Fording	
Mode of operation	Tele-operated, autonomous

3.10 Black Knight
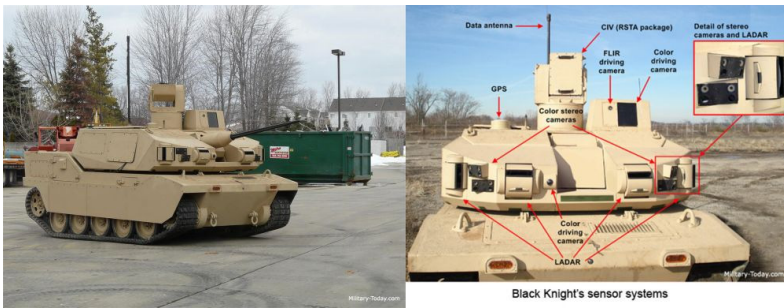
Fig. 12. Black Knight and its sensors

Table 9. Technical data of GRUNT vehicle

Weight	450 kg
Length x Width x Height	2.79 x 1.52 x 1.91 m
Engine power	
Max speed	30 km/h
Endurance	-
Gradient/side slope	15°/-
Vertical step	
Trench	
Fording	
Mode of operation	Tele-operated, autonomous

3.11 Guardium

Guardium, developed by G-NIUS Unmanned Ground Systems LTD, is intended to perform missions including convoy security, reconnaissance, surveillance, combat logistic support and also programmed patrols along border routes. Furthermore, it can autonomously respond. The vehicle is equipped with daylight and night-vision camera, metal detector and observation mast (Fig. 11b). A group of vehicles can also cooperate in the network. Vehicle can carry various types of equipment including weapon and non-lethal weapon systems. Platform can work in tele-operated and autonomous mode. Table 10 provides technical data of the vehicle.

Table 10. Technical data of Guardium vehicle

Weight	1400 kg
Length x Width x Height	2.95 x 1.8 x 2.2 m
Engine power	
Max speed	50 km/h
Endurance	24 h
Gradient/side slope	15°/-
Vertical step	
Trench	
Fording	
Mode of operation	Tele-operated, autonomous

Table 11. Technical data of Black Knight vehicle

Weight	9500 kg
Length x Width x Height	4.98 x 2.44 x 2 m
Engine power	300 hp
Max speed	77 km/h
Endurance	
Gradient/side slope	
Vertical step	
Trench	
Fording	
Mode of operation	Tele-operated, autonomous

The Black Knight was developed by BAE Systems (Military Today). The purpose of the vehicle is to show capabilities of unmanned tele-operated and autonomous performance. The vehicle could be used for reconnaissance, surveillance and investigation of hazardous areas. Human operator controlling the Black Knight is located inside Bradley guiding vehicle but there is also an option of control via portable device. In autonomous mode vehicle uses sensors like LADAR, thermal camera and GPS for maneuvering and avoiding obstacles (Fig. 12). The vehicle is equipped with 25 mm cannon and coaxial 7.62 mm gun.

Maneuverability of described vehicle allows it to follow the tanks. Technical data of described vehicle are shown in Table 11.

4   Perspectives and Directions of Unmanned Ground Vehicle Development

Asymmetry of contemporary battlefield causes losses not only in equipment but after all in soldiers. So, there is the reason for searching the ways of gaining advantage over the enemy by implementation modern technologies in military equipment and weapons system. New technologies are supposed to achieve the ability of detection, identification and elimination the threats of asymmetric warfare. The main issue is soldiers protection. Their operations in the dangerous areas should be minimized by implementing the unmanned systems: remotely controlled, automatic and in the most advanced solutions – autonomous. To be fully autonomous the artificial technology, navigation, communication techniques should be developed. It is very important to develop the power supply systems.

The lessons learned experiences gained in combat missions indicate the need of changing the concept of use the forces by development of new operational capabilities based on usage of newest technologies and techniques to defense against new threats like Improvised Explosive Devices (IEDs). IEDs being relatively cheap and simple technology of irregular troops or terrorists but one of the most dangerous threats of asymmetric warfare are able to cause heavy losses to regular forces. These and other threats determine the research efforts to develop the techniques and technologies involving unmanned ground vehicles applications. As they are exposed on risk of being destroyed in the explosion, they should be relatively inexpensive but on the other hand equipped with necessary set of sensors and effectors for proper navigation, reconnaissance, detection and elimination the threats and also efficient communication, control and propulsion system allowing to perform mission with minimum or without human interaction. To be relatively cheap it is worth to focus on modular solutions of the systems to make possible dedicated usage of unmanned ground systems. Finding compromise between these criteria is very difficult and demands building of interdisciplinary consortia of scientific and industrial entities. The permanent end user interaction in all phases of development process and also in the whole life cycle management of the system is necessary.

5   Summary

The current threats generate the need for new capabilities. There is a great impact of new technologies on military applications of unmanned ground vehicles. They create new areas of usage of these systems. Asymmetric warfare weapons like Improvised Explosive Devices determines requirements for UGVs.

There have been presented history, classifications and perspectives of UGVs in this paper. Then some examples of remote controlled, tele-operated and autonomous vehicles have been presented.

Considering advantages of unmanned system applications to the modern warfare and possible progress in remotely controlled and autonomous platforms we can summarize that they significantly reduce the human losses in nowadays conflicts. Evolution of unmanned military vehicles allows them to take up the missions currently reserved for manned solutions.

Application of unmanned vehicles allows to perform military operations in the areas inaccessible for human due to the chemical, biological, nuclear, thermal and other environmental hazards.

References

[1]   All-Purpose Remote Transport System (ARTS) Capabilities Demonstration

[2]   United States Army Communications-Electronic Command Research, Development & Engineering Center Fort Belvoir, Virginia 22060-5806 (2002), `http://www.itep.ws/pdf/ARTS.pdf`

[3]   Arditi, D., Kale, S., Tangkar, M.: Innovation in Construction Equipment and Its Flow into the Construction Industry. Journal of Construction Engineering and Management 123(4) (December 1997), Бронетехника в Фотографиях, `http://serkoff.narod.ru/photoalbum170.html`

[4]   Digger DTR, `http://www.digger.ch/`

[5]   Dok-Ing, `http://dok-ing.hr`

[6]   Frontline Robotics, `http://www.frontline-robotics.com`

[7]   G-NIUS Unmanned Ground Systems LTD, `http://www.g-nius.co.il`

[8]   General Dynamics Robotic Systems, `http://www.gdrs.com/robotics/programs/program.asp?UniqueID=27`

[9]   Global Security. Multifunction Utility/Logistics Equipment Vehicle (MULE) UGV (1 Ton)

[10] Robotic Infantry Support System (RISS), `http://www.globalsecurity.org/military/systems/ground/fcs-mule.htm`

[11] Hoggett, R.: 1967 – "Shakey" – Charles Rosen, Nils Nilsson, Bertram Raphael et al (American) (2005)

[12] Jabłoński J.: Japońskie goliatyYi-GO. Inne oblicza historii, `http://ioh.pl/artykuly/pokaz/japoskie-goliaty-yigo,1102/` Skotnicki M.: from Muzeum Wojska Polskiego, `http://www.muzeumwp.pl/emwpaedia/pojazd-gasienicowy-sd-kfz-303a-goliath.php.`

[13] Mężyk, A., Skowron, K.: Modern power transmission systems for tracked vehicles, High Speed Tracked Vehicles (Szybkobieżne Pojazdy Gąsienicowe) (31) nr. 3, 2012r., OBRUM sp. z o.o. Gliwice (November 2012)

[14] Mężyk, A., Nawrat, A.: APG - pierwszy polski pojazd gąsienicowy o napędzie hybrydowym. Rap. Wojsko Tech. Obron. nr. 10, s. (2011) 72-73 Military-Today

[15] Internet source, `http://www.military-today.com/engineering/m1_panther_2.htm` (visited January 05, 2013)

[16] Internet source, `http://www.military-today.com/apc/black_knight.htm` (visited January 05, 2013)

[17] Munk, S.: Information Capabilities for Robots of the Future Battlefield. Academic and Applied Research in Military Science (AARMS) 2(2), 199–208 (2003)

[18] National Robotics Engineering Center (NREC), Crusher Unmanned Combat Vehicle, `http://www.rec.ri.cmu.edu/projects/crusher`

[19] National Robotics Engineering Center (NREC), Gladiator, `http://www.rec.ri.cmu.edu/projects/flyer/gladiator.pdf`

[20] Newton, M.: Peaceful Robots Armed to the Teeth (2011), `http://www.annalsofamericus.com/terrordome-2-0/peaceful-robots-armed-to-the-teeth`

[21] Saska, P., Krzystała, E., Mężyk, A.: An analysis of an explosive shock wave impact onto military vehicles of contemporary warfare. J. Kones, Powertrain Transp. 18(1), 515–524 (2011)

[22] Spawar Systems Center Pacific, Mobile Detection Assessment and Response System (MDARS) `http://www.public.navy.mil/spawar/Pacific/Robotics/Pages/MDARS.aspx` Широкорад А. Б. Чудо-оружие СССР: Тайнысоветскогооружия. — М.: Вече (2005)

[23] Tesla, N.: Method of an Apparatus for Controlling Mechanism of Moving Vessels or Vehicles, U.S. Patent No. 613809 (1898), `http://cyberneticzoo.com/?p=1628`

[24] Tesla, N.: My Inventions (1921)

[25] Hightech-Edge. The Crusher – DARPAs Six Wheeled Autonomous Robot, `http://www.hightech-edge.com/crusher-darpa-autonomous-robot-iphone-xbox-controller/1417`

[26] U.S. Army, `http://usarmy.vo.llnwd.net/e2/-images/2009/02/19/30634/`

[27] U.S. Army Developmental Test Command. (2009, February 12). Testing of Unmanned Ground Vehicle (UGV) Systems (Test Operations Procedure (TOP) 2-2-540) (2009) Военный Альбом, `http://waralbum.ru/10342/`

[28] Wickersham, E.E.: Land Torpedo, U.S. Patent No. 1407989 (1922)

[29] Wikimedia, `http://upload.wikimedia.org/wikipedia/commons/c/cb/Bundesarchiv_Bild_146-1980-053-53%2C_Sprengpanzer_%22Goliath%22.jpg`

Estimation of Solution of Discrete Linear Time-Varying System

Adam Czornik, Aleksander Nawrat, and Michał Niezabitowski

Abstract. In this paper we propose the upper, and in some cases, lower bounds for norm of solution of linear discrete time-varying system by coefficients matrices. We show that our estimates have two merits. Firstly, we do not need to know eigenvalues or spectral norm of matrices because we can simply calculate it by matrix coefficients. Secondly, our bounds are also valid in case of singular matrices. Moreover, in the paper we present an upper estimate for stationary system.

Keywords: time-varying discrete linear systems, growth bounds, stability, Lyapunov exponents.

1 Introduction

Consider the linear discrete time-varying system

$$x(n+1) = A(n)x(n), n \geq 0 \tag{1}$$

where $A = (A(n))_{n \in N}$, $A(n) = [a_{ij}(n)]_{i,j=1,\ldots,s}$ is a sequence of s-by-s real matrices. By $\|\cdot\|$ we denote the Euclidean norm in R^s and the induced operator norm. The transition matrix is defined as

$$\mathscr{A}(m,k) = A(m-1)\ldots A(k)$$

for $m > k$ and $\mathscr{A}(m,m) = I$, where I is the identity matrix. For an initial condition x_0 the solution of (1) is denoted by $x(n,x_0)$ so

Adam Czornik · Aleksander Nawrat · Michał Niezabitowski
Silesian University of Technology, Institute of Automatic Control,
Akademicka 16 Street, 44-101 Gliwice
e-mail: {Adam.Czornik,Aleksander.Nawrat,
        Michal.Niezabitowski}@polsl.pl

$$x(n, x_0) = \mathscr{A}(n, 0) x_0.$$

The main result of this paper is to present an upper, and in some cases, a lower bound for norm of solution of system (1) by elements of matrices $A(n)$. Estimation problem of the solutions of continuous linear systems in terms of the coefficients is discussed in literature (for example see [1], Chapter IV, §6). The author shows on examples that is impossible to judge objectively, which of the presented there estimates is in general better. This problem is also discussed in [3], [15] and [16].

Estimation problem for the solution of dynamical systems is closely related to the concept of Lyapunov exponents. Now we present the definitions.

Let $a = (a(n))_{n \in \mathbb{N}}$ be a sequence of real numbers. The numbers (or the symbol $\pm\infty$) defined as

$$\lambda(a) = \limsup_{n \to \infty} \frac{1}{n} \ln |a(n)|$$

is called the characteristic exponent of sequence $(a(n))_{n \in \mathbb{N}}$.

For $x_0 \in \mathbb{R}^s, x_0 \neq \mathbf{0}$ the Lyapunov exponent $\lambda_A(x_0)$ of (1) is defined as characteristic exponent of $(\|x(n, x_0)\|)_{n \in \mathbb{N}}$, therefore

$$\lambda_A(x_0) = \limsup_{n \to \infty} \frac{1}{n} \ln \|x(n, x_0)\|.$$

It is well known [4] that the set of all Lyapunov exponents of system (1) contains at most s elements, say $-\infty < \lambda_1(A) < \lambda_2(A) < \ldots < \lambda_r(A) < \infty, r \leq s$ and the set $\{\lambda_1(A), \lambda_2(A), \ldots, \lambda_r(A)\}$ is called the spectrum of (1).

For exhaustive presentation of theory of Lyapunov exponents we recommend the following literature positions: [2], [4]. Problem of estimation of Lyapunov exponents is discussed in [5]-[9], [12]-[14] and [18].

In the paper we will also use the following conclusion from publication [10] and [11].

Theorem 1. *Suppose, that for system (1) we have*

$$\lim_{n \to \infty} A(n) = A. \tag{2}$$

Then, Lyapunov exponents of system (1) coincides with logarithms of moduli's eigenvalues of matrix A.

2   Main Results

Let introduce the following notations:

$$\bar{a}_{ij}(p) = \begin{cases} a_{ij}(p) & \text{for } i \neq j \\ a_{ii}(p) - 1 & \text{for } i = j \end{cases}, \tag{3}$$

$$\widetilde{a}_{ik}(p) = \begin{cases} a_{ik}(p) \text{ for } i \neq k \\ a_{ii}(p) + 1 \text{ for } i = k \end{cases}, \tag{4}$$

$$a_{jk}^{(i)}(p) = \overline{a}_{ij}(p)\widetilde{a}_{ik}(p), \tag{5}$$

$$b(p) = \frac{1}{2} \sum_{i,j,k=1}^{s} \left| a_{jk}^{(i)}(p) + a_{kj}^{(i)}(p) \right|. \tag{6}$$

The next Theorem contains the main result of our paper.

Theorem 2. *For any solution $x(n, x_0)$ of system (1) the estimate*

$$\|x(n+1, x_0)\|^2 \leq \|x_0\|^2 \prod_{p=0}^{n} (b(p) + 1), \tag{7}$$

is valid for any $n \in \mathbb{N}$. Moreover, if $b(n) < 1$ for all n, then

$$\|x_0\|^2 \prod_{p=0}^{n} (1 - b(p)) \leq \|x(n+1, x_0)\|^2 \tag{8}$$

is also valid for all $n \in \mathbb{N}$.

Proof. Take a solution of (1)

$$x(p, x_0) = [x_1(p), ..., x_s(p)]^T$$

with nonzero initial condition. We have

$$x_i(p+1) = \sum_{j=1}^{s} a_{ij}(p)x_j(p), \ i = 1, ..., s$$

and

$$x_i(p+1) - x_i(p) = \sum_{j=1}^{s} \overline{a}_{ij}(p)x_j(p),$$

$$x_i(p+1) + x_i(p) = \sum_{k=1}^{s} \widetilde{a}_{ik}(p)x_k(p).$$

Multiplying the last two identities we obtain

$$x_i^2(p+1) - x_i^2(p) = \sum_{j,k=1}^{s} \overline{a}_{ij}(p)\widetilde{a}_{ik}(p)x_j(p)x_k(p) = \sum_{j,k=1}^{s} a_{jk}^{(i)}(p)x_j(p)x_k(p).$$

Adding up these equalities for $i = 1, \dots, s$ we get

$$\|x(p+1)\|^2 - \|x(p)\|^2 = \sum_{i,j,k=1}^{s} a_{jk}^{(i)}(p)x_j(p)x_k(p)$$

and therefore

$$\left| \|x(p+1)\|^2 - \|x(p)\|^2 \right| \leq \frac{1}{4} \sum_{i,j,k=1}^{s} \left| a_{jk}^{(i)}(p) + a_{kj}^{(i)}(p) \right| \left(x_j^2(p) + x_k^2(p) \right) \leq$$

$$\frac{1}{2} \sum_{i,j,k=1}^{s} \left(\left| a_{jk}^{(i)}(p) + a_{kj}^{(i)}(p) \right| x_j^2(p) \right) \leq$$

$$\frac{1}{2} \left(\sum_{j=1}^{s} x_j^2(p) \right) \sum_{i,j,k=1}^{s} \left| a_{jk}^{(i)}(p) + a_{kj}^{(i)}(p) \right| = \|x(p)\|^2 b(p).$$

Now, for natural $p = 0, \ldots, n$ the following inequality

$$- \|x(p)\|^2 b(p) \leq \|x(p+1)\|^2 - \|x(p)\|^2 \leq \|x(p)\|^2 b(p)$$

holds.

Dividing the last inequality by $\|x(p)\|^2$ we obtain

$$-b(p) \leq \frac{\|x(p+1)\|^2}{\|x(p)\|^2} - 1 \leq b(p),$$

and therefore

$$\prod_{p=0}^{n} (1 - b(p)) \leq \frac{\|x(n+1)\|^2}{\|x(0)\|^2} \leq \prod_{p=0}^{n} (1 + b(p))$$

Finally, multiplying the last inequality by $\|x(0)\|^2$, our upper (7) and lower (8) estimates follow immediately what ends the proof.

The next four examples illustrate our estimates.

Example 1. Consider system (1) with $(A(n))_{n \in N}$ given by

$$A(n) = \begin{bmatrix} \sqrt{2}\sin n & \frac{1}{n^3+10} \\ \frac{1}{n^2+20} & \sqrt{2}\cos n \end{bmatrix}.$$

Namely, its elements are as follows

$$\begin{array}{ll} a_{11}(n) = \sqrt{2}\sin n & a_{12}(n) = \frac{1}{n^3+10} \\ a_{21}(n) = \frac{1}{n^2+20} & a_{22}(n) = \sqrt{2}\cos n \end{array}.$$

Applying the above-mentioned elements of $(A(n))_{n \in N}$ to (3) and (4) we obtain (5) in the following form

$$a_{11}^{(1)}(n) = \bar{a}_{11}(n)\tilde{a}_{11}(n) = (a_{11}(n))^2 - 1 = 2\sin^2 n - 1$$

$$a_{12}^{(1)}(n) = \bar{a}_{11}(n)\tilde{a}_{12}(n) = (a_{11}(n) - 1)\, a_{12}(n) = \frac{\sqrt{2}\sin n - 1}{n^3 + 10}$$

$$a_{21}^{(1)}(n) = \bar{a}_{12}(n)\tilde{a}_{11}(n) = a_{12}(n)\,((a_{11}(n)) + 1) = \frac{\sqrt{2}\sin n + 1}{n^3 + 10}$$

$$a_{22}^{(1)}(n) = \bar{a}_{12}(n)\tilde{a}_{12}(n) = (a_{12}(n))^2 = \frac{1}{(n^3 + 10)^2}$$

$$a_{11}^{(2)}(n) = \bar{a}_{21}(n)\tilde{a}_{21}(n) = (a_{21}(n))^2 = \frac{1}{(n^2 + 20)^2}$$

$$a_{12}^{(2)}(n) = \bar{a}_{21}(n)\tilde{a}_{22}(n) = a_{21}(n)\,(a_{22}(n) + 1) = \frac{\sqrt{2}\cos n + 1}{n^2 + 20}$$

$$a_{21}^{(2)}(n) = \bar{a}_{22}(n)\tilde{a}_{21}(n) = (a_{22}(n) - 1)\, a_{21}(n) = \frac{\sqrt{2}\cos n - 1}{n^2 + 20}$$

$$a_{22}^{(2)}(n) = \bar{a}_{22}(n)\tilde{a}_{22}(n) = (a_{22}(n))^2 - 1 = 2\cos^2 n - 1$$

Because,

$$b(n) = \frac{1}{2} \sum_{i,j,k=1}^{s} \left| a_{jk}^{(i)}(n) + a_{kj}^{(i)}(n) \right| =$$

$$\frac{1}{2}\left[\left| a_{11}^{(1)}(n) + a_{11}^{(1)}(n) \right| + \left| a_{12}^{(1)}(n) + a_{21}^{(1)}(n) \right| + \left| a_{21}^{(1)}(n) + a_{12}^{(1)}(n) \right| + \right.$$

$$\left| a_{22}^{(1)}(n) + a_{22}^{(1)}(n) \right| + \left| a_{11}^{(2)}(n) + a_{11}^{(2)}(n) \right| + \left| a_{12}^{(2)}(n) + a_{21}^{(2)}(n) \right| +$$

$$\left. \left| a_{21}^{(2)}(n) + a_{12}^{(2)}(n) \right| + \left| a_{22}^{(2)}(n) + a_{22}^{(2)}(n) \right| \right]$$

$$\frac{1}{2}\left[\left| 2\sin^2 n - 1 + 2\sin^2 n - 1 \right| + \left| \frac{\sqrt{2}\sin n - 1}{n^3 + 10} + \frac{\sqrt{2}\sin n + 1}{n^3 + 10} \right| + \right.$$

$$\left| \frac{\sqrt{2}\sin n + 1}{n^3 + 10} + \frac{\sqrt{2}\sin n - 1}{n^3 + 10} \right| + \left| \frac{1}{(n^3 + 10)^2} + \frac{1}{(n^3 + 10)^2} \right| +$$

$$\left| \frac{1}{(n^2 + 20)^2} + \frac{1}{(n^2 + 20)^2} \right| + \left| \frac{\sqrt{2}\cos n + 1}{n^2 + 20} + \frac{\sqrt{2}\cos n - 1}{n^2 + 20} \right| +$$

$$\left. \left| \frac{\sqrt{2}\cos n - 1}{n^2 + 20} + \frac{\sqrt{2}\cos n + 1}{n^2 + 20} \right| + \left| 2\cos^2 n - 1 + 2\cos^2 n - 1 \right| \right] =$$

$$\frac{1}{2}\left[4\left| \sin^2 n - \frac{1}{2} \right| + \frac{4\sqrt{2}}{n^3 + 10}|\sin n| + \frac{2}{(n^3 + 10)^2} \right.$$

$$\frac{2}{(n^2+20)^2} + \frac{4\sqrt{2}}{n^2+20}|\cos n| + 4\left|\cos^2 n - \frac{1}{2}\right|\right] =$$

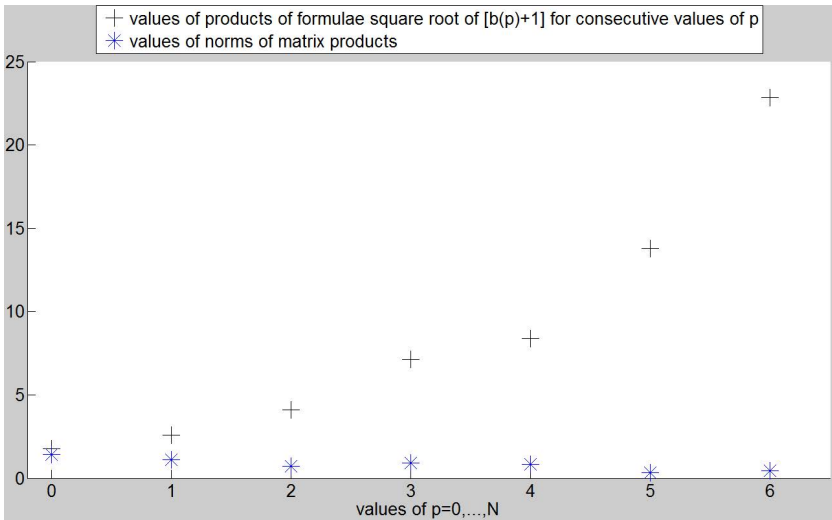$$2\left|\sin^2 n - \frac{1}{2}\right| + \frac{2\sqrt{2}}{n^3+10}|\sin n| + \frac{1}{(n^3+10)^2} +$$

$$\frac{1}{(n^2+20)^2} + \frac{2\sqrt{2}}{n^2+20}|\cos n| + 2\left|\cos^2 n - \frac{1}{2}\right|$$

varies between 0 and 2.5 it implies that for any solution $x(n,x_0)$ of system (1) only the upper estimate (7)

$$\|x(n+1,x_0)\| \leq \|x_0\| \prod_{p=0}^{n} \sqrt{(b(p)+1)}$$

is valid for all n. The numerical values of the solution and bound are presented in Figure (1)

Fig. 1. Our upper estimate and values of norms of matrix products

From this example we can only estimate an upper bound for growth rate.

Example 2. Consider system (1) with $(A(n))_{n \in N}$ given by

$$A(n) = \begin{bmatrix} \sin n & \frac{1}{n^3+10} \\ \frac{1}{n^2+20} & \cos n \end{bmatrix}.$$

Namely, its elements are as follows

$$a_{11}(n) = \sin n \quad a_{12}(n) = \frac{1}{n^3+10}$$
$$a_{21}(n) = \frac{1}{n^2+20} \quad a_{22}(n) = \cos n.$$

Applying the above-mentioned elements of $(A(n))_{n \in N}$ to (3) and (4) we obtain (5) in the following form

$$a_{11}^{(1)}(n) = \bar{a}_{11}(n)\tilde{a}_{11}(n) = (a_{11}(n))^2 - 1 = \sin^2 n - 1$$

$$a_{12}^{(1)}(n) = \bar{a}_{11}(n)\tilde{a}_{12}(n) = (a_{11}(n) - 1)\, a_{12}(n) = \frac{\sin n - 1}{n^3 + 10}$$

$$a_{21}^{(1)}(n) = \bar{a}_{12}(n)\tilde{a}_{11}(n) = a_{12}(n)\,((a_{11}(n)) + 1) = \frac{\sin n + 1}{n^3 + 10}$$

$$a_{22}^{(1)}(n) = \bar{a}_{12}(n)\tilde{a}_{12}(n) = (a_{12}(n))^2 = \frac{1}{(n^3 + 10)^2}$$

$$a_{11}^{(2)}(n) = \bar{a}_{21}(n)\tilde{a}_{21}(n) = (a_{21}(n))^2 = \frac{1}{(n^2 + 20)^2}$$

$$a_{12}^{(2)}(n) = \bar{a}_{21}(n)\tilde{a}_{22}(n) = a_{21}(n)\,(a_{22}(n) + 1) = \frac{\cos n + 1}{n^2 + 20}$$

$$a_{21}^{(2)}(n) = \bar{a}_{22}(n)\tilde{a}_{21}(n) = (a_{22}(n) - 1)\, a_{21}(n) = \frac{\cos n - 1}{n^2 + 20}$$

$$a_{22}^{(2)}(n) = \bar{a}_{22}(n)\tilde{a}_{22}(n) = (a_{22}(n))^2 - 1 = \cos^2 n - 1$$

Despite the fact that

$$b(n) = \frac{1}{2} \sum_{i,j,k=1}^{s} \left| a_{jk}^{(i)}(n) + a_{kj}^{(i)}(n) \right| =$$

$$\frac{1}{2}\left[\left| a_{11}^{(1)}(n) + a_{11}^{(1)}(n) \right| + \left| a_{12}^{(1)}(n) + a_{21}^{(1)}(n) \right| + \left| a_{21}^{(1)}(n) + a_{12}^{(1)}(n) \right| + \right.$$

$$\left| a_{22}^{(1)}(n) + a_{22}^{(1)}(n) \right| + \left| a_{11}^{(2)}(n) + a_{11}^{(2)}(n) \right| + \left| a_{12}^{(2)}(n) + a_{21}^{(2)}(n) \right| +$$

$$\left. \left| a_{21}^{(2)}(n) + a_{12}^{(2)}(n) \right| + \left| a_{22}^{(2)}(n) + a_{22}^{(2)}(n) \right| \right] =$$

$$\frac{1}{2}\left[\left| \sin^2 n - 1 + \sin^2 n - 1 \right| + \left| (\sin n - 1)\frac{1}{n^3 + 10} + (\sin n + 1)\frac{1}{n^3 + 10} \right| + \right.$$

$$\left| (\sin n + 1)\frac{1}{n^3 + 10} + (\sin n - 1)\frac{1}{n^3 + 10} \right| + \left| \frac{1}{(n^3 + 10)^2} + \frac{1}{(n^3 + 10)^2} \right| +$$

$$\left| \frac{1}{(n^2 + 20)^2} + \frac{1}{(n^2 + 20)^2} \right| + \left| \frac{1}{n^2 + 20}(\cos n + 1) + \frac{1}{n^2 + 20}(\cos n - 1) \right| +$$

$$\left| \frac{1}{n^2+20}(\cos n - 1) + \frac{1}{n^2+20}(\cos n + 1) \right| + \left| \cos^2 n - 1 + \cos^2 n - 1 \right| \right] =$$

$$\frac{1}{2}\left[2\left|\sin^2 n - 1\right| + 2\left|\frac{\sin n}{n^3+10}\right| + 2\left|\frac{\sin n}{n^3+10}\right| + 2\left|\frac{1}{(n^3+10)^2}\right| + $$

$$2\left|\frac{1}{(n^2+20)^2}\right| + 2\left|\frac{\cos n}{n^2+20}\right| + 2\left|\frac{\cos n}{n^2+20}\right| + 2\left|\cos^2 n - 1\right| \right] =$$

$$\left|\sin^2 n - 1\right| + 2\left|\frac{\sin n}{n^3+10}\right| + \frac{1}{(n^3+10)^2} + $$

$$\frac{1}{(n^2+20)^2} + 2\left|\frac{\cos n}{n^2+20}\right| + \left|\cos^2 n - 1\right|$$

are more and more smaller but always greater than 1, it implies that for any solution $x(n,x_0)$ of system (1) only the upper estimate (7)

$$\|x(n+1,x_0)\| \le \|x_0\| \prod_{p=0}^{n} \sqrt{(b(p)+1)}$$

is valid for all n. The numerical values of the solution and bound are presented in Figure (2)
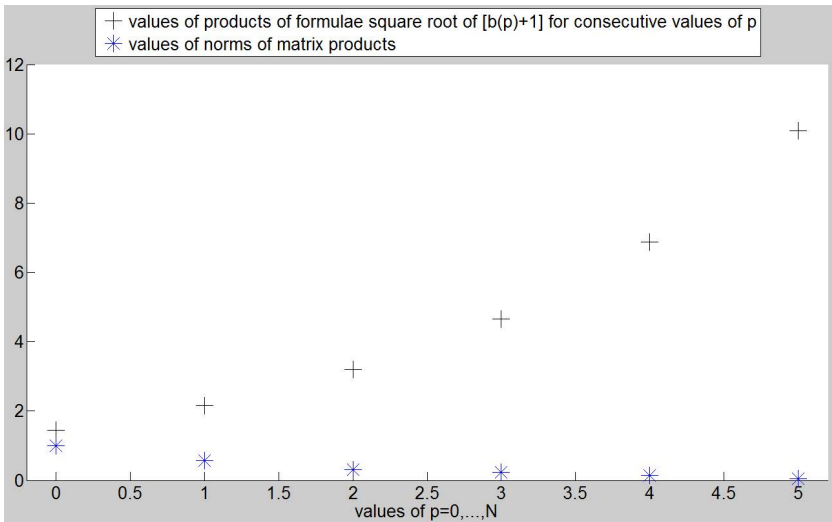

Fig. 2. Our upper estimate and values of norms of matrix products

As previously, we can only estimate an upper bound for growth rate.

Example 3. Consider system (1) with $(A(n))_{n \in N}$ given by

$$A(n) = \begin{bmatrix} \frac{\sin n}{5} + 1 & \frac{1}{n+10} \\ \frac{1}{n+20} & \frac{\cos n}{5} + 1 \end{bmatrix}.$$

Namely, its elements are as follows

$$\begin{array}{ll} a_{11}(n) = \frac{\sin n}{5} + 1 & a_{12}(n) = \frac{1}{n+10} \\ a_{21}(n) = \frac{1}{n+20} & a_{22}(n) = \frac{\cos n}{5} + 1 \end{array}.$$

Applying the above-mentioned elements of $(A(n))_{n \in N}$ to (3) and (4) we obtain (5) in the following form

$$a_{11}^{(1)}(n) = \bar{a}_{11}(n)\tilde{a}_{11}(n) = (a_{11}(n))^2 - 1 = \frac{\sin^2 n + 10\sin n}{25}$$

$$a_{12}^{(1)}(n) = \bar{a}_{11}(n)\tilde{a}_{12}(n) = (a_{11}(n) - 1) a_{12}(n) = \frac{\sin n}{5n + 50}$$

$$a_{21}^{(1)}(n) = \bar{a}_{12}(n)\tilde{a}_{11}(n) = a_{12}(n)((a_{11}(n)) + 1) = \frac{10 + \sin n}{5n + 50}$$

$$a_{22}^{(1)}(n) = \bar{a}_{12}(n)\tilde{a}_{12}(n) = (a_{12}(n))^2 = \frac{1}{(n^3 + 10)^2}$$

$$a_{11}^{(2)}(n) = \bar{a}_{21}(n)\tilde{a}_{21}(n) = (a_{21}(n))^2 = \frac{1}{(n^2 + 20)^2}$$

$$a_{12}^{(2)}(n) = \bar{a}_{21}(n)\tilde{a}_{22}(n) = a_{21}(n)(a_{22}(n) + 1) = \frac{10 + \cos n}{5n + 100}$$

$$a_{21}^{(2)}(n) = \bar{a}_{22}(n)\tilde{a}_{21}(n) = (a_{22}(n) - 1) a_{21}(n) = \frac{\cos n}{5n + 100}$$

$$a_{22}^{(2)}(n) = \bar{a}_{22}(n)\tilde{a}_{22}(n) = (a_{22}(n))^2 - 1 = \frac{\cos^2 n + 10\cos n}{25}$$

Because,

$$b(n) = \frac{1}{2} \sum_{i,j,k=1}^{s} \left| a_{jk}^{(i)}(n) + a_{kj}^{(i)}(n) \right| =$$

$$\frac{1}{2} \left[\left| a_{11}^{(1)}(n) + a_{11}^{(1)}(n) \right| + \left| a_{12}^{(1)}(n) + a_{21}^{(1)}(n) \right| + \left| a_{21}^{(1)}(n) + a_{12}^{(1)}(n) \right| + \right.$$

$$\left| a_{22}^{(1)}(n) + a_{22}^{(1)}(n) \right| + \left| a_{11}^{(2)}(n) + a_{11}^{(2)}(n) \right| + \left| a_{12}^{(2)}(n) + a_{21}^{(2)}(n) \right| +$$

$$\left. \left| a_{21}^{(2)}(n) + a_{12}^{(2)}(n) \right| + \left| a_{22}^{(2)}(n) + a_{22}^{(2)}(n) \right| \right] =$$

$$\frac{1}{2}\left[\left|\frac{\sin^2 n + 10\sin n}{25} + \frac{\sin^2 n + 10\sin n}{25}\right| + \left|\frac{\sin n}{5n+50} + \frac{10+\sin n}{5n+50}\right| + \right.$$

$$\left|\frac{10+\sin n}{5n+50} + \frac{\sin n}{5n+50}\right| + \left|\frac{1}{(n^3+10)^2} + \frac{1}{(n^3+10)^2}\right| +$$

$$\left|\frac{1}{(n^2+20)^2} + \frac{1}{(n^2+20)^2}\right| + \left|\frac{10+\cos n}{5n+100} + \frac{\cos n}{5n+100}\right| +$$

$$\left.\left|\frac{\cos n}{5n+100} + \frac{10+\cos n}{5n+100}\right| + \left|\frac{\cos^2 n + 10\cos n}{25} + \frac{\cos^2 n + 10\cos n}{25}\right|\right] =$$

$$\frac{1}{2}\left[\frac{2}{25}\left|\sin^2 n + 10\sin n\right| + \frac{4}{5n+50}\left|5+\sin n\right| + \frac{2}{(n+10)^2} + \right.$$

$$\left.\frac{2}{(n+20)^2} + \frac{4}{5n+100}\left|5+\cos n\right| + \frac{2}{25}\left|\cos^2 n + 10\cos n\right|\right] =$$

$$\frac{1}{25}\left|\sin^2 n + 10\sin n\right| + \frac{2}{5n+50}\left|5+\sin n\right| + \frac{1}{(n+10)^2} +$$

$$\frac{1}{(n+20)^2} + \frac{2}{5n+100}\left|5+\cos n\right| + \frac{1}{25}\left|\cos^2 n + 10\cos n\right|$$

vary between 0.2 and 1 it implies simultaneously that for any solution $x(n,x_0)$ of system (1) the estimates (7) and (8)

$$\|x_0\|\prod_{p=0}^{n}\sqrt{(1-b(p))} \le \|x(n+1,x_0)\| \le \|x_0\|\prod_{p=0}^{n}\sqrt{(b(p)+1)}$$

are valid for all n. The numerical values of the solution and bounds are presented in Figure (3)

In this example we are able to estimate also the lower bound for growth rate.

Example 4. Consider system (1) with $(A(n))_{n\in N}$ given by

$$A(n) = \begin{bmatrix} 1 & \frac{1}{n^3+10} \\ \frac{1}{n^2+20} & 1 \end{bmatrix}. \tag{9}$$

Namely, its elements are as follows

$$\begin{array}{ll} a_{11}(n) = 1 & a_{12}(n) = \frac{1}{n^3+10} \\ a_{21}(n) = \frac{1}{n^2+20} & a_{22}(n) = 1 \end{array}.$$

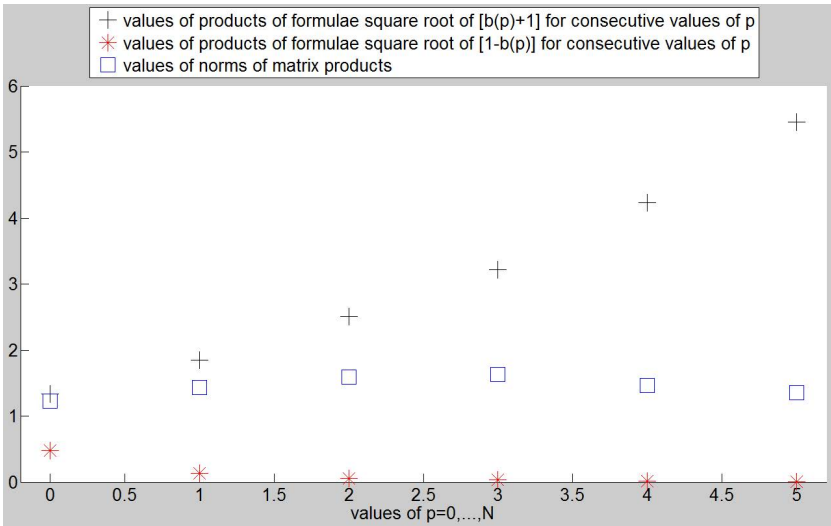Applying the above-mentioned elements of $(A(n))_{n\in N}$ to (5) and (3) we obtain (5) in the following form

Fig. 3. Our upper and lower estimates, and values of norms of matrix products

$$a_{11}^{(1)}(n) = \overline{a}_{11}(n)\widetilde{a}_{11}(n) = (a_{11}(n))^2 - 1 = 0$$

$$a_{12}^{(1)}(n) = \overline{a}_{11}(n)\widetilde{a}_{12}(n) = (a_{11}(n) - 1)\, a_{12}(n) = 0$$

$$a_{21}^{(1)}(n) = \overline{a}_{12}(n)\widetilde{a}_{11}(n) = a_{12}(n)\, ((a_{11}(n)) + 1) = \frac{2}{n^3 + 10}$$

$$a_{22}^{(1)}(n) = \overline{a}_{12}(n)\widetilde{a}_{12}(n) = (a_{12}(n))^2 = \frac{1}{(n^3 + 10)^2}$$

$$a_{11}^{(2)}(n) = \overline{a}_{21}(n)\widetilde{a}_{21}(n) = (a_{21}(n))^2 = \frac{1}{(n^2 + 20)^2}$$

$$a_{12}^{(2)}(n) = \overline{a}_{21}(n)\widetilde{a}_{22}(n) = a_{21}(n)\, (a_{22}(n) + 1) = \frac{2}{n^2 + 20}$$

$$a_{21}^{(2)}(n) = \overline{a}_{22}(n)\widetilde{a}_{21}(n) = (a_{22}(n) - 1)\, a_{21}(n) = 0$$

$$a_{22}^{(2)}(n) = \overline{a}_{22}(n)\widetilde{a}_{22}(n) = (a_{22}(n))^2 - 1 = 0$$

Because

$$b(n) = \frac{1}{2} \sum_{i,j,k=1}^{s} \left| a_{jk}^{(i)}(n) + a_{kj}^{(i)}(n) \right| =$$

$$\frac{1}{2} \left[\left| a_{11}^{(1)}(n) + a_{11}^{(1)}(n) \right| + \left| a_{12}^{(1)}(n) + a_{21}^{(1)}(n) \right| + \left| a_{21}^{(1)}(n) + a_{12}^{(1)}(n) \right| + \right.$$

$$\left| a_{22}^{(1)}(n) + a_{22}^{(1)}(n) \right| + \left| a_{11}^{(2)}(n) + a_{11}^{(2)}(n) \right| + \left| a_{12}^{(2)}(n) + a_{21}^{(2)}(n) \right| +$$

$$\left. \left| a_{21}^{(2)}(n) + a_{12}^{(2)}(n) \right| + \left| a_{22}^{(2)}(n) + a_{22}^{(2)}(n) \right| \right] =$$

$$\frac{1}{2}\left[|0| + \left|0 + \frac{2}{n^3+10}\right| + \left|\frac{2}{n^3+10} + 0\right| + \left|\frac{1}{(n^3+10)^2} + \frac{1}{(n^3+10)^2}\right| + \right.$$

$$\left.\left|\frac{1}{(n^2+20)^2} + \frac{1}{(n^2+20)^2}\right| + \left|\frac{2}{n^2+20} + 0\right| + \left|0 + \frac{2}{n^2+20}\right| + |0|\right] =$$

$$\frac{1}{2}\left[4\left|\frac{1}{n^3+10}\right| + 2\left|\frac{1}{(n^3+10)^2}\right| + 2\left|\frac{1}{(n^2+20)^2}\right| + 4\left|\frac{1}{n^2+20}\right|\right] =$$

$$\frac{2}{n^3+10} + \frac{1}{(n^3+10)^2} + \frac{1}{(n^2+20)^2} + \frac{2}{n^2+20} = \frac{2n^3+21}{(n^3+10)^2} + \frac{2n^2+41}{(n^2+20)^2}$$

tends to zero it implies simultaneously that for any solution $x(n,x_0)$ of system (1) the estimates (7) and (8)

$$\|x_0\| \prod_{p=0}^{n} \sqrt{(1-b(p))} \le \|x(n+1,x_0)\| \le \|x_0\| \prod_{p=0}^{n} \sqrt{(b(p)+1)}$$

are valid for all n. The numerical values of the solution and bounds are presented in Figure (4)
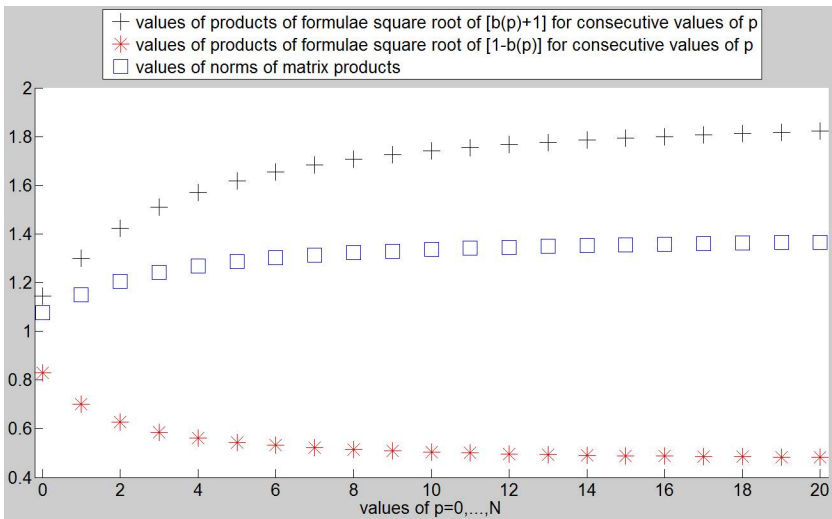

Fig. 4. Our upper and lower estimates, and values of norms of matrix products

By contrast with previous 3 examples here we can both estimate a growth rates and, what is more important, decide about stability of system (1).

It is well known (see [17]), that an infinite product $\prod\limits_{p=0}^{\infty}(x(p)+1)$ with positive

$x(p)$ converges if and only if the series $\sum\limits_{p=0}^{\infty}x(p)$ converges. Also similarly, if $0 <$

$x(p) < 1$ holds, then $\prod\limits_{p=0}^{\infty}(1-x(p))$ approaches a non-zero limit if and only if the

series $\sum\limits_{p=0}^{\infty}x(p)$ converges. Therefore, from Theorem 2 we obtain the following result
about stability.

Corollary 1. *If the series* $\sum\limits_{p=0}^{\infty}b(p)$, *where* $b(p)$ *are given by (6), converges, then (1)*
is stable.

It is clearly that in Example (4) the series $\sum\limits_{p=0}^{\infty}b(p)$ is convergent, and therefore
system (1) is stable.

Observe that from Theorem 1 we know that Lyapunov exponents of system (1)
with coefficients given by (9) are all equal to zero. But it doesn't imply that the
system is stable.

Bound of norm of a matrix power by coefficients is a particular case of our es-
timate. Our result is also valid for stationary systems and we will ilustrate it by an
example of 2-by-2 matrix.

Example 5. Consider system (1) with all $A(n)$ equal to A, where

$$A = \begin{bmatrix} e & f \\ g & h \end{bmatrix}.$$

Namely, its elements are as follows

$$\begin{array}{ll} a_{11}(n) = e & a_{12}(n) = f \\ a_{21}(n) = g & a_{22}(n) = h \end{array}.$$

Applying the above-mentioned elements of A to (5) and (3) we obtain (5) in the
following form

$$a_{11}^{(1)}(n) = \overline{a}_{11}(n)\tilde{a}_{11}(n) = (a_{11}(n))^2 - 1 = e^2 - 1$$
$$a_{12}^{(1)}(n) = \overline{a}_{11}(n)\tilde{a}_{12}(n) = (a_{11}(n) - 1)\,a_{12}(n) = (e-1)f$$
$$a_{21}^{(1)}(n) = \overline{a}_{12}(n)\tilde{a}_{11}(n) = a_{12}(n)\,((a_{11}(n)) + 1) = (e+1)f$$
$$a_{22}^{(1)}(n) = \overline{a}_{12}(n)\tilde{a}_{12}(n) = (a_{12}(n))^2 = f^2$$
$$a_{11}^{(2)}(n) = \overline{a}_{21}(n)\tilde{a}_{21}(n) = (a_{21}(n))^2 = g^2$$
$$a_{12}^{(2)}(n) = \overline{a}_{21}(n)\tilde{a}_{22}(n) = a_{21}(n)\,(a_{22}(n) + 1) = g\,(h+1)$$
$$a_{21}^{(2)}(n) = \overline{a}_{22}(n)\tilde{a}_{21}(n) = (a_{22}(n) - 1)\,a_{21}(n) = g\,(h-1)$$
$$a_{22}^{(2)}(n) = \overline{a}_{22}(n)\tilde{a}_{22}(n) = (a_{22}(n))^2 - 1 = h^2 - 1$$

Finally,

$$b(n) = \frac{1}{2} \sum_{i,j,k=1}^{s} \left| a_{jk}^{(i)}(n) + a_{kj}^{(i)}(n) \right| =$$

$$\frac{1}{2} \left[\left| a_{11}^{(1)}(n) + a_{11}^{(1)}(n) \right| + \left| a_{12}^{(1)}(n) + a_{21}^{(1)}(n) \right| + \left| a_{21}^{(1)}(n) + a_{12}^{(1)}(n) \right| + \right.$$

$$\left| a_{22}^{(1)}(n) + a_{22}^{(1)}(n) \right| + \left| a_{11}^{(2)}(n) + a_{11}^{(2)}(n) \right| + \left| a_{12}^{(2)}(n) + a_{21}^{(2)}(n) \right| +$$

$$\left. \left| a_{21}^{(2)}(n) + a_{12}^{(2)}(n) \right| + \left| a_{22}^{(2)}(n) + a_{22}^{(2)}(n) \right| \right] =$$

$$\frac{1}{2} \left[\left| e^2 - 1 + e^2 - 1 \right| + 2 \left| (e-1)f + (e+1)f \right| + \left| f^2 + f^2 \right| + \right.$$

$$\left. + \left| g^2 + g^2 \right| + 2 \left| g(h+1) + g(h-1) \right| + \left| h^2 - 1 + h^2 - 1 \right| \right] =$$

$$\frac{1}{2} \left[2 \left| e^2 - 1 \right| + 4 \left| ef \right| + 2 \left| f^2 \right| + 2 \left| g^2 \right| + 4 \left| gh \right| + 2 \left| h^2 - 1 \right| \right] =$$

$$\left| e^2 - 1 \right| + 2 \left| ef \right| + f^2 + g^2 + 2 \left| gh \right| + 2 \left| h^2 - 1 \right|$$

For any a, b, c, d we have

$$b(p) = \left| e^2 - 1 \right| + 2 \left| ef \right| + f^2 + g^2 + 2 \left| gh \right| + 2 \left| h^2 - 1 \right|$$

Adding 1 we obtain

$$b(p) + 1 = \left| e^2 - 1 \right| + 2 \left| ef \right| + f^2 + g^2 + 2 \left| gh \right| + 2 \left| h^2 - 1 \right| + 1$$

$$\|A^n\| \leq \left(\sqrt{\left| e^2 - 1 \right| + 2 \left| ef \right| + f^2 + g^2 + 2 \left| gh \right| + 2 \left| h^2 - 1 \right| + 1} \right)^n$$

$$\|A^n\| \leq \left(\sqrt[2]{b(p) + 1} \right)^n$$

Assuming $a, d > 1$, $b, c > 0$ our estimate can be simplified as follows

$$b(p) = (e+f)^2 + (g+h)^2 - 2$$

$$b(p) + 1 = (e+f)^2 + (g+h)^2 - 1$$

$$\|A^n\| \leq \left(\sqrt{(e+f)^2 + (g+h)^2 - 1} \right)^n$$

$$\|A^n\| \leq \left(\sqrt[2]{b(p) + 1} \right)^n$$

3 Conclusion

In this paper we have obtained upper and lower bounds for norm of solution of linear discrete time-varying system in terms of coefficients of matrices $A(n)$. It is interesting that to calculate our bounds we do not need to know eigenvalues or spectral norm of matrices because we can simply calculate it by matrix coefficients. It is also worth to notice that our bounds are also valid in case of singular matrices. Moreover, in the paper, as the corollary of our results, we have obtained an upper estimate for stationary system.

Presented solutions can be widely used in the algorithms of data transmission [19], [20] and control developed by the research team from Silesian University of Technology. The proposed method can be particularly useful for high-compression algorithms where the key parameter is the time of computation. A time series analysis can bring a significant increase of efficiency of the communication system between the UAV and mobile control station. The presented methods could also be used for communication channel modeling applications. In particular important is the ability to apply to applications related to cryptography and signal variability analysis and validation of quality of encryption algorithms.

References

1. Adrianova, L.Y.: Introduction to Linear Systems of Differential Equations, vol. 146. AMS Bookstore (1995)
2. Arnold, L., Crauel, H., Eckmann, J.P. (eds.): Lyapunov Exponents. Proceedings of a Conference, held in Oberwolfach, May 28-June 2. Lecture Notes in Mathematics, vol. 1486. Springer, Berlin (1991)
3. Awad, L.R., El-Kholy, E.M., El-Bendary, S.: On the Estimation of Solutions for Some Linear Systems of Differential Equations. Acta Mathematica Sinica, New Series 14(1), 41–46 (1998)
4. Barreira, L., Pesin, Y.: Lyapunov exponents and Smooth Ergodic Theory. Univ. Lecture Ser., vol, 23. Amer. Math Soc., Providence (2002)
5. Li, C., Chen, G.: Estimating the Lyapunov exponents of discrete systems. Chaos 14(2), 343–346 (2004)
6. Li, C., Xia, X.: On the bound of the Lyapunov exponents for continuous systems. Chaos 14(3), 557–561 (2004)
7. Czornik, A., Jurgas, P.: Set of possible values ofmaximal Lyapunov exponents of discrete time-varying linear system. Automatica 44(2), 580–583 (2008)
8. Czornik, A., Nawrat, A.: On new estimates for Lyapunov exponents of discrete time-varying linear systems. Automatica 46(4), 775–778 (2010)

9. Czornik, A.: Bounds for characteristic exponents of discrete linear time-varying systems. Journal of the Franklin Institute-Engineering and Applied Mathematics 347(2), 502–507 (2010)

10. Czornik, A., Mokry, P., Niezabitowski, M.: On a Continuity of characteristic exponents of linear discrete time-varying systems. Archives of Control Sciences 22(LVIII), 17–27 (2012)

11. Czornik, A., Niezabitowski, M.: O parametrycznej zale żności wykładników Lapunowa dyskretnych układów liniowych. In: XVIII Krajowa Konferencja Automatyzacji Procesów Dyskretnych w Zakopanem September 19-22, Analiza procesów dyskretnych, Tom I, pp. 41–48 (2012)

12. Czornik, A., Niezabitowski, M.: Lyapunov Exponents for Systems with Unbounded Coefficients. - To appear in Dynamical Systems: An International Journal (2012)

13. Czornik, A., Nawrat, A., Niezabitowski, M.: On the Lyapunov exponents of a class of the second order discrete time linear systems with bounded perturbations. - To appear in Dynamical Systems: An International Journal (2012)

14. Key, E.S.: Lower bounds for the maximal Lyapunov exponent. Journal of Theoretical Probability 3(3), 477–487 (1990)

15. Leonov, G.A.: Strange Attractors and Classical Stability Theory. Nonlinear Dynamics and Systems Theory 8(1), 49–96 (2008)

16. Leonov, G.A.: Strange Attractors and Classical Stability Theory. St. Petersburg University Press (2009)

17. Rudin, W.: Real and Complex Analysis, 3rd edn. McGraw Hill, Boston (1987)

18. Smith, R.A.: Bounds for the characteristic exponents of linear systems. Proc. Camb. Phil. Soc. 61, 889–894 (1965)

19. Topór-Kamiński, T., Żurkowski, R., Grygiel, M.: Selected methods of measuring the delay in data transmission systems with wireless network interfaces. Acta Phys. Pol. A 120(4), 748–754 (2011)

20. Topór-Kamiñski, T., Krupanek, B., Homa, J.: Delays models of measurement and control data transmission network. In: Nawrat, A., Simek, K., Świerniak, A. (eds.) Advanced Technologies for Intelligent Systems of National Border Security. SCI, vol. 440, pp. 257–278. Springer, Heidelberg (2013)

Virtual Reality Technology for Military and Industry Training Programs

Marek Koźlak, Antoni Kurzeja, and Aleksander Nawrat

Abstract. This paper presents how the Virtual Reality (VR) technology and Computer Graphics (CG) is used nowadays by industry to reduce productions costs, minimize learning curve and eliminates hazard situations. Few examples of procedural training and VR simulators are being presented, as well as the usage of CG for military training and troops support.

1   Introduction

In production industries it is already a standard to use Virtual Reality and its methods to improve product development, increase quality and optimize final design. Computer visualizations and analysis software significantly helps to reduce growing production costs and allows to avoid prototypes manufacture and arduous testing in science laboratories. This speeds up development project and improves communication between engineers, allowing for intuitive experience and data exchange while using intelligible environment of virtual reality. Today's competitive business climate intensifies the need for well-trained operators with all types of skills and in all industries. Companies are pushing facilities to their limits, while both processes and automated systems are becoming more and more complicated. The projected retirement of many experienced operators in the near future sets the stage for a young workforce. The question is how to maintain a

Marek Koźlak · Aleksander Nawrat
Silesian University of Technology, Technopark, ul. Konarskiego 18C,
44-100 Gliwice, Poland
e-mail:{marek.kozla,anawrat}@polsl.pl

Marek Koźlak · Antoni Kurzeja
Ośrodek Badawczo-Rozwojowy Urządzeń Mechanicznych "OBRUM" sp. z o.o.,
ul. Toszecka 102, 44-117 Gliwice, Poland,
e-mail: {mkozlak,akurzeja}@obrum.gliwice.pl

profitable production rate and secure a safe and effective work environment with personnel that is new to the job. This is where 3D communications are becoming ubiquitous, independent of specialized software and formats, and cost effective. The use of 3D data and tools is helping accelerate the communication of information. Disconnecting 3D data from burdened systems and making this data available for all people in the organization is considered an important objective that significantly improves the communication quality while reduce time and costs.

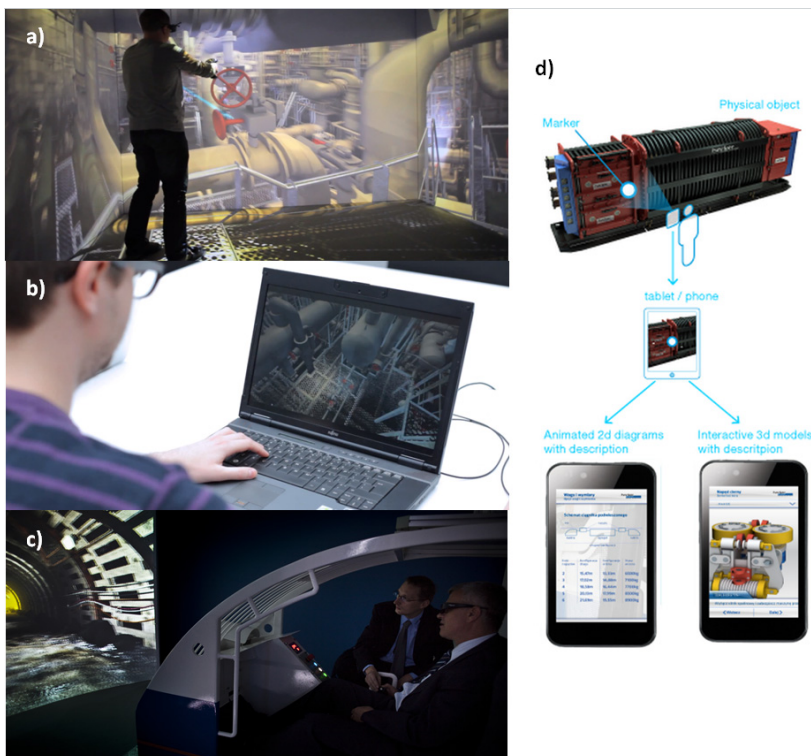## 2   Virtual Reality for Industry

With safe virtual environments, the ability to make and learn from mistakes while performing complicated procedures and instructions is a hallmark of the way to designs training and educational solutions. Within this 'learning by doing' approach, a user can quickly identify a problem, ask questions, or receive just-in-time mentoring about any consequences of his actions. Photorealistic 3D models of detailed equipment and full-scale facilities are just the beginning. By reusing this data in a real-time software environment, a virtual instructor can interactively guide students through even the most advanced assembly service, maintenance checklist or safety procedure.

The objective of all operator training is to improve a skill set as rapidly and effectively as possible. The realism associated with Virtual Reality training greatly accelerates learning and skill acquisition. In fact, the combination of VR and traditional training has been proven effective again and again.

Having the ability to improve asset utilization, reuse complex models, and visit hazardous locations virtually using 3D simulated environments allows time savings to accumulate. An example of time savings is creating a virtual walkthrough of a production facility. Realistic 3D display technology allows to tour a facility virtually from just about anywhere emulating real-life experiences and remote collaboration among teams. In Fig. 1. a virtual simulator of LNG vessel compressor room operated by Exxon Mobile is presented. Using 1:1 full scale immersive display system an operator is being trained on over 100 pressure valves functionality, which is not possible in real life due to a cost restrains and potential risk. Such a system might be classified as an "Operator Training Simulator" (OTS) which is fundamental to production facility operations and abnormal situation management. OTS allows beginners to learn the basics, while more experienced staff are able to deal with unusual or emergency situations in a safe environment.

Final model quality, physics simulation and equipment behavior control decides how the trainees will absorb the instruction and retain what they learned in their exercise. Almost any machine might be reconstructed as a 3D interactive model with real and virtual controllers or cockpits. These simulators, often called Synthetic Environmental Trainers (SET), blurs the difference between the simulation and the real work environment. SET can dramatically shorten the learning curve, improve operator's skill and support mastery for certification and compliance. As an example Fig. 1. presents a typical simulator where true cockpit of the vehicle was combined with 3D stereoscopic real time environment.

Since last few years CG technologies supports industry with another very powerful training toolkit in the form of Augmented Reality Instructions. ARI delivers computer generated maintenance and operational information on top of visible objects. See-through glasses project digitized models and information layered on top of the existing environment. Operators can interact with equipment controls while service step-by-step instructions augment the user's experience. Applications and simulators can be designed to appear on the mobile devices such as electronic tablets or smartphones, replacing printed material with always current, best practice instructions. This solutions help to transform an employee with general understanding of an environment or equipment into the knowledge worker for the 21st century. Fig. 1. presents an example of ARI project implemented for mining equipment service and weekly maintenance.

Fig. 1. Virtual Reality training simulators developed by i3D in 2012 for mining industry: a) CAVE immersive simulator developed for Exxon Mobile (OTS), b) Exxon Mobile interactive simulator displayed on a standard laptop, c) Synthetic Environmental Trainer with physical controllers developed for Becker Warkop, d) Augmented Reality Instructions for Android devices developed for Becker Warkop (sources: i3D, Exxon Mobile, Becker Warkop 2012)

Regardless which of the three mentioned above types of Virtual Reality simulators are being used, the general benefits of VR listed below are significant:

- **More Proficient Operators**. Experienced personnel make fewer errors; they can identify upcoming process disruption earlier and initiate the adequate steps and actions to avoid or minimize any detrimental effects.
- **Risk Reduction & Enhanced Skills Development**. Synthetic Environmental Trainers expose operators to a wide range of environment conditions and teach them how to deal with emergencies and unusual conditions in safe and secure conditions – preventing loss & injury when real crises occur.
- **Knowledge Capture for More Effective Training**. The ability to measure what a trainee is doing right or wrong immediately in the virtual work environment provides accurate data on the effectiveness of training and enhanced operator personal skills.
- **Reduced Loss of Production during Training**. Using Operator Training Simulators instead of production machines allows the production process to continue uninterrupted.
- **Increased Crew Efficiency**. Competent and well-trained employees perform tasks quickly and efficiently ensuring product quality and contributing to the development of the company.
- **Average Production per Machine** Improvement. Highly motivated and knowledgeable personnel are more likely to exploit the full potential of equipment, increasing average annual production per machine.
- **Reduced Machine Wear and Damage**. Simulators help operator better understand the machinery, reducing risk of improper use and potential breakage.
- **Improved Reliability and Quality**. Well-trained personnel is able to face more complex tasks, defining new quality standards.

3   Virtual Reality for Defense

Since the begging of CG (Computer Graphics) technology development, Virtual Reality (VR) has been used to support several US army defense projects as well as their command centers. Nowadays, VR software and display equipment go beyond many standard limitations and allow users to communicate and cooperate with each other in digital world as well as reduce the costs and the number of real exercises needed for military personnel training. Presently, computer applications are mostly used to train military pilots and tank crews in safe environments. Soldiers steps into a physical mockup of the vehicle surrounded with projection screens which in the real time generate 3D world around their perception.

The most important assets of the military forces is their experience and the knowledge acquired on the ground in combat. Military officials become concerned how to transfer this knowledge to a young man, ages 18 to 24, in the best effective way to enhance their skills and their ability to think in complex environments.

During the standard military exercises, life of the soldier is usually not in danger. This makes it very hard to study his individual behavioral characteristic, his

ability to analyze threats, identify emerging situation and decision making process under a life – threatening situation. VR allows to arrange dangerous combat conditions in potentially safe environment. Lesson learned would be very important to detect suspicious behavior and actions of individuals. Through such a virtual experience, we can select the best people for the job and prepare them for the mission.

But present VR combat solutions also has some major drawbacks. For example, all the simulators are located in the air-conditioned environments, where soldiers do not feel heat or cold, they do not get tired carrying full weight backpack while walking through the quaggy terrain. Possibility to go through the walls without collision detection also makes it more gaming than serious training.

With today's technology and fast grown of the computer graphics, this might be improved. Among the numerous of standard military Synthetic Environmental Trainers (SET), each year more advanced and complex "first response" simulators are being deployed in the army which brings troops training to the next level. One of such a modern systems is the most common one named VIRTSIM offered commercially on the market by Raytheon. "Utilizing cutting edge software, VIRTSIM creates real-life scenarios for users to immerse themselves in tactical training activities" (source: Raytheon).

Advanced first response simulators based on Virtual Reality technology gives us a significant benefits:

- **Repeatability** – each mission can be repeated many times, results might be stored, and played to analyze and compare individual behave.
- **Knowledge transfer** – years of ground in combat experience might be captured and documented for young soldiers training.
- **Safe training** – the highest risk possible combat scenarios might be simulated to deceive soldiers perception without putting them for any physical risk of injury.
- **Economic factor** – soldiers deployment might take place without moving expensive military equipment and troops to foreign country or ally polygons, ammunition and fuel expenses are eliminated.
- **Behavior evaluation** – VR allows to detect suspicious behavior and actions of individuals in dangerous combat conditions, and their decision making process.

Custom made systems integrates real environments with advanced Virtual and Augmented Reality technologies, which delivers innovative and up-to date training solutions to the military. Additionally Virtual Reality applications are commonly used as a therapy treatment for military veterans to deal with Post Traumatic Stress Disorder. By recreating an exact combat situation, dangerous and stress location or past battle conditions, therapist can manipulate veterans to effect their perception and help to deal with psychology outcomes as well as reduce veterans trauma.
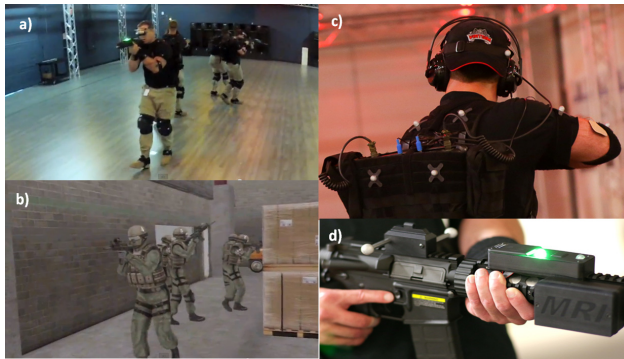
Fig. 2. Example of the first response military simulator offered commercially on the market: a) Picture of the training hall with soldiers equipped with tracking system, Head Mounted Display glasses, electric shock bandages and weapon replicas, b) Solders as a 3D avatars in simulation environment, c) Individual equip per solder, d) Fire arms replica with tracking system (sources: Raytheon 2012)

Fig. 3. Post Traumatic Stress Disorder behavior research using immersive CAVE display system (source: i3D 2012)

4   VR for Safety

Every year emergencies from man-made to natural disasters, take their toll on businesses and industry in lives and costs. This can be changed. Business and industry can limit injuries and damages and return more quickly to normal operations if they plan ahead. Management today is augmenting their recovery plans and safety trainings for effective emergency preparedness with 3D models and simulations of a facility, locale or specific situations.

One of the best ways to prevent and control occupational injuries, illnesses and deaths is to "design out" or minimize hazards and risks early in the design process. Using 3D models and simulations of building, structures, work environments,

machinery and equipment are cost-effective means to enhance occupational safety and health.

Classic safety training is generally comprised of several days of lectures supplemented with simple video presentations and compute-based training (CBT) modules. Focused primarily on knowledge transfer, this classic approach does not fully engage trainees to develop problem solving or critical thinking skills.

Virtual Reality changes the approach with meaningful interactive 3D content designed to actively engage students and keeps them focused on the subject matter, encouraging discussion while working within the environment virtually. Research has shown that trainees use gaming-type applications are much better prepared and retain the instruction longer. Interactive 3D technology is a flexible way to represent and experience safely complex, potentially hazardous processes or environments regardless of the geography or industry. With VR technology, engineers are able to analyze risky scenarios and minimize potential incident-prone areas, also VR works to make employees or even soldiers more aware of potential hazards at a site, the proper use of safety equipment and the procedures to maximize everyone's safety should problems occur.

Safety training should be continuous and ongoing. New devices, new technologies, new processes, all require new safety instruction, protocols and practice. Fig.4. presents an example of typical step by step approach safety application developed by i3D for Oil and Gas industry leader, where safety protocols decides of the life of many.
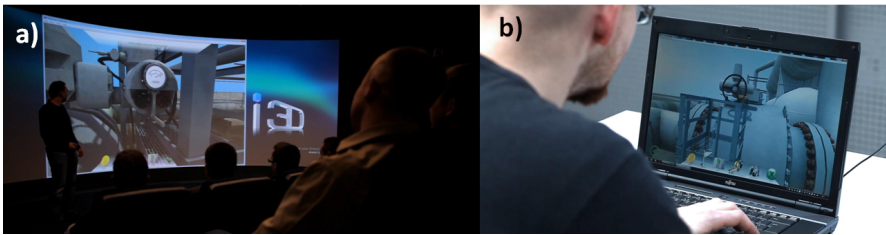
Fig. 4. Gas and oil separator unit safety instruction developed in 2011 by i3D using Quazar3D real-time interactive environment: a) classroom with 3D stereoscopic projection system, b) individual safety test on a laptop (source: i3D, 2011)

5   Summary

Thanks to newly affordable, newly accessible VR technology, it's a brand new day in Information Communications. Teams working virtually and collaboratively in 3D are the norm for the 21st century workforce. By detaching 3D data from complex systems and making this data accessible to all people in the organization, VR methodology dramatically improves communication effectiveness while reducing time and costs.

Synthetic Environmental Trainers and Operator Training Simulators continuously evaluates and monitors each individual student's actions, quickly identifying weak spots that require additional attention teaching the most effective way and best working practices. Virtual Reality simulators optimize the training cycle while providing a very high standard in terms of skills improvement and safety consciousness. Simulators and Augmented Reality Instructions can be used for beginners' basic training, or to help experienced operators refine their skills to increase production levels.

References

[1]   i3D (i3D S.A.), `http://www.i3dinc.com/`
[2]   BP (British Petrolium),
      `http://www.bp.com/sectiongenericarticle800.do?`
      `categoryId=9040152&contentId=7073365`
[3]   Becker Warkop,
      `http://www.becker-mining.com/runtime/cms.run/doc/`
      `English/987/News.html?newsid=107`
[4]   `http://www.youtube.com/watch?v=_GTICfs3JG4`
[5]   Exxon Mobile, `http://poland.texasresearchbizwire.com/node/7`
[6]   `http://www.youtube.com/watch?v=baOegjxWJsA&list=UUC4K5jBv`
      `hNAbU2EwWe54JEQ&index=8`
[7]   Raytheon, `http://www.raytheon.com/newsroom/feature/virtsim/`
[8]   Raytheon,
      `http://www.raytheon.com/newsroom/rtnwcm/groups/ncs/`
      `documents/content/rtn12_ncs_virtsim_brochure.pdf`

Verifying Unmanned Land Vehicle Vision System Configuration Using Serious Gaming Solution

Marek Koźlak, Antoni Kurzeja, and Aleksander Nawrat

Abstract. In this article is described used in Research and Development Center of Mechanical Appliances OBRUM sp. z o.o. method of vehicle R&D cycle support using serious gaming (SG) solution. Implemented in OBRUM sp. z o.o. solution is described on example of Multipurpose Engineering Machine (WMI) with remote control functionality requirement. Short serious gaming introduction with WMI characteristic familiarize reader with study object. Short description of how SG is used in R&D cycle of modernization and concept vehicle R&D. Conclusion summarizes OBRUM sp. z o. o. experience and presents specific application of research results.

1   Introduction

Research and Development Center of Mechanical Appliances "OBRUM" Sp. z o. o. is a part of Bumar Group, and as a main research and development center is conducting a series of programs in support of the national defense. For over 40 years OBRUM realizes modernization, short series manufacture and product implementation in cooperation with reputed universities and defense industry from around the world. Today OBRUM provides full R&D cycle of:

Marek Koźlak · Aleksander Nawrat
Silesian University of Technology, Technopark, ul. Konarskiego 18C,
44-100 Gliwice, Poland
e-mail: {marek.kozla,anawrat}@polsl.pl

Marek Koźlak · Antoni Kurzeja
Ośrodek Badawczo-Rozwojowy Urządzeń Mechanicznych "OBRUM" sp. z o.o.,
ul. Toszecka 102, 44-117 Gliwice, Poland
e-mail: {mkozlak,akurzeja}@obrum.gliwice.pl

- Trucked vehicle – PT91, WZT3, MID, MG-20,
- Wheeled vehicle – WMI, MS-20,
- Simulation and Training systems – BESKID-3, SK-1, SK-1 PLATOON

1.1   Serious Gaming – VBS2

Serious gaming is successfully used for training for more than 10 years. SG solutions developed by defence or civil industry are focused in most cases on First Person Perspective or Third Person Perspective simulation of single solider, team, platoon or company level. The main objective of training using serious game is to improve:

- battlefield awareness,
- teamwork inside single squad or team,
- operation tactics,
- communication

Contemporary graphics, easy configurable high fidelity models, enhanced physics and varied available environments opens new possibilities of usage for SG solution. In company like Research and Development Centre of Mechanical Appliances where next to training and simulation system development we run number of analyses and case study at unmanned systems development. Simulation systems development tools is also used in vehicle development, serious game is being use both for simulation and analysis. OBRUM is using Virtual Battlespace 2 (VBS2) as main Serious Gaming solution for S&T system development and prototypes analyses. Virtual Battlespace 2 (http://products.bisimulations.com/development) is a COTS solution used by American, Canadian, Australian and many other army's for tactical training to company level. VBS2 is based on ARMA2 graphic engine, using NVidia PhysX provide sufficient for initial systems analysis fidelity of prepared vehicle 3D models.

At the stage of preliminary analysis OBRUM system designers, software engineers and mechanical designers identified SG used by OBRUM for S&T systems development as a useful for listed above subject analyses:

- HMI interfaces development – testing,
- Vision system configuration prototyping,
- Conceptual vehicles usage verification,
- Controllability analyses,
- Promotion and concept vehicle presentation.

1.2   Object of Study – Base Chassis of Multipurpose Engineering Machine (WMI)

This article discusses conducted analyses for vision system developed for Multipurpose Engineering Machine (WMI) fig. 1 developed and presented by OBRUM in year 2012 on International Defence Industry Exhibition MSPO 2012.

WMI is technology demonstrator of wheeled engineering machine developed in a purpose of direct in convoy engineering support.

The base chassis of WMI is based on 2-axles wheeled drive system, including 4x4 drive. Chassis is equipped with controlled suspension including opportunity to lock and adjust the height, both shock absorbing axles with calibration of twist of the machine (alignment), highly effective brakes at high wheels with ABS systems, clearance about 350 mm, wheels with single terrain tyres of high capacity including pressure control system. Vehicle drive is composed of combustion engine of power about 250 kW. Maximum velocity of the vehicle is about 80 km/h.

WMI vehicle weight including basic equipment of a loader shall equal about 16,500 kg, vehicle width 2.55-3 m, height up to 2.7 m, length up to about 7.5 m.

WMI has a possibilities to lift up to 5,0 tonnes on front work tool, crab drive mode and remote control possibilities.

During machine development, mechanical, electrical designers with OBRUM research department conducted series of analyses to fulfil vehicle technical and tactical requirements.

Remote control capabilities, for unmanned mode was achieved by developed in OBRUM control system that give us the same steering capabilities inside and outside of control cab.

Fig. 1. WMI photography without front work tool, showing front working tool adapter (source: OBRUM)

2   Analysis

Analyzing requirements and SG possibilities, defined following analyses to be conducted to determinate:

1. Vision system configuration:
    a. Number of cameras,
    b. Cameras placement,
    c. Minimal image resolution of transferred to control panel vision signal.
2. Controllability using designed vision system.

In this article we discuss developed in OBRUM development department method on a example of defining vision system camera placement.

2.1 WMI for VBS2 Model Construction

First step of preparation for system analyses using VBS2 is 3D model development.

For purposes of WMI analyses we used CAD/CAM model built in used by OBRUM R&D department SolidWorks. Model prepared for production of technology demonstrator is a source of surface 3D model for VBS2 model development tool – OXYGEN. After preparation of model skeleton and textures config file is prepared. Config file in VBS2 contains all information about model used in VBS2 simulation. One of many configuration parameters is PhysX parameters that describes model physic such as weight, mass centre, materials and others. After finishing configuration of VBS2 model we can use it in VBS2 scenario and control it with keyboard, HID devices such as steering wheel, pedals or other earlier implemented HMI interfaces.

In the phase of development machine specification and 3D models of chassis designer establish proposed vision system configuration, which are a base point for camera placement. During 3D model preparation for VBS2, as many camera points on model is set as construction of the machine allows. After game model is prepared we develop simplified HMI interface or implement existing solution for operator to control the machine in virtual environment.

2.2 Scenario Preparation

To determinate proper camera placement for remote control of engineering machine we have to build a set of test scenarios. Trial scenarios will be used as a test ground and let chose optimal configuration to achieve point 1b of virtual machine tests.

To fulfil requirement of safe remote control of Multifunctional Engineering Machine (WMI) was prepared 4 scenarios. Every scenario was played by the same operator using the same HMI interface. For full credibility of conducted test for every configuration 3 set of test were conducted in slightly different configuration (to avoid user remember obstacles configuration).

For vision system configuration was prepared the fallowing scenarios:

1. Maneuvering in urban areas,
2. Road clearing – obstacles remove,
3. Precise working tool operation,
4. Tow and winch operating.

2.3 Trials Examples

Showed above example of 3D scenario configurator in VBS2. Precise objects placement is possible thanks to available measure tools fig. 2 and 3.

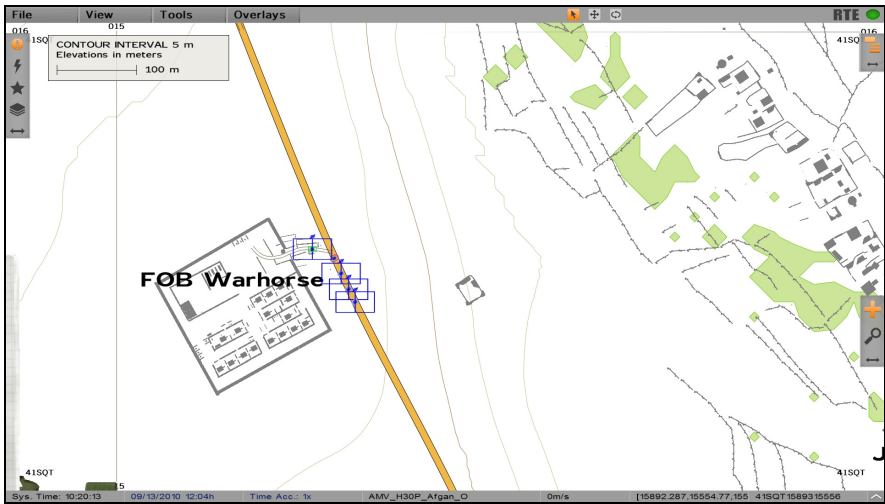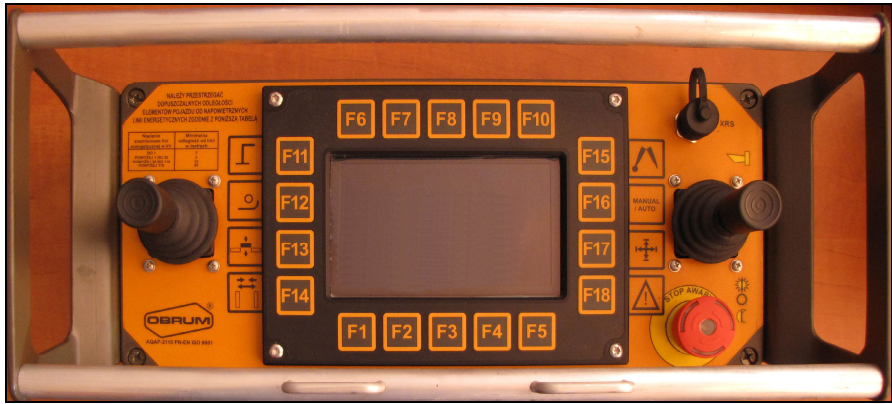**Fig. 2.** Scenario screen 3D camera view


Fig. 3. Scenario screen tactical view

Fig. 4. HMI interface example used for machine control (developed for MS-20 – 20m bridge layer) control panel

Tactical scenario view allows operator to see full scenario and like at battlefield plan its actions.

HMI interface fig. 4 used for VBS2 model control was MS-20 control panel (20m bridge layer MS-20) and PC with 24' LCD screen for camera view.
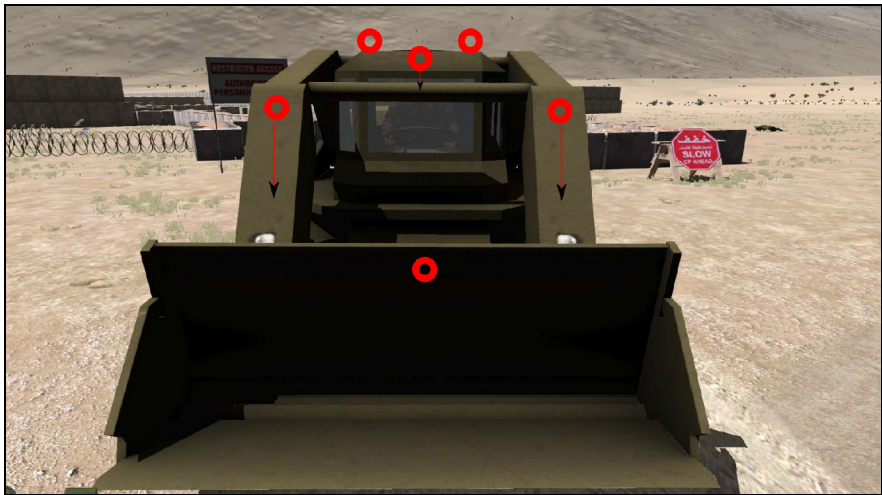
Fig. 5. Verified camera position at working tool and cabin

Verified camera position fig. 5 at working tool and cabin. Camera position verification during trials was prepared in several different configuration taken into account machine construction, operator proposal and hardiness of used cameras. Camera view change required VBS2 model config file edition and change.

Fig. 6. Camera at work tool view point example

Showed above camera views fig. 6 were displayed at 22" LCD screen in configuration:

- 1 view per screen – using two 22" LCD screen,
- 2 per screen – using one 22" LCD screen,
- Switchable configuration.

2.4 Implementation of Test Result

During conducted trials OBRUM engineers specified vision system configuration for next phase of WMI project, 3 axis PINIA. Developed solution contains:

- Optimal camera configuration, divided into specific operation usage modes of machine,
- Optimal camera placement,
- Requirement for communication link,
- Requirement for camera resolution and view angle,
- Proposed HMI configuration,
- Controllability analyse.

3 Conclusions

During test and trials of developed in OBRUM modernization and concept vehicles, ware defined fallowing conclusion of using Serious Gaming in R&D cycle of vehicle:

1. Serious gaming can by successfully used in manned and unmanned vehicle research and development cycle, for:
   a. Conception verification,
   b. Subsystem configuration analyses, such as:,
      i. Vision systems,
      ii. Interior HMI configuration,
      iii. Remote control panel configuration,

      c.   Controllability analysis,

      d.   Tactical usage verification,

      e.   Controllability when towing,

      f.   Promotion (advert) and concept vehicle usage demonstration.

2. Proposed solution can help engineers running analyses, concept works or vehicle modernization to solve the problems of:

      a.   Controllability analyses,

      b.   Inside and outside cabin visibility,

      c.   Vision systems configuration,

      d.   HMI interface configuration,

However serious game that using only simplified physic models or inaccurate data about model can issues difficulties with simulation fidelity. Conducting tests and trials at VBS2 models of concept machines there is a problem of building high fidelity physic and construction model for under construction vehicles – that translate to only indicative controllable test results.

Developed in OBRUM solution for concept testing in most affordable, fastest and giving best results method of concept vehicle verification and development.

References

[1] Pasieka, D., Wocka, P.: Research and Development Center of Mechanical Appliances OBRUM sp. z o.o. Journal of KONES Powertrain and Transport 18(1) (2011)

[2] Buck, W.: Trends in Immersive Environments, Future Solutions Allied Command Transformation Norfolk, Virginia, United States of America, ITEC (2011)

Conclusions

Vision based systems are commonly used in the area of automatic control, especially in Unmanned Aerial Vehicles (UAV). Drones with their special selected parameters gives infinite opportunities in improvement and development of vision surveillance algorithms, also in areas such as geodesy, cartography and meteorology. Majority of the applications are based on sensors, for example video or thermal imaging cameras. Consequently, it is essential to develop new video acquisition devices and design methodologies. However, there are a lot of challenges in the area of vision, which were presented and discussed in this book.

One of the most important issue in the area of automatic control is visual surveillance. The main idea is to detect special targets and abnormal situations due to their characteristic features, like size or character of movement. It is necessary to detect features using real time processing. However, the time of computation limits the process of detection from live video stream. While the process of detection of abnormal objects or situations is time consuming, the following process of real time object tracking minimize the computation time. This fact can be used for surveillance purposes, for creation of automatic target sentry turrets and for creation of control algorithms of camera gimbal placed in the UAVs. Moreover, information obtained from tracking can be used for higher level algorithms, such as object or activity recognition.

Drones are used in different weather conditions and during day or night time. Due to this fact, it is essential to improve algorithms of video acquisition and innovate the video acquisition devices. During flight in harsh conditions the wind can cause an unexpected rotation of the UAV object. The road and position of the drone can be corrected by entering the special mechanical construction – gimbal. However, this solution is not sufficient enough, and even after entering solutions presented above operating in harsh weather conditions can lead to blockage of the mechanical system. Challenges lie also in the other field of video acquisition. Visible light cameras often cover only a small part of the magnetic spectrum and they are very sensitive for dust, smoke, pollution and other weather inconveniences. Therefore, thermal cameras should be used more often. Video acquisition devices equipped with thermal cameras can be used for more accurate target detection, tracking and recognition in low light and harsh weather conditions not only during the day, but also during the night. There is a big need for development and improvement of the existing video acquisition devices. Such devices should be characterized mainly by small weight, low energy consumption and high resistance to temperature and vibrations.

Control algorithms are another important issues in development of UAV. There are three main applications of vision based algorithms in this area. UAV objects can be controlled by sending commands by human terrestrial operator using gestures. Systems recognizing gestures might significantly improve the quality of control. The other approach is to use aerial vision information. However, the biggest challenges here are stabilization and denoising of the video stream, calibration, in order to perform distortion compensation, and improvement of intensity of illumination or acquisition noise, for example due to high temperature of the device surroundings. The third application of vision based control algorithms is navigation of UAVs in an unknown dynamically changing environment. Geodesic terrain maps are commonly used in this area. However, there are a lot of disadvantages related with this approach. Such maps are often outdated and they are not include information about some tall buildings or flora. The big problem here is also connected with the appearance of other flying units in a local environment of UAVs. Control of the drones and planning a mission using 3D maps is an important issue and big challenging problem. Therefore, it should be solved in order to simplify and precise the process of navigation in a dynamically changing environments.

An important task during designing and construction of UAVs is process of testing: simulations and real life experiments. The first step of testing is utilization of data using advanced simulation environments. The UAV navigation algorithms can be implemented and followed by established trajectory. At the same time, it is possible to observe video streams acquired from virtual cameras, which are placed under UAV object. The video stream from a camera should be wirelessly transmit to human operator using ground base station, and should be encrypted due to the high risk of wireless data capture. Thus, a significant network bandwidth and dedicated image and sound compression algorithms are required.

The aim of simulation tests and real life experiments are to obtain positive results using simulations. Such results are considered as a first stage of development and improvement of classification and detection algorithms. Multiple sources of information are used to improve the quality of recognition. But the other problem is arising here. The increased amount of information sometimes can results in deterioration of real time processing. Therefore, dimensional reduction and clustering algorithms should be used to reduce the amount of data.

The area of UAV development is broad and essentially new. Therefore, the algorithms and methods used in this field should be improved and increased. All of the presented solutions are supported by analysis of applied techniques, analysis of new methods and results, and inspiring discussions. The new methods applied in this area show promising future, however, still there are a lot of challenging tasks for scientists and developers, which should be discussed and solved.

Author Index